Investigating Novel Inhibitors of Epithelial - Mesenchymal Transition (EMT) and Cancer Stem Cells (CSCs) in Pancreatic Cancer

By

Ruochen Dong
Bachelor of Medicine., Xi'an Jiaotong University, 2012

Submitted to the graduate degree program in Pharmacology and the Graduate Faculty of the University of Kansas in partial fulfillment of the requirements for the degree of Doctor of Philosophy.

_____
Committee Chair: Qi Chen, PhD

_____
Dan A. Dixon, PhD

_____
Bruno Hagenbuch, PhD

_____
Wen-Xing Ding, PhD

_____
Udayan Apte, PhD

Date Defended: 02/05/2020

The dissertation committee for Ruochen Dong certifies that this is
the approved version of the following dissertation:

Investigating Novel Inhibitors of Epithelial - Mesenchymal Transition (EMT) and Cancer Stem Cells (CSCs) in Pancreatic Cancer

_____

Chair: Qi Chen, PhD

_____

Graduate Director: Bruno Hagenbuch, PhD

Date Approved: 4/27/2020

Abstract

Pancreatic cancer is the 4th leading cause of cancer-related death in the U.S. in 2019. The five-year survival rate for all stages combined is only 9%, which is the lowest among all types of cancer. The current chemotherapeutic regimens for pancreatic cancer, including gemcitabine, FOLFIRNOX, and nab-paclitaxel, only provide limited benefits to the patients, due to low response rate and/or intolerable toxicities. Pancreatic cancer is enriched with cancer stem cells (CSCs), which contribute to its high metastatic tendency and resistance to treatments. The formation of CSCs is highly associated with cancer cell epithelial-mesenchymal transition (EMT), which contributes to the plasticity of cancer cells and comprises an initial step for metastasis. Inhibiting EMT and CSCs in pancreatic cancer could potentially inhibit pancreatic cancer progression, metastasis, and drug resistance.

Various efforts have been made to develop anti-tumor agents through modulation of important signaling pathways involved in EMT and CSCs. However, there has not been a clinical success in a specific inhibitor to CSCs, or the EMT process. Extracts from medicinal plants have been rich sources for compounds possessing activities to attenuate CSC characteristics. These compounds contribute to the suppression of tumor progression and aggressiveness in various degrees. A great amount of synthetized small molecules have also been studied in targeting regulating factors of EMT and CSCs. Recent studies revealed that RNA binding proteins have the potential to serve as a therapeutic target in cancer management. The role of RNA binding proteins in EMT and CSCs is a research topic of increasing interests. The overall goal of this dissertation is to develop several approaches to discover and investigate novel EMT and CSC inhibitors for pancreatic cancer.

We first investigated extracts of two traditional medicinal plants, Pao Pereira extract (Pao) and *Rauwolfia vomitoria* extract (Rau) for their anti-pancreatic CSC activities. Data demonstrated that Pao and Rau preferentially inhibited the viability of pancreatic CSC population, compared with the whole cancer cell population. Consistently, the expression of CSC-related genes, *DPPA4*, *ESRRB* and *TCL1A*, and β-catenin target genes, *BCL2L2* and *COX2* were significantly suppressed with Pao and Rau treatment. The tumorigenicity was also inhibited by Pao and Rau in subcutaneous pancreatic cancer xenograft mouse models. Pao and Rau demonstrated potent anti-pancreatic CSC effect *in vitro* and *in vivo* and are worth further investigation. (Chapter 4 and Chapter 5)

Next, we investigated the role of an RNA binding protein, HuR, in pancreatic cancer EMT and CSCs. Our data showed that knockdown of HuR in pancreatic cancer cells significantly inhibited cell migration, invasion, and stem-like features. Consistently, knockdown of HuR led to the inhibition of EMT by upregulating epithelium marker Claudin-1 and downregulating mesenchymal marker Vimentin and Snail. Restoration of HuR in HuR deleted (KO) pancreatic cancer cells enhanced migration and enriched CSC population. RNP-IP assay and dual-luciferase reporter assay identified that *SNAI1* mRNA directly bound to HuR through an AU-rich elements (AREs) dependent way. The data demonstrated that inhibition of HuR destabilized *SNAI1* mRNA, and subsequently reduced Snail protein levels, resulting in the EMT and CSCs inhibition in pancreatic cancer cells. (Chapter 6)

We then developed a small molecule inhibitor of HuR, KH-3, and evaluated the activities of KH-3 on pancreatic cancer EMT and CSCs. Our data showed that KH-3 directly bound to HuR and interfered the binding of HuR with its target mRNAs. As an HuR/mRNA disruptor, KH-3 treatment successfully mimicked the effects of HuR knockdown in pancreatic cancer cell lines:

KH-3 significantly inhibited pancreatic cancer cell migration, invasion, tumor sphere formation and EMT. In an orthotopic pancreatic cancer mouse model, KH-3 significantly inhibited tumor growth and metastasis. Importantly, loss of target analyses showed that KH-3 exerted its anti-pancreatic cancer effect in an HuR dependent way *in vitro* and *in vivo*. In conclusion, KH-3 serves as a potent and specific HuR/mRNA disruptor and inhibits pancreatic cancer EMT and CSCs *in vitro* and *in vivo*. As the first of its class, KH-3 can serve as a drug-lead for developing agents that comprehensively inhibit pancreatic cancer growth, metastasis, and treatment resistance. (Chapter 7)

Overall, studies in this dissertation resulted in the identification of three novel EMT and CSC inhibitors, which can be further investigated in pre-clinical and clinical studies for their anti-tumor efficacy. These three EMT and CSC inhibitors each have their own merits and shortcomings. Natural plant extracts, Pao and Rau, have potent anti-pancreatic CSC activities with limited toxicity, thus hold the potential to combine with conventional chemotherapy agents. However, as compounds mixtures, Pao and Rau need future purification and isolation for clinical applications. The compound KH-3 was identified as a novel HuR inhibitor and provided a novel drug-lead for pancreatic cancer management. More studies on the pharmacokinetics, pharmacodynamics, and the combination of KH-3 with conventional chemotherapeutic agents are worth investigation. We hope that the work we have accomplished in this dissertation could add to our knowledge of a new mechanism on EMT and CSC regulation and contribute towards discovery of new drugs for pancreatic cancer.

Acknowledgement

First, and most of all, I would like to express my gratitude to my mentor Dr. Qi Chen for accepting me as her student and allowing me to pursue my PhD research work. I am very grateful for her guidance, continuous support and encouragement.

I would like to thank my committee members, Dr. Dan A. Dixon, Dr. Bruno Hagenbuch, Dr. Wen-Xing Ding and Dr. Udayan Apte for their support and guidance. I also would like to thank my previous committee member Dr. Luciano DiTacchio, for his advice and support during my PhD program. I especially thank my mentor Dr. Qi Chen and all my committee members for their help in writing this dissertation.

I would like to thank our collaborator Dr. Liang Xu and his post-doctoral fellow Dr. Xiaoqing (Sarah) Wu at the University of Kansas for providing the compound KH-3, and MIA PaCa2 HuR KO cells for my research work, and to thank them for their support and help.

I would like to thank Dr. Jeanne Drisko and Jean Sunega at the University of Kansas Medical Center for their support with my research project.

I would like to thank Dr. Dan Dixon at the University of Kansas Medical Center for providing HuR plasmid for my dissertation research work.

I would also like to thank Dr. Shrikant Anant at the University of Kansas Medical Center for providing HPNE cells for my research work.

I would like to thank Dr. Sitta Sittampalam at the National Center for Advancing Translational Sciences, NIH for providing MRC-5 cells for my research work.

I would like to thank Richard Hastings at the flow cytometry core laboratory of KUMC for training and helping me with flow cytometry technology.

I would like to thank the current members in Dr. Qi Chen's lab, Tao (Dylan) Wang and Ping Chen, and former members, Kishore Polireddy, Yan Ma, Yu Jun, Ying Zhang, Enlong Ma, and Iman Joker. This dissertation could not have been accomplished without your support.

I would also like to thank all the faculties and staffs of the Department of Pharmacology, Toxicology and Therapeutics for their help and encouragement.

I would like to express my deepest gratitude to my dear parents, my wife, and my daughter for their endless support.

I would also like to thank all my friends, whose direct or indirect help me during my PhD program.

Grant support in this dissertation: The work in chapter 4 and chapter 5 was supported by a research grant provided by the Beljanski Foundation. The Beljanski Foundation had no influence on the design, performance, data collection, data analysis or manuscript preparation of the study.

The work in chapter 6 and chapter 7 was supported by the National Institutes of Health grant R21 CA198265 (to Dr. Qi Chen) and in part by R01 CA191785 (to Dr. Liang Xu and Dr. Jeffrey Aubé).

Conflicts of interest: The author declare that there is no conflict of interest in relating to this dissertation.

Table of Contents

List of Figures

List of Tables

Chapter 1. Introduction

1.1. Pancreatic cancer

Pancreatic cancer is the 4th leading cause of cancer-related death in the United States and is expected to be the second by 2030 [1]. The latest estimation from American Cancer Society demonstrated that 56,770 people (men=29,940, women=26,830) will be diagnosed with pancreatic cancer in 2020 and 45,750 (men=23,800, women=21,950) will die from it [2]. Currently, there are no efficient early detection methods for pancreatic cancer since most early stage patients do not have specific or recognizable symptoms. For the small percentage of patients (about 9%) diagnosed with local disease, the 5-year survival is only 26%. For about 53% of the patients diagnosed at an advanced stage, the 5-year survival is only 2%, which is the lowest among all types and stages of malignancies [2].

1.1.1. Histology of pancreatic cancer

The pancreas is an organ of both digestive (exocrine) and endocrine functions in vertebrates. The exocrine pancreas comprises more than 95% of the pancreatic mass and consists of acinar cells, ductal epithelium cells, and associated connective tissues, vessels, and nerves. As an exocrine organ, the acinar cells in the pancreas secrete pancreatic juice, which contains a variety of digestive enzymes, into the duodenum through the pancreatic duct. As an endocrine gland, the pancreas secretes a variety of hormones, including glucagon, insulin, and somatostatin, into the blood vessel. The islets of Langerhans are the functional units of the endocrine pancreas, which are consisted of alpha cells, beta cells, delta cells, epsilon cells, and PP cells. Thus, pancreatic cancer, theoretically, may refer to neoplasms originated from any of the cells of the pancreas.

Among all the neoplasms originated from the pancreas, pancreatic ductal adenocarcinoma (PDAC) is the most common type (> 90%), and thus the term "pancreatic cancer" usually refers

to this type only [3]. PDAC can arise in any location in the pancreas, though it is most often (60%-70%) found in the head of the pancreas [4]. Three types of precursor lesions are associated with PDAC: pancreatic intraepithelial neoplasia (PanIN), intraductal papillary mucinous neoplasm (IPMN), and mucinous cystic neoplasm (MCN) [5]. (**Fig. 1.1**)

As the most well studied pancreatic cancer precursor, PanIN can be graded into four stages, PanIN-1A, PanIN-1B, PanIN-2, and PanIN-3, based on the histological and cytological atypia. PanIN-1A is characterized by tall columnar cells with basally located nuclei and abundant supranuclear mucin. The nuclei shape is usually slightly atypia. The epithelial lesions of PanIN-1B are similar to PanIN-1A and are usually in a papillary, micropapillary, or basally pseudostratified structure. PanIN-2 is characterized by flat or papillary mucinous epithelial lesions with nuclear abnormalities, such as loss of polarity, nuclear crowding, and enlarged nuclei. PanIN-3 is characterized by papillary or micropapillary lesions, true cribriforming luminal necrosis, and cytologic abnormalities. Histologically, PanIN-3 can be diagnosed with the budding off of small clusters of epithelial cells into the lumen and luminal necrosis. Cytologically, PanIN-3 lesions are usually characterized by a loss of nuclear polarity and dystrophic goblet cells, which have lumen-oriented nuclei and basement membrane-oriented mucinous cytoplasm [6-8]. (**Figure 1.1**)

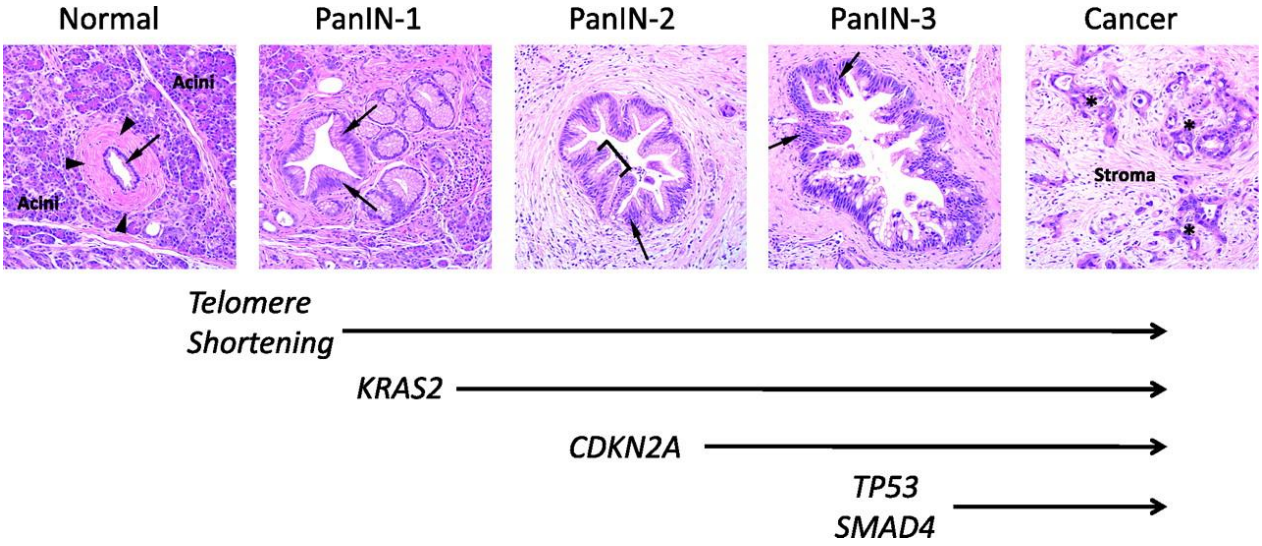

Figure 1.1 Morphological and genetic progression model of pancreatic carcinogenesis [8]. Histology images demonstrate normal pancreatic ducts and three grades of PanINs: PanIN-1, 2, and 3, which eventually develop to PDAC. Early genetic alterations, such as *KRAS* mutations and *CDKN2A* loss, and late genetic alterations, such as *TP53* loss and *SMAD4* loss, are represented at the bottom.

Reprinted with permission from Iacobuzio-Donahue, C.A., Genetic evolution of pancreatic cancer: lessons learnt from the pancreatic cancer genome sequencing project. Gut, 2012. **61**(7): p. 1085-94.

IPMN and MCN are less common precursor lesions. IPMNs are neoplasms that initiate within the pancreatic ducts characterized by the production of mucin and papillary proliferation of ductal epithelium [9]. Although IPMNs usually have a favorable prognosis, some IPMNs can transform from benign tumors to malignant tumors. Based on the histological characteristics, IPMNs can be classified into four types: intestinal type (villous dark cell type), gastric type (papillary clear cell type), pancreatobiliary type, and oncocytic type (compact cell type) [9]. Those four types of IPMNs have critical prognostic significance due to their abilities to develop into carcinomas. Studies have shown that the development of carcinomas derived from IPMNs is rarely found in gastric type, but frequently found in intestinal type, whereas the oncocytic type and pancreatobiliary type will commonly develop into malignancies.

MCNs are rare precursor lesions and are developed exclusively (>95%) in women [10]. The lesions are usually located in the distal pancreas, and it can also occur in the liver and gallbladder [11]. In MCNs, mucin-producing cysts are surrounded by ovarian-like stroma. The unique ectopic ovarian-like stroma is thought to be seeded from primordial ovarian cells at an early stage of embryonic development [12]. According to the WHO criteria, MCNs are classified as MCNs with low grade dysplasia (adenoma), moderate dysplasia (borderline neoplasm), high grade dysplasia (carcinoma *in situ*), and invasive carcinoma [13-15]. MCNs usually have a favorable prognosis, unless developing into invasive tumors (~16%). The 5-year disease-specific survival for noninvasive MCNs was 100%, and for those with invasive cancer, 26% [13]. (**Fig. 1.2**)

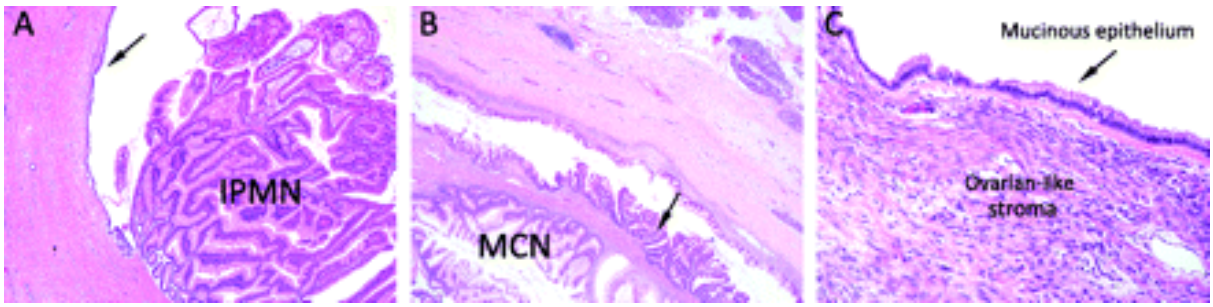

Figure 1.2 Cystic precursors of pancreatic cancer [8]. (A) Low power view of an IPMN. (B) Low power view of an MCN. (C) Higher power view of the MCN shown in (B). The ovarian-like stroma underlies the mucinous epithelium was demonstrated.

Reprinted with permission from Iacobuzio-Donahue, C.A., Genetic evolution of pancreatic cancer: lessons learnt from the pancreatic cancer genome sequencing project. Gut, 2012. **61**(7): p. 1085-94.

1.1.2. Molecular characteristic of pancreatic cancer

Studies in the past three decades have identified a broad spectrum of genetic variations that are involved in pancreatic cancer tumorigenesis, progression, invasion, and metastasis. Here, we focus on the gene mutations that are most commonly found in driving PDAC tumorigenesis, including mutations in *KRAS*, *p16/CDKN2A*, *TP53*, and *SMAD4*.

The *KRAS* proto-oncogene

KRAS mutations are found in nearly all PDAC patients, and thus PDAC is thought to be the most *RAS*-addicted cancer [16]. The *KRAS* gene encodes a 21.6 kDa membrane-localized GTPase transforming protein KRAS. *KRAS* gene was first identified as an oncogene in Kirsten Rat Sarcoma virus in 1982 [17]. The *KRAS* gene belongs to the *RAS* gene family. The *RAS* gene family includes *HRAS*, *KRAS* and *NRAS*. In mammalian cells, *KRAS* gene encodes two protein variants, KRAS4A and KRAS4B [18]. As the other RAS proteins, KRAS protein comprises two domains: the guanosine nucleotides binding G domain, which contains five conserved G1-G5 motifs that directly bind to GDP/GTP, and a C-terminal membrane targeting region, which determines the cell membrane anchoring and regulates post-translational modification [19].

KRAS protein is a GTPase and serves as a binary ON-OFF molecular switch in regulating a variety of cellular pathways involved in cell proliferation, differentiation, and survival. KRAS protein is continuously cycling between its active guanosine triphosphate (GTP)-bound state (ON) and its inactive guanosine diphosphate (GDP)-bound state (OFF). As an essential molecular switch, the KRAS ON-OFF switching is tightly controlled by GTPase-activating proteins (GAPs) and guanine nucleotide exchange factors (GEFs) [19]. GAPs activate intrinsic GTPase activity of RAS protein to hydrolyze GTP into GDP, and GEFs aid in the exchange of

GDP for GTP [20, 21]. In normal cells, KRAS is predominantly in the GDP-bound inactive form. Multiple extracellular stimulations, such as growth factors and cytokines, can activate KRAS into the KRAS-GTP bound form. On the other hand, mutations in *KRAS* gene lead to the production of constitutively activated KRAS protein. Genetic studies revealed that missense mutations that encode single amino acid primarily happened at codon 12 and codon 13 [22, 23]. These mutations lead to KRAS protein locked in GTP-bound form and constitutively active, resulting in overstimulation of downstream signaling pathways to drive cancer progression.

KRAS mutation was widely found in pancreatic cancer (90%), colon cancer (50%) and lung cancer (~30%), which are the three major types of cancer lead to the cancer-related death in the U.S. [24-26]. *KRAS* mutation serves as an initiating genetic event for PDAC, followed by several other genetic mutations to drive the transformation from normal pancreatic tissue to PDAC [27, 28]. During the transformation progress from pancreatic ductal epithelium to PanIN lesions, *KRAS* mutation frequency was more than 90% [29]. The activation of KRAS engages in various downstream effector pathways, which are characterized by a RAS association (RA) domain or RAS-binding domain (RBD), including the RACGEF-RAC1 Small GTPase Effector signaling network, the RALGEF-RAL small GTPase effector signaling network, the PI3K/AKT/mTOR effector signaling network, and the RAF-MEK-ERK singling network. For example, active KRAS interacts with the RAF serine threonine kinases, ARAF, BRAF, and CRAF/RAF1, which are the three most significant effectors in KRAS signaling axis. The activation of RAF kinases initiates a cascade of phosphorylation events, resulting in the phosphorylation and activation of MEK1/2 serine/tyrosine/threonine kinases and ERK1/2 serine/threonine kinases. Activated MEK1/2 and ERK1/2 then phosphorylate several cytoplasmic and nuclear substrates, many of which are transcription factors that regulate the expression of genes involved in cell survival

signaling, e.g. MYC, which is required for the maintenance of RAS-driven tumors [30-32]. The RAS-RAF-MEK-ERK signaling cascade is a crucial effector in the initiation and maintenance of KRAS-driven tumors. In a mouse model, genetic deficiency in MEK1/2 or ERK1/2 blocked non-small cell lung cancer (NSCLC) progression driven by $Kras^{G12D}$ mutation [33]. An ERK inhibitor, SCH772984, significantly inhibited tumor growth in *KRAS*-mutant pancreatic cancer patient-derived xenograft (PDX) mouse, in association with MYC suppression [34].

The PI3K-AKT-mTOR signaling network also drives oncogenesis in *KRAS* mutated cells [35]. Activated KRAS binds to the RAS-binding domain (RBD) of the p110 subunit of PI3K. The binding phosphorylates phosphotidylinositol-4,5-bisphosphate (PIP2), resulting in the formation of plasma membrane-associated phosphotidylinositol-3,4,5-bisphosphate (PIP3). PIP3 then activates a variety of downstream proteins, including PDK1 and AKT [36]. The activated AKT phosphorylates many other proteins that can further promote cell growth. Therefore, the inhibition of PI3K signaling suppresses KRAS-driven oncogenesis in pancreatic cancer. For example, the pancreas-specific disruption of *PI3K p110α* gene prevented the transformation and development of PDAC in $Kras^{G12D/+}$, $Ptf1a^{Cre/+}$ mice [37].

Although *KRAS* mutations is the predominant mutation in pancreatic cancer, the *KRAS* mutation alone is not sufficient to drive the progression from PanIN to PDAC. *Pdx1-Cre*; *LSL-*$Kras^{G12D}$ mice developed PanIN by 26 weeks but did not progressed into metastatic tumors [38]. Several other genetic mutations are required in PDAC progression.

The *P16/CDKN2A* tumor suppressor gene

The *P16* gene, also known as cyclin-dependent kinase Inhibitor 2A (*CDKN2A)*, is a tumor suppressor gene located on chromosome 9p21 [39]. By binding to cyclin-dependent kinase 4

(CDK4), the p16 protein inhibits phosphorylation of various growth factors and regulatory factors in the G1 phase of the cell cycle. *P16* is one of the most frequently mutated and inactivated tumor suppressor genes in all types of cancer, especially in pancreatic cancer. The mutation frequency in sporadic pancreatic cancer is about 95% [24, 25, 40]. *P16* gene inactivation happens with different types of mutation, such as the loss of heterozygosity, homozygous deletion, or promoter silencing. It has been shown that loss of function in *P16/CDKN2A* cooperates with activation in *KRAS* to drive the PanIN transformation and PDAC progression. The $p16^{-/-}$; *LSL- Kras*^{G12D}; *Pdx1-Cre* mice and $p16^{flox/flox}$; *LSL- Kras*^{G12D}; *Pdx1-Cre* mice developed PDAC and had significantly reduced median survival (15.5± 3.8 weeks, n=36, and 25.5± 8.9 weeks, n=16, respectively) compared with $p16^{+/+}$; *LSL- Kras*^{G12D}; *Pdx1-Cre* mice, which has significantly longer median survival (~15 months) [41]. Moreover, re-expression of p16 in MIA PaCA-2 cells significantly reduced the primary xenograft growth, angiogenesis, and lymphatic metastasis in an orthotopic mouse model [42]. Clinical studies have found that the loss of *P16* expression in PDAC patients was highly correlated with lymph node metastasis (p=0.040) and advanced stages (p=0.015) [43].

The *TP53* tumor suppressor gene

The *TP53* gene is one of the most frequently mutated genes in all types of cancer and is mutated in ~75% of pancreatic cancers [24, 28]. As a tumor suppressor protein, p53 transcriptionally activates target genes, e.g. p21, in response to cellular stress and thus induces apoptosis or cell growth arrest. The mutation of *TP53* frequently results in the expression of $p53^{R175H}$ protein, rather than loss of protein expression [44]. *TP53* mutation usually appears in the later stage of PanINs that have already acquired significant features of dysplasia. Given that most $Kras^{G12D}$-expressing pancreatic cells are selectively lost from the pancreas, the mutation of KRAS alone is

not sufficient to drive PDAC transformation. The loss or mutation of *TP53* allows the retention of $Kras^{G12D}$-expressing cells and thus drives the PDAC progression. PDAC formation was compared between two lines of transgenic mouse models. The *Pdx1-Cre-GFP, LSL-*$Kras^{G12D/+}$, *LSL-*$Trp53^{R172P/+}$ ($KP^{p21}C$) mice have mutant *KRAS* and mutant *TP53* but still induce p21 and cell cycle arrest. The *Pdx1-Cre-GFP, LSL-*$Kras^{G12D/+}$, *LSL-*$Trp53^{R172H/+}$ (KPC) mice have *KRAS* mutation and a complete loss of function of *TP53*. Data showed that the $KP^{p21}C$ mice did not form PDAC (0/9), and the KPC mice had PDAC (7/9) (P = 0.01). The *Pdx1-Cre-GFP, LSL-*$Kras^{G12D/+}$, *LSL-*$Trp53^{loxP/+}$ ($KP^{fl}C$) mice, which had *KRAS* mutation and heterozygous loss of *TP53*, was also used to compare with the KPC mice. The $KP^{fl}C$ mice formed PDAC but did not form liver metastatic lesions (0%), whereas 65% of the KPC mice had liver metastasis (P<0.001) [44]. These results indicated that the loss function of *TP53* in *P21* activation, combined with mutant KRAS drives PDAC transformation, progression, and metastasis.

The *SMAD4* tumor suppressor gene

SMAD4, also known as MADH4 (Mothers against decapentaplegic homolog 4,) or DPC4 (deleted in pancreatic cancer-4), is a tumor suppressor protein encoded by *SMAD4* gene. SMAD4 exerts its tumor suppressor function by acting as a transcriptional factor, in association with SMAD2/SMAD3. The heterotrimeric SMAD2/SMAD3-SMAD4 complex is translocated into the nucleus in response to the activation of TGF-β signaling pathways, resulting in the activation of genes involved in cell growth inhibition, such as *P21* and *P27* [45, 46]. The loss or inactivation of *SMAD4* occurs in ~50% of pancreatic cancers and is associated with poor prognosis [47]. However, *Pdx1-Cre,* $Smad4^{lox/lox}$ mice is not able to initiate PanIN or PDAC, indicating that *SMAD4* loss alone is not sufficient for the transformation. Activation of KRAS is required, as the *Pdx1-Cre,* $Kras^{G12D/+}$, $Smad4^{lox/lox}$ mice showed significantly accelerated

progression of PanIN and PDAC [48, 49]. *SMAD4* loss has also been shown to associate with the metastasis of KRAS-driven PDAC [50, 51]. A study in 89 PDAC patients demonstrated that *SMAD4* mutations were significantly associated with poor overall survival (11.5 months vs. 14.2 months, $p = 0.006$) [47].

1.1.3. The clinical management of pancreatic cancer

Diagnosis and staging

Early and precise detection and diagnosis are critical challenges for pancreatic cancer management. Usually, the tests and procedures to detect, diagnose, and stage pancreatic cancer are done at the same time. The general tests and procedures include physical examination, medical history, blood chemistry, CA 19-9 Radioimmunoassay (RIA), medical imaging-related technics (CT scan, PET scan, Ultrasound, and MRI), and biopsy [52, 53]. Unfortunately, pancreatic cancer may not cause noticeable signs or symptoms in the early stages. While presenting, the signs or symptoms are not specific, which include jaundice, pain in the upper or middle abdomen and back, loss of appetite, feeling tired, and weight loss for unknown reasons. These signs and symptoms are highly like the signs and symptoms of many other illnesses, for example, liver illness and gallbladder illness. Thus, pancreatic cancer is tough to be detected and diagnosed at early stages. Most pancreatic cancer patients are diagnosed as advanced stages with limited treatment options and unsatisfied prognosis.

Pancreatic cancer can be categorized into five stages (stage 0-IV) based on tumor size, lymphatic invasion, and/or distant metastasis. Stage 0 pancreatic cancer (carcinoma *in situ*) is the stage that only abnormal cells, rather than solid tumors, can be found in the pancreas. In stage I pancreatic

cancer, the solid tumor is formed but limited in the pancreas. Base on the size of the tumor, stage I pancreatic cancer can be further divided into stage IA (tumor size < 2 cm) and stage IB (2 cm<tumor size <4 cm). When tumor size is larger than 4 cm, it is classified as stage II, with stage IIA does not have lymphatic invasion. In stage IIB and above, the tumor starts to demonstrate invasiveness and aggressiveness to local lymph nodes and distant organs. The major criterion for stage IIB pancreatic cancer is that the tumor invades into one to three adjacent lymph nodes. Stage III and stage IV pancreatic cancer are characterized by either more than four adjacent lymph nodes invasion or major adjacent blood vessels invasion (Stage III), or distant organ metastasis (Stage IV).

Treatment – surgery and radiotherapy

The treatment options and the prognosis for pancreatic cancer are dependent on the stages. Surgical removal is the only curative therapy but is only for ~10 % of patients with a respectable tumor, typically Stage I and Stage II. Whipple procedure (pancreaticoduodenectomy) is the most common surgical procedure when the tumor is limited to the head of the pancreas, which is commonly found in PDAC patients (60–70%) [54]. This procedure removes the head of the pancreas containing the solid tumor, along with the gallbladder, part of the intestine, part of the stomach, and bile duct. The remaining body and tail of the pancreas will be left to exert the physiological digestive and endocrine function of the pancreas. Distal pancreatectomy and total pancreatectomy are operations for tumor in the tail of the pancreas. However, these surgeries are less common due to the increased risk of infection and severe side effects [55-57]. When pancreatic cancer is progressed into invasive and metastatic stages (Stage III and IV), a surgical removal could be considered as a palliative operation to relieve the symptoms of the patients.

Considering the aggressiveness of pancreatic cancer, patients with all stages usually need additional chemotherapy and radiation therapy to achieve a favorable prognosis.

The role of radiation therapy (RT) in the adjuvant settings for locally advanced resectable pancreatic cancer is controversial. Early trials did not suggest a role of adjuvant RT in pancreatic cancer, until in 1985, the Gastrointestinal Tumor Study Group (GITSG) conducted a trial that laid the foundation of chemoradiation therapy (CRT) for pancreatic cancer in the United States [58]. In this trial, 43 patients underwent curative resection of PDAC without evidence of intraperitoneal diseases were enrolled. The radiotherapy was administered in a split-course way, with a total dose of 40 Gy and a 2-week treatment break. Fluorouracil (5-FU) was administrated as the chemotherapy agent during the first 3 days of each RT course, followed by a weekly administration for 2 years or until tumor recurrence was noted. The survival benefits were observed in CRT patients: the median disease-free survival (DFS) was 11 months in CRT patients, compared with the 9 months DFS of surgery-alone patients; the median survival (MS) was 20 months in CRT patients, compared with 11 months of surgery-alone patients. The GITSG trial demonstrated a benefit of CRT in adjuvant settings, which then became standard adjuvant therapy of pancreatic cancer, particularly in the United States. In 1998, the European Organization for Research and Treatment of Cancer (EORTC) conducted another trial involving 218 PDAC patients [59]. RT was delivered in a similar way as in the GITSG trial, while the chemotherapy (CT) was administrated only during the RT. Long-term follow-up demonstrated no significance in 5-year overall survival (OS) with CRT (25% (CRT) vs. 22% (surgery alone)) and 10-year OS with CRT (17% (CRT) vs. 18% (surgery alone)) [60]. Another trail, which involved 289 PDAC patients, was designed by European Study Group for Pancreatic Cancer (ESPAC) in 2004, also showed that CRT did not have survival benefits with a 5-year survival

rate of 10%, compared with a 5-year survival rate of 20% in patients who did not receive CRT [61]. Thus, there are still debates on the effect of RT as an adjuvant setting in pancreatic cancer treatment. More recent trials reported that neoadjuvant CRT might have the potential to improve survival in early stage pancreatic cancer patients. In the phase-III PREOPANC-1 trial by the Dutch Pancreatic Cancer Group, 246 resectable or borderline-resectable pancreatic cancer patients were involved [62]. The preoperative neoadjuvant CRT regimen consisted of 15 fractions of radiation at 2.4 Gy in addition with gemcitabine. Both neoadjuvant CRT arm and control arm were followed by a cycle of adjuvant gemcitabine treatment. The results demonstrated that the neoadjuvant CRT patients have longer overall survival (17.1 months vs. 13.5, p=0.047), compared with the non-neoadjuvant resection patients [63].

Treatment - chemotherapy

Chemotherapy was commonly used as an adjuvant or neoadjuvant regimen in both resectable and unresectable pancreatic cancer patients. Gemcitabine, 5-fluorouracil (5-FU), oxaliplatin, albumin-bound paclitaxel, cisplatin, and irinotecan are widely used in pancreatic cancer chemotherapy, with gemcitabine the most commonly used. Gemcitabine (2', 2'-difluoro-2'-Deoxycytidine; dFdC) was patented in 1983 and was approved for medical use in 1995 [64], Since then, gemcitabine has been applied to various carcinomas, including pancreatic cancer, lung cancer, breast cancer, and ovarian cancer [29, 65-67]. Gemcitabine is transported into cells via a variety of transporters, such as SLC29A1, SLC28A1, and SLC28A3 [68]. The cytoplasmic gemcitabine is phosphorylated by deoxycytidine kinase (DCK) to gemcitabine triphosphate (2',2'-difluorodeoxycytidine 5'-triphosphate; dFdCTP), which is the pharmacological active form. The structural similarity of dFdCTP to deoxycytidine triphosphate (dCTP) makes gemcitabine to act as a nucleoside analog [69]. The incorporation of gemcitabine into the DNA leads to the

masked chain termination in DNA prolongation, thus inhibits DNA synthesis. Gemcitabine also inhibits ribonucleotide reductase (RNR). The metabolite gemcitabine diphosphate (2',2'-difluorodeoxycytidine 5'-diphosphate; dFdCDP) inhibits RNR and depletes the dCTP pool for DNA synthesis, resulting in cell death [70].

Randomized clinical trials proved that gemcitabine increased the overall survival of pancreatic cancer patients. A phase II trial in 1994 demonstrated that partial response was observed in five of the enrolled patients (11% of total), with a median duration of 13 months and improved performance status [71]. In 1997, 126 advanced, unresectable stage pancreatic cancer patients were enrolled in a randomized trial to evaluate the effectiveness of gemcitabine versus 5-FU [72]. This study showed that patients with gemcitabine treatment experience better clinical benefits, including less analgesic consumption and pain intensity and better Karnofsky performance status, comparted with 5-FU treated patients (23.8 % vs. 4.8%). The median survival and 1-year survival rate in gemcitabine-treated patients were also improved compared with 5-FU treated patients (5.65 months vs. 4.41 months; and 18% vs. 2%, respectively). Despite the low response rate (approximate 10%) and multiple side effects, gemcitabine has been used as the first-line chemotherapeutic agent for pancreatic cancer in the past two decades. Besides the benefit gained in advanced stage patients, gemcitabine was also shown to improve the overall survival in pancreatic cancer patients with surgically resectable diseases, especially in neoadjuvant settings [73-75]. As the Charite Onkologie (CONKO) trial demonstrated, the median survival of patients with surgery and adjuvant gemcitabine treatment improved to 22.8 months, compared with 20.2 months in the observation patients who did not receive specific anticancer treatment [76]. The 5-year survival also improved to 21% with gemcitabine adjuvant therapy, compared to 9% without.

Nab-paclitaxel, also known as nanoparticle albumin-bound paclitaxel or Abraxane®, is recently approved as a first-line chemotherapeutic agent for pancreatic cancer. Paclitaxel exerts its effect as a microtubule disruptor, leading to the defects in mitotic spindle assembly and cell division [77]. Paclitaxel was first evaluated in a phase II clinical trial to treat unresectable and metastatic PDAC as a single agent in 1997 [78]. However, only minimal activity was observed in patients, with an 8% response rate, a 5 months median survival and a moderate toxicity. The major limitation of paclitaxel is its low water solubility (~0.4 μg/mL); thus, it is usually formulated in polyoxyethylated castor oil (Cremophor EL) and dehydrated ethanol (50/50, v/v) [79]. However, Cremophor EL has serious side effects, which limit its usage in pancreatic cancer patients [80]. Despite many positive *in vitro* and *in vivo* data, early clinical studies did not show benefit of paclitaxel in treating pancreatic cancer. Advanced stage PDAC patients hardly responded to paclitaxel treatment as a single agent or had limited response rate (~10%) to the combination of paclitaxel with other chemotherapy agents, including 5-FU, bryostatin, and granulocyte colony-stimulating factor (G-CSF), with limited improvement of median survival (~6 month) [78, 81-86]. The nano-delivered system was applied to improve solubility with generally low toxicity. In 2005, the FDA approved nab-paclitaxel for the treatment of metastatic breast cancer [87]. Clinical studies demonstrated that advanced PDAC patients had an improved response to nab-paclitaxel (~32%), with a median survival of 7.3 months [88]. The combination of nab-paclitaxel and gemcitabine also showed favorable effects on advanced PDAC patients in a large-scale phase III trial involved in 842 patients, with a response rate of ~23% and a median survival of ~8.5 months, compare with gemcitabine alone treatment patients [89, 90]. Now, nab-paclitaxel has been considered as a first-line chemotherapeutic agent in PDAC patients when combined with gemcitabine. The effect of nab-paclitaxel in PDAC is still under investigation. More than

100 clinical studies are undergoing to evaluating nab-paclitaxel in PDAC patients in combination with more than 50 novel agents (www.clinicatrials.gov).

Other chemotherapeutic agents used in treatment of pancreatic cancer include fluorouracil (5-FU), cisplatin, and irinotecan. 5-FU has a long history as a chemotherapeutic agent against varieties of carcinomas [91]. As a pyrimidine analog and a pro-drug, the metabolites of 5-FU can induce cell death in rapidly dividing cells by either inhibiting the thymidylate synthase or incorporating into DNAs and RNAs, resulting in the termination of DNA and RNA synthesis. 5-FU and other fluoropyrimidines-based drugs, such as capecitabine and tegafur, have been widely used in pancreatic cancer chemotherapy [92]. Cisplatin and irinotecan are other conventional chemotherapy drugs that are used to improve the survival of pancreatic cancer patients by acting as a DNA adducting/damaging agent and a topoisomerase inhibitor, respectively.

As mono-regimen chemotherapy has only limited benefits on the overall survival of pancreatic cancer patients, combination chemotherapy is sought. Theoretically, combination chemotherapy can reduce the chance of drug resistance and can target multiple therapeutic targets to achieve synergistic effects. For these purposes, numerous efforts had been made to develop gemcitabine-based combination therapy in pancreatic cancer management. Except for the recent success in nab-paclitaxel, most of the efforts had failed. Randomized controlled clinical trials in the past two decades showed modest improvements in the overall survival with additional toxicity by combining other agents to gemcitabine [93-100]. However, success was achieved with a non-gemcitabine regimen, FOLFIRINOX, which is a combination of oxaliplatin, irinotecan, fluorouracil, and folinic acid. A randomized controlled clinical trial demonstrated that the overall responses, median overall survival and 1-year survival in FOLFIRINOX treated patients were significantly improved, compared with gemcitabine treated patients (54/171 vs. 16/171; 11.1

months vs. 6.8 months; 48.4% vs. 20.6%; respectively) [101]. However, the incidence of grade 3 and grade 4 adverse effects was significantly increased, including neutropenia, thrombocytopenia, anemia, diarrhea, and sensory neuropathy, which limited the use of FLOFIRINOX in patients with poor conditions.

Taken together, PDAC is one of the most lethal types among all carcinomas, with various gene mutations and high heterogenicity. Chemotherapy is commonly used as an adjuvant or neoadjuvant setting in both resectable and unresectable pancreatic cancer patients. For many patients with advanced stages of disease, chemotherapy is the only option applicable. However, current chemotherapeutic agents only provide limited benefits to PDAC patients, with low response rate and significant toxicity. The development of better agents for PDAC management is an urgent and unmet need.

1.2. Epithelial – mesenchymal transition (EMT)

1.2.1. Basics of EMT

Epithelial-mesenchymal transition (EMT) is a crucial cellular program involved in both physiological and pathological progress. Based on the context in which EMT occurs, EMT can be categorized into three types [102]. Type I EMT occurs during embryonic development, while type II EMT occurs during tissue regeneration and wound healing, and type III EMT occurs during a variety type of carcinoma progressions.

In the physiological aspect, EMT plays an essential role in embryogenesis, tissue morphogenesis, and wound healing. On the other hand, EMT has been shown to be one of the initial steps for carcinoma cells to overcome original cell adherents and turn into a more metastatic, malignant phenotype. During this reversible cellular process, epithelial cells progressively lose their surface adhesion molecules and cell polarity, and then transform from the epithelium-state cells into the spindle-shaped, mesenchymal morphology, resulting in the increased mobility and invasiveness [102, 103]. (**Fig. 1.3**)

The lateral cell-cell junctions, including tight junctions, adherent junctions, gap junctions, and desmosomes, are the base structures to hold the epithelial cells together. In addition, the cell-basement membrane adhesion and apical-basal polarity of the epithelial cells are maintained by hemidesmosomes. The activation of EMT leads to the downregulation of several specific epithelial molecules, among which E-cadherin is one of the most crucial [104]. E-cadherin is a transmembrane protein, which contains a C-terminal cytoplasmic tail, including a membrane proximal cytoplasmic/conserved domain (MPCD) and a β-catenin binding domain (CBD), a transmembrane region and five N-terminal Ca+ dependent extracellular cadherin repeats (EC1-5). E-cadherin is linked to the cell cytoskeleton by forming the CBD/β-catenin/α-catenin/EPLIN

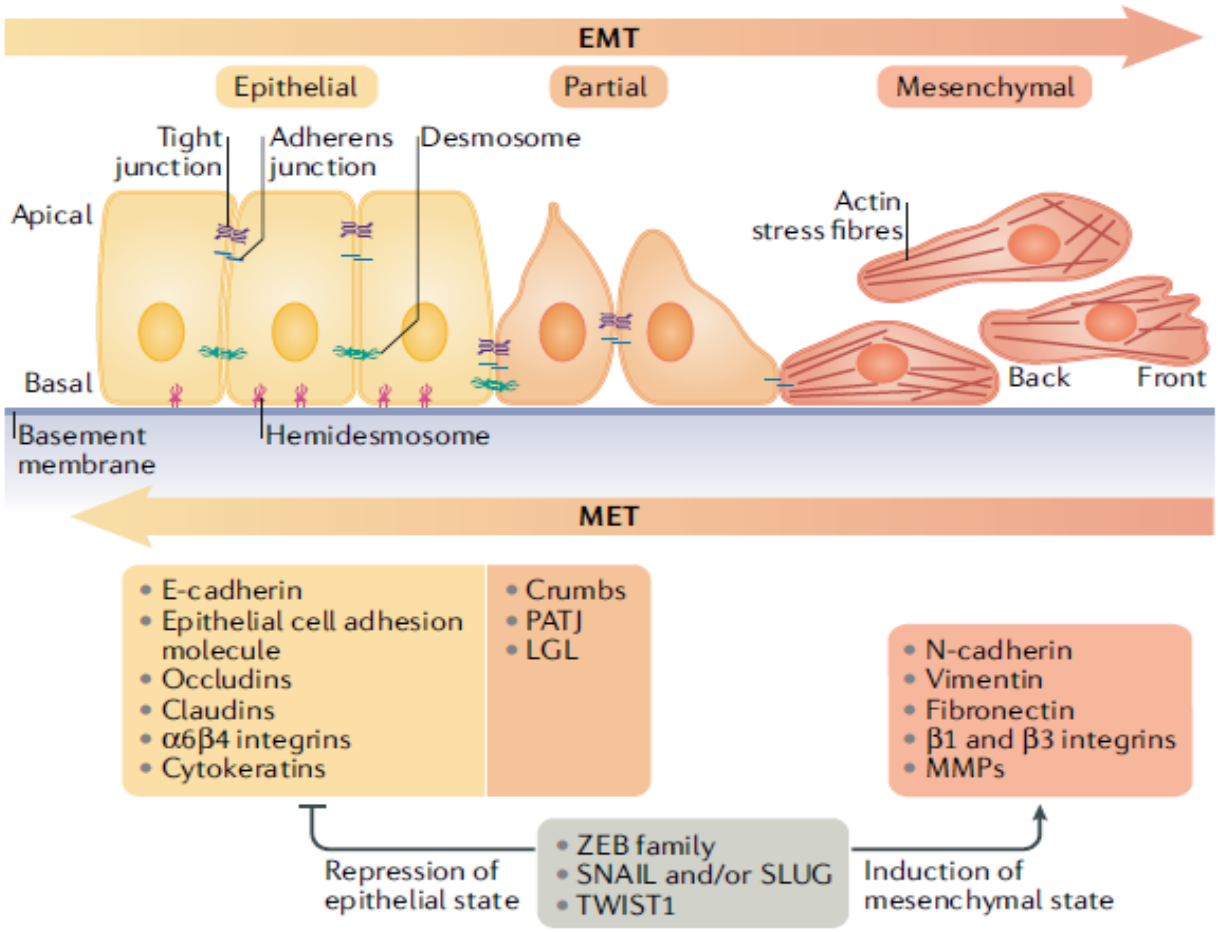

Figure 1.3 Schematic diagram of a typical EMT progress [103]. During EMT progression, epithelial cells lose cell-cell attachment, cell-basal membrane attachment, and transform into a spindle-like mesenchymal phenotype. The expression of several EMT markers are changed, with epithelial markers (yellow) decreased and mesenchymal markers (orange) increased. EMT-related transcriptional factors (gray) regulate the expression of EMT markers. EMT is a reversible process. Mesenchymal – Epithelial transition is the reversed process of EMT.

Reprinted with permission from Dongre, A. and R.A. Weinberg, New insights into the mechanisms of epithelial-mesenchymal transition and implications for cancer. Nat Rev Mol Cell Biol, 2019. 20(2): p. 69-84.

(or vinculin)/F-actin structure. EC1 is the most distal extracellular domain, and have a conserved tryptophan 2 (Trp 2) residue and a conserved HAV tripeptide sequence, which are crucial to form the E-cadherin homodimers in adjacent cells [105, 106]. The E-cadherin homodimers create a firm linkage between the cytoskeleton of adjacent cells. Studies illustrated that loss of E-

cadherin expression played a central role in the process of EMT in cancer cells. In pancreatic cancer, partial or complete loss of E-cadherin was widely observed (~50%) and was associated with advanced stage, lymph node metastasis, and poor prognosis [107-109].

Other adhesion molecules are also required in the cell-cell adhesion in the epithelial cell layer. Claudin family proteins, along with occludin family proteins and junction adhesion molecules (JAM), compose the tight junction, which holds cells together and maintains the cell polarity by acting as a paracellular barrier [110]. Claudins are 20-34 kDa four-time transmembrane proteins, with both C-terminal and N-terminal located in the cytoplasm, and two conserved extracellular loops. The large extracellular loop of Claudin-1 can regulate ion selectivity in paracellular transport [111]. Two highly conserved cysteine residues within the large loop can form a disulfide bond and thus increase the Claudin-1 protein stability. The formation of Claudin dimers between adjacent cell membranes relies on the hydrophobic interactions between two shorter second extracellular loops. The C-terminal end of Claudins contains a PDZ-binding motif, which can interact with several tight junction-associated proteins, such as zonula occludens-1 (ZO-1), and PDZ domain containing proteins, such as MUPP1 [112, 113]. The C-terminal can also be phosphorylated and affect the localization and functions of Claudins.

The role of claudins in cancer is controversial. Studies using patient samples showed that claudins were down-regulated in various cancers. Claudin-1 has been found to be down-regulated in breast cancer, colorectal cancer, and prostate cancer [114-117]. Claudin-7 was reduced in breast cancer, esophagus cancer, and prostate cancer [117-119]. These reports showing loss of claudins in cancers are consistent with the concept that tumorigenesis is accompanied by a disruption of tight junctions, a process that may lead to loss of cohesion, gain of invasiveness, and lack of differentiation in cancer cells. However, other studies also using

patient samples had conflicting findings that claudins were up-regulated in many types of cancer. Claudin-1 was found to be upregulated in breast cancer, colorectal cancer, and gastric cancer [120-124]. Claudin-7 was also found upregulated in breast cancer, gastric cancer, and ovarian cancer [121, 125, 126]. The discrepancy may result from the different patient population, specimen collection, and different detection methods. For example, some studies in colorectal cancer only evaluated membrane stanning of Claudin-1 [122], whereas other studies considered both nuclear and membrane stanning [115, 123]. These controversial data imply that Claudins act more than components of the tight junctions in carcinoma. Indeed, the function of Claudin-1 in carcinoma may rely on its cellular localization and is different in different types of cancer. In colorectal cancer, the nuclear localized Claudin-1 has been reported to be an EMT inducer by either directly inhibiting E-cadherin transcription or activating β-catenin/TCF/LEF-1 signaling pathway, and thus promoted tumor growth and metastasis [123]. In liver cancer, Claudin-1 induced EMT by activating the c-Abl-Ras-Raf-1/ERK1/2 signaling pathway [127]. Paradoxically, several studies demonstrated that Claudin-1 acted as a tumor suppressor in lung cancer and gastric cancer [128, 129]. In pancreatic cancer, current studies suggested that Claudin-1 served as a suppressor in tumor progression and metastasis. Downregulation of Claudin-1 promoted pancreatic cancer cell proliferation by inhibiting the TNF-α induced apoptosis [130, 131].

Several cytoskeleton proteins also contribute to EMT progression. The cytoskeleton is a dynamic structure, which is consisted of actin-based microfilaments, tubulin-based microtubules, and intermediate filaments [132]. The intermediate filaments contain various proteins depending on the cell types. Due to the lack of structural polarity, intermediate filaments function as supporting components in the cytoskeleton, rather than cell motility components. Vimentin is a type III

intermediate filament and the most widely distributed intermediate filament protein in eukaryotic cells. In addition, Vimentin is one of the major cytoskeletal components in mesenchymal cells. Thus, it has been used as a mesenchymal marker in EMT progression [133]. The upregulation of Vimentin was found to be correlated with the malignancy of various types of cancer, including breast cancer, prostate cancer, lung cancer, and pancreatic cancer [134-137]. Studies showed that Vimentin not only acted as an EMT marker, but also contributed to EMT progression in cancer cells. Vimentin has been proved to induce changes in cell shape, motility, and adhesion during EMT [133]. The depletion of Vimentin in breast cancer cells led to reduced cell proliferation and migration by inducing cytoskeleton reorganization [138]. Vimentin was also correlated with Slug mediated EMT progression in colorectal cancer and breast cancer [139, 140].

1.2.2. EMT-inducing transcription factors (EM-TFs) in EMT progression

The initiation and progression of EMT are orchestrated by various transcription factors. Of importance in pancreatic cancer are Snail/Slug, ZEB1/ZEB2, TWIST1/TWIST2, and β-catenin, which are controlled by several EMT related signaling pathways [104] (**Fig. 1.4**).

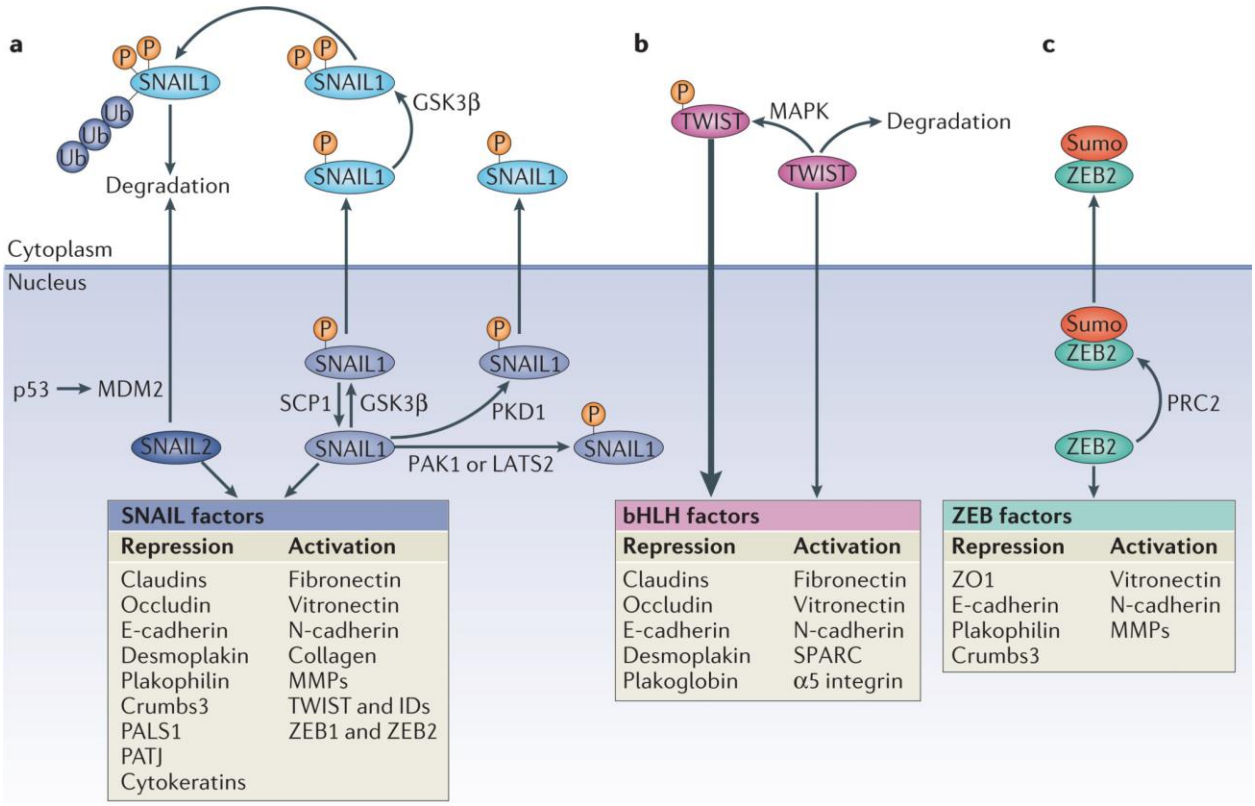

Figure 1.4 The function and regulation of major EMT-TFs, including Snail, Twist, and ZEB2 [104]. Snail, Twist, and ZEB2 were regulated in different mechanisms. As transcriptional factors, the target genes of Snail, TWIST, and ZEB2 were also listed.

Reprinted with permission from Lamouille, S., J. Xu, and R. Derynck, Molecular mechanisms of epithelial-mesenchymal transition. Nat Rev Mol Cell Biol, 2014. 15(3): p. 178-96.

Snail family transcription factors

Zinc finger protein SNAI1 (Snail) is a crucial EMT-TF by repressing the expression of adhesion molecules, such as E-cadherin and Claudins. Snail homologs have been found in many species. There are three Snail family proteins in vertebrates: SNAI1 (Snail), SNAI2 (Slug), and SNAI3 (Smuc) [141]. The Snail family proteins have similar structures. A conserved C-terminal zinc-finger DNA binding domain, which contains four to six Cys2His2 type zinc fingers, can bind to the E-box motif (5′-CANNTG-3′) in promoters of target genes. The N-terminal contains a

conserved SNAG (Snail/Gfi) domain, which interacts with several transcriptional co-repressors and epigenetic remodeling complexes, such as histone decetylas1/2 (HDAC1/2), Sin3A and polycomb repressive complex 2 (PRC2) [142]. The central part of Snail family proteins is responsible for protein degradation, stabilization, and transportation. A serine-rich domain (SRD) located in the central of Snail family protein can be phosphorylated by various kinases, typically glycogen synthase kinase-3β (GSK-3β). The phosphorylation in SRD leads to Snail degradation by β-Transducin repeat-Containing Protein (β-TrCP) [143]. Snail can also be degraded by several ubiquitin ligases, such as FBXL14 [144]. The nuclear export sequence (NES) located in the central of Snail family proteins is responsible for the nuclear export of Snail family proteins by interacting with CRM1 [145].

Snail proteins contain DNA-binding motifs and control target gene expression through epigenetic regulation. The conserved SNAG (Snail/Gfi) domain on the N-terminal of Snails recruits chromatin remodeling factors, resulting in an epigenetic modification on histones. For example, Snail recognizes and binds to the E-box of E-cadherin promoter, and then recruits SIN3A-HDAC1/2 complex to deacetylate histone H3 and histone H4, leading to the suppression of E-cadherin expression [146]. Similarly, with this epigenetic regulation, Snail proteins regulate the expression of several other epithelial-related proteins, including Claudins, Occludins, and ZO-1. Downregulation of these epithelial molecules results in EMT progression. On the other hand, Snail possess an indirect positive regulatory function by interacting with other transcriptional factors. For example, Snail interacted with β-catenin and activated β-catenin/TCF or β-catenin/LEF-1 transcription complexes, resulting in the upregulation of mesenchymal proteins, such as N-cadherin, Vimentin, and Fibronectin [147-149]. Snail and Slug also increased cancer stem cell (CSC) features by enhancing the expression of genes related to stemness [150].

The upregulation of Snail and Slug were widely observed in pancreatic cancer cell lines and tissues. About 78% of pancreatic cancer cases showed a moderate to strong Snail expression, and 50% displayed a positive expression of Slug [151]. Using different criteria, Tao Yin et al. reported that 20 out of 56 (36%) pancreatic cases were identified as Snail positive phenotype [152]. The expression of Snail in pancreatic cancer has a close correlation with lymph node invasion and distant metastasis. The overexpression of Snail in pancreatic cancer cells demonstrated enhanced metastatic and invasive ability in orthotopic xenograft models [152, 153].

Inhibition of Snail leads to inhibition in tumor progression, metastasis, and tumorigenicity in many types of cancer, including breast cancer, lung cancer, colon cancer, and pancreatic cancer [154, 155]. Thus, Snail has the potential to serve as a therapeutic target against carcinomas. A recently developed Snail inhibitor, GN-25, has been reported to reverse the EMT phenotype and EMT markers in *KRAS*-mutated *SNAIL*-transduced human mammary epithelial cells (HMLEs) [156].

As a crucial EMT regulator, the expression of Snail is tightly controlled by various signaling pathways, including the canonical WNT signaling pathway, the TGF-β signaling pathway, and the Notch signaling pathway, which are discussed in **Chapter 1.2.3**.

ZEB family transcription factors (ZEB1/ZEB2)

Zinc finger E-box-binding (ZEB) family transcription factors are characterized by the presence of two zinc finger clusters that account for E-box recognition and DNA binding, and a homeodomain in the central. Similar to Snail family proteins, ZEB family proteins contain various binding domains for its coactivators or corepressors, including a coactivator histone

acetyltransferase p300 (p300) and p300/CBP-associated factor (PCAF) binding domain, a Smad interaction domain, and a C-terminal-binding protein (CtBP) interaction domain [157]. ZEB family proteins recognize the E-box on target DNA through its zinc finger clusters, and then recruit corepressors or coactivators to regulate the expression of target genes. For example, ZEB1 directly binds to the E-box of *CDH1* promoter, and then recruits the CtBP/HDAC transcriptional co-repressors, and/or the switch/sucrose non-fermentable (SWI/SNF) chromatin-remodeling protein BRG1, leading to the inhibition of *CDH1* transcription and decreased expression of E-cadherin [158].

As a pivotal EMT inducer, the dysregulation of ZEB1 expression is observed in various types of cancer, including lung cancer, liver cancer, colon cancer, and pancreatic cancer [159-162]. Rhodes LV et al. showed that the overexpression of ZEB1 and ZEB2 enhanced the migration, invasion, and tumorigenicity in triple-negative breast cancer cells [163]. The activation of TGF-β signaling and upregulation of ZEB1 were shown to enhance metastasis in lung cancer and colon cancer [164, 165]. In pancreatic cancer, the upregulation of ZEB1 and ZEB2 was correlated with advanced stages, enhanced metastasis and poor prognosis [166]. ZEB1 also contributes to chemo-resistance in cancer. Inhibition of ZEB1 led to the inhibition of cell proliferation and metastatic characteristics and restored chemosensitivity in ovarian cancer, lung cancer, and pancreatic cancer [167-169]. Therefore, ZEB1 is also a promising therapeutic target in cancer management. Unfortunately, there is no potent and specific ZEB1 inhibitor to date.

TWIST family transcription factors (TWIST1/TWIST2)

The twist-related protein (TWIST) family transcription factors belong to the super-family of basic helix-loop-helix (bHLH) transcription factor and serve as both activators and repressors of

target genes transcription. The N-terminal of the TWIST1 protein is responsible for the protein-protein interactions with coactivators or corepressors, for example, PCAF, CREB-binding protein (CBP), p300, and HDACs [170, 171]. The recruited p300/CBP/PCAF coactivator complex activates the transcription of target genes through its intrinsic histone acetyltransferase (HAT) activity, whereas the recruitment of HDACs inhibits the transcription of target genes. Two nuclear localization signals (NLSs), which are responsible for nuclear transportation and localization, are also located in the N-terminal of the TWIST1 protein. An HLH DNA-binding domain is localized in the center of TWIST proteins, which can form homo- or heterodimers with other E-box binding proteins to recognize and bind to the E-box of target gene promoters [170]. The C-terminal of TWIST1 protein contains a TWIST-box domain, which can bind to Runt-domain transcription factors (Runx) to exert transcription activation activity. The choice of target genes of TWIST1 protein is based on the selection of its bindings patterners, which is controlled by the phosphorylation status of TWIST1 [172].

TWIST1 and TWIST2 are major EMT regulators in embryonic development, wound healing, and carcinogenesis, by upregulating mesenchymal molecules and downregulating epithelial molecules. TWIST1 recruits the methyltransferase SET8 to monomethylate H4K20, which is associated with the repression of E-cadherin promoters and activation of N-cadherin promoters [173]. In PDAC tissues, the expression of TWISTs is weak, but still significantly increased compared with IPMN and non-neoplastic pancreas [151]. In pancreatic cancer cell lines, the expression of TWISTs is not detectable in MIA PaCa2, PANC-1, BxPC-3, ASPC-1, and HS766T cells and is low to moderate in Capan-1, Capan-2, and CFPAC-1 cells [174]. However, TWISTs were upregulated in hypoxia conditions [175]. Considering that pancreatic cancers are usually undergone hypoxia, TWISTs may play a role in the invasive behavior of pancreatic

tumors. Numerous studies have shown that inhibition of TWISTs inhibited the growth, metastasis, and tumorigenicity in various types of cancer, including breast cancer, melanoma, and pancreatic cancer [176-179].

1.2.3. Singling pathways in EMT progression

EMT is orchestrated by a complex network of signaling pathways, including Wnt signaling pathways, TGF-β signaling pathways, Notch signaling pathways, and JAK/STAT signaling pathways. In the EMT process, activation of these singling pathways ultimately leads to the induction of server essential EMT-TFs, such as Snail, Slug, ZEB1/2, and TWIST1/2, resulting in suppression of epithelial molecules and upregulation of mesenchymal molecules [103, 104]. (**Fig. 1.5**)

Wnt signaling pathway

Three Wnt signaling pathways have been identified in response to the binding of Wnt ligands to the Frizzled family cell surface receptors: the canonical Wnt signaling pathway, the non-canonical Wnt-calcium pathway, and the non-canonical planar cell polarity pathway [180]. Among them, the canonical Wnt signaling pathway is extensively studied and is associated with EMT progression.

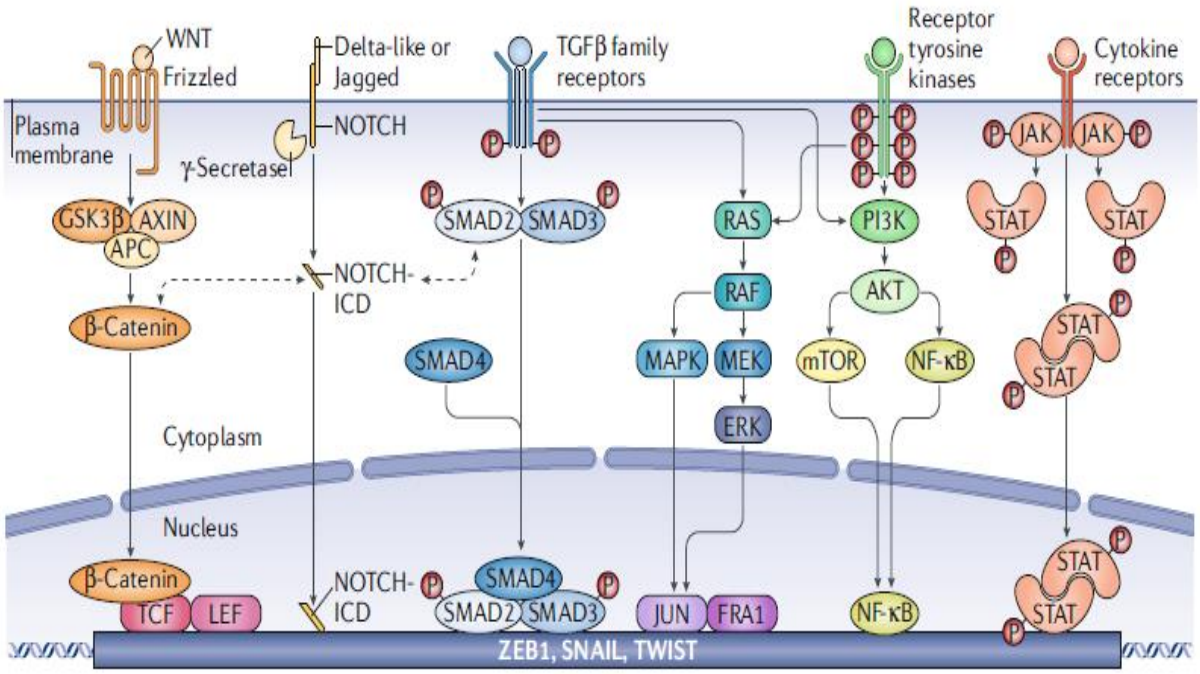

Figure 1.5. Singling pathways involved in EMT, including Wnt signaling pathway, Notch signaling pathway, TGF-β signaling pathway, NF-kB signaling pathway, JAK/STAT signaling pathway [103]. EMT-TFs, such as Snail, ZEB1, and TWIST, are ultimately activated with the activation of EMT-related signaling pathways, resulting in EMT progression.

Reprinted with permission from Dongre, A. and R.A. Weinberg, New insights into the mechanisms of epithelial-mesenchymal transition and implications for cancer. Nat Rev Mol Cell Biol, 2019. 20(2): p. 69-84.

The canonical Wnt signaling pathway modulates its signaling transduction thought the regulation of β-catenin degradation. As a dual-functional protein, β-catenin serves as an adhesion molecule when it is located on the cell membrane, whereas serves as a transcription factor when it is in the nucleus. The level of cellular β-catenin is controlled by a β-catenin destruction complex, which consists of Axin, adenomatous polyposis coli (APC), glycogen synthase kinase-3β (GSK-3β) and casein kinase 1 α (CK1α) [180]. The Axin/APC/GSK-3β/CK1α complex phosphorylates β-catenin, resulting in β-catenin ubiquitination by β-TrCP, and subsequent proteasomal degradation. The degradation of β-catenin prevents cytosolic and nuclear accumulation of β-

catenin. When the canonical Wnt signaling is initiated by the binding of Wnt ligands to the Frizzled-LRP5/6 receptor complex, the dishevelled (Dsh/Dvl) protein is recruited to the membrane. The membrane Dsh/Dvl provides docking sites for Axin and GSK-3β, thus leads to the dissociation of the Axin/APC/GSK-3β/CK1α complex and the relieving of β-catenin degradation. The stabilized β-catenin translocates into the nucleus and serves as a transcriptional factor by forming a complex with DNA bound T cell factor/lymphoid enhancer factor (TCF/LEF) to activate the transcription of Wnt target genes [181].

Many EMT-related genes have been identified as direct target genes of β-catenin, including Slug, ZEB1, and TWIST [181]. Although Snail is not a direct target gene of β-catenin, the expression of Snail is regulated by the canonical Wnt signaling pathway in a different manner. Snail contains a β-catenin-like canonical motif, which supports its GSK3β-dependent phosphorylation, β-TrCP-directed ubiquitination, and proteasomal degradation [182]. Thus, the activation of canonical Wnt signaling suppresses the phosphorylation and degradation of Snail, leading to the upregulation of Snail. Moreover, Snail promotes the expression of Wnt target genes by directly interacting with β-catenin. Studies have shown that the upregulation of Snail contributed to the increased responses to Wnt signaling in cancer cells. Overexpression of Snail in colon cancer led to increased expression of Wnt target genes, whereas downregulation of endogenous Snail by siRNA reduced Wnt target gene expression [148]. Consistently, pharmacological inhibition of canonical Wnt signaling inhibits EMT. PRI-724 is a first-in-class small molecule inhibitor for the canonical Wnt signaling pathway by inhibiting the interaction between β-catenin and its transcriptional coactivator, CBP. Preclinical studies of PRI-724 in pancreatic cancer suggested that this agent promoted differentiation of chemotherapy-insensitive cancer stem cells and tumor-initiating cells, inhibited stroma formation, and decreased metastatic potential [183, 184].

A Phase Ib clinical trial (NCT01764477) demonstrated that PRI-724 combined with gemcitabine was safe and demonstrated modest clinical activity [185, 186]. Whether the Wnt inhibitor PRI-724 has clinical effects needs further investigation.

TGF-β signaling pathway

The transforming growth factor-β (TGF-β) pathway is one of the most important EMT-regulation pathways in various types of cancer. The activation of TGF-β pathway is initiated by binding of TGF-β ligands, including TGF-β isoforms activins and bone morphogenetic proteins (BMPs), to TGF-β family receptors (TβRs), resulting in the phosphorylation of SMAD2 and SMAD3/5. The phosphorylated SMAD2 and SMAD3/5 form a trimeric SMAD complex with SMAD4, which then translocates into the nucleus and serves as a transcriptional factor to regulate the expression of downstream genes involved in cell growth, proliferation, and EMT [187]. Transcriptional activation of EMT-TFs, such as Snail, Slug, ZEB1, and TWIST, has been shown to be essential for TGF-β mediated EMT induction in different types of cancer [188].

The TGF-β pathway activates EMT through several different mechanisms of action. The trimeric SMAD complex promotes the transcription of mesenchymal genes, such as *VIM* and *FN1*, and EMT-TFs, such as *SNAI1*, *SNAI2*, *ZEB1*, and *TWIST1* [187]. The upregulation of these EMT-TFs further inhibits the expression of epithelial proteins, including E-cadherin, Claudins, and Occludins, resulting in EMT. The upregulated EMT-TFs also create a positive feedback loop to help the cells maintain the EMT status by upregulating the TGF-β ligands [189, 190]. Moreover, TGF-β signaling induces EMT through non-canonical pathways (non-SMAD pathways) by activating Raf/MEK/ERK signaling pathway, PI3K/AKT/mTOR pathway, JNK/p38 MAPK signaling cascades, and Rho-like GTPases signaling pathways [187, 191].

The inhibition of TGF-β pathway leads to the inhibition of EMT in many types of cancer and is a promising target for pancreatic cancer therapy. Galunisertib (LY2157299) is a small molecule TFG-β inhibitor developed by Eli Lilly, and its effects on various types of cancer have been evaluated by several phase II/III clinical trials on rectal cancer (NCT02688712), metastatic prostate cancer (NCT02452008), and unresectable pancreatic cancer (NCT01373164). The combination of galunisertib with gemcitabine has shown favorable effects on the overall survival (OS), progression free survival (PFS) and overall response rate (ORR) of unresectable pancreatic cancer patients, comparted with the patients receive placebo with gemcitabine (OS: 8.9 months vs 7.1 months; PFS: 4.11 months vs 2.86 months; ORR: 10.6% vs 3.8%, respectively) [192].

Notch signaling pathway

The Notch signaling pathway is primarily involved in controlling cell differentiation, proliferation, and apoptosis. The activation of Notch signaling starts with the binding of Notch ligands, such as Delta-like ligands (Delta-like 1, 3, 4) and Jagged family ligands (Jagged-1 and 2), to the Notch receptors (Notch 1-4). The binding of Notch ligands with Notch receptors triggers a proteolytic cleavage by γ-secretase, leading to the generation and releasing of Notch intracellular domain (NICD), which is an active fragment of Notch [193]. NICD translocates into the nucleus, where it forms a complex with a transcriptional factor, recombination signal binding protein for immunoglobulin kappa J region (RBPJ or CPF1), and activators, mastermind-like protein 1 (MAML1) and p300, to activate the transcription of Notch target genes involved in cell growth, proliferation, and apoptosis, such as *CCND1*, *MYC*, *TP53*, and *P21* [194].

The activation of Notch signaling has been shown to associate with EMT in several types of cancer [195]. Notch singling pathway regulates the transcription of several EMT- TFs, such as

Snail and Slug. In pancreatic cancer, upregulation of Notch receptors and Notch ligands promoted EMT and tumor progression [196, 197]. Paradoxically, other studies demonstrated a tumor-suppressive role of Notch signaling in the development of PanIN [198, 199]. Several Notch signaling inhibitors, such as nirogacestat (PF-03084014) and crenigacestat (LY3039478) have been developed by targeting γ-secretase and showed favorable effects against the progression, metastasis, and chemoresistance of prostate cancer and liver cancer *in vitro* and *in vivo* [200, 201]. Currently, phase II clinical trials (e.g. NCT01981551; NCT02836600) are on-going to evaluate the effects of Notch inhibitors on advanced solid tumors. Overall, the comprehensive involvement of Notch signaling in cancer progression and EMT is still under investigation and could provide valuable information for novel Notch inhibitors in drug development.

Other EMT-related signaling pathways

In addition to the signaling pathways mentioned above, many other signaling pathways have been shown involved in EMT progression in cancer, such as NF-Kb pathway and JAK/STAT pathway [202, 203]. Similar to TGF-β, Wnt, and Notch pathways, the activation of these pathways ultimately leads to the upregulation of EMT-TFs, such as Snail, ZEB1, and TWIST, resulting in the decreased epithelial molecules, the increased mesenchymal molecules, and the progression of EMT.

Taken together, EMT is a crucial factor in pancreatic cancer progression and metastasis. The inhibition of EMT by targeting EMT-TFs or EMT-related signaling pathways has promise to be an efficient strategy in pancreatic cancer management.

1.3. Cancer stem cells (CSCs)

1.3.1. The basic of CSCs

Tumor cells are heterogeneous in many features, even in the same bulk of a tumor. They are heterogeneous in morphology, metabolism, proliferation and metastatic ability, as well as harboring different genetic mutations or combinations of mutations [204]. Cancer stem cell (CSC) theory states that a hierarchical cellular structure of tumor cells roots the heterogeneity. In the bulk of a tumor, three basic functional groups of cancer cells can be identified: the CSCs, the cancer progenitor cells, and the mature cancer cells. The CSCs are the minority in the whole cell population, with the ability of self-renewal and differentiating towards all other types of cancer cells in a tumor. CSCs share many characteristics with normal stem cells. One important characteristic is self-renewal. Depending on various micro-environmental signals, a CSC can divide and generate two daughter CSCs, or a daughter CSC and a progenitor cancer cell, or two progenitor cells. The daughter CSCs do not differentiate and keep all the features of the parent CSCs, whereas the progenitor cells will further divide and differentiate. Progenitor cancer cells are the fast dividing cancer cells, but they have reduced capacity of self-renewal and have a limited number of divisions. Although CSCs are usually in a quiescent state, they have the infinity number of divisions throughout the lifespan of the tumor [205].

As early as in the 1950s, a study found that a certain subpopulation of cancer cells isolated from mouse peritoneal fluid showed specific karyotype [206]. In the 1960s and 1970s, more evidence revealed that a minor subpopulation of cancer cells demonstrated the characteristics of stem cells with self-renewal ability and the ability to differentiate into mature cancer cells [207-209]. The concept of CSCs was formed in the 1990s, as Lapidot et al. and Bonnet et al. identified a CD34+ CD38- subpopulation of cancer cells in acute myeloid leukemia (AML) and found these cells

were responsible for the initiation of derivative leukemia in immune-deficient mice. They also found that CD34+CD38+ or CD34- leukemia cells did not have tumor-initiating ability [210, 211]. Subsequent studies identified CSC activities in almost all types of solid tumors, including prostate cancer, colon cancer, lung cancer, breast cancer, liver cancer, and pancreatic cancer [212-217]. In 2006, the definition of a CSC was given by American Association for Cancer Research (AACR) as "a cell within a tumor that possesses the capacity to self-renew and to cause the heterogeneous lineages of cancer cells that comprise the tumor" [218].

CSCs are mainly characterized by its stemness (self-renewal) features, including the ability to form tumor spheres *in vitro*, to initiate tumor *in vivo*, and the upregulation of stemness-related pathways and molecules (e.g. SHH pathway and Nanog). Moreover, studies have shown that CSCs played essential roles in drug resistance, tumor metastasis, and recurrence [219-221]. In breast cancer and pancreatic cancer, the CD44+ subpopulation demonstrated enhanced metastatic ability [215]. Isolated CD44+/CD24- breast CSCs were able to initiate primary tumors in an orthotopic site and subsequently generate lung metastasis [222]. In pancreatic cancer, orthotopic implantation of CXCR4+/CD133+ pancreatic CSCs produced distant liver metastasis [223].

The connection of CSCs and EMT is also shown by the existing of circulating tumor cells (CTCs). Studies showed that CTCs is correlated with tumor metastasis and prognosis in a variety of solid tumors, including metastatic breast cancer, colon cancer, and prostate cancer [224-226]. CTCs have CSC activity and features. Isolated CTCs from melanoma patients were shown to initiate metastasis *in vivo* [227]. CTCs isolated from breast cancer patients also demonstrated enriched CD44+CD24- CSC phenotype [228]. It is hypothesized that CSCs in a primary tumor can enter the circulation and then become circulating CSCs, which is a critical subset of CTCs. However, it is not clear yet whether CTCs directly contribute to the formation of metastatic

lesion or are simply an indicator of tumor progression and metastasis. The relationship of CSCs and CTCs remains to be determined.

The mechanisms by which CSCs become drug resistant are not well understood yet. Mechanisms could include upregulation of ATP-binding cassette (ABC) transporters, such as ATP-binding cassette super-family G member 2 (ABCG2), or ATP-binding cassette sub-family B member 1 (ABCB1 or MDR1), which enhance the efflux of chemotherapeutic drugs from the cytosol [229-231]. The drug resistance may also be due to the quiescent status of the CSCs, as most chemotherapy and radiation therapy target fast-dividing cells [232]. Other properties may also contribute, such as overexpressed detoxifying enzymes, enhanced DNA repair ability, and overexpression of anti-apoptotic proteins [220]. The existing of drug-resistant CSCs in the tumor may lead to the failure of chemotherapy and radiation therapy. Investigating the mechanisms of drug resistance related to CSCs is necessary and could provide valuable information to design novel therapeutic approaches.

There are still many gaps of knowledge in the origin and biology of CSCs. Currently, there are two major hypothetical theories to explain the origin of CSCs. In the “embryonal rest theory”, CSCs are thought to be derived from the embryonal resting normal stem cells (NSC). Several experiments showed that the genetic nutation in NSCs led to neoplastic growth [233, 234]. It was also reported that glioma in a patient receiving fetal neural stem cell transplantation was identified as a donor origin rather than host origin, suggesting that dysregulated NSCs can grow into tumors [235]. There are also studies in hematological malignancies showing that CSCs coming from transformed bone marrow derived cells (BMDCs) [236]. However, emerging evidence has shown that CSCs may be derived from the progenitor or differentiated mature cancer cells [205, 223, 237, 238]. In the “dedifferentiation theory”, progenitor or mature cancer

cells undergo mutations to regain the property of self-renewal [239]. This theory emphasizes the plasticity of cancer cells in dedifferentiating into a stem-like status, regulated by signals in the microenvironment (niche) and likely through EMT process [240, 241].

In order to identify and study CSCs, multiple cell markers have been used. There have been no universal markers to pinpoint all CSCs in different tumors. Instead, combinations of CSC markers have shown the ability to identify a subpopulation of cells with significantly increased stemness features. Multiple cell surface antigens have been used as CSC markers. In solid tumors, CSCs were first isolated from breast cancer cells. A CD44+ CD24- subpopulation of breast cancer cells demonstrated higher tumorigenic ability compared to the rest of the breast cancer cells [215]. Thus CD44+CD24- were identified and now commonly used as CSC markers for breast cancers. The upregulation of CD44 was then found to be associated with enriched CSC population in prostate cancer and pancreatic cancer [212, 217]. Many other cell surface antigens have also been identified as CSC markers, such as CD133 (liver cancer, breast cancer, brain cancer, lung cancer, pancreatic cancer), CD166 (colon cancer, lung cancer), CXCR4 (pancreatic cancer, glioma), and leucine-rich repeat-containing G-protein coupled receptor 5 (LGR5, liver cancer, gastric cancer, pancreatic cancer) [242-245]. The embryonic stem cell related Yamanaka factors can also be used as CSC markers, including octamer-binding transcription factor 4 (OCT4), sex determining region Y-box 2 (SOX2), Kruppel-like factor 4 (KLF4), and c-Myc [246-248]. Aldehyde dehydrogenase 1 (ALDH1) is another CSC marker normally used in breast cancer and leukemia. The increased activity of ALDH1 has been demonstrated to be correlated with increased tumorgenicity in chronic myelogenous leukemia (CML) [249]. However, ALDH does not seem to be a CSC marker in prostate tumors [250]. Besides these markers, cell-permeable dyes are able to indicate a side population that exhibits similar characteristics as

CSCs, as CSCs have enhanced efflux due to upregulated ABCG2 transporters. Therefore, the side population is also used in studies of CSCs. For example, the staining of a cell-permeable DNA binding fluorophore dye, DyeCycle™ Violet (DCV), has been used as an indicator of CSC side population (DCV- cells) in A549 and H460 lung cancer cells [251].

In pancreatic cancer, Li et al demonstrated that the CD44+/CD24+/EpCAM+ subpopulation in patient-derived xenograft (PDX) tumor samples consisted less than 1% of whole pancreatic cancer cell population and possessed the abilities of self-renewal and producing differentiated progenitor cancer cells and had increased expression of the sonic hedgehog signaling [217]. There was a 100-fold increase in tumorigenicity of CD44+/CD24+/EpCAM+ pancreatic cancer cells compared with the CD44-/CD24-/EpCAM- cells. As few as ~100 of the CD44+/CD24+/EpCAM+ cells initiated tumors in nude mice with indistinguishable histological features to the original human tumors [215, 217]. Other studies found that a widely used CSC marker in different types of cancer, CD133, was also upregulated in pancreatic CSCs, accompanied with significantly increased tumorigenicity [252, 253]. Therefore, CD44+/CD24+/CD133+/EpCAM+ cell population is a reliable combination of markers to identify and isolate pancreatic CSCs [254]. Many studies used CD44+/CD24+/EpCAM+ to identify pancreatic CSCs.

1.3.2. CSCs and EMT

Numerous studies revealed that EMT and CSCs are highly correlated in many ways. Firstly, tumors with enriched CSCs show higher metastatic ability with upregulated EMT-TFs and EMT-related molecules. The inhibition of CSCs led to the inhibition of metastatic ability and EMT features [219, 255]. On the other hand, induction of EMT increased the number of CSCs and

enhanced tumor initiation ability [241]. Inhibition of EMT-TFs inhibited both EMT and stemness features, such as tumor sphere formation ability and tumorigenicity *in vivo* [256]. Furthermore, EMT and CSCs share many regulating signaling pathways, such as Wnt signaling pathway and Notch signaling pathway. The suppression of these pathways impairs both EMT progression and CSC features in tumors.

Tumors with enriched CSC population have upregulated EMT-related molecules and have increased metastatic abilities. The CD44+CD24-ALDH+ CSC population from head and neck cancer patients demonstrated promoted EMT progression with increased expression of Snail and Vimentin, and suppressed expression of E-cadherin [257]. Similarly, the CD44+ CSC population of H1299 NSCLC cells has increased EMT features with upregulated N-cadherin and Vimentin [258]. In pancreatic cancer cells, a study showed that CD133 facilitated EMT progression by modulating the expression of Slug and N-cadherin [259]. The PANC-1 tumor spheres were reported to have enhanced EMT progression with decreased E-cadherin and increased N-cadherin [260].

The Induction of EMT helps maintain the stemness feature in CSCs. The activation of EMT, induced by TWIST1, Snail, or TGF-β, induced enrichment of CD44+/CD24- population in human mammary epithelial cells HMLER, and increased tumorigenicity of the cells [261, 262]. In breast cancer patient tissues, a metaplastic, low Claudin and low E-cadherin "EMTed" subtype had an enriched CD44+/CD24- population [263]. The silencing of Snail expression in pancreatic cancer cells decreased an ALDH+ side population and impaired the tumorigenicity *in vivo* [264]. The inhibition of EMT by targeting EMT-TFs also leads to the inhibition of CSCs. Studies have shown that the inhibition of ZEB1 and Snail led to the inhibition of CSC population

and tumorigenicity in several cancer types, including colorectal cancer and pancreatic cancer [265-267].

1.3.3. The signaling pathways in CSCs

Several cellular signaling pathways that drive and maintain the stemness in CSCs have been identified, of importance are Wnt signaling pathway, JAK/STAT signaling pathway, Hedgehog signaling pathway, and Notch signaling pathway.

The Wnt signaling pathway and the Notch signaling pathway

In the canonical Wnt signaling pathway, nuclear β-catenin is the key to regulate the stemness feature in CSCs. Studies have shown that increased levels of β-catenin enhanced the tumor sphere formation capacity in gastric cancer cells [268]. Activation of the canonical Wnt signaling pathway also upregulated the expression and activity of Telomerase, which is a pivotal factor in controlling stem cells and cancer progression [269]. The constitutively activated Wnt signaling has been shown to be essential to maintain stemness feature, including tumor sphere formation, enriched side population *in vitro*, and tumorigenicity, CSC phenotype (CD44+OCT+) *in vivo*, in gastric cancer cell lines [268].

Inhibition of Wnt signaling has the potential to inhibit EMT progression and stemness features in cancer. Currently, several Wnt signaling inhibitors have been developed and are undergoing clinical testing in conjunction with chemotherapies. PRI-724 is a first-in-class small molecule inhibitor for the canonical Wnt signaling pathway. Several other small molecule Wnt signaling inhibitors, such as SM08502 and CGX1321, has also been identified. Early phase clinical trials

are current on going to evaluate the safety and efficacy of SM08502 and CGX1321 on advance solid tumors [NCT03355066, NCT03507998, NCT02675946].

It has been revealed that pancreatic CSCs expressed higher levels of Notch-1, compare with the no-CSC population or the whole cancer cell population [270]. The activation of Notch signaling by exogenous Notch ligands induced the enrichment of CSC population and promoted the tumor sphere formation in pancreatic cancer cells. Consistently, the inhibition of Notch signaling by either γ -secretase inhibitors or Hes1 shRNA led to the inhibition of CSC population and tumorgenicity *in vitro* and *in vivo* [197]. The upregulated Notch expression was also correlated with poor survival and poor prognosis in PDAC patients [271]. As Notch signaling is involved in both EMT progression and CSCs, the activation of Notch signaling in pancreatic cancer has been shown to promote cell proliferation, migration and tumorigenicity [197, 272]. Currently, the Notch signaling inhibitors are mainly targeting γ -secretase. For example, a γ -secretase inhibitor, RO4929097, is undergoing multiple clinical trials on pancreatic cancer [NCT01232829], colon cancer [NCT01116687], melanoma [NCT01196416] and sarcoma [NCT01154452] for its safety and efficacy.

The JAK/STAT Pathway

The JAK/STAT signaling pathway contains the Janus kinase (JAK1-3 and TYK2), the signal transducer and activator of transcription proteins (STAT1-4, STAT5A, STAT5B, and STAT6) and cytokine receptors [273]. In response to the binding of multiple extracellular ligands, such as chemicals and cytokines, the cytokine receptors dimerize and bring the receptor-associated JAKs into proximity. The receptor-associated JAKs then phosphorylate each other on tyrosine residues in their activation loops, leading to the activation of their kinase activity. The activated JAKs

phosphorylate tyrosine residues on the cytokine receptors, leading to the generation of docking sites for STATs. STATs bind to the phosphorylated tyrosine on the receptor and then are phosphorylated by JAKs, resulting in the dissociation of JAKs from the receptor docking sites and the hetero- or homodimerization of phosphorylated STATs. Like many other transcription factors, dimerized STATs translocate into the nucleus and then serve as transcription factors in association with other coactivators, such as CBP/P300 complex and HATs [274, 275].

Studies have shown that the activation of JAK/STAT signaling pathway helped maintain the stemness features in different types of cancer. In breast cancer cells, the activation of JAK/STAT signaling pathway resulted in an enrichment of CD44+CD24- CSC population [276]. The activation of JAK/STAT signaling pathway was also detected in the CD133+/CD44+ prostate CSC population while they were forming the tumor spheres [277]. On the other hand, CSC population exhibited upregulated JAK/STAT activation. The colon CSC (ALDH+/CD133+) population exhibited an enhanced expression of STAT3 phosphorylation, compared with both ALDH-/CD133-cells population and unsorted whole cell population, indicating the upregulation of JAK/STAT signaling pathway in CSCs [278, 279]. Consistently, the inhibition of STATs was shown to inhibit the clonogenicity and tumorigenicity in prostate cancer [280]. In pancreatic cancer, the inhibition of JAK/STAT pathway led to decreased Mucin 4 expression in Capan1 and CD18/HPAF cells, resulting in suppression of cell proliferation and metastasis [281].

Targeting JAK/STAT pathway is a promising strategy to inhibit CSCs and tumor metastasis. Several STAT inhibitors have been developed and tested in pre-clinical and clinical trials. Niclosamide is a selective inhibitor on phosphorylation of STAT3 and has no obvious inhibitory effects against the activation of other STAT family proteins, such as STAT1 or STAT5. Recent studies have demonstrated that niclosamide inhibited proliferation, metastasis, drug resistance,

and radioresistance in various types of cancer, including breast cancer, ovarian cancer, lung cancer, and hepatocellular cancer [282-288]. Interestingly, the JAK/STAT is a shared signaling pathway by EMT, thus the inhibition of JAK/STATS signaling pathway has the potential to inhibit both EMT and CSCs. Indeed, niclosamide also reversed EMT in breast cancer cells through the suppression of IL-6/STAT3 signaling axis [285]. Currently, multiple phase I/II clinical trials are underway to evaluate the effect of niclosamide in colon cancer (NCT02687009) and prostate cancer (NCT02532114, NCT03123978, NCT02807805). In addition, clinical trials have been conducted with another JAK1/2 inhibitor, Ruxolitinib. Current results only demonstrated modest effects of Ruxolitinib on breast cancer, colon cancer, and pancreatic cancer (NCT02955940, NCT01423604).

The hedgehog signaling pathway

The hedgehog (HH) signaling pathway is crucial in generating specialized cells and maintaining the proper cell differentiation during development. Three hedgehog homologs have been identified in mammals, including desert hedgehog (DHH), indian hedgehog (IHH) and sonic hedgehog (SHH) [289]. The SHH is the best-studied hedgehog homolog in the vertebrates. The ~45 kDa SHH precursor is autocatalytically processed to produce an ~20 kDa N-terminal signaling domain (SHH-N) with signaling activity. The SHH-N is then secreted from its producing cell and serves as a paracrine SHH ligand on adjacent cells with the participation of protein Dispatched (DISP). The binding of SHH-N with Patched-1 or Patched-2 (PTCH1 or PTCH2) receptor relieves the inhibition of cell surface protein Smoothened (SMO), which is repressed by the PTCH receptor in the absence of SHH ligands. The relieving of SMO inhibition further leads to the activation of SHH transcriptional factors, GLI family zinc finger proteins (GLIs), including activators CLI1, GLI2, and repressor GLI3 [290]. Similar to many other

transcription factors, the activated GLIs translocate into the nucleus and then regulate the transcription of SHH target genes, such as *CCND1* and *P21*, with the assistant of other coactivators or corepressors.

Dysregulation of SHH signaling has been found in most cancers. SHH signaling activates the expression of many genes involved in cell proliferation, differentiation, invasion, and survival. GLI1 and GLI2 have been proved to directly activate the transcription of *NANOG*, which is a major CSC-related transcription factor, thus enhance the self-renewal and stemness potential in medulloblastomas [291]. In highly invasive and aggressive glioblastoma, the stemness genes (e.g. *OCT4*, *NANOG*, *SOX2*, and *BMI1*) were found upregulated with the activation of SHH signaling through CLI1 [292]. The activation of SHH signaling in pancreatic CSCs is also significantly higher than non-CSC population, indicating that SHH helped maintain the self-renewal ability in pancreatic CSCs [293].Consistently, the inhibition of SHH signaling leads to the inhibition of stemness features in different types of cancer. It has been shown that the inhibition of SHH signaling preferentially enhanced the sensitivity of CD133+ glioma cells to temozolomide treatment [294]. Pharmacological inhibition of SHH signaling also inhibited the CSC population in anaplastic thyroid cancer cells and inhibited the expression of stemness genes, such as *NANOG*, *CD44*, and *OCT4*, in colon CSCs [295, 296]. In pancreatic cancer, the inhibition of SHH signaling resulted in reduction of stemness features via BMI1 downregulation and reduction of chemoresistance by downregulating the expression of ABCG2 [297].

Inhibitors targeting SHH signaling pathway factors, such as SHH and SMO, were developed and tested in several clinical trials. Vismodegib, a SHH inhibitor, was a “first in the class” drug approved by FDA for basal cell carcinoma in 2012. Currently, this drug is undergoing several clinical trials on prostate cancer (NCT02115828), ovarian cancer (NCT00959647) and pancreatic

cancer (NCT01088815, NCT01537107, NCT01195415). The combination of vismodegib with gemcitabine inhibited the percentage of CD44+/CD24+/EpCAM+ population from 4.79% to 3.09% with a 30-days treatment, indicating the suppression of CSCs in the advanced pancreatic cancer patients (NCT01195415). Vismodegib and other SHH inhibitors are worth further investigation to serve as new therapeutic strategies in pancreatic cancer management.

In summary, the enriched CSCs in pancreatic cancer contribute to the metastasis and chemo-resistance, which are major challenges in pancreatic cancer management. The development of CSC inhibitors is urgent and necessary. Considering the technical limitations to pinpoint CSCs for drug discovery, the development of CSC inhibitors by targeting on EMT-TFs and EMT-related molecules could be an alternative and effective way. The close relationship between EMT and CSCs provide a strategy to inhibit both EMT and CSCs, ultimately leading to the inhibition of tumor metastasis and chemo-resistance.

1.4. Post-transcriptional regulation in pancreatic cancer EMT and CSCs

In eukaryote cells, the genetic information usually flows from DNAs to RNAs, then to proteins. mRNAs are the major genetic information carriers between DNAs, the primary genetic information carrier, and proteins, the ultimate functional units. After transcription, mRNAs undergo a series of processes before proteins are translated. The post-transcriptional regulation is the regulatory method in mRNA processing, which kicks in between the transcription and translation. Post-transcriptional regulation is mainly conducted by RNA binding proteins (RPBs), which involved in various steps in mRNA processing, such as alternative splicing, mRNA capping, polyadenylation and mRNA turnover. Another important post-transcriptional regulator is microRNAs (miRNAs) [298].

Depending on the genetic cause of regulatory changes, the gene regulation can be categorized into two categories. The *cis*-regulatory elements, including promoters, enhancers, silencers, adenylate-uridylate-rich elements (AU-rich elements or AREs), are usually non-coding DNA or RNA sequences contained within the genes being regulated. The *trans*-regulatory elements, including transcription factors, miRNAs, RBPs, are usually diffusible molecules that can regulate the expression of unlinked genes through binding to the *cis*-elements. Both miRNAs and RBPs are *trans*-regulatory elements and exert their function by binding to *cis*-regulatory elements, such as AREs.

Studies have shown that the regulation of EMT and CSCs is controlled at both transcriptional level and post-transcriptional level. Several post-transcriptional regulators have been found to be correlated with PDAC carcinogenesis, metastasis and prognosis.

1.4.1. micro-RNAs in pancreatic cancer EMT and CSCs

A microRNA (miRNA) is a small non-coding RNA molecule (containing about 22 nucleotides) found in plants, animals, and some viruses, which functions in RNA silencing and post-transcriptional regulation of gene expression. miRNAs regulate the expression of ~ 60% of protein coding genes of the human genome [299]. miRNAs function via base-pairing with target sequences in the 3' untranslated region (3'UTR) of mRNAs [300]. In animals, the base-pairing between miRNAs and mRNAs are not complete complementary, instead, the base-pairing between a highly conserved 6-8 nucleotides "seed" sequence near the 5′ of the miRNAs and the 3'UTR of mRNAs is required for the specific binding of miRNA with mRNAs [301]. The binding then recruits an RNA-induce silencing complex (RISC) to form a microRNA ribonucleoprotein complex (miRNP), which containing several proteins, such as RNase III Dicer and Argonaute, to exert endonuclease activity [302]. The miRNAs silence the mRNAs by translational suppression or inducing mRNA degradation [303, 304].

miRNAs are conserved and are thought to be a essential component in genetic regulation. Recent research shows that miRNAs play important roles in cancer metastasis and EMT [305]. Different micro-RNAs can achieve their specific regulatory functions by serving as either onco-miRNAs or tumor suppression miRNAs. An important tumor suppression miRNA family involving in cancer metastasis regulation is miR-200 family. miR-200 family directly targets ZEB1 and ZEB2 mRNAs, suppresses their expression, and consequently reliefs their suppression on E-cadherin expression [306]. By these mechanism, miR-200 family inhibits EMT and leads to the inhibition of tumor metastasis. Upregulation of miR-200 reversed EMT and induced gemcitabine sensitivity in gemcitabine-resistant PDAC cells [307]. However, the boundary of onco-microRNAs and tumor suppressor microRNAs is not absolute. In some circumstances a tumor

suppressor miRNA can become an onco-miRNA. For example, the tumor suppressor miR-200 has also been shown to promote the last step of metastasis, in which migrating cancer cells undergo mesenchymal-epithelial transition (MET) during their colonization at distant organs [308, 309]. By using a series of isogenic cell lines from mouse mammary carcinoma, Dykxhoorn DM et al. demonstrated that the miR-200 family was highly expressed only in the metastatic cells (4T1 cells) but not in the non-metastatic cells, which are unable to colonize (4TO7 cells), invasion and intravasation (67NR), and extravasation (168FARN). The overexpression of miR-200c in both metastatic 4T1 cells and non-metastatic 4TO7 cells promoted MET and colonization in both primary site (mammary fat pad) and metastatic site (lung) [308, 310]. miRNAs regulate tumor metastasis not only by inhibition of EMT, but also by other mechanisms. For example, another tumor suppressor miRNA, miR-34, inhibited the expression of Sirtuin 1, leading to an increase in p53 acetylation and increased expression of p21 and p53 upregulated modulator of apoptosis (PUMA) [311]. Both p21 and PUMA are transcriptional targets of p53 and regulate the cell cycle and apoptosis, respectively. Thus, the up-regulation of miR-34 induces cancer cells apoptosis and cell cycle arrested, which can also inhibit cancer metastasis.

Taken together, miRNAs are post-transcriptional regulators by modulating mRNA translation and degradation. Recent studies also revealed that crosstalk between miRNAs and RBPs are important to regulate mRNA biology, which are discussed in **Chapter 1.4.2**.

1.4.2. RNA-binding proteins (RBPs) and ARE binding proteins (AUBP) in pancreatic cancer EMT and CSCs

There are many RBPs with diverse functions. To exert the RNA-binding function, RBPs contain one or multiple RNA-recognition and binding domains, including RNA-binding domain (RBD, also known as RNA recognition motif, RRM), K-homology (KH) domain, RGG (Arg-Gly-Gly) box, SAM domain, zinc finger (ZnF), double stranded RNA-binding domain (dsRBD), cold-shock domain, and the Piwi/Argonaute/Zwille (PAZ) domain [312, 313]. The large numbers of RBPs in eukaryotes enable a highly specific post-transcriptional process to orchestrate gene expressions. RBPs exert their function in almost every aspect of RNA biology, including pre-mRNA splicing, polyadenylation, RNA capping, RNA transporting, RNA localization, RNA translation and RNA turnover [314]. In this section, we mainly focus on the RBPs that recognize the AREs in the 3'UTR of mRNAs (ARE binding proteins or AUBPs), which mainly regulate the RNA turnover.

In general, AUBPs exert their biological function through binding to the AREs in target mRNAs. AREs are typically 50-150 nucleotides present within 3′ UTRs of short-lived mRNAs of cytokines, proto-oncogenes, and growth factors. AREs has been identified in ~8% of human genes, indicating that AUBPs are crucial in gene regulation and must be tightly regulated [315-317]. AREs are one of the *cis*-regulatory elements responsible for rapid degradation of short-life mRNAs. Currently, three classes of AREs have been identified. Class I AREs have dispersed AUUUA motif in the context of U-rich sequence. Class II AREs have overlapped AUUUA motifs in the context of U-rich sequence. Class III AREs are U-rich only without AUUUA pentamers [318].

AUBPs function as *trans*-regulatory elements by recognizing and binding to the *cis*-regulatory elements, usually AREs, of target mRNAs. The binding of AUBPs relies on the RNA-binding domains, typically the RRMs. The canonical RRMs fold into an αβ sandwich structure with four anti-parallel β-sheets and two α-helix packed against the β-sheets. The RNA binding residues, namely RNP 1 and RNP 2, are located in the central strands of the β-sheet and are highly conserved in different RRMs [319, 320]. The β-sheet surface of an RRM can bind to four to six nucleotides; thus, the recognition and binding of a longer mRNA requires the formation of a binding pocket by several RRMs [321]. Recent studies revealed that RRMs also involved in protein-protein interactions, typically leading to the AUBP homodimerization when bind to target mRNAs [322].

The AUBPs regulate the expression of target genes by influencing mRNA degradation, stabilization and/or translation. Thus, the AUBPs can be further characterized into degradation factors, such as AU-binding factor 1 (AUF1), Tristetraprolin (TTP), KH domain-slicing regulatory protein (KSRP), stabilization factors, such as human antigen R (HuR), and translational control proteins, such as T-cell intracellular antigen 1 (TIA-1) and TIA-1 related protein (TIAR). The functional classification is not absolute. For example, the mRNA stabilization factor, HuR, can also inhibit translation of target mRNAs by recognizing and binding to the internal ribosome entry site (IRES), which mediates the cap-independent translation, on the 5'UTR of a small subset of target mRNAs [64]. Here, we mainly focus on one of the most studied AUBPs, HuR.

Human antigen R (HuR)

The human antigen R (HuR), also known as embryonic lethal abnormal vision-like protein 1 (ELAVL1), belongs to the ELAVL/Hu proteins family, which is composed of four highly conserved members: the neuron specifically expressed HuB/ELAVL2, HuC/ELAVL3, HuD/ELAVL4, and ubiquitously expressed HuR/ELAVL1 [323, 324]. HuR is consisted of three highly conserved canonical RRMs, with RRM1 and RRM2 on the N-terminal, and RRM3 on the C-terminal. RRM1 and RRM2 are most conserved motifs across Hu family proteins and function in tandem to bind to the AREs in the 3'UTR of target mRNAs [324, 325]. The role of RRM3 is less clear. Recent studies revealed that the RRM3 is a multifunction domain that involved in HuR homodimerization and HuR-mRNA interaction [326]. A 60-residue basic hinge domain is located in between of the RRM1/RRM2 and RRM3. The HuR nucleocytoplasmic shutting sequence (HNS) within the hinge domain is required for translocation of HuR between nucleus and cytoplasm, in cooperating with several transport machinery components, such as exportin-1 (XPO1, CRM1), transportins, and importins [323, 327]. The cytoplasmic localization is required for HuR to exert its mRNA stabilizing ability.

HuR is usually considered as an mRNA stabilizer by protecting a large numbers of target mRNAs from degradation, which encode proteins involved in various pathologies, especially inflammation and cancer [328] (**Fig. 1.6)**. For example, HuR has been proved to directly bind to the mRNAs of *CCND1*, *CDKN1A*, *TGFB1*, *VEGFA*, *COX2*, and *MMP9* [329-333]. Interestingly, *HUR* mRNA has been proved to be stabilized by HuR protein itself via the binding of HuR with

the AREs in *HUR* mRNA, indicating a positive feedback loop of HuR expression when cells are attempt to survival under stimulation conditions [334, 335].

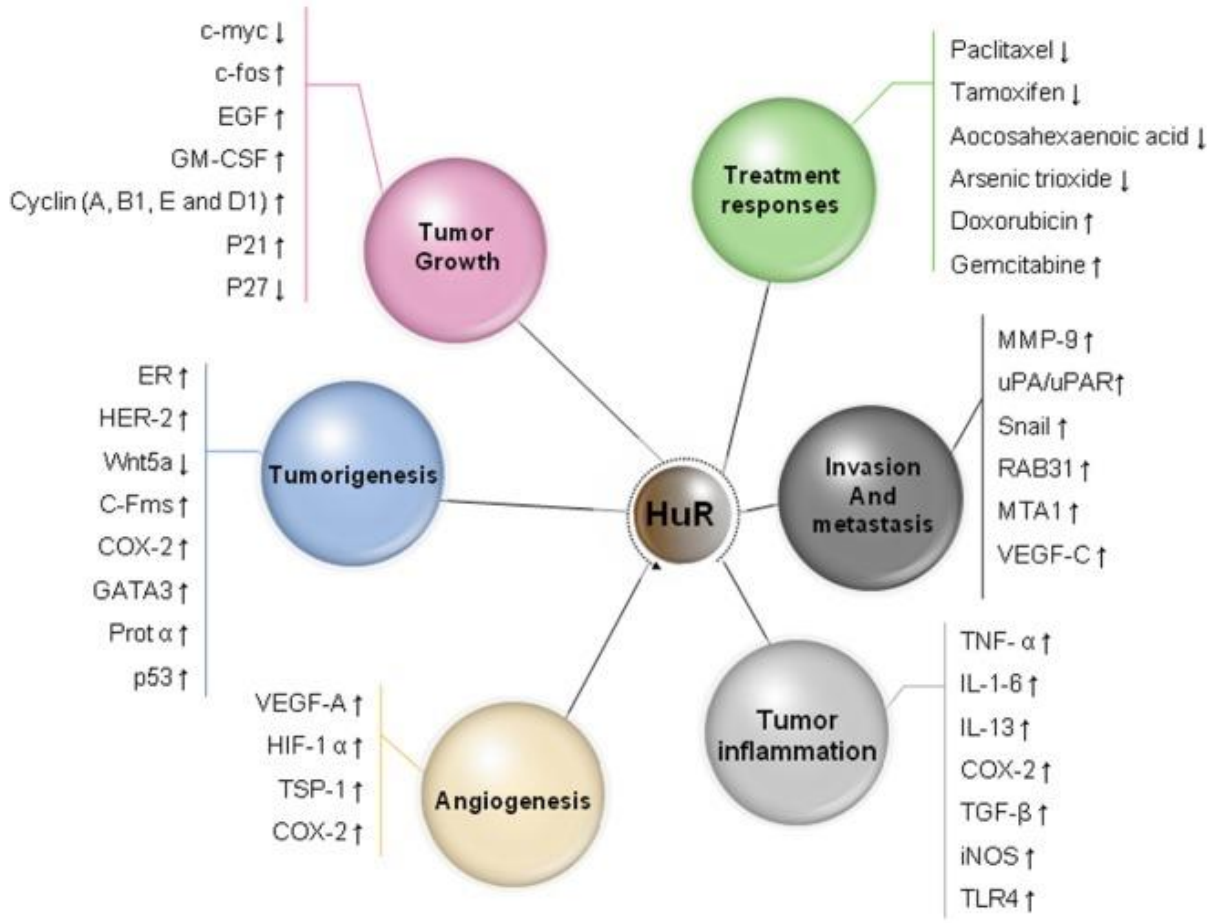

Figure 1.6 The various functions of HuR in cancer-related events [329]. HuR exerts its function by regulating the stability or translation of target mRNAs involved in cancer-related events. Up arrows demonstrate that the proteins were upregulated, or the drugs were sensitized with increased HuR, vice versa.

The exact mechanisms by which HuR protects its target mRNAs from rapid degradation are not well understood yet. The competitive binding of HuR against other AUBPs, especially RNA decay AUBPs, to the same AREs may be an explanation. RNA decay AUBPs, e.g. tristetraprolin (TTP), exert the mRNA decay function thought the recruitment of deadenylation complexes. In mammalian cells, three major deadenylation complexes has been identified: the Ccr4/Caf1/Not (Caf1) complex, the poly A-specific ribonuclease (PARN) complex, and the Pan2/Pan3 complex [336, 337]. TTP recruits the Caf1 deadenylation complexes when binds to target AREs, and then conducts a 3'-5' RNA decay in the exosomes or a 5'-3' Xrn1-dependent RNA decay in the processing-bodies (P-bodies) [338, 339]. The binding of HuR to target mRNAs blocks the binding of RNA decay factors, such as TTP, AUF-1, or microRNAs, disrupting the recruitment of mRNA degradation complexes, such as exosomes, p-bodies, or RISCs [335, 340].

HuR also serves as a translational promoter or suppressor. HuR has been shown to promote the translation of hypoxia-inducible factor-1α (HIF-1α), X-linked inhibitor of apoptosis protein (XIAP), and B-cell lymphoma 2 (BCL-2) [341-343]. The mechanisms of this promoted translation by HuR are not clear yet, and apparently independent of mRNA stabilization. Several studies indicated that the HuR-associated inhibition of other translational repressors, such as TIA-1 and microRNA/RISCs, may cause the translational upregulation of target mRNAs [344, 345]. Less commonly, HuR can also serve as a translational suppressor. In these circumstances, HuR binds to the 5'UTR, instead of the 3'UTR, of a mall subset of target mRNAs, such as *CDKN1B*, *THBD*, and *IGF1R* mRNA, by recognizing the IRES sequence. The binding of HuR with IRES inhibits the assembly and initiation of both cap-dependent and cap-independent translation machinery, resulting in the translationally repression of target mRNAs [346-349]. HuR can also bind to the 3'UTR and recruit a let-7/RISC complex to inhibit mRNA translation

[350]. In summary, HuR exerts its *trans*-regulatory element effects in several ways, usually leading to the stabilization of target mRNAs, which encode proteins involved in cancer and other pathological events.

The abundance and localization of HuR in cells are tightly controlled. As a pivotal factor in response to stimulations, the abundance of HuR is regulated on transcriptional level, post-transcriptional level, translational level and post-translational level. Studies have shown that the activation of PI3K/AKT signaling pathway or the overexpression of Smad1 protein promoted the transcription of *HUR* mRNA [351, 352]. On the post-transcriptional level, several miRNAs, such as miRNA-570-3p, miRNA-519, and miRNA-125a, have been proved to inhibit HuR expression through the nucleotides specific binding and the recruitment of RISCs [353-355]. The degradation of HuR was mediated by ubiquitination at residue lysine-182 followed by proteasome-mediated proteolysis. This heat shock induced ubiquitination process was antagonized by the phosphorylation of HuR by checkpoint kinase 2 (CHK2) [356].

HuR is predominantly in the nucleus (>90%), however, the nuclear function of HuR is largely unknow, except for a proposed function in pre-RNA splicing [357, 358]. The cytoplasmic localization is necessary for HuR to modulate the expression of target mRNAs [324, 359]. In general, the post-translational modifications, usually phosphorylation, of residues within the HNS determine the intracellular localization of HuR. For example, phosphorylation of HuR at serine-158 and serine-221 by protein kinase c-α (PKC-α) promoted the cytoplasmic translocation of HuR and enhanced the binding affinity of HuR to *COX2* mRNA in response of ATP treatment [360]. On the contrary, the phosphorylation of HuR by cyclin-dependent kinase 1 (CDK1) at serine-202 induced nuclear HuR accumulation during cell cycle phase G2 [361]. The phosphorylation in the residues within RRMs impairs the RNA binding and regulatory abilities

of HuR. For instance, the phosphorylation of HuR by CHK2 at serine-88, serine-100, and threonine-118, which are all located within RRM1/RRM2, impaired the binding affinity of HuR to *SIRT1* mRNA in response to oxidative stress [362]. Taken together, the expression and localization of HuR is orchestrated by multiple factors, indicating the vital role of HuR in post-transcriptional regulation.

HuR has been found to be abundant and primarily located in the cytoplasm in pancreatic cancer patients [363]. The overexpression and cytoplasmic localization of HuR were thought to be a response of PDAC to microenvironmental stressors, such as chemotherapy, hypoxia, and nutrient deprivation [364, 365]. PDAC has high level of hypoxia, which is one of the reasons for chemoresistance. Recent studies showed that HuR regulated the hypoxia-induced chemoresistance by stabilizing the mRNA of proto-oncogene *PIM1* in pancreatic cancer cells. In chronic hypoxia condition, HuR translocated from the nucleus into the cytoplasm and bound to the 3' UTR of *PIM1* mRNA, which is a prominent chemoresistant factor by phosphorylating and inactivating apoptotic factors, such as bcl-2-associated death promoter (BAD). Inhibition of HuR significantly sensitized pancreatic cancer cells to oxaliplatin and 5-FU under physiologic low oxygen conditions [366]. In addition, HuR protected PDAC against nutrient deprivation and gemcitabine treatment by stabilizing isocitrate dehydrogenase 1 (IDH1), which is a nicotinamide adenine dinucleotide phosphate (NAPDH)-generating enzyme. The increased IDH1 minimized intracellular ROS, resulting in PDAC cell survival and chemoresistance [367]. However, an early study showed that overexpression of HuR sensitized pancreatic cancer cells to gemcitabine treatment by stabilizing deoxycytidine kinase (dCK), which is the key enzyme for gemcitabine metabolism and activation [363]. Several subsequent studies indicated that cytoplasmic localization of HuR also sensitized PDAC and breast cancer to 5-FU treatment through

stabilizing FOXO1 or dCK [368-370]. Even pancreatic cancer patients with high expression level of HuR may have better response to gemcitabine/5-FU treatment, there is no evidence that the overexpression of HuR can benefit pancreatic cancer patients. In fact, HuR level is associated with metastasis and poor prognosis.

Cytoplasmic abundance of HuR has the potential to serve as a predictive marker for prognosis. In invasive ductal breast cancer patients, the abundance of cytoplasmic HuR was highly correlated with the high TNM grades, tumor size, and poor prognosis [371-373]. However, the prognostic role of HuR in pancreatic cancer is controversial. Early studies have shown that high cytoplasmic HuR level was correlated with advanced T stages, but was a favorable marker for the gemcitabine response and overall survival with gemcitabine treatment [363, 374]. Later, a large scale phase III clinical trial by the same group demonstrated that the disease-free survival (DFS) and overall survival (OS) of gemcitabine treated patients was not associated with cytoplasmic HuR expression [370]. Further studies are needed to validate HuR as a predictive and prognostic marker in pancreatic cancer.

Numerous studies have revealed that the dysregulation of HuR is correlated with invasiveness, metastasis, EMT, and CSC features in various types of cancer. Cytoplasmic accumulation of HuR was significantly increased in tumors with lymphatic/vascular invasion compare with tumors without lymphatic/vascular invasion in bladder cancer, breast cancer, and colon cancer [375-377]. In osteosarcoma, knockdown of HuR repressed osteosarcoma cell migration, invasion, chemoresistance, and stemness (indicated by suppressed sphere formation and decreased OCT4 and Nanog), through the suppression of yes-associated protein 1 (YAP) activation [378]. In breast cancer cells, a β-catenin/HuR post-transcriptional machinery has been found to promote tumor growth and CSC phenotype in response to hypoxia, by stabilizing *SNAI2*

and *CA9* mRNAs [379]. In pancreatic cancer, a study found that HuR silencing significantly impaired the malignant characteristics of PDAC cells, including migration, invasion, and sphere formation abilities [380]. However, the direct targets of HuR in PDAC malignance was not identified and validated in this study. In summary, HuR is considered to be a stress response factor of PDAC to conquer harsh tumor microenvironment, such as hypoxia, nutrient deprivation, and chemotherapy, resulting in the adaptive survival of PDAC cells. The inhibition of HuR holds the potential to inhibite PDAC proliferation, chemoresistance, invasion, and metastasis.

Considering the importance of HuR in carcinogenesis, to date, many efforts has been made on the development of small molecule HuR inhibitors. MS-444 is the first in class HuR inhibitor, which mainly inhibit the HuR homodimerization. MS-444 was isolated from the culture broth of a bacterial strain KY7123 and was initially discovered as a myosin light chain kinase inhibitor [381]. MS-444 inhibits HuR homodimerization before RNA binding, and thus leads to the interruption of HuR trafficking and suppression of HuR cytoplasmic localization. MS-444 exhibits activities in inhibiting tumor progression, tumorigenicity, and chemoresistance in several types of cancer. Blanco FF et al. found that MS-444 inhibited colon cancer cell proliferation *in vitro* and tumorigenicity *in vivo* by inhibiting HuR trafficking and cytoplasmic localization [382]. In malignant glioma, MS-444 inhibited the proliferation and invasion of highly chemoresistant brain tumor initiating cells (BTICs) [383]. In pancreatic cancer, MS-444 inhibited an hypoxia-induced protein, PIM1, and significantly enhanced the sensitivity of PDAC cells to oxaliplatin and 5-FU treatment [366]. Several other HuR inhibitors have different mechanisms of action. Dihydrotanshinone-I (DHTS), which is a natural compound extracted form *salvia miltiorrhiza*, bound to the inter-domain region between RRM1 and RRM2 of HuR,

thus disrupted the binding of HuR with target mRNAs [384]. In colon cancer, DHTS inhibited the tumor sphere formation and tumor growth in an HuR dependent manner [385]. However, DHTS has paradoxical effects on HuR inhibition. DHTS only interrupted the HuR/mRNA complex with low AU-rich density mRNAs, whereas promoted the binding of HuR to high AU-rich density mRNAs. Pyrvinium pamoate, an FDA-approved anthelminthic drug, is recently identified as a novel HuR inhibitor. Pyrvinium pamoate activated the AMP-activated kinase/importin α1 cascade, and thus inhibited CDK1 dependent HuR cytoplasmic localization [386].

A recent fluorescence polarization assay based high-throughput screening of ~6000 compound was carried out by our collaborators, and successfully identified a cluster of potential HuR disruptors. In this study, Wu X et al. screened ~6000 compounds from an FDA-approved drug library and a KU Chemical Methodologies and Library Development Center (CMLD) compound library (www.cmld.ku.edu). The screen yields 38 positive hits. Among them, CMLD-2 was the most potent in HuR/mRNA disrupting. CMLD-2 also demonstrated cytotoxicity effects on colon cancer cells and pancreatic cancer cells. The IC_{50} of CMLD-2 on normal cells, WI-38, was significantly lower than it was in colon cancer and pancreatic cancer cells, indicating the potential of CMLD-2 to serve as a therapeutic agent against colon cancer and pancreatic cancer. Numerous other HuR disruptors, such as tanshinone mimics, quercetin and b-40, dehydromutactin, and okicenone are currently under investigation [387-390].

Taken together, HuR has been considered as a novel and promising therapeutic target in cancer managements. However, there are still gaps of knowledge on how HuR is involved in the invasiveness and stemness features of PDAC. In addition, there is no success in HuR inhibitors in clinical trials for their anti-tumor effects. There is a need in developing novel HuR inhibitors

that directly interrupt the binding of HuR with its target mRNAs. The comprehensive investigation on the role of HuR in PDAC also benefits the development of HuR inhibitors for PDAC management.

Chapter 2. Statement of Purpose

The purpose of this study is to develop and investigate anti-tumor agents, including natural sourced products and synthetic small molecule compounds, on inhibiting pancreatic cancer EMT and CSCs *in vitro* and *in vivo*. We hypothesized that: 1) the inhibition of pancreatic cancer EMT and CSCs could inhibit pancreatic cancer metastasis and tumorgenicity; 2) The inhibition of the RNA binding protein HuR could contribute to the inhibition of pancreatic cancer EMT and CSCs. To test our hypothesis, we performed studies by focusing on the following specific aims.

2.1. Specific aim 1: To investigate the anti-tumor effects of medical plant extracts on pancreatic CSCs *in vitro* and *in vivo*. (Chapter 4 and 5)

Extracts of two traditional medical plants, Pao Pereira (Pao) and *Rauwolfia vomitoria* (Rau), were tested for their activities against pancreatic cancer cells. Their activities in inhibiting the CSC population were examined using *in vitro* and *in vivo* models.

MTT assay was used to test the cytotoxicity of the two natural products on a panel of pancreatic cancer cell lines, including PANC-1, MIA PaCa2, AsPc-1, BxPc-3, and HPAF-2, and compared with immortalized normal fibroblast cells, MRC5. Tumor sphere formation assay and pancreatic CSC surface markers (CD24+CD44+EpCAM+) analysis were performed to test the effects of Pao and Rau on inhibiting pancreatic CSC population. A DCV staining-based flow cytometry cell sorting was developed to isolate a side population with enriched pancreatic CSCs (DCV- cells) from the whole cell population. The cytotoxicity of Pao and Rau on unsorted cells, non-CSC-like cells (DCV+), and CSC-like cells (DCV-) was examined with MTT assay and tumor sphere formation assay. Western blot was utilized to examine the level of Nanog and nuclear β-catenin as stem feature related proteins. Moreover, the expression of β-catenin downstream target genes and CSC-related genes was examined with RT-qPCR. *In vivo* tumorigenicity of pancreatic

cancer cells with the treatment of Pao or Rau was examined with a subcutaneous pancreatic cancer xenograft mouse model.

2.2. Specific aim 2: To investigate the function of the RNA binding protein HuR in pancreatic cancer EMT and CSCs. (Chapter 6)

Our working hypothesis is that HuR stabilizes the mRNAs of EMT and CSC-related genes, thus promotes pancreatic cancer EMT and CSCs. A loss-of-function model and a gain-of-function model were used to test our hypothesis.

siRNA based HuR knockdown and CRISPR/Cas 9 HuR gene deletion were both performed as an *in vitro* model for a loss-of-function analysis. With this model, we tested cell migration, invasion, stemness features, and the level of EMT markers and EMT-TFs with following assays: wound healing assay and boyden chamber invasion assay were performed to test cell mobility, migration, and invasion. Tumor sphere formation assay was utilized to examine the stemness features. The level of EMT markers and EMT-TFs, including Claudin-1, Vimentin, ZO-1, and Snail was examined by using western blot and immunofluorescence staining.

The restoration of HuR in HuR KO MIA PaCa2 cells was performed for a gain-of-function analysis. With this model, we tested cell migration ability, the level of EMT markers and EMT-TFs by using wound healing assay and western blot.

Ribonucleoprotein immunoprecipitation (RNP-IP) and RNA decay assay were then performed to examine the binding of HuR with target mRNAs. The binding motifs of target mRNAs were then examined with dual luciferase reporter assay. Nude mice with subcutaneously inoculated HuR KO MIA PaCa2 cells were utilized as an *in vivo* loss-of-function model. Tumorigenicity was then tested by evaluating tumor formation rate and tumor growth in this model.

2.3. Specific aim 3: To investigate the activity of a novel HuR inhibitor against pancreatic cancer EMT and CSCs. (Chapter 7)

The working hypothesis is that pharmacological inhibition of HuR inhibits pancreatic cancer EMT and CSCs. We utilized a novel small molecule, namely KH-3, as a pharmacological inhibitor of HuR, to test our hypothesis.

Given that KH-3 had a source coming from HDAC inhibitor structural derivatives, western blot was first used to test the residue HDAC inhibition effect of KH-3, compare with SAHA and MS-175. Fluorescence polarization assay, alpha assay, and surface plasmon resonance assay were used to verify that KH-3 is an HuR inhibitor by directly binding to HuR and disrupting HuR/mRNA complex. The cytotoxicity of KH-3 on different pancreatic cancer cell lines, including PANC-1, MIA PaCa2, and BxPc-3, as well as an immortalized normal pancreatic ductal cell line, hTERT-HPNE was examined with MTT assay. Wound healing assay, boyden chamber invasion assay, and tumor sphere formation assay were utilized to test cell migration, invasion, and stemness features with KH-3 treatment. Western blot and immunofluorescence staining were applied to detect the expression of EMT signature proteins with KH-3 treatment. RNP-IP assay, RNA-decay assay, and dual-luciferase reporter assay were performed to test the disruption of HuR/mRNA binding with KH-3 treatment. In addition, a loss-of-target analysis was performed with wound healing assay as an *in vitro* model and subcutaneous xenograft mice as an *in vivo* model. The effects of KH-3 on pancreatic cancer progression and metastasis was tested in an orthotropic xenograft mouse model.

Chapter 3. Materials and Methods

3.1. Cell culture and cell viability assay

Pancreatic cancer cell lines (PANC-1, MIA PaCA2, AsPC-1, HPAF-II, and BxPc-3) were from the American Type Culture Collection (Manassas, VA). An immortalized human pancreatic ductal epithelial cells line (hTERT-HPNE) was donated by Dr. Shrikant Anant at the University of Kansas Medical Center. An immortalized human lung epithelial cell line (MRC-5) were provided by Dr. Sitta Sittampalam at the National Center for Advancing Translational Sciences, NIH. All cells were sub-cultured in our lab in recommended media supplemented with 10% fetal bovine serum (FBS) (Sigma Aldrich, St. Louis, MO), 100 units/ml penicillin/streptomycin (Sigma Aldrich, St. Louis, MO) at 37 °C in a humidified 5% CO_2 atmosphere.

MTT assay was used for cell viability detection. Cells were plated into 96 well plates at a starting density of 3000 cells/well (for 72 hours treatment) or 5000 cells/well (for 48 hours treatment). At the end of treatment, the media was replaced with 120 µL/well fresh media containing 0.5 mg/ml MTT (3-(4,5-dimethylthiazol-2-yl)-2,5-diphenyltetrazolium bromide) (Sigma Aldrich, St. Louis, MO). The plates were incubated for 4 more hours at 37°C in a humidified 5% CO_2 atmosphere. Formazan crystals were then dissolved by 100 µL/well DMSO. Cell viability was obtained by measuring the purple color at an absorbance wavelength of 570 nm on a micro-plate reader (BioTek, Winooski, VT).

3.2. Wound healing assay (Scratch assay)

Cells were seeded into 24-well plate and cultured to reach >90% confluence. Scratch was made by scraping a straight line in the central of cell monolayer with a 100 µL sterile pipette tip. Cells were washed immediately with sterile PBS to remove debris. Photographs were captured at 0 hours of treatment, and multiple time points during the treatment, with 20x magnification. The

extent of wound healing was calculated by 100% - [(area of the remaining scratch at specific time point ÷ areas of original scratch at 0 hours) x 100%].

3.3. Matrigel invasion assay

Cells were seeded into the boyden chambers (BD Biosciences, San Jose, CA) that were either pre-coated or not coated with 1 mg/ml matrigel (BD Bioscience, San Jose, CA), at 1 x 10^4 cells per chamber in 0.5% FBS containing media. Boyden chambers were then inserted into 24 well plates, with 10% FBS containing media outside the chamber as a chemo-attractor. At the indicated time points in each experiment, the remaining cells inside the chamber were carefully removed using cotton swab. Cells that invaded to the bottom-side of the chamber were washed twice with cold PBS and fixed with 100% ice cold methanol for 10 minutes on ice. Fixed cells were then stained with 0.05% crystal violet for 10 minutes at room temperature and photographed with 10x magnification for cell counting. At least 3 fields per boyden chamber were imaged. Cell number in each image was measured using image J.

3.4. RNA isolation, cDNA synthesis, and real-time PCR

Total RNA was extracted from cells or tissue samples using TRIZOL reagent according to the manufacturer's protocol (Invitrogen, Grand Island, NY). cDNA synthesis was performed with 1 µg of total RNA using Omniscript RT kit according to manufacturer's protocol (Qiagen, Valencia, CA). cDNA was then diluted 1:4 in DEPC treated nanopure water and used for further analysis. Real-time PCR was performed using Bio-Rad iQ iCycler detection system with iQ SYBR green supermix (Bio-Rad Laboratories Ltd, Hercules, CA). Reactions were performed in a total volume of 10 µL, including 5 µL of 2x iQ SYBR green supermix, 1µL of primers at 20 pmol/µL, and 1 µL of cDNA template. All reactions were carried out in at least triplicates for each sample. GAPDH or 18S rRNA was used as housekeeping gene for normalization. Gene

expression quantification used the ΔΔCT method and $2^{(-\Delta\Delta CT)}$ was used as the relative expression changes for each gene. RT-qPCR primers were synthetized by Integrated DNA Technologies (Coralville, IA) and were listed in Table 3.1. RT-qPCR conditions were listed in Table 3.2.

Table 3.1. RT-qPCR primers used in RT-qPCR analysis.

Target mRNA	Sense primer (5' – 3')	Antisense primer (5' – 3')
18s RNA	GGGAGGTAGTGACGAAAAATAACAAT	CCCTCCAATGGATCCTCGTT
BCL2L2	GCGGAGTTCACAGCTCTATAC	AAAAGGCCCCTACAGTTACCA
BMI1	TACTCCAGTGCAGTCTCCTC	TCCCATCTTTCCTAACACAG
Claudin-1	CCTCCTGGGAGTGATAGCAAT	GGCAACTAAAATAGCCAGACCT
Cox-2	CTGGCGCTCAGCCATACAG	CGCACTTATACTGGTCAAATCCC
Dppa4	AAAAGCAAGAAGGGAGAGTGA	CGGAGATTGCACTGAACTGA
E-Cadherin	CGAGAGCTACACGTTCACGG	GGGTGTCGAGGGAAAAATAGG
Essrb	TCAGAGAGCAGCCCATACCT	GCGTCACAAACTCCTCCTTC
GAPDH	CCAGGTGGTCTCCTCTGACTTCAACA	AGGGTCTCTCTCTTCCTCTTGTGCTC
HuR	ACCAGGCGCAGAGATTCA	GGTTGTAGATGAAAATGCACCAG
MMP14	GGCTACAGCAATATGGCTACC	GATGGCCGCTGAGAGTGAC
MSI1	TAAAGTGCTGGGGCAATCG	TCTTCTTCGTTCGAGTCACCA
MYC	TCCCTCCACTCGGAAGGAC	CTGGTGCATTTTCGGTTGTTG
Nanog	ACCTATGCCTGTGATTTGTGG	AAGAGTAGAGGCTGGGGTAGG
Nucleostemin	CAGAGATCCTCTTGGTTGCAG	AATGAGGCACCTGTCTCCTC
Oct4	GAGAATTTGTTCCTGCAGTGC	GTTCCCAATTCCTTCCTTAGTG
Slug	CGAACTGGACACACATACAGTG	CTGAGGATCTCTGGTTGTGGT
Snail	TCGGAAGCCTAACTACAGCGA	AGATGAGCATTGGCAGCGAG
Sox2	ATGGGTTCGGTGGTCAAGTC	GTGGATGGGATTGGTGTTCTC
Tbx3	GAAGAAGAGGTGGAGGACGA	ATTCAGTTTCGGGGAACAAG
Tcl1	GATACCGATCCTCAGACTCCA	GAGGGACAGAAGGGACAGAA
TWIST1	GTCCGCAGTCTTACGAGGAG	GCTTGAGGGTCTGAATCTTGCT
ZEB1	GATGATGAATGCGAGTCAGATGC	ACAGCAGTGTCTTGTTGTTGT
ZEB2	CAAGAGGCGCAAACAAGCC	GGTTGGCAATACCGTCATCC
Zfx	TGATTCCAGGCAGTACCAAAC	TGACGAAAACCCTTACCACAC
ZO-1	ATGGAGGAAACAGCTATATGGGA	CCTGTGAAGCGTCACTGTATG
β-catenin	CATCTACACAGTTTGATGCTGCT	GCAGTTTTGTCAGTTCAGGGA

Table 3.2. RT-qPCR conditions used in RT-qPCR analysis.

Cycling Step	Temperature	Hold Time (m:s)	Number of Cycles
Initial denaturation and enzyme activation	95°C	3:00	1
Denaturing	95°C	0:15	40
Annealing	55-60°C	0:30	
Extension	72°C	0:30	
Melt curve analysis	55-95°C(in 0.5°C increments)	0:30	1

3.5. HuR knockdown/overexpression

Recombinant pcDNA3.1 HuR-flag Plasmid (p-HuR) was provided by Dr. Dixon at the University of Kansas, and the empty vector pcDNA3.1+ (p-Vec) were purchased from Addgene (Cambridge, MA). HuR siRNA was synthetized by Integrated DNA Technologies (Coralville, IA), (Sense: 5'-rGrArGrGrCrArArUrUrArCrCrArGrUrUrUrCrATT-3'; Antisense: 5'-rUrGrArArArCrUrGrGrUrArArUrUrGrCrCrUrCTT-3'). Allstars negative control siRNA was purchased from Qiagen (Qiagen, Germantown, MD). Plasmids were transfected with lipofectamine™ 3000 reagent (Invitrogen, Grand Island, NY), and siRNAs were transfected with lipofectamine™ RNAiMAX reagent (Invitrogen, Grand Island, NY), according to the manufacturer's protocol. The transfection time was 24 hours for siRNAs and 48 hours for plasmid in all the experiments. HuR protein level was detected by western blot.

3.6. CRISPR/Cas9 knockout of HuR gene

The lentiCRISPRV2 vector was purchased from AddGene (Watertown, MA) and the control single guide RNAs (sgRNAs) and HuR sgRNAs were cloned into the vector following published

procedures [391, 392]. The HuR lentiviral sgRNA or control sgRNA were co-transfected into HEK293FT cells with the packaging plasmids pMD2.G and psPAX2 (both from AddGene). MIA PaCa-2 cells were infected with virus medium and then selected with 1.0 µg/mL puromycin. Single clones were generated by limited dilution.

3.7. Ribonucleoprotein immunoprecipitation (RNP-IP) Assay

Total lysate of MIA PaCa-2 HuR wide-type (WT) cells, MIA-PaCa-2 HuR knockout (KO) cells, and KH-3 treated MIA PaCa-2 HuR WT cells (KH-3 2 µM, 24 hours) were prepared and then immunoprecipitated with anti-HuR or normal rabbit IgG (Cell Signaling Technology, Beverly, MA) using the immunoprecipitation kit (protein G) according to the manufacturer's protocol (Roche, Basel, Switzerland). RNaseOUT™ Recombinant Ribonuclease Inhibitor (Invitrogen, Grand Island, NY) was supplemented in all steps at the concentration of 100 U/mL to prevent RNA degradation. In the KH-3 treated cells, KH-3 was supplemented in all steps at the concentration of 2 µM. Total RNA was then extracted from the immunoprecipitation products by using TRIZOL reagent according to the manufacturer's protocol (Invitrogen, Grand Island, NY), and RT-qPCR was used for analysis of interested mRNAs.

3.8. Dual luciferase reporter construction and Dual-Glo luciferase reporter assay

The full-length 3'-UTR of Snail mRNA (full length) was synthesized by Genewiz (South Plainfield, NJ). The two truncated 3'- UTRs of Snail mRNA (ΔAREs, and AREs) were cloned from total RNA of MIA PaCa-2 cells using the PCR primers and PCR conditions described in Table 3.3. The ΔAREs sequence does not containing any AU-rich HuR binding elements, whereas the AREs sequence contains the major part of the AU-rich elements in the 3'-UTR of Snail mRNA as demonstrated in Fig 6.12 A. A Sanger sequencing was then performed by Genewiz (South Plainfield, NJ) to verify the fidelity of ΔARE and AREs. Full length, ΔAREs,

and AREs were digested with SalI (5') / XbaI (3') and then ligated into pmiGLO dual luciferase reporter plasmid (Promega, Madison, WI), respectively, using T4 DNA Ligase (Promega, Madison, WI). The transformation of JM109 competent cells (Promega, Madison, WI) with the re-constructed plasmids were then performed for plasmids cloning. Re-constructed plasmids were then extracted by using PureYield™ Plasmid Miniprep System (Promega, Madison, WI).

In Dual-Glo luciferase reporter assay, MIA PaCA-2 HuR KO cells were co-transfected with pmirGLO dual luciferase reporter plasmid with or without the constructions (either full length, ΔAREs, AREs, or empty reporter) (Promega, Madison, WI) and pCDNA-3.1+-HuR (or empty vector) by using Lipofectamine 3000 reagent (Invitrogen, Grand Island, NY). KH-3 was added at 24 hours, and the dual-glo luciferase reporter assay was performed at 48 hours using Dual-Glo® Luciferase Assay System (Promega, Madison, WI).

Table 3.3. PCR primers and other conditions used in the construction of dual-luciferase plasmid in luciferase reporter assay.

Sequences	Primers (5' – 3')		PCR condition	Enzyme digestion, ligation and transformation condition
ΔAREs	Sense	AATCTCTAGACCCTC GAGGCTCCCTC	98 °C, 30 s; 98 °C, 10 s/55 °C, 30 s/66 °C, 5 m – 10 cycles; 98 °C, 10 s/60 °C. 10 s/72 °C, 30 s – 30 cycles; 72 °C, 5 m	Enzyme digestion: SalI/XbaI 10U, 37°C, 3 hours; Ligation: 2.5 or 5ng of insert DNA and 50ng of linearized vector using a standard ligation protocol; Transformation: JM109 competent.
	Antisense	GACCGTCGACGGTC TTCATCAAAGTCCTG		
AREs	Sense	AATCTCTAGACAGGC AGCTATTTCAGC	98 °C, 30 s; 98 °C, 10 s/44 °C, 30 s/66 °C, 5 m – 10 cycles; 98 °C, 10 s/60 °C. 10 s/72 °C, 30 s – 30 cycles; 72 °C, 5 m	
	Antisense	GACCGTCGACTTTAA TATATAAATTAACTGC		
Whole Length	Synthesized by GENEWIZ			

3.9. SDS PAGE and western blot

Cells were lysed with RIPA buffer containing protease inhibitors and phosphatase inhibitors (Sigma Al), followed by sonication for 10 seconds. BCA method was used for protein quantification (Pierce BCA protein assay kit, Waltham, MA). SDS-PAGE and Western blot was performed as routine: 10 µg total protein (2 µg protein for nuclear and cytoplasmic proteins) was run on a 10% SDS-PAGE gel, and then transferred to PVDF membrane (ED Millipore, Burlington, MA) overnight at 4 °C. Membrane was then blocked with 5% blocking grade blocker (Bio-Rad, Hercules, CA) in 1xTBS-T (Tween-20, 0.1%) for 2 hours at room temperature with constant shaking. Primary and secondary antibodies were from Cell Signaling Technology Inc. (Danvers, MA): rabbit anti-clauidn-1 (1:250), rabbit anti-vimentin (1:1000), rabbit anti-snail (1:500), rabbit anti-β-catenin (1:1,000), rabbit anti-vinculin (1:1,000), rabbit anti-Histone H3 (1:2,000), rabbit anti-Nanog (1:2,000), mouse anti-β-actin (1:2,000), goat anti-rabbit or anti-mouse IgG (1:5,000); or Millipore (Burlington, MA): rabbit anti-HuR (1:1000). Primary antibodies were incubated overnight at 4 °C and secondary antibodies were incubated at room temperature for 2 hours. Blots were established using a chemiluminescence detection kit (Pierce ECL western blotting substrate/Pierce ELC+ western blotting substrate, Thermo Scientific, Rockford, IL).

3.10. Immunofluorescence and immunohistochemistry

Cells grown on 8-well chamber slide were treated and then fixed in 4% paraformaldehyde and blocked in blocking buffer (1x PBS + 5% Goat serum + 0.3%Triton X-100) at room temperature for 1 hour. Rabbit anti-clauind-1 primary antibody (1:200, Cell Signaling Technology, Beverly, MA) was incubated overnight at 4 °C. Anti-rabbit IgG (H+L), F(ab')2 Fragment (Alexa Fluor® 488 Conjugate) secondary antibody (1:500, Cell Signaling Technology, Beverly, MA) was

incubated at room temperature for 2 hours. Nucleus were then stained overnight with a DAPI-containing ProLong® Gold Antifade Reagent (Cell Signaling Technology, Beverly, MA).

Paraffin-embedded tumor sections (5 μM thick) were deparaffinized and then rehydrated by serial incubation in xylene, 100% ethanol, 95% ethanol, and distilled deionized water. Endogenous peroxide was blocked by hydrogen peroxide blocking buffer provided in mouse and rabbit specific HRP/DAB (ABC) detection IHC kit (Abcam, Cambridge, UK) at room temperature for 10 minutes. Antigen retrieval was performed in boiling citrate buffer for 5 minutes followed by sub-boiling temperature for 20 minutes. Mouse anti-HuR primary antibody (1:500, Santa Cruz Biotechnology, Santa Cruz, CA) was incubated overnight at 4 °C. Biotinylated goat anti-polyvalent antibody and DAB were provided in mouse and rabbit specific HRP/DAB (ABC) detection IHC kit (Abcam, Cambridge, UK) and were used to develop the tumor sections. All the sections were then counterstained with hematoxylin.

3.11. mRNA stability assay

MIA PaCa-2 HuR WT and MIA PaCa-2 HuR KO cells were treated with actinomycin D at the concentration of 5 μg/mL to block transcription. Cells were collected for total RNA extraction at 0 hours, 0.5 hours, 1 hour, 2 hours, and 3 hours after actinomycin D treatment.

In KH-3 treated MIA PaCa-2 WT group, cells were treated with actinomycin D for 30 minutes at the concentration of 5 μg/mL, followed by adding KH-3 at the concentration of 2 μM. Cells were collected for total RNA extraction at 0 hours, 0.5 hours, 1 hour, 2 hours and 3 hours after KH-3 treatment. Gene expression was analyzed by using RT-qPCR and normalized to 18S rRNA.

3.12. Tumor sphere formation assay

Single cell suspension was planted into 96 well ultra-low attachment plates (Corning Inc., Corning, NY) at a density of 100 cells/well in stem cell media and incubated at 37°C in a humidified atmosphere of 95% air and 5% CO_2. The stem cell media consist of DMEM (Corning Inc., Corning, NY) supplemented with 1x B-27 supplement, 20 ng/mL human basic fibroblast growth factor, 20 ng/mL epidermal growth factor, 100 units/mL penicillin/streptomycin (Invitrogen, Grand Island, NY), and 4 μg/mL heparin calcium salt (Fisher Scientific, Pittsburg, PA). Tumor spheres were counted after 14 days under the microscope. Size of the spheres was measured using Image J software.

3.13. Flow cytometry in pancreatic CSCs detection

Cells were exposed to various concentrations of the plant extract Pao or Rau for 24 hours or 48 hours. Cells were then washed three times in PBS and re-suspended in binding buffer (PBS supplemented with 0.1% bovine serum albumin) for 15 minutes. PE conjugated anti-CD24 antibody, PE-Cy7 conjugated anti-CD44 antibody, and APC conjugated anti-EpCam antibody (Biolegend, San Diego, CA) were added into Pao-treated cell suspension and incubated for 15 minutes according to the manufacturer's protocol. Cells were then washed three times in PBS before flow cytometry analysis with BD LSR II flow cytometer (BD Biosciences, San Jose, CA). Data was normalized to cell death (normalized CSC population = original CSC population detected with flow cytometry x % cell viability detected with MTT assay).

The plant extract Rau has strong auto-fluorescence in 2 ranges of emission wavelength: 400 nm - 600 nm and 800 nm - 900 nm, which overlap the emission wavelength of many fluorescent labeling molecules. Therefore, we used PE-Cy7 conjugated CD24 and APC conjugated EpCam

antibodies as indicative markers for pancreatic CSCs (CD24+EpCam+) to avoid overlapping with Rau auto-fluorescence.

3.14. Flow cytometry in pancreatic cancer side population cell sorting

Dye Cycel Violet (DCV) (Invitrogen, Grand Island, NY) was used for staining of the non-CSC population. Cells that efficiently exclude DVC from cytoplasm are considered CSC-like population (DCV negative cells). MIA PaCa-2 cells were suspended at a density of $1x10^6$ cells/ml in DMEM supplemented with 10% FBS and 10 mM HEPES. DCV (10 µM) were added and incubated for 30 minutes at room temperature. Cells were then washed twice in PBS and re-suspend in DMEM supplemented with 10% FBS and 10mM HEPES for 1 hour. Cells were transferred to ice-cold HBSS/2%FBS/10mM HEPES buffer right before flow cytometry sorting. The DCV negative and positive cells were separately collected for further analysis. Gate setting was performed by using cells treated with a pump inhibitor Verapamil (200 µM) prior to DCV staining.

3.15. Fluorescence polarization (FP) assay

pTBSG-HuR and pTBSG-RRM1/2 plasmids encoding full-length human antigen R (HuR) and the RNA recognition motifs 1 and 2 (RRM1/2, residues G18-N186) of HuR, respectively, were constructed by KU COBRE-PSF Protein Purification Group. Musashi1 (MSi1) RNA oligo (5′-GCUUUUAUUUAUUUUG-3′ with 3 ′ fluorescein or 3 ′ biotin) was purchased from Dharmacon (Thermo Scientific, Lafayette, CO). RNAs were pretreated by heating at 95°C for 5 minutes and immediately cooling on ice for 5 minutes. In the fluorescence polarization assay, experiments were performed in 96-well black plates (Corning, Corning, NY) with a final volume of 100 µl using the BioTek Synergy H4 plate reader (Biotek, Winooski, VT). 25 nM full-length HuR and 2 nM fluorescein labeled Msi1 RNA oligo were added to the assay buffer (20 mM HEPES pH 7.4,

150 mM NaCl, 1 mM DTT and 0.05% (v/v) pluronic F-68) with a final volume of 100 μL and incubated at room temperature for 30 minutes. Compounds with five doses (2 nM-20 μM) were added to the wells prior to the protein-RNA complex. Anisotropy measurements were taken after incubation at room temperature for 2 hours. IC50 was calculated via sigmoid fitting of dose response curve using Prism 5.0. Ki was calculated using free online software. (http://sw16.im.med.umich.edu/software/calcki/).

3.16. Amplified Luminescent Proximity Homogeneous Assay (Alpha assay)

Experiments were performed in 96-well white 1/2 area plate (Perkin Elmer, Waltham, MA) with a final volume of 50 μL. Multiple doses of compounds were added to the wells first, followed by pre-formed RRM1/2-Msi1 complex (100 nM RRM1/2 protein and 25 nM Msi1 RNA), donor beads and acceptor beads (Perkin Elmer, 20 μg/mL final concentration). Measurements were taken after incubation at room temperature for 2 hours. IC50 and Ki were determined as described in FP assay.

3.17. Surface Plasmon Resonance (SPR) assay

The SPR experiments were performed using a BIACORE 3000 (GE Healthcare) at 20 °C and used to study the binding interaction of KH-3 with either full length HuR or RRM1/2 of HuR. The ligands, HuR or RRM1/2 were immobilized using the standard primary amine coupling reaction and followed by standard procedures. The sensor chip surface was initially activated with a 1:1 mixture of N-hydroxysuccinimide (NHS, 115 mg/mL) and N-(3- dimethyl-aminopropyl)-N'-ethyl-carbodiimide-hydrochloride (EDC, 750 mg/mL) for 7 minutes each with a flow rate of 5 μL/minute. Full-length HuR protein or RRM1/2 protein was then applied to the flow cells in 10 mM sodium acetate, pH 4.5, and immobilized to a density of 7200 RU and 3800 RU (response units), respectively. An adjacent flow cell was left blank to serve as a reference

surface. The activated carboxylic acid groups were quenched with a 7-minute injection of ethanolamine (1 M, pH 8.5). To collect kinetic binding data, compound KH-3 in 20 mM HEPES pH7.4, 150 mM NaCl, 3 mM EDTA, 0.05% p20 (v/v), 5% DMSO (v/v), were injected over the flow cells at the indicated concentrations at a flow rate of 60 μL/minute and at 20 °C. The complex was allowed to associate for 4 minutes and dissociate for 3 minutes. Considerable care was taken to prevent contamination. Samples were carefully injected to avoid carryover effects and the system was carefully washed before injection of each new sample. The sample flow rate was set at 60 μL/minute to determine the kinetic and equilibrium constant. The equipment surfaces were washed extensively with buffer solution to restore the surfaces before each binding experiment. Data analysis was performed using BIA evaluation software. Data analysis and sensor grams were automatic corrected for nonspecific bulk refractive index effects. Standard procedures for the 1:1 Langmuir binding fit model were used for the kinetic analysis of ligand binding to the protein.

3.18. Pancreatic cancer xenograft mouse model for Pao or Rau treatment

All animal studies followed a protocol approved by the Institutional Animal Care and Use Committee of the University of Kansas Medical Center #2015-2247. One-time treatment and repeated treatment were used for measurement of tumorigenicity. In the one-time treatment model, pancreatic cancer cells, PANC-1, were used for tumor inoculation at 3 different numbers: $2x10^4$ cells per injection, $2x10^5$ cells per injection, or $1 x10^6$ cells per injection. PANC-1 cells were suspended in PBS as single cell suspension and then mixed with either 200 mg/mL Pao, Rau or PBS. At each cell injection number, cells mixed with Pao or Rau were injected subcutaneously into the left flank of female Ncr nu/nu mouse, and cells mixed with PBS into the

right flank of the same mouse. Ten mice were used for each cell number. Tumor formation and tumor size were monitored and measured daily with a caliper.

In the repeated treatment model, single cell suspension of PANC-1 cells were mixed with 200 mg/mL Pao or Rau and then inoculated into both left and right flanks of 10 female Ncr nu/nu mice at 2 x 10^5 cells per injection. Treatment started the next day with oral gavage of 20 mg/kg Pao or Rau respectively, 5x per week for 3 weeks. Control group (10 mice) was inoculated with the same number of cells in PBS and was gavaged with equivalent volume of saline solution. Tumor formation and tumor size were monitored and measured daily with a caliper.

3.19. Pancreatic cancer xenograft mouse model for KH-3 treatment

All animal procedures were approved by the Institutional Animal Care and Use Committee at the University of Kansas Medical Center under the protocol #2015-2247. Dose of KH-3 was pre-determined by a dose finding pilot experiment to be 100 mg/kg body weight, intraperitoneal injection (IP), 3x weekly. All treatment concerning KH-3 used this dose regimen. A 5-FU treatment group with 50 mg/kg, intraperitoneal injection (IP), 2x weekly was included as a chemo-treatment positive control. Control mice were intraperitoneally injected with the vehicle solution for KH-3 (5% Tween-80, 5% ethanol) and at the same volume as KH-3 treated mice.

A subcutaneous tumor model was used to determine tumor formation rate. MIA PaCa-2 HuR WT cells or MIA-PaCa-2 HuR KO cells were inoculated into the flank of female Ncr nu/nu mouse at the number of 2x10^6 cells in PBS. Tumor formation was closely monitored daily, and tumor size was measured 3 times/week using a digital caliper.

An orthotopic pancreatic tumor model was used to determine treatment effects of KH-3. Luciferase-expressing PANC-1 cells (PANC-1–Luc, multi-clones) were established by the

Preclinical Proof of Concept Core Laboratory (University of Kansas Medical Center, Kansas City, KS). At the inoculation, female Ncr nu/nu mice (donor mice, n=5) was put under anesthesia by inhalation of 2-5% isoflurane, and a small subcostal laparotomy was performed. The pancreas was carefully identified and lifted with tweezers, and 2×10^5 PANC-1-Luc cells in 50 μL PBS were injected into the tail of pancreas. After 11 days, the solid tumors inside the pancreas of these donor mice were resected. Normal pancreatic tissues surrounding the tumor bulk were carefully removed. The tumor tissues were minced into small pieces of 1 mm^3 cube and implanted into the recipient nude mice (n=30). At the implantation, a tissue pocket was created in the pancreas of the recipient nude mice with eye scissors, and one tumor tissue cube was implanted into the tissue pocket. The peritoneum and skin were closed using wound clips. After 11 days, wound clips were removed and the recipient mice were scanned for xenograft formation using an IVIS imaging system (Waltham, MA) upon intraperitoneal injection of 150 mg/kg D-luciferin. Mice were grouped into control group (n=9), KH-3 treatment group (n=10), and 5-FU treatment group (n=10) based on tumor burden. Treatment commenced as described, with weekly follow-up imaging. Treatment lasted for 5 weeks, and gross necropsy was performed at the end of treatment.

3.20. Data analysis

Statistical analysis was performed using SPSS software. Student's t-test was utilized when compare the means between two independent samples in normal distribution. One-way ANOVA with Tukey's test was utilized when compare the means between more than two independent samples in normal distribution. Mann-Whitney's U test was utilized when compare the means between two independent samples in abnormal distribution. A difference was considered significant at the $p < 0.05$ level. Correlation was analyzed by Pearson Test.

Chapter 4. Extract of the Medicinal Plant Pao Pereira Inhibits Pancreatic CSCs *In Vitro* and *In Vivo*

This chapter has previously been published as an open access article (CC BY-NC) and is reprinted here with adaptations. Dong, R., Chen, P., & Chen, Q. (2018). Extract of the Medicinal Plant Pao Pereira Inhibits Pancreatic Cancer Stem-Like Cell *In Vitro* and *In Vivo*. Integrative cancer therapies, 17(4), 1204–1215.
Retrieved from https://doi.org/10.1177/1534735418786027

Natural products have been a rich resource for bioactive anticancer agents. They are used in folk medicines all over the world and have been used by oncologic patients and integrative medicine practitioners for many years. Pao Pereira (*Geissospermum vellosii*) is an Amazonian tree in the Apocynaceae family. This family of plants have been used as a folk medicine in South American to treat a variety of health-related conditions, including cancer [393]. A number of compounds isolated from this family of plants were reported to have antiplasmodial [394], antiviral [395], and antiparasitic [396] bioactivities. The extract of the bark of Pao Pereira (Pao) has long been used in complementary and alternative medicine on cancer patients, and has been reported recently to have tumor inhibitory effect toward prostate, ovarian and pancreatic cancers [393, 397-399]. We previously reported that Pao induced pancreatic cancer cells apoptosis, and inhibited pancreatic tumor growth in mice [398]. The combination of Pao and gemcitabine showed synergistic antitumor effects [398]. Here, we investigated the activities of Pao in inhibiting pancreatic CSCs both *in vitro* and *in vivo*.

4.1. Results

4.1.1. Pao inhibited pancreatic tumor spheroids formation *in vitro*

Five different human pancreatic cancer cell lines (PANC-1, MIA PaCa-2, AsPC-1, HPAF-II, and BxPC-3) and an immortalized epithelial cell line (MRC-5) were treated with Pao, and cell viability was detected after 48 hours. Pao inhibited proliferation of all five cancer cells (**Fig. 4.1. A**), with IC_{50} values ranging from 125 to 325 μg/mL. The noncancerous epithelial cell MRC-5 was less affected, with a higher IC_{50} value of 547 μg/mL (**Fig. 4.1. B**). These results are consistent with our previous studies that Pao inhibited the overall proliferation of pancreatic cancer cells [398].

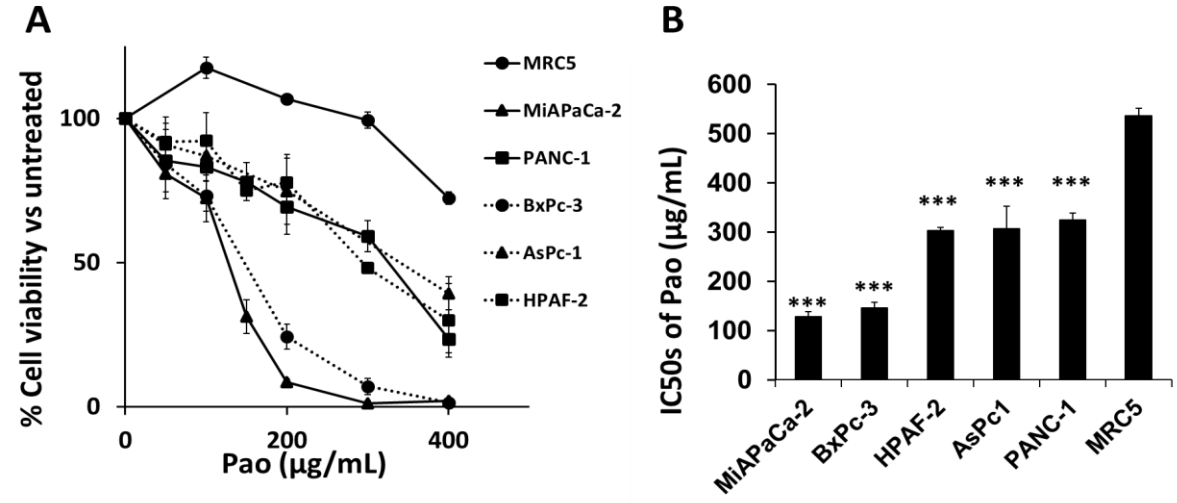

Figure 4.1. Inhibition of the proliferation of pancreatic cancer cells by Pao. (A) Dose-response curves. Human pancreatic cancer cells PANC-1, AsPC-1, HPAF-II, BxPC-3, and MIA PaCa-2 were exposed to serial concentrations of Pao for 48 hours. Cell viability was detected by MTT assay. An immortalized noncancerous epithelial cell line, MCR-5, was subjected to the same treatment. (B) IC50 values of Pao in pancreatic cancer cells and MRC-5 cells. ***$p < .001$ compared with the IC50 of MRC5 cells by one-way ANOVA-Tukey's test. All values are expressed as means ± SD of three independent experiments, each done in triplicates.

To investigate inhibition in CSCs, tumor spheroid formation was detected. The ability to form tumor spheroids is an indication of CSCs' self-renewal and tumorigenic capacity *in vitro*. When cancer cells are cultured in serum-free, nonadherent conditions, the non-CSC population dies by anoikis, whereas CSCs overcome anoikis and go through division leading to formation of tumor spheroids [400, 401]. At the concentration of 50 µg/mL, Pao significantly reduced the number of the PANC-1 tumor spheroids (**Fig. 4.2. A, B**). At the concentration of 100 µg/mL and above, Pao completely eliminated the PANC-1 tumor spheroids (**Fig. 4.2. A, B**). The estimated IC_{50} value for PANC-1 spheroids inhibition is 27 µg/mL. In comparison, the IC_{50} value of Pao to the bulk of PANC-1 cells is about 300 µg/mL (**Fig. 4.1. A**). In the bulk PANC-1 cell population, 100 µg/mL of Pao inhibited the overall proliferation by 20%, whereas 100% tumor spheroids were

inhibited at this concentration (**Fig. 4.2. A**). MIA PaCa-2 pancreatic cancer cells were also subjected to Pao treatment for detection of tumor spheroids. Similar results were obtained. Pao reduced the number of the MIA PaCa-2 spheroids at 50 μg/mL, and completely inhibited spheroid formation at 100 μg/mL and above (**Fig. 4.2. C, D**). The estimated IC_{50} value is 35 μg/mL (**Fig. 4.2. D**), which is much lower than the IC_{50} value to the bulk MIA PaCa-2 cells (**Fig. 4.1. A**).

The side population of cells that exclude dyes is indicative of CSCs [402, 403]. MIA PaCa-2 cells were sorted by flow cytometry to separate CSC-like side populations by DCV staining. Both DCV− cells (CSC-like) and DCV+ (non-CSC-like) cells were collected and treated with Pao. Cell viability was examined by MTT assay. Pao inhibited viability in all unsorted, DCV+ and DCV− cells, with preference in inhibiting DCV− cells (**Fig. 4.2. E**). The estimated IC_{50}s were 147 μg/mL in unsorted cells, 145 μg/mL in DCV+ cells, and 84 μg/mL in DCV− cells. This suggests that Pao preferentially inhibits CSC-like cells.

DCV− cells formed large spheroids as expected. While some cell spheroids were also formed in DCV+ cell culture, they were significantly smaller (**Fig. 4.2. F**). The spheroid formation in DCV+ cells may be due to the DCV staining, and the sorting method is not an exclusive method to pin-point CSCs, as to date there is no efficient way to pinpoint pancreatic CSCs. The DCV staining and sorting, rather, provided us a side population enriched with "stemness." Pao at 50 μg/mL inhibited spheroids from both DCV− and DCV+ populations (**Fig. 4.2. F**), a result consistent with those in unsorted cells.

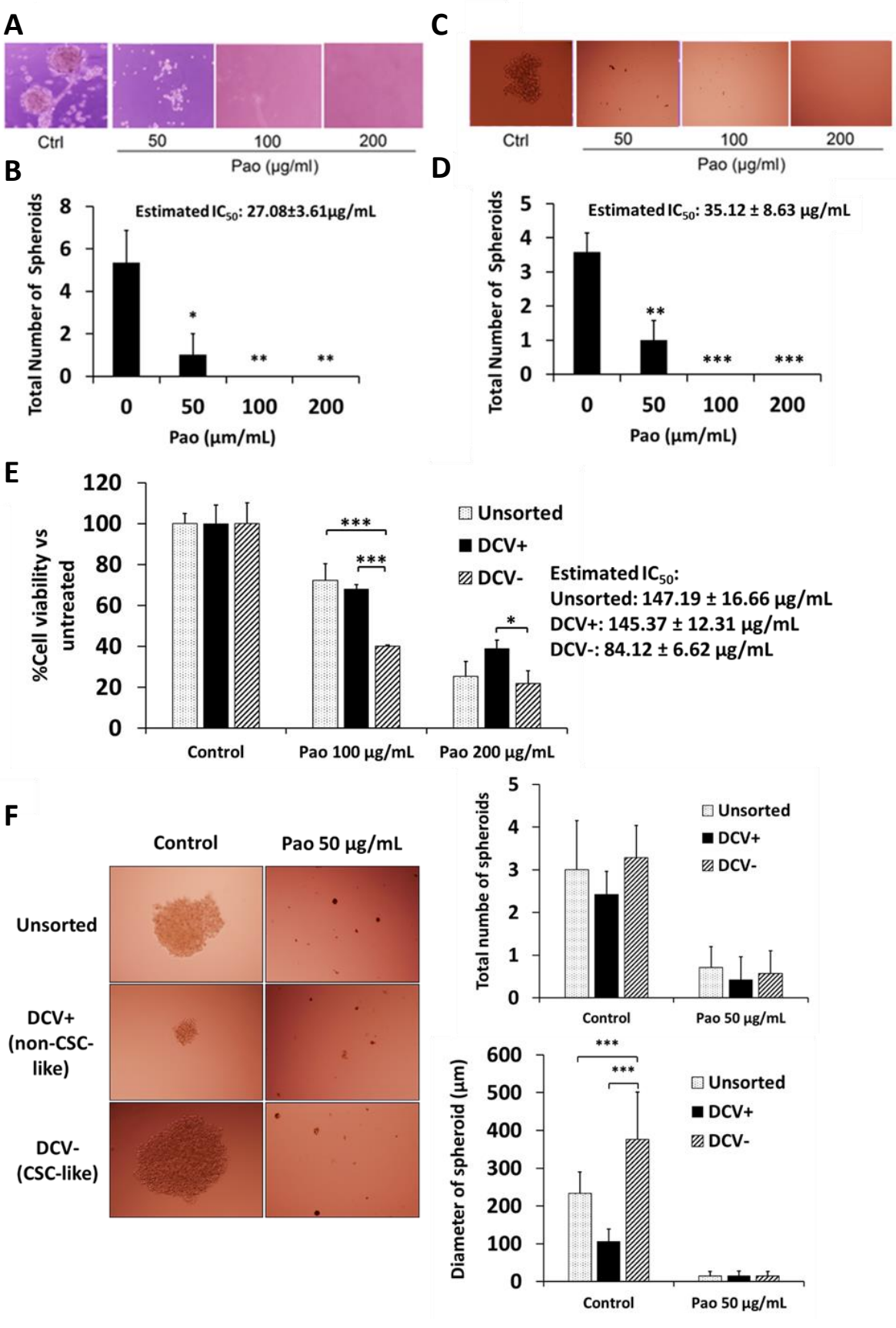
A
Ctrl
50
100
200
Pao (µg/ml)
C
Ctrl
50
100
200
Pao (µg/ml)
B
Estimated IC50: 27.08±3.61µg/mL
Total Number of Spheroids
Pao (µm/mL)
D
Estimated IC50: 35.12 ± 8.63 µg/mL
Total Number of Spheroids
Pao (µm/mL)
E
%Cell viability vs untreated
Unsorted
DCV+
DCV-
Estimated IC50:
Unsorted: 147.19 ± 16.66 µg/mL
DCV+: 145.37 ± 12.31 µg/mL
DCV-: 84.12 ± 6.62 µg/mL
Control
Pao 100 µg/mL
Pao 200 µg/mL
F
Control
Pao 50 µg/mL
Unsorted
DCV+ (non-CSC-like)
DCV- (CSC-like)
Total numbe of spheroids
Unsorted
DCV+
DCV-
Control
Pao 50 µg/mL
Diameter of spheroid (µm)
Unsorted
DCV+
DCV-
Control
Pao 50 µg/mL

Figure 4.2. Inhibition of pancreatic tumor spheroids by Pao. (A) Representative images of the PANC-1 spheroids with and without Pao treatment. PANC-1 single-cell suspension was plated into 24-well ultra-low attachment plates at a density of 5000 cells/well in stem cell media. Tumor spheroids were counted after four weeks. (B) Number of PANC-1 spheroids (means ± SD of three independent experiments). (C) Representative images of the MIA PaCa-2 spheroids with and without Pao treatment. MIA PaCa-2 single-cell suspension was plated into 96-well ultra-low attachment plates at a density of 100 cells/well in stem cell media. Tumor spheroids were counted after two weeks. (D) Number of MIA PaCa-2 spheroids (means ± SD of three independent experiments). (E) Cell proliferation of unsorted cells, DCV+ cells (non CSCs-like) and DCV− cells (CSC-like) with Pao treatment for 48 hours (means ± SD of three independent experiments). (F) Representative images of the MIA PaCa-2 spheroids from unsorted cells, DCV+ cells and DCV− cells with and without Pao treatment. Number and size of MIA PaCa-2 spheroids are shown in bar graph. *$p < 0.05$; **$p < 0.01$; ***$p < 0.001$, compared with untreated control by one-way ANOVA-Tukey's test.

4.1.2. Pao reduced number of pancreatic cancer stem-like cells *in vitro*

The CSC population can be identified by specific cell surface markers. In pancreatic cancer, a subpopulation of cells with high expression of surface markers CD44, CD24, and EpCAM (CD44+ CD24+ EpCAM+ cells) were reported to possess strong self-renewal ability and the ability to produce differentiated progeny and to generate new tumors in mice that were histologically identical to parent tumors [404]. Here, we use these markers as indicative markers for pancreatic CSCs and detected changes in these markers with Pao treatment. PANC-1 cells were treated with Pao for 24 or 48 hours at 50, 100 or 200 μg/mL. CD44, CD24, and EpCAM were examined by immune staining and flow cytometry analysis. Pao reduced the CD44+ CD24+ EpCam+ population at both 24- and 48-hour treatment (**Fig. 4.3. A, B**). In the control group, CD44+ CD24+ EpCam+ cells constituted 7.5% to 9% of the whole population. At the concentration of 200 μg/mL, Pao significantly reduced CD44+ CD24+ EpCam+ cells to 3.05% at 24-hour treatment (**Fig. 4.3. A**), and to 0.37% at 48 hours (**Fig. 4.3. B**). At a lower concentration of 100 μg/mL, Pao reduced the triple positive cells to 2.31% at 48-hour treatment (**Fig. 4.3. B**), which was still a significant reduction compared with control (**Fig. 4.3. B**). We

estimated that the IC_{50} value at 24-hour treatment was 152.97 ± 41.68 µg/mL, and at 48-hour treatment it was 99.53 ± 6.95 µg/mL (**Fig. 4.3. A, B**).

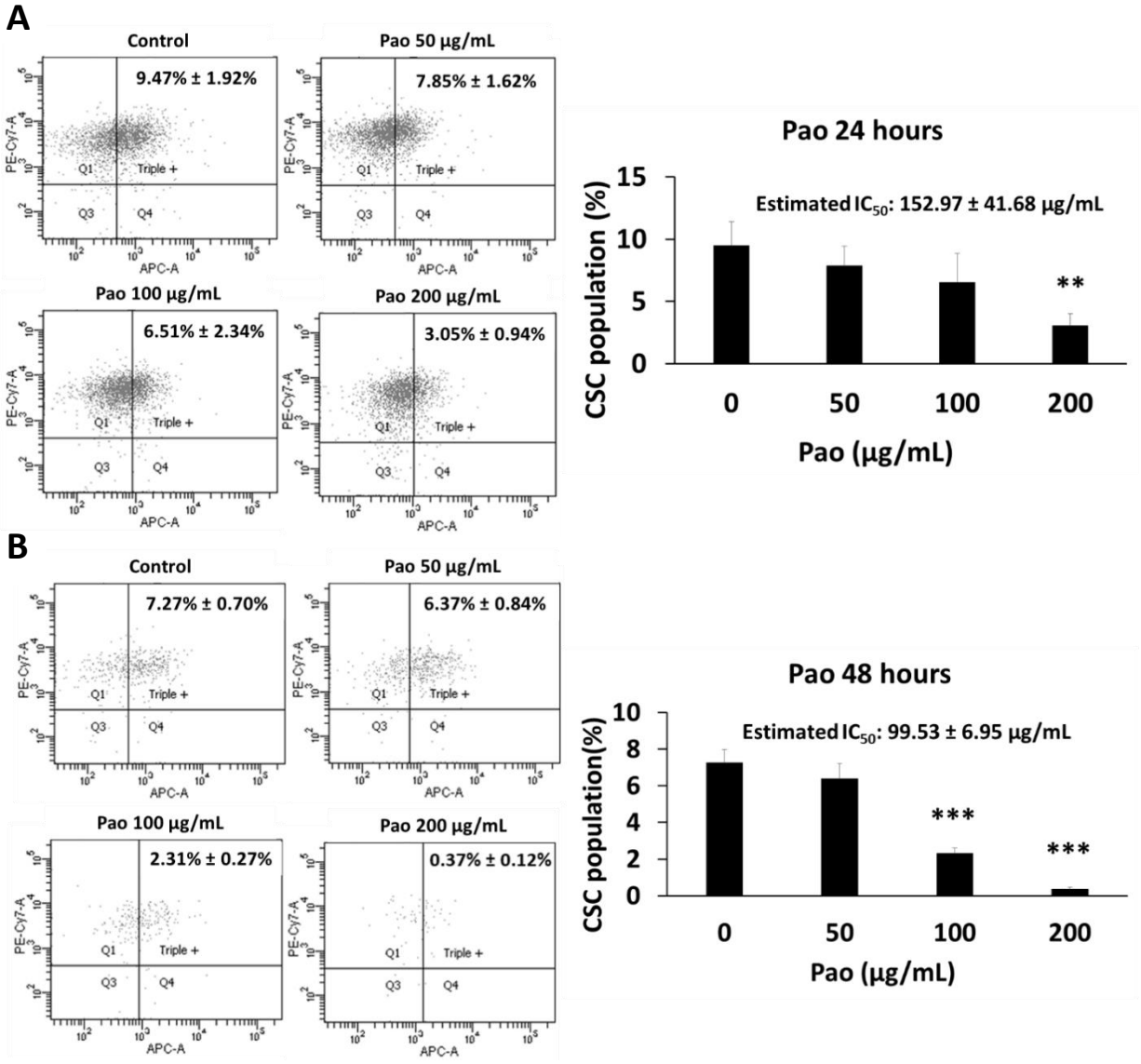

Figure 4.3. Inhibition of CSC population by Pao. PANC-1 cells were treated with Pao for 24 hours (A) and 48 hours (B) at indicated concentrations. Cells were then stained with fluorescent conjugated antibodies for CD24, CD44, and EpCam, followed by flow cytometry analysis. Left panels show EpCam (APC) and CD44 (PE-Cy7) positive cells under CD24 (PE) positive gate. The percentages of CD24+ CD44+ EpCam+ cells were quantified and shown in the bar graph (mean ± SD of three experiments). The data were normalized to cell death. **p < 0.01; ***p < 0.001 compared with untreated group by one-way ANOVA-Tukey's test.

4.1.3. Pao inhabited CSCs relate gene expression *in vitro*

Canonical Wnt/β-catenin signaling pathway plays an important role in maintaining the self-renewal and spheroid formation capacities of CSCs [405, 406]. Accumulation of β-catenin in the nucleus as a transcriptional factor is a hallmark of Wnt/β-catenin pathway activation [181]. Here, the cytoplasmic and nuclear fractions of the PANC-1 cells were each examined for β-catenin levels with or without Pao treatment. Pao 100 μg/mL at 24 and 48 hours reduced the level of β-catenin in both nucleus and cytoplasm, with more severe reduction in nucleus (**Fig. 4.4. A**). A panel of β-catenin downstream target genes, including BCL2L2, COX-2, MMP14, and MYC, were examined by RT-qPCR (**Fig. 4.4. C**). None of these genes were changed at 24-hour treatment. However, at 48-hour treatment, the expression of BCL2L2 and COX-2 was significantly decreased, consistent with Wnt/β-catenin signaling pathway inhibition.

Studies have shown that a stem cell related gene Nanog can induce β-catenin phosphorylation and therefore enhance its degradation, and consequently inhibit Wnt signaling pathway [407]. We therefore examined the expression of Nanog by Western blot. Nanog was increased at 24 hours of Pao treatment but was decreased at 48 hours of Pao treatment (**Fig. 4.4. B**). We postulate that increase in Nanog at the earlier time point suppressed nuclear β-catenin levels, and then the feedback from decreasing β-catenin levels caused inhibition in Nanog expression at a later time point [408, 409]. As a result, both Nanog and the Wnt signaling pathway were inhibited by Pao. A panel of other CSC-related genes were also examined by RT-qPCR, which are reported to be important for CSC initiation and maintenance [410]. Data showed that the expressions of *DPPA4*, *ESRRB*, and *TCL1* were inhibited with 48-hour Pao treatment (**Fig. 4.4. D**).

Taken together, Pao treatment has an early effect in increasing Nanog expression, which leads to β-catenin phosphorylation and degradation, thereby repressing nuclear β-catenin level. The decreasing nuclear β-catenin level negatively influences Nanog expression. Pao treatment may also directly inhibit β-catenin nuclear accumulation. Both can result in an overall suppression of both Nanog and nuclear β-catenin levels (**Fig. 4.4. E**). The full mechanism of Pao-induced CSC inhibition is worth further investigation.

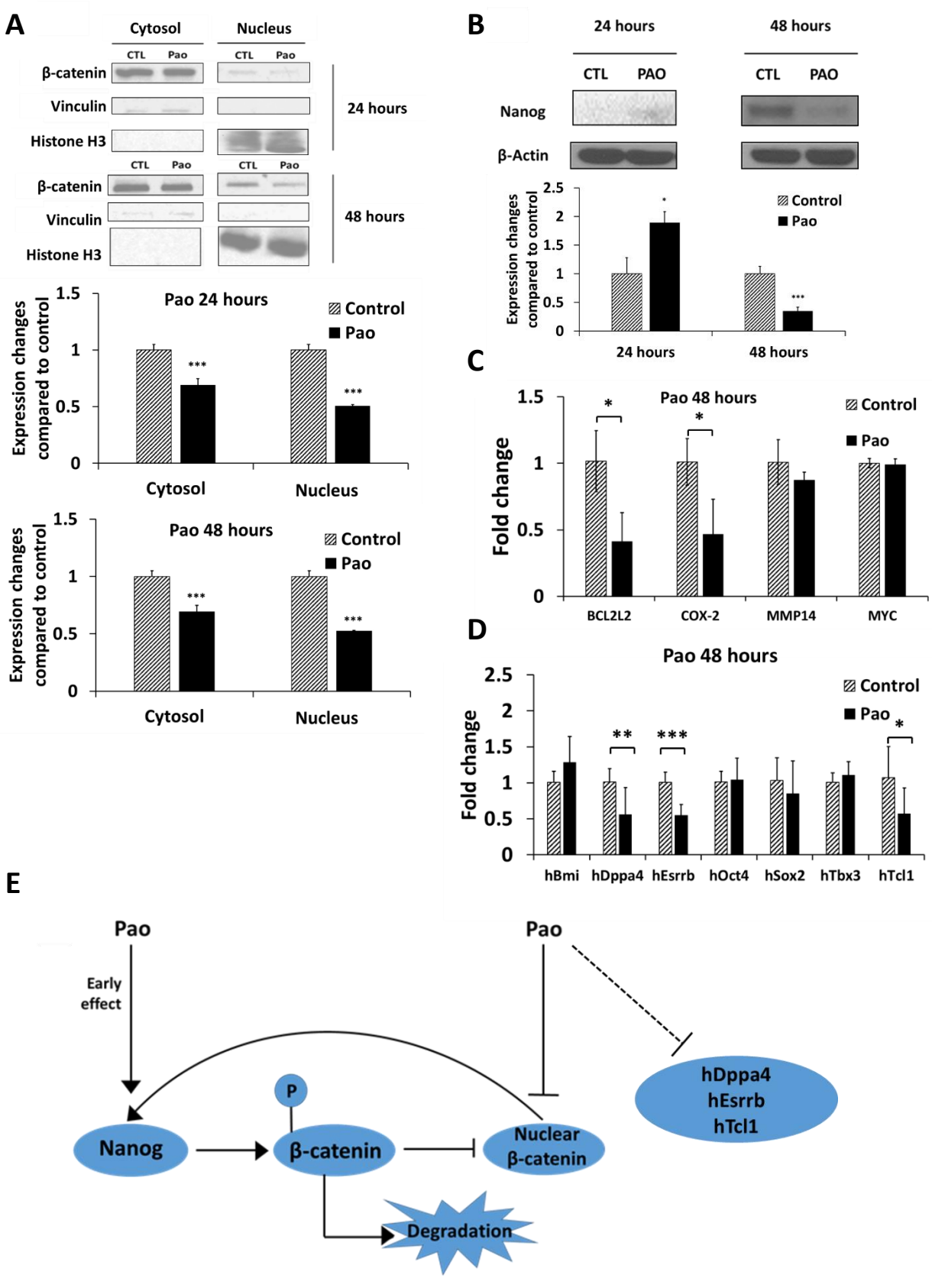
A
Cytosol
Nucleus
CTL
Pao
β-catenin
Vinculin
Histone H3
24 hours
48 hours
Pao 24 hours
Pao 48 hours
Control
Pao
Expression changes compared to control
Cytosol
Nucleus
B
24 hours
48 hours
CTL
PAO
Nanog
β-Actin
C
Fold change
BCL2L2
COX-2
MMP14
MYC
D
hBmi
hDppa4
hEsrrb
hOct4
hSox2
hTbx3
hTcl1
E
Pao
Early effect
P
Nanog
β-catenin
Nuclear β-catenin
hDppa4
hEsrrb
hTcl1
Degradation

Figure 4.4. Decreased expression of CSC-related genes and proteins by Pao. PANC-1 cells were treated with Pao at 100 μg/mL for 24 and 48 hours. (A) β-Catenin levels in cytoplasmic and nuclear fractions, detected by Western blot. Vinculin was a loading control for cytoplasmic proteins, and histone H3 was a loading control for nuclear fraction. Bar graph shows band density normalized to loading control and compared to untreated cells. (B) The expression of Nanog, detected by Western blots. Bar graph shows band density normalized to loading control and compared to untreated cells. (C) The expression of β-catenin downstream target genes at 48 hours of Pao treatment, detected by RT-qPCR. (D) The expression of CSC-related genes after 48 hours Pao treatment, detected by RT-qPCR. (E) Postulated mechanism of Pao inhibiting Nanog and nuclear β-catenin. Pao treatment has an early effect in increasing Nanog expression, which leads to β-catenin phosphorylation and degradation, therefore represses nuclear β-catenin level. The decreasing nuclear β-catenin level negatively influences Nanog expression. Pao treatment may also directly inhibit β-catenin nuclear accumulation. Both can result in an overall suppression of Nanog and nuclear β-catenin levels. Pao also inhibited the RNA level of CSC-related genes, such as *DPPA4*, *ESRRB* and *TCL1*. *$p < 0.05$; **$p < 0.01$; ***$p < 0.001$ compared with the untreated control group by Student's t-test.

4.1.4. Pao inhibited pancreatic CSCs *in vivo*

Tumorigenicity was examined in immunocompromised mice to evaluate the inhibitory activity of Pao against pancreatic CSCs *in vivo*. A one-time treatment was performed first using inoculation of different numbers of PANC-1 cells at limited dilutions. Respectively, 2×10^4 cells, 2×10^5 cells, and 1×10^6 cells were mixed with 200 μg/mL Pao and injected subcutaneously into the left flanks of nude mice (N = 10). As control, the same number of cells were mixed with PBS and inoculated into the right flanks of the same mouse. At all three numbers of cell injections, neither a delay nor a reduction of rate in tumor formation was found (**Fig. 4.5. A, C, E**). The one-time Pao treatment tended to reduce the size of tumors at the 2×10^4 and 2×10^5 cells groups, but there was no significant difference compared with control groups (**Fig. 4.5. B, D, F**).

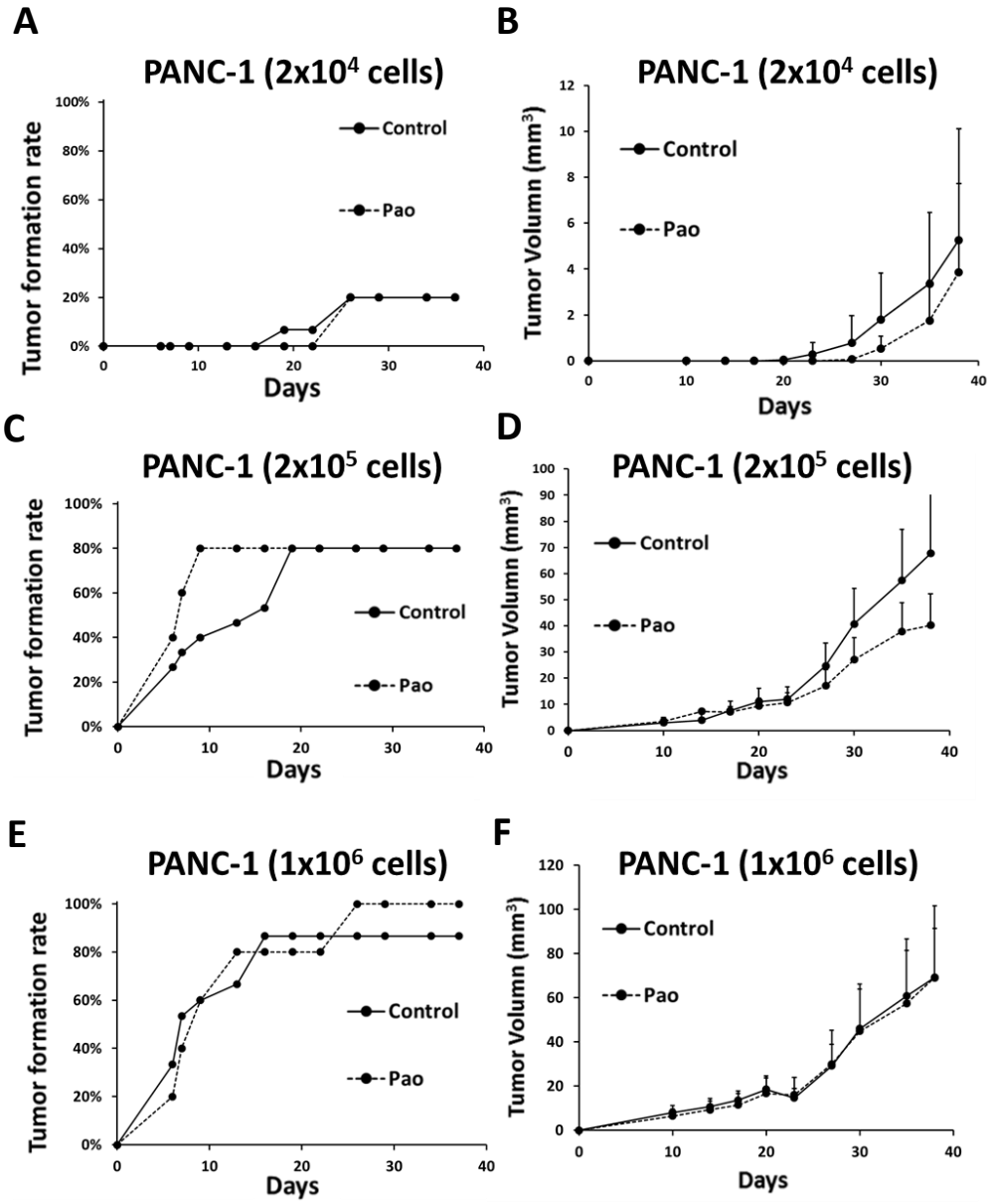

Figure 4.5. Effects of one-time Pao treatment on PANC-1 tumor formation in nude mice. (A, B) 2×10^4 PANC-1 cells, (C, D) 2×10^5 PANC-1 cells, and (E, F) 1×10^6 PANC-1 cells were mixed with 200 μg/mL Pao, and then inoculated into the left flank of each mouse. The same number of PANC-1 cells were mixed with phosphate buffered saline (PBS) and inoculated into the right flank of each mouse. A total of 10 mice were used for each cell number. The tumor formation rate (A, C, E) was defined as the number of tumors observed at a specific day / 10 × 100%. Tumor size (B, D, F) was measured by caliper, and the tumor volume was calculated using the formulation: tumor volume = width × width × length/2.

As the one-time Pao treatment failed to reduce the rate of tumor formation, we conducted repeated treatment with oral administration of Pao. The cell number was selected to be 2×10^5 per injection. Mice (N = 10) were injected subcutaneously at both left and right flanks with PANC-1 cells mixed with 200 μg/mL of Pao. Treatment started the next day and lasted for 3 weeks with oral gavage of 20 mg/kg Pao, 5 times per week. Control mice (N = 10) were inoculated with the same number of cells mixed with PBS and were gavaged with equivalent volumes of saline.

Both the rate and time of tumor formation were significantly reduced by Pao treatment (**Fig. 4.6. A**). At day 6, tumor formation rate in control group reached 80%, while in Pao-treated group it was only 10%. At day 20, when the treatment stopped, all mice in control group were bearing tumors on both flanks (100% tumor formation), while the Pao-treated group only had 30% tumor formation. All mice were kept for 2 more months after treatment had stopped. At the end of the experiment, the Pao treatment group had a maximum of 65% tumor formation, compared with the 100% tumor formation in the control group. These data indicate that Pao administration at 20 mg/kg orally eliminated CSCs in 35% of the injection sites.

Growth of the formed tumors was also inhibited by Pao treatment compared with the control group (**Fig. 4.6. B**). A long-term inhibitory effect in tumor growth was observed after treatment had stopped (**Fig. 4.6. B**). Adverse effects were monitored during the treatment and no adverse effects were observed. Body weight showed no difference between the treated and the control group (**Fig. 4.6. C**).

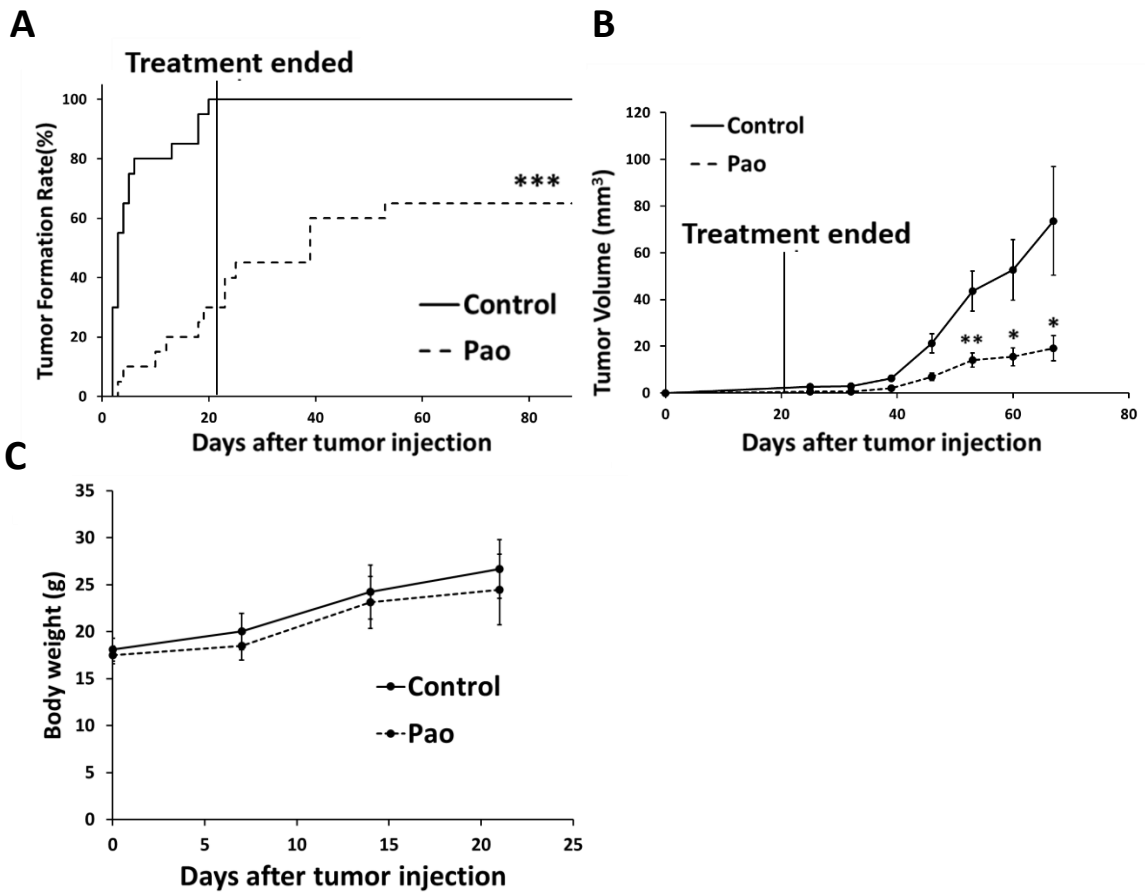

Figure 4.6. Effects of repeated Pao treatment on PANC-1 tumor formation and tumor growth in nude mice. (A) Tumor formation rate. A total of 2×10^5 PANC-1 cells were mixed with 200 µg/mL Pao (Pao) or phosphate buffered saline (PBS; control) and inoculated at both flanks of nude mice (N = 10 for each group). Treatment started the next day and lasted for three weeks with oral gavage of 20 mg/kg Pao (Pao) or saline (control) five times per week. ***$p < 0.001$ by log-rank test. (B) Longitudinal tumor growth. Tumor size was measured every three days by a caliper. Tumor volume = width × width × length/2. (C) Body weight of mice during treatment of three weeks. *$p < 0.05$; **$p < 0.01$; ***$p < 0.001$ compared with untreated control group by Student's t-test.

4.2. Discussion

In this study, we demonstrated both *in vitro* and *in vivo* that the extract of the plant Pao Pereira (Pao) inhibited pancreatic CSCs. Previously, we have reported that Pao induces apoptosis in pancreatic cancer cells and sensitizes pancreatic cancer cells to gemcitabine treatment [398]. Independent of its apoptosis-inducing activity, the CSCs inhibition could be another reason contributing to Pao-induced gemcitabine sensitivity. Taken together, the benefits of Pao in pancreatic cancer treatment are worth investigation clinically, especially in combination with current chemotherapies.

To date, there has been no efficient method to pinpoint a pancreatic CSC and maintain and amplify it for drug development purposes. Functional assays such as tumor spheroid assay and tumorigenicity in mice are commonly used [411]. The use of chromosomal dye [402, 403] or several cell surface markers are powerful to identify and isolate a subpopulation enriched with stem-like features [404]. In our studies here, we did not only rely on CSCs isolated and separately treated. First, it is difficult to obtain and maintain a pure CSC population [412]. Second, isolated CSCs might lose their natural environment in the bulk population [413]. Instead, we treated the bulk of pancreatic cancer cells, and a side population, and examined the CSC specific outcomes. The inhibitory results from our studies are not likely due to the general cytotoxicity of Pao to the bulk of cancer cells, because Pao has an IC_{50} value of 300 µg/mL in 48 hours of treatment toward the bulk of PANC-1 cells and has a much lower IC_{50} value of 153 µg/mL for the reduction of CD44+ CD24+ EpCam+ cells at a shorter treatment time of 24 hours, and 99.53 µg/mL at 48 hours. Furthermore, in the tumor spheroid formation assay, Pao has an IC_{50} of 27 µg/mL in inhibiting the number of spheroids. These data suggest that Pao has a preferential inhibitory activity toward pancreatic CSCs.

The mechanism(s) by which Pao induces CSC inhibition needs to be further investigated. Our study showed that Pao reduced both Nanog and nuclear β-catenin level of PANC-1 cells, which are important in stem cell initiation and maintenance. Pao also reduced mRNA levels of several CSC-related genes, namely *DPPA4*, *ESRRB*, and *TCL1*. The mechanism through which Pao interacts with Nanog, β-catenin singling pathway and/or the other CSC genes needs to be further investigated in depth. Moreover, as this plant preparation contains a complex mixture of natural compounds, it is possible that Pao affects other molecular targets and pathways that lead to CSC inhibition.

Previous studies on the extract of Pao showed the inhibitory effect on proliferation on pancreatic, ovarian and prostate cancers [393, 397-399]. Our animal data here showed promising effects of Pao in inhibiting tumorigenicity and tumor growth, at a dose and administration route that can be easily translated into clinical use. No toxic side effects were observed in mice at this dosage. The inhibition in tumorigenicity implies a possible role of Pao in the prevention of cancer, in addition to data indicating a treatment role. Given that the extracts of Pao Pereira are consumed by the American public as a health supplement, the safety, toxicity, and effects of Pao as an anticancer agent should be further investigated clinically.

Chapter 5. Inhibition of Pancreatic Cancer Stem Cells by *Rauwolfia vomitoria* Extract

This chapter has previously been published as an open access article (CC BY-NC-ND). The result section and discussion section are reprinted here without adaptations. Dong, R., Chen, P., Chen, Q. Inhibition of pancreatic cancer stem cells by Rauwolfia vomitoria extract. Oncology Reports 40.6 (2018): 3144-3154.
Retrieved from https://doi.org/10.3892/or.2018.6713

Herbal preparations of Rauwolfia vomitoria (Rau), a tropical shrub in the family Apocynaceae, is a traditional folk medicine in Africa used to treat a variety of conditions, including hypertension [414, 415], fever [416, 417] , gastrointestinal diseases [418], liver diseases [419], and cancer [420]. The extract as a whole mixture is widely used as a health supplement. Extracts from the root bark of this plant are enriched with β-carboline alkaloids and indole alkaloids [421]. β-carboline alkaloids have been reported to have several bioactivities, including antitumor effects [422, 423]. In our previous study, it was reported that an extract of Rau, with its hypotensive component reserpine removed, induced pancreatic cancer cell apoptosis, and inhibited pancreatic tumor growth in mice [424]. The combination of Rau and gemcitabine showed synergistic antitumor effects [424]. In the present study, the activities of the same extract on inhibiting pancreatic CSCs *in vitro* and *in vivo* were investigated.

5.1. Results

5.1.1. Inhibition of pancreatic cancer tumor spheroid formation *in vitro*.

Five human pancreatic cancer cell lines (PANC-1, MIA PaCa-2, AsPC-1, HPAF-II and BxPC-3) and an immortalized epithelial cell line (MRC-5) were treated with various concentrations of Rau, and cell viability was detected 48 hours later. Rau inhibited the proliferation of all five cancer cells **(Fig. 5.1. A)**, with IC_{50} values ranging between 140 and 317 μg/ml. The non-cancerous MRC-5 epithelial cell line was less affected by Rau treatment, with a higher IC_{50} value of 567 μg/ml **(Fig. 5.1. B)**. These results are consistent with our previous findings that Rau inhibited the overall proliferation of pancreatic cancer cells [424].

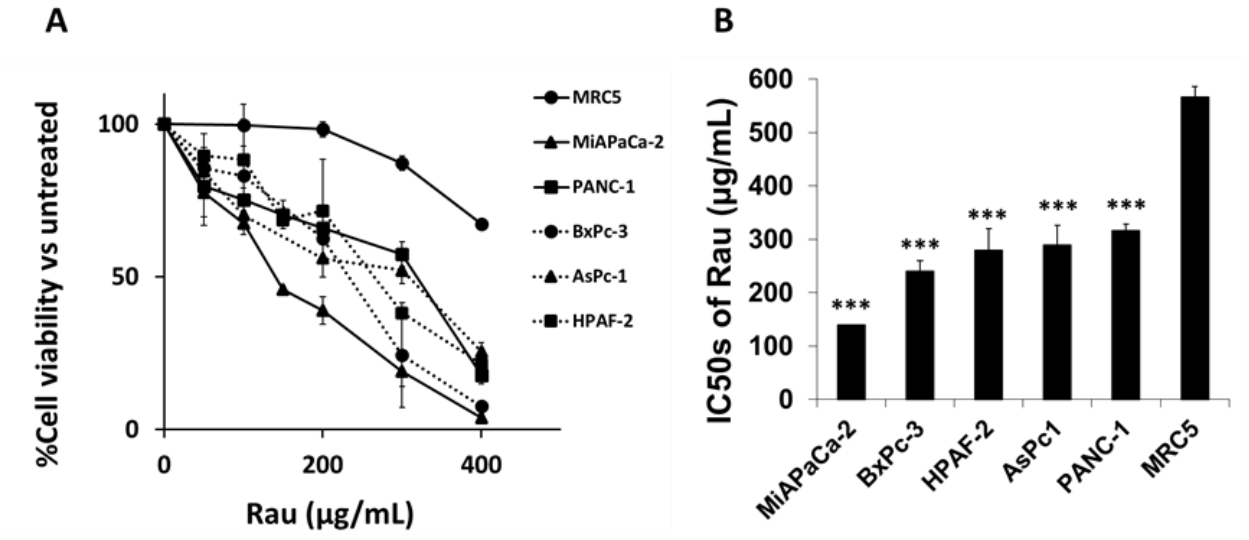

Figure 5.1. Inhibition of the proliferation of pancreatic cancer cells by Rau. (A) Dose-response curves. Human PANC-1, AsPC-1, HPAF-II, BxPC-3 and MiA PaCa-2 pancreatic cancer cells were exposed to serial concentrations of Rau for 48 hours. Cell viability was detected using a 3-(4, 5-dimethylthiazol-2-yl)-2, 5-diphenyltetrazolium bromide assay. An immortalized non-cancerous MCR-5 epithelial cell line was subjected to the same treatment. (B) IC50 values of Rau in pancreatic cancer cells and MRC-5 cells. ***P<0.001, compared with the IC50 of MRC-5 cells. All values are expressed as the mean ± standard deviation of three independent experiments each performed in triplicate. Rau, Rauwolfia vomitoria; IC50, 50% inhibitory concentration.

To investigate the inhibitory effect of Rau in CSCs, a tumor spheroid formation assay was performed. The ability to form tumor spheroids is an *in vitro* indication of the tumorigenic capacity and self-renew ability of CSCs. When cancer cells are cultured in non-adherent, serum-free conditions, non-CSC populations die by anoikis, whereas CSCs overcome anoikis and go through division leading to the formation of tumor spheroids [400, 401]. Single cell suspensions were treated with Rau and tumor spheroids were counted 4 weeks later. Data showed that Rau significantly reduced the number of the PANC-1 tumor spheroids at the concentrations of 50 and 100 µg/ml, and completely eliminated the tumor spheroids at 200 µg/ml (**Fig. 5.2. A, B**). The estimated IC50 value for tumor spheroids inhibition is 39.44 µg/ml. By contrast, the IC_{50} value

of Rau to the bulk of PANC-1 cells was 317 µg/ml (**Fig. 5.1. B**). The MIA PaCa-2 pancreatic cancer cells were also treated by Rau for the detection of tumor spheroids. Similar results were obtained. Rau reduced the number of the MIA PaCa-2 spheroids at 50 µg/ml, and completely inhibited spheroid formation at ≥100 µg/ml (**Fig. 5.2. C, D**). The estimated IC_{50} value of 34 µg/ml (**Fig. 5.2. D**) was lower than the IC_{50} value for the bulk of the MIA PaCa-2 cells (**Fig. 5.1. A**).

Cells with stemness features are reported to exclude dyes as side populations [402, 403]. In order to separate the CSC-like population, MIA PaCa-2 cells were sorted using flow cytometry with DCV staining. The DCV− cells (CSC-like) and DCV+ (non CSC-like) cells were collected and treated with Rau. Rau inhibited the viability in all unsorted, DCV+ and DCV− cells, preferentially inhibiting DCV− cells (**Fig. 5.3. A**). The estimated IC_{50} values were 162 µg/ml in unsorted cells, 177 µg/ml in DCV+ cells and 122 µg/ml in DCV− cells. This result suggested that Rau preferentially inhibited CSC-like cells.

Tumor spheroid formation was detected. Although cell spheroids were also formed in the DCV+ cell culture, they were significantly smaller (**Fig. 5.3. B**). By contrast, DCV− cells formed large spheroids, as expected. As there is currently no exclusive way to pin-point pancreatic CSCs, the formation of spheroids in DCV+ cells may due to the remaining CSC-like cells in the DCV+ population. However, the DCV staining and sorting provided a side population enriched with ‘stemness’. Rau at 50 µg/ml inhibited spheroids in the DCV− and DCV+ populations (**Fig. 5.3. B**), a result consistent with those in unsorted cells.

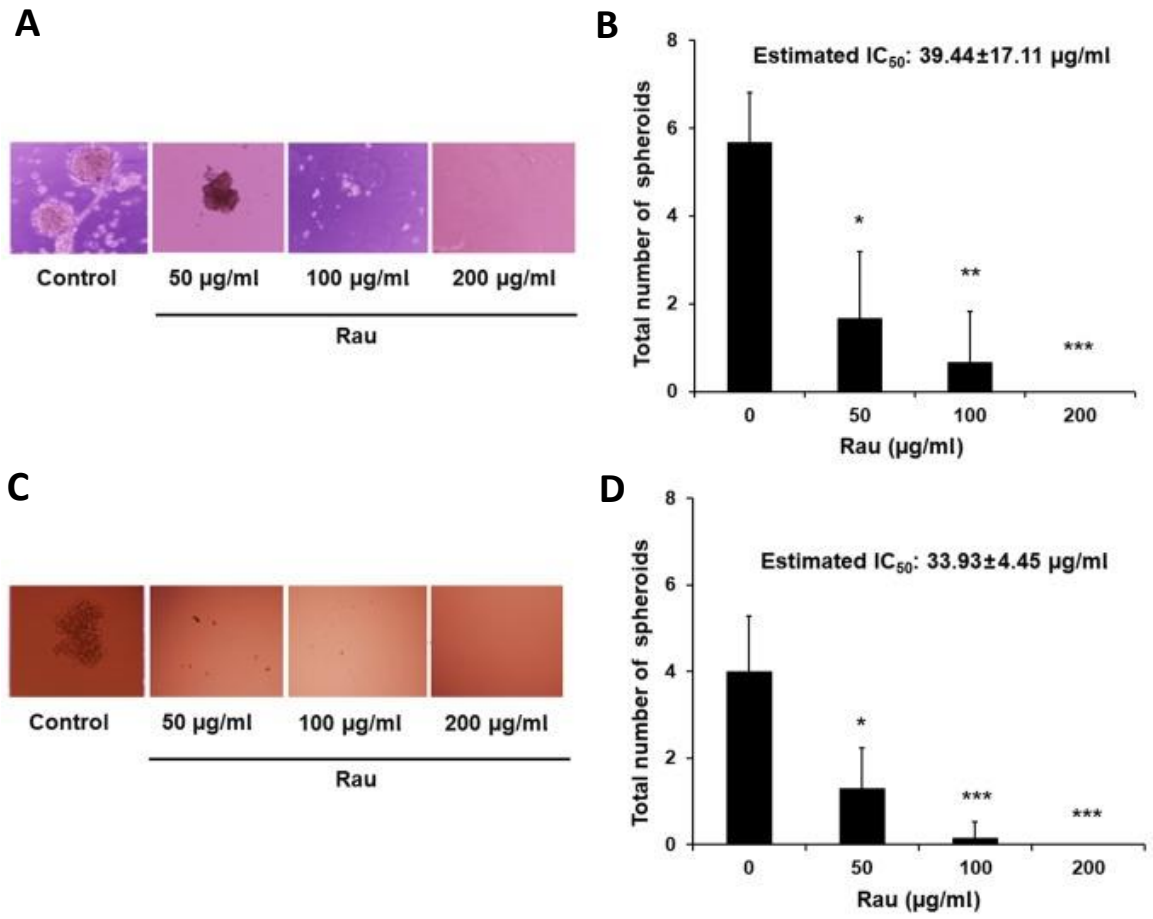

Figure 5.2. Inhibition of pancreatic tumor spheroids by Rau. (A) Representative images of the spheroids with and without Rau treatment (magnification, ×10). A PANC-1 single-cell suspension was plated into 24-well ultra-low attachment plates at a density of 5,000 cells/well in stem cell media. Tumor spheroids were counted 4 weeks later. (B) Number of PANC-1 spheroids (mean ± standard deviation of three independent experiments). *P<0.05, **P<0.01 and ***P<0.001, compared with the untreated control. (C) Representative images of the MIA PaCa-2 spheroids with and without Rau treatment. MIA PaCa-2 single-cell suspension was plated into 96-well ultra-low attachment plates at a density of 100 cells/well in stem cell media. Tumor spheroids were counted 2 weeks later. (D) Number of MIA PaCa-2 spheroids (mean ± standard deviation of three independent experiments). Rau, Rauwolfia vomitoria; IC50, 50% inhibitory concentration.

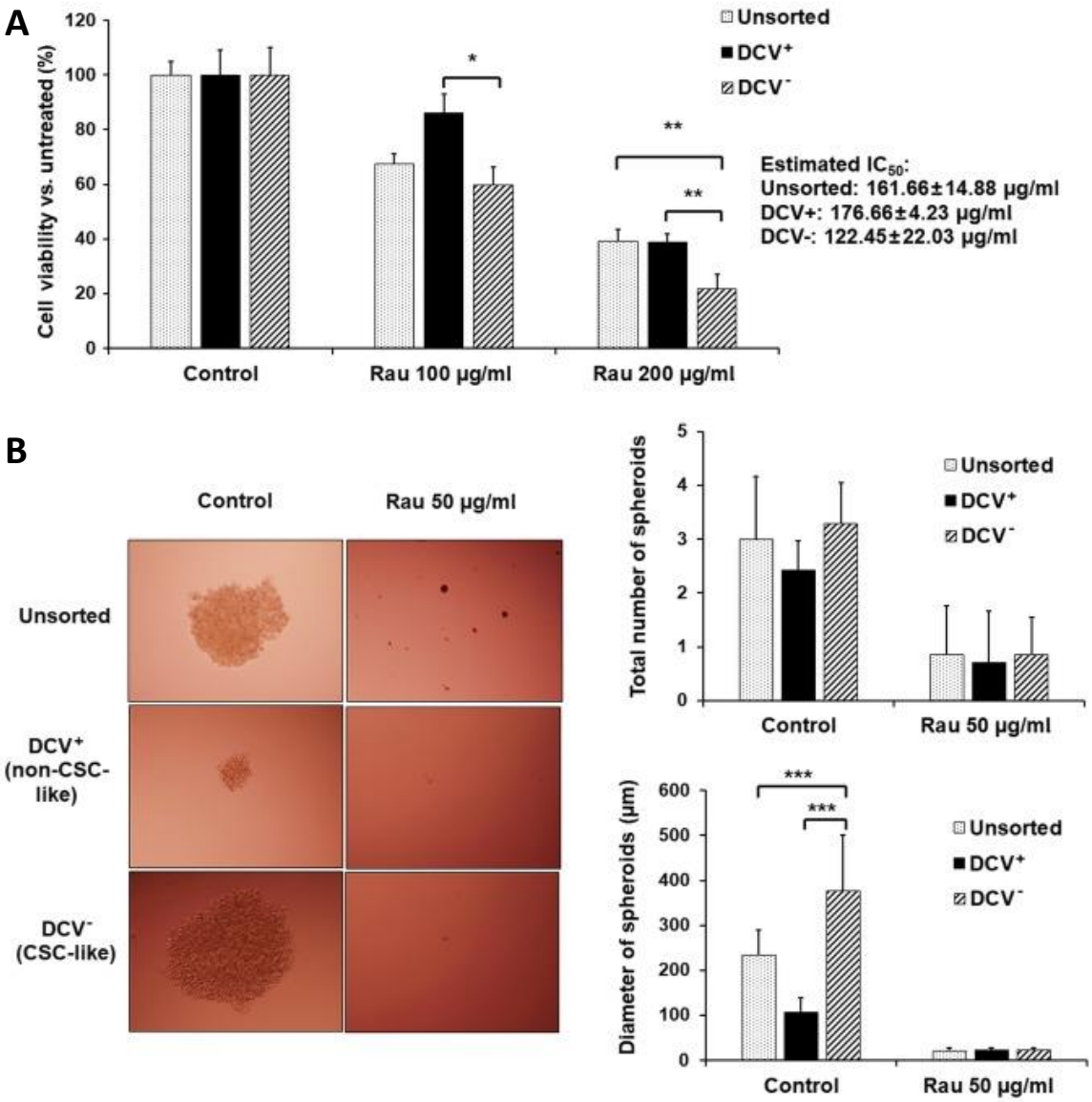

Figure 5.3. Inhibition of pancreatic CSC-like subpopulations by Rau. (A) Cell proliferation of unsorted cells, DCV+ cells (non-CSC-like) and DCV− cells (CSC-like) with Rau treatment for 48 hours (mean ± standard deviation of three independent experiments). (B) Representative images of the MIA PaCa-2 spheroids from unsorted cells, DCV+ cells and DCV− cells with and without Rau treatment (magnification, ×10). The number and size of MIA PaCa-2 spheroids are shown in bar graph. *P<0.05; **P<0.01 and ***P<0.001. CSC, cancer stem cell; Rau, Rauwolfia vomitoria; DCV, Dye Cycle Violet; IC50, 50% inhibitory concentration.

5.1.2. Reduction of the CSC marker-positive cell population.

The effects of Rau on CSCs in a shorter time period were also examined. The PANC-1 cells were treated with Rau for 24 or 48 hours at concentrations of 50, 100 or 200 µg/ml. The pancreatic CSC markers CD24 and EpCAM were examined by immune staining followed by flow cytometric analysis. Rau reduced the CD24+EpCam+ cell population following 24 and 48 hours treatment (**Fig. 5.4. A, B**). In the control groups, CD24+EpCam+ cells consisted of 6.50–10.72% of the whole population. At the concentration of 200 µg/ml, Rau significantly reduced CD24+EpCam+ cells to 2.52–2.95% following 24 and 48 hours of treatment (**Fig. 5.4. A, B**). At a lower concentration of 100 µg/ml, Rau also significantly reduced the CD24+EpCam+ cells to 2.99–5.22% following 24 and 48 hours of treatment (**Fig. 5.4. B**). It was estimated that the IC50 value at 24-h treatment was 142.04±12.40 µg/ml, and at 48 hours treatment was 126.09±12.51 µg/ml (**Fig. 5.4. A, B**), and these values were lower than the IC50 values for the bulk tumor cells. These data are consistent with the results above showing that Rau preferentially inhibited pancreatic CSCs.

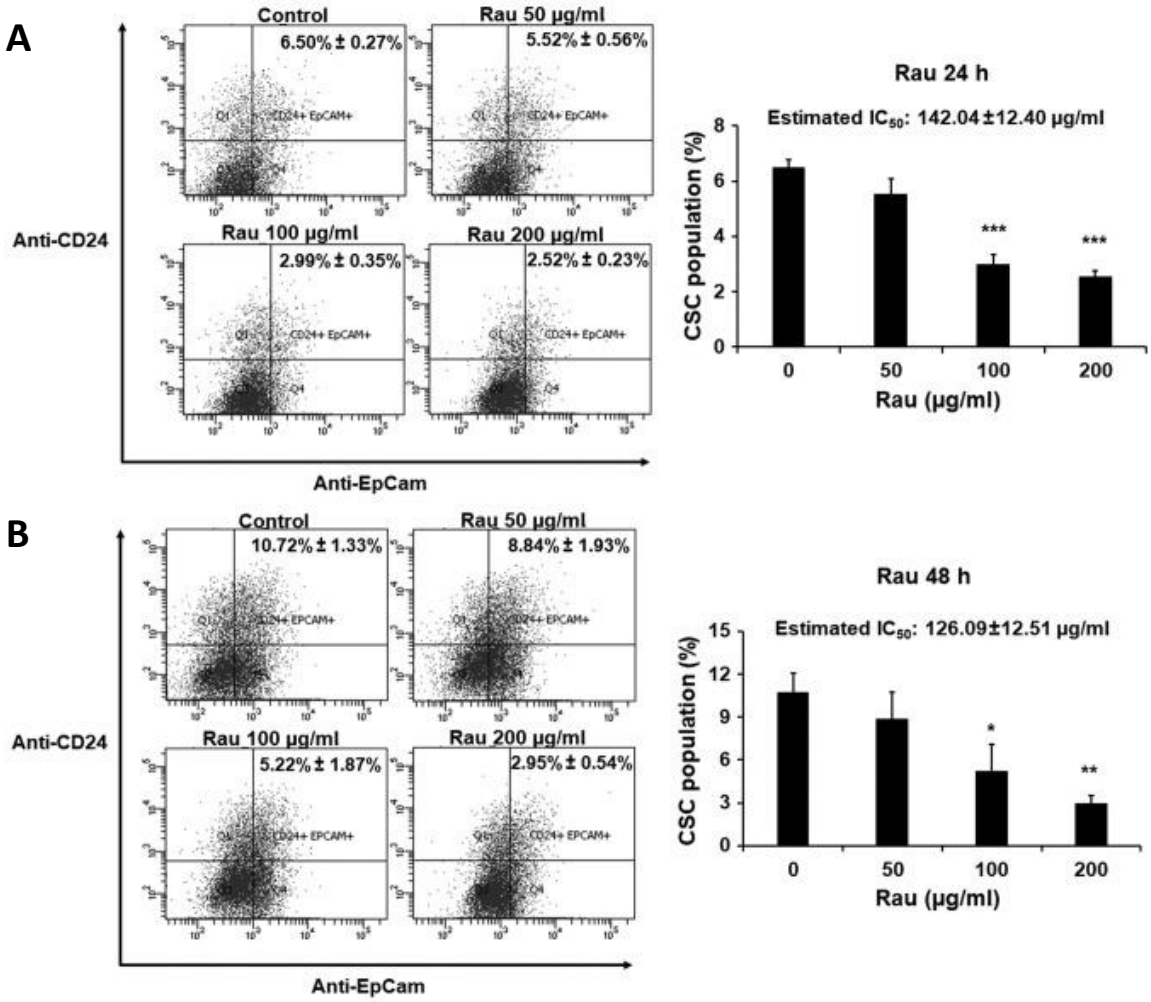

Figure 5.4. Inhibition of CSC populations by Rau. PANC-1 cells were treated with Rau for (A) 24 and (B) 48 hours at the indicated concentrations. Cells were then stained with fluorescent conjugated antibodies for CD24 and EpCam, followed by flow cytometric analysis. Left panels show the EpCam (APC) and CD24 (PE) positive cells. The percentages of CD24+EpCam+ cells were quantified and shown in the bar graph (mean ± standard deviation of three experiments). The data were normalized to cell death. *P<0.05; **P<0.01; ***P<0.001, compared with the untreated group. CSC, cancer stem cell; Rau, Rauwolfia vomitoria; IC50, 50% inhibitory concentration.

5.1.3. Inhibition of CSCs relate gene expression *in vitro*.

One of the essential pathways in maintaining the self-renewal and spheroid formation capacities of CSCs is activation of the canonical Wnt/β-catenin signaling pathway [405, 406]. When there is active Wnt signaling, the β-catenin degradation complex in the cytosol dissociates, and β-catenin accumulates in the nucleus and functions as a transcriptional factor to upregulate genes that promote CSC stemness, including Nanog [181]. In the present study, the cytoplasmic and nuclear fractions of the PANC-1 cells were each examined for β-catenin levels with or without Rau treatment. Treatment with Rau (100 µg/ml) for 24 and 48 hours reduced the levels of β-catenin in the nucleus (**Fig. 5.5. A**), whereas the cytoplasmic β-catenin levels were not changed (**Fig. 5.5. A**). A panel of β-catenin downstream target genes, including B-cell lymphoma 2-like 2 (BCL2L2), cyclooxygenase-2 (COX-2), matrix metalloproteinase (MMP)14 and MYC, were examined by RT-qPCR analysis (**Fig. 5.5. B**). Following treatment for 48 hours, the expression of MYC was significantly decreased by Rau treatment, which is consistent with Wnt/β-catenin signaling pathway inhibition. Studies have shown that the stem cell-related gene Nanog has the ability to induce β-catenin phosphorylation and enhances its degradation [407]. Therefore, the present study examined the expression of Nanog by western blot analysis. Nanog was increased following 24 hours of Rau treatment, and was then decreased following 48 hours of Rau treatment (**Fig. 5.5. C**). It was hypothesized that the increase in Nanog at the earlier time point enhanced β-catenin degradation and therefore suppressed nuclear levels of β-catenin. The suppressed β-catenin levels subsequently resulted in inhibition of the expression of Nanog at a later time-point [408, 409]. As a result, the Nanog and Wnt signaling pathway was suppressed by Rau.

A panel of other CSC-related genes were also examined by RT-qPCR analysis [410]. Data showed that the expression levels of developmental pluripotency associated 4 *(DPPA4)*, estrogen related receptor β *(ESRRB)* and SRY-box 2 *(SOX2)* were inhibited following 48 hours of Rau treatment (**Fig 5.5. D**).

Taken together, Rau treatment had an early effect in increasing the expression of Nanog, which led to the phosphorylation and degradation of β-catenin and repressed the nuclear level of β-catenin. The decreasing level of nuclear β-catenin negatively affected the expression of Nanog. Rau treatment also appeared to directly inhibit the nuclear accumulation of β-catenin and other CSC-related genes, including MYC, resulting in the overall suppression of Nanog and nuclear β-catenin (**Fig. 5.5. E**). The full mechanism of Rau-induced CSC inhibition warrants further investigation.

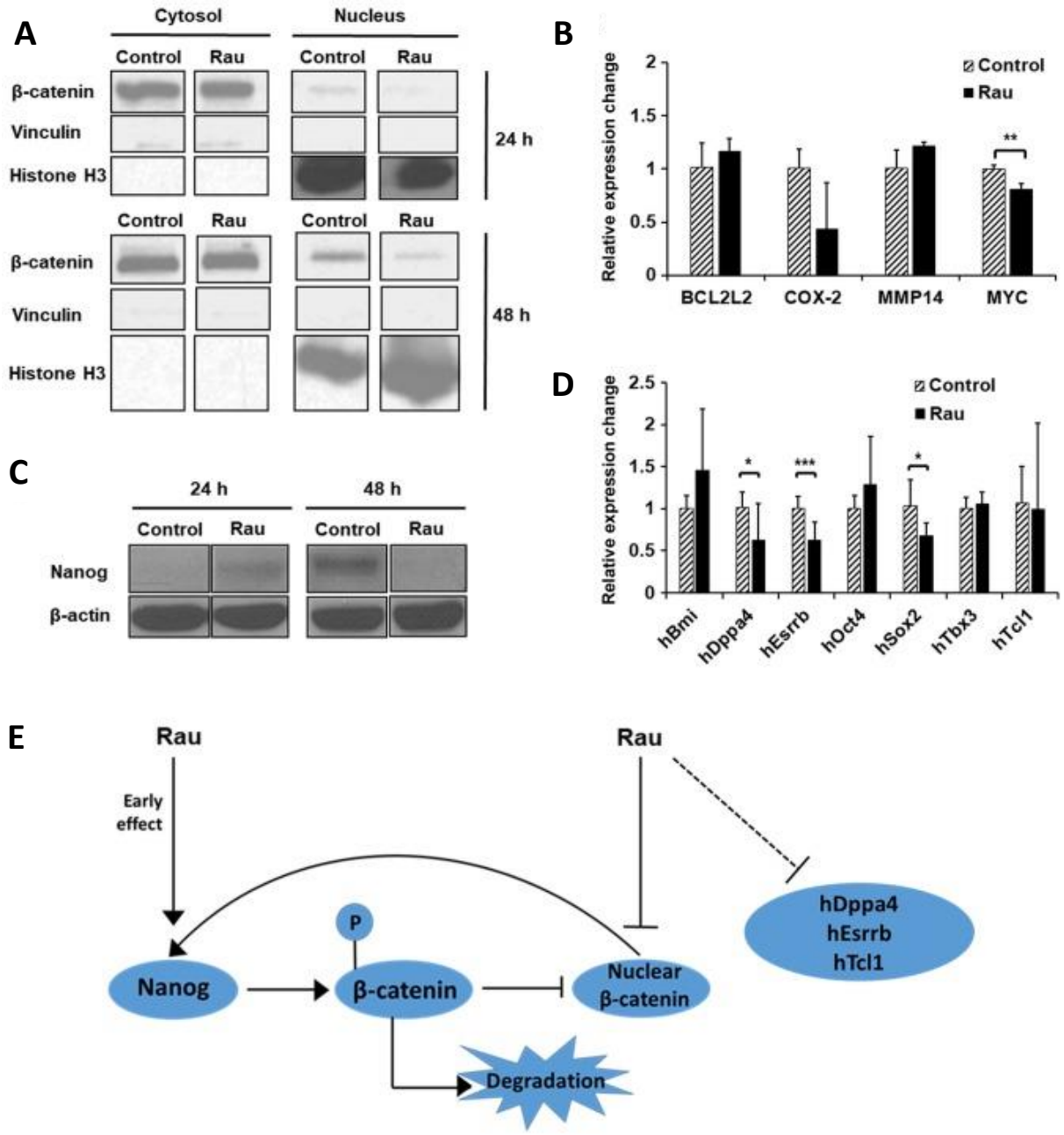

Figure 5.5. Decrease of nuclear β-catenin by Rau. PANC-1 cells were treated with Rau at 100 μg/ml for 24 and 48 hours. (A) Expression of β-catenin was detected by western blot analysis in cytoplasmic and nuclear fractions. Vinculin was a loading control for cytoplasmic proteins, and histone H3 was a loading control indicative for the nuclear fraction. (B) Expression of β-catenin downstream target genes at 48 hours of Rau treatment, detected by RT-qPCR analysis. (C) Expression of Nanog was detected by western blot analysis. (D) Expression of CSC-related genes following 48 hours of Rau treatment, detected by RT-qPCR analysis. (E) Suggested mechanism of Rau inhibiting Nanog and nuclear β-catenin. Rau treatment has an early effect in increasing the expression of Nanog, which leads to the phosphorylation and degradation of β-catenin, which represses nuclear β-catenin. The decreasing level of nuclear β-catenin negatively influenced the expression of Nanog. Rau treatment also appeared to directly

inhibit β-catenin nuclear accumulation. Both can result in overall suppression of levels of Nanog and nuclear β-catenin. Rau also inhibited the RNA level of CSC-related genes, including Dppa4 and Esrrb. *P<0.05; **P<0.01; ***P<0.001, compared with the untreated control group. Rau, Rauwolfia vomitoria; RT-qPCR, reverse transcription-quantitative polymerase chain reaction; BCL2L2, B-cell lymphoma 2-like 2, COX-2, cyclooxygenase-2, MMP14, matrix metalloproteinase 14; Dppa4, developmental pluripotency associated 4, Esrrb, estrogen related receptor β; Oct4, octamer-binding transcription factor 4; Tbx3, T-box 3; Tcl1, T cell leukemia 1.

5.1.4. Inhibition of pancreatic CSCs *in vivo*.

The inhibitory effects of Rau against pancreatic CSCs were examined *in vivo* by tumorigenicity in immunocompromised mice. Single treatment was performed first using inoculation of different numbers of PANC-1 cells at limited dilutions. The cells (2×10^4, 2×10^5 and 1×10^6) were mixed with 200 μg/ml Rau and injected subcutaneously into the left flanks of nude mice (n=10), respectively. For the control, the same number of cells were mixed with PBS and inoculated into the right flanks of the same mouse. The results are shown in **Fig. 5.6. A-F**. At the lowest inoculation number (2×10^4 cells), the tumor formation rate was low and no difference was observed between the treated and untreated groups. At the highest inoculation number (1×10^6 cells per injection), the untreated group reached a maximum of 90% tumor formation and the treated group reached 80%, with no significant difference between the two. There was also no difference in the growth of the formed tumors between the treated and untreated groups. At 2×10^5 cells per injection, the single Rau treatment significantly inhibited the tumor formation rate. The growth of the formed tumors was also inhibited.

As single Rau treatment showed limited effect on the inhibition of tumor formation rate and tumor size, repeated treatment was performed with oral administration of Rau. The optimal cell number for injection was selected as 2×10^5 per injection. The mice (n=10) were injected subcutaneously in the left and right flanks with PANC-1 cells mixed with 200 mg/ml of Rau.

Treatment started the following day and lasted for 3 weeks with oral gavage of 20 mg/kg Rau, five times per week. The control mice (n=10) were inoculated with the same number of cells mixed with PBS and were administered with equivalent volumes of saline.

The rate of tumor formation and time of tumor formation were significantly different between the control and treated groups (**Fig. 5.7. A**). At day 6, the tumor formation rate in the control group reached 80%, whereas that in the Rau-treated group was only 35%. At day 20 when the treatment had stopped, all mice in the control group were bearing tumors on both flanks (100% tumor formation), whereas the Rau-treated group only had 65% tumor formation. All mice were kept for 2 months following the end of treatment. At the end of the experiment, the Rau-treated group had a maximum of 85% tumor formation, compared with 100% tumor formation in the control group. These data indicated that Rau administration at 20 mg/kg orally eliminated CSCs in 15% of the injection sites.

The growth of the formed tumors was not significantly inhibited by Rau treatment compared with the control group, which indicated the lack of a long-term inhibitory effect on tumor growth following the end of treatment (**Fig. 5.7. B**). No adverse effects were observed in either group during the treatment (**Fig. 5.7. C**).

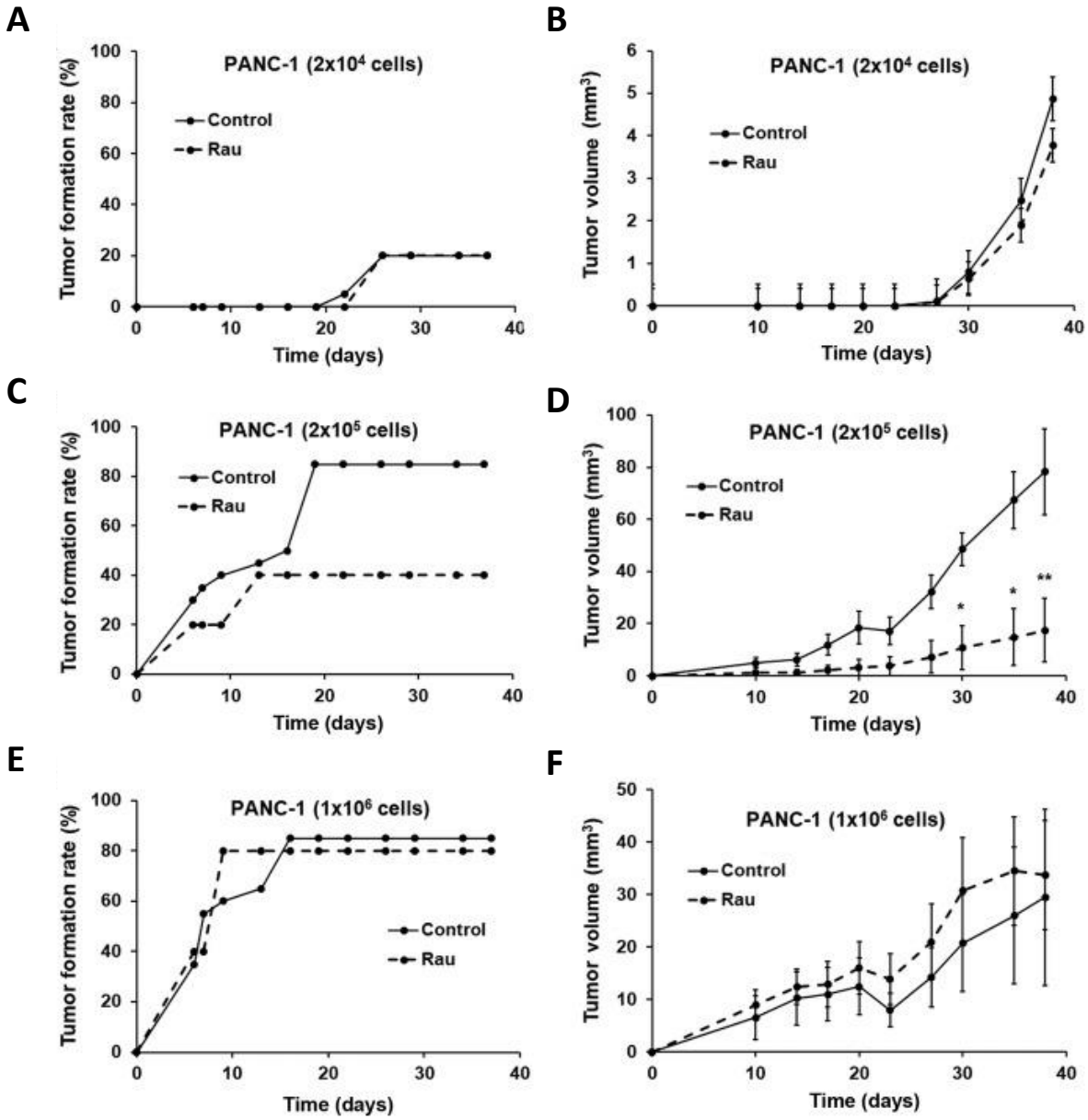

Figure 5.6. Effects of single Rau treatment on PANC-1 tumor formation in nude mice. (A) Tumor formation rate and (B) tumor size at 2×10^4 PANC-1 cells; (C) Tumor formation rate and (D) tumor size at 2×10^5 PANC-1 cells; (E) Tumor formation rate and (F) tumor size at 1×10^6 PANC-1 cells. PANC-1 cells were mixed with 200 μg/ml Rau, and then inoculated into the left flank of each mouse. The same density of PANC-1 cells were mixed with PBS, and inoculated into the right flank of each mouse. A total of 10 mice were used for each cell number. The tumor formation rate was determined as: Number of tumors observed on a specific day/10 × 100%. Tumor size was monitored weekly using calipers and tumor volume was calculated using the following formula: Tumor volume = width × width × length/2. *P<0.05; **P<0.01. Rau, Rauwolfia vomitoria.

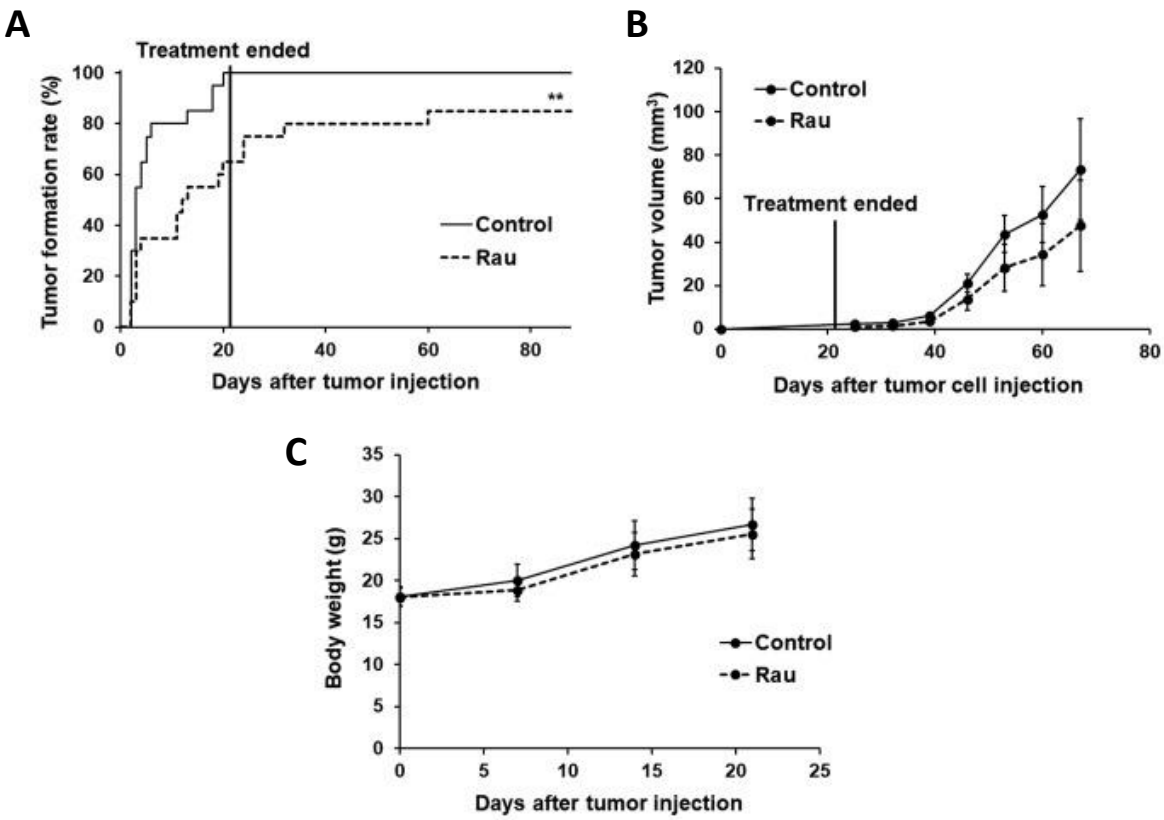

Figure 5.7. Effects of repeated Rau treatment on PANC-1 tumor formation and tumor growth in nude mice. (A) Tumor formation rate. 2×10^5 PANC-1 cells were mixed with 200 mg/ml Rau or PBS (control), and inoculated at both flanks of nude mice (n=10 for each group). Treatment started the next day and lasted for 3 weeks with oral gavage of 20 mg/kg Rau or saline (control) five times per week. **P<0.01 by log-rank test. (B) Longitudinal tumor growth. Tumor size was measured weekly using calipers. Tumor volume = width × width × length/2. (C) Body weight of mice during treatment for 3 weeks. Rau, Rauwolfia vomitoria.

5.2. Discussion

Targeting CSCs has been an attractive strategy for developing novel treatments with the aim of eliminating the entire cancer cell population. However, targeting CSCs has been challenging. First, as CSCs are only a small population in the bulk of cancer cells, anticancer agents that have cytotoxicity to the bulk of cancer cells do not necessarily inhibit CSCs [425, 426]. CSCs possess self-renewal ability and are able to give rise to new tumors [413]. CSCs are also found to be drug resistant [220, 229]. The mechanism by which CSCs become drug resistant remains to be fully elucidated. A partial reason is the quiescent status of CSCs in a growing tumor. Other potential mechanism are the upregulated expression of the ABCG2 transporter, which facilitates the efflux of chemotherapeutic drugs from the cytosol [229], overexpression of detoxifying enzymes, enhanced DNA repair ability, and overexpression of anti-apoptotic proteins [220]. Given the roles of CSC in tumor generation, metastasis and drug resistance, the identification and development of novel drugs that can inhibit CSCs may lead to a promising outcome in the comprehensive inhibition of tumor growth, metastasis and recurrence, and overcoming drug resistance. In the present study, it was demonstrated that the Rau extract inhibited pancreatic CSCs *in vitro* and *in vivo*. Previously, it was reported that the same Rau extract induced the apoptosis of pancreatic cancer cells and sensitized pancreatic cancer cells to gemcitabine treatment [424]. The inhibition of CSCs may be another factor contributing to Rau-induced gemcitabine sensitivity in addition to its apoptosis-inducing activity. The data suggested that Rau had preferential inhibitory effects towards pancreatic CSCs and also inhibited the bulk of cancer cells. This may be advantageous in cancer therapy as one treatment inhibits CSC and non-CSCs. The overall inhibitory effect in non-CSC and CSCs results in the inhibition of tumor growth, whereas the inhibition in CSCs is likely also to reduce metastasis and chemotherapy resistance.

Given the lack of treatment options for pancreatic cancer, the benefits of Rau in pancreatic cancer treatment warrant further investigation, particularly in combination with current chemotherapies.

Dye exclusion and CSC surface markers are used in CSC isolation and provide consistent data for the enrichment of pancreatic CSCs. However, there has not been an efficient method to definitively identify and isolated a pure pancreatic CSCs and maintain/amplify them for drug development purposes [404]. Functional assays, including tumor spheroid assays and tumorigenicity in mice are commonly used [411]. Due to the difficulties in obtaining and maintaining a pure CSC population [412], the isolated CSCs may lose their natural environment in the bulk population [413]. In the present study, the bulk of pancreatic cancer cells were treated, in addition to a dye-excluding side population, and the CSC-specific outcomes were examined. The inhibition of CSCs was shown and was not likely due to the general cytotoxicity of Rau to the bulk of cancer cells. The data showed that Rau had an IC50 value of 317 μg/ml over 48 hours of treatment towards the bulk of PANC-1 cells, and had markedly lower IC50 values of 126.9–142.04 μg/ml for the reduction of CD24+EpCam+ cells at a shorter treatment time of 24–48 h. Furthermore, in the tumor spheroid formation assay, Rau had an IC50 value of 39.44 μg/ml in inhibiting the number of spheroids. These data suggested that Rau had a preferential inhibitory activity towards pancreatic CSCs.

The data obtained in the present study showed that Rau reduced protein levels of nuclear β-catenin and Nanog in PANC-1 cells, which are important in stem cell initiation and maintenance. Rau also reduced the mRNA levels of several CSC-related genes, namely *DPPA4*, *ESRRB* and *SOX2*. The in-depth mechanism underlying how Rau interacts with Nanog and/or the β-catenin signaling pathway requires further investigation. In addition, as plant extracts contain a complex

mixture of natural compounds, it is possible that Rau also affects other molecular targets and pathways that lead to its CSC inhibitory effect.

Previous studies on extracts of Rau showed inhibitory effects on the proliferation on pancreatic, ovarian and prostate cancer [420, 424, 427]. The data from animal experiments in the present study revealed the promising effects of Rau in inhibiting tumorigenicity, at a dose and administration route that can be easily translated into clinical use. No toxic side-effects were observed in mice at this dosage. The inhibition of tumorigenicity indicated the possible role of Rau in the prevention of cancer, in addition to data indicating a treatment role. As extracts of Rauwolfia vomitoria are consumed by the American public as a health supplement, the safety, toxicity and effects of Rau as an anticancer agent require further investigation clinically.

Chapter 6. Downregulation of HuR Suppresses Pancreatic Cancer EMT, Metastasis and CSCs

The RNA binding protein, HuR, is highly expressed in pancreatic cancer compared with normal tissues [363]. Elevated HuR nuclear and cytoplasmic levels are correlated with advanced stages in pancreatic cancer, and influence patient prognosis and survival rate. Downstream HuR targets include mRNAs that encode proteins involved in almost every hallmark characteristics of cancer. HuR is a putative target for cancer treatment.

How HuR regulates cancer cell EMT and CSCs is not well understood. Understanding the involvement of HuR in cancer cell EMT and CSCs will not only add to our knowledge of the regulation of EMT and CSCs, but also provide a novel approach for design of drugs targeting EMT and CSCs. In this chapter, we aim to fill the gap in understanding the role of HuR in pancreatic cancer cell EMT and CSCs.

6.1. Results

6.1.1. Suppression of HuR inhibited pancreatic cancer EMT

To study the role of HuR in pancreatic cancer cell EMT, we inhibited the expression of HuR in pancreatic cancer cell lines by either transfecting siRNAs targeting HuR mRNA (si-HuR) or performing a CRISPR/Cas9 based HuR gene deletion. Si-HuR transfection was performed in both PANC-1 and Mia PaCa2 cells for 24 hours. Cell morphology of the transfected cells changed to a more epithelium-like state, characterized by decreased spindle-like appearance, decreased cell length/width ratio, and/or enlarged cell diameter (**Fig. 6.1.**). The expression of EMT markers was then examined using western blot. Consistent with the morphological changes, the expressions of signature EMT markers in both PANC-1 and MIA PaCa2 cells were altered. The epithelial marker Claudin-1 was significantly upregulated, the mesenchymal marker Vimentin was downregulated, and the EMT-TFs Snail was significantly decreased (**Fig. 6.2. A**).

The expression of Claudin-1 was further confirmed by immunofluorescence staining. Results clearly showed an increased expression of Claudin-1 (**Fig. 6.2. B**).

Permanent deletion of HuR gene in MIA PaCa2 cells was performed by using a CRISPR/Cas-9 method. The deletion caused a depletion of HuR protein in MIA PaCa2 cells as we expected. Similar to the observations in the Si-HuR cells, the morphology of HuR-deleted cells (HuR KO) showed a more epithelium-like state compared with the control cells (HuR WT) (**Fig. 6.1.**). The expression of EMT markers was also altered, with an increase in Claudin-1, and a decrease in Vimentin and Snail, which were consistent with the protein expression profiles in si-HuR knockdown cells (**Fig. 6.2.**).

We then re-expressed HuR in the HuR KO MIA PaCa2 cells and expected that the EMT markers would be restored. MIA PaCa2 HuR KO cells were transfected with pCDNA 3.1-HuR plasmid to achieve the HuR restoration, with parallel pCDNA 3.1 empty plasmid transfected HuR KO cells as control. HuR re-expression in MIA PaCa2 HuR KO cells decreased the epithelial markers Claudin-1 and ZO-1, and increased the mesenchymal marker Vimentin, and Snail (**Fig. 6.3.**).

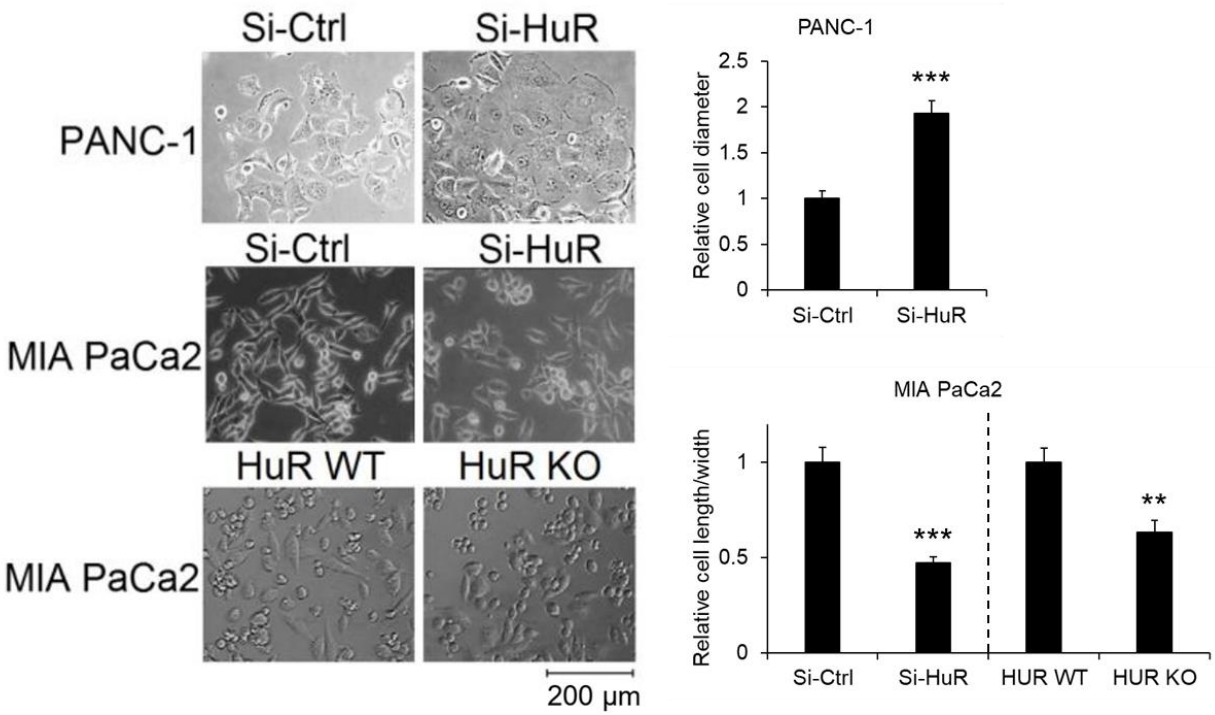

Figure 6.1. Morphological characteristics of PANC-1 and MIA PaCa-2 cells with and without HuR knockdown or deletion. Si-HuR were cells transfected with si-RNA targeting HuR mRNA for 24 hours, and Si-Ctrl were cells transfected with scramble si-RNA for 24 hours. Images were obtained at 24 hours after transfection. HuR KO were MIA PaCa2 cells with HuR gene deletion using CRISPR/Cas9. HuR WT were MIA PaCa-2 cells transfected with control sgRNA. Cell diameter and/or length/width ratio was measure using Image J software with 10 cells per sample. **$p < 0.01$; ***$p < 0.001$ by Student's t-test.

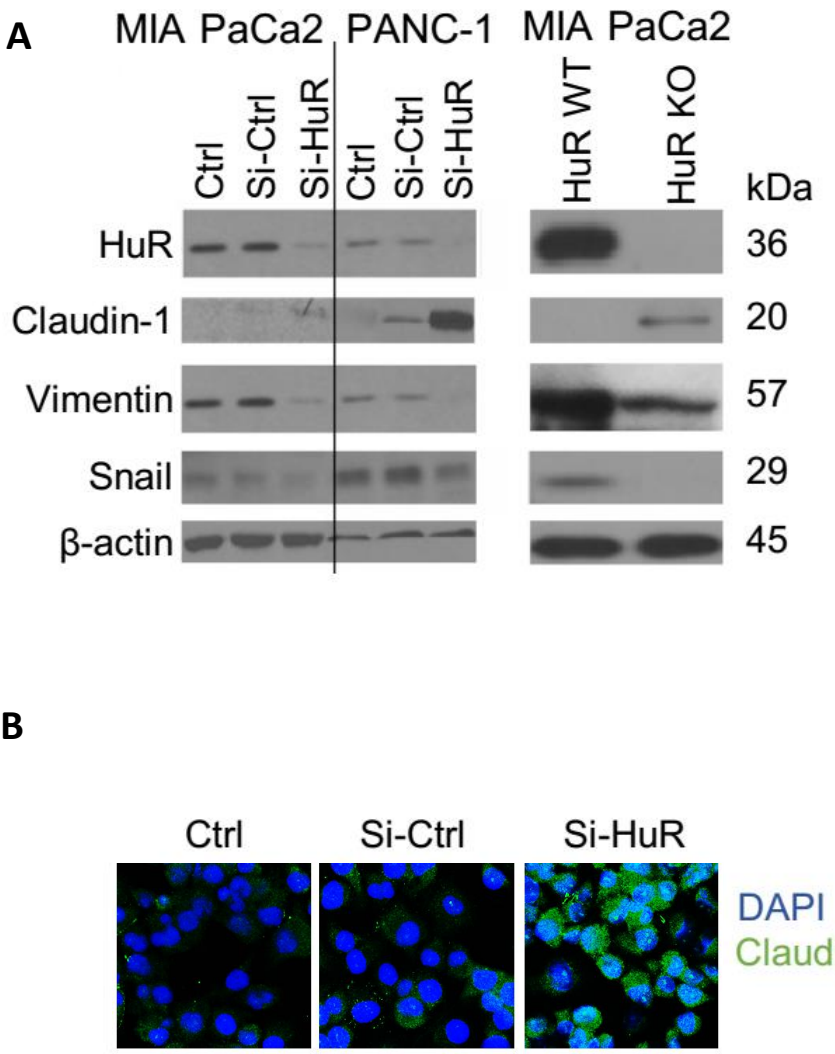

Figure 6.2. The suppression of HuR decreased expression of mesenchymal markers and promoted expression of epithelial markers in pancreatic cancer cells. (A) Western blot of HuR and EMT markers using cell extracts of MIA PaCa-2 and PANC-1 cells. β-actin was used as a loading control. Cells were transfected with either Si-Ctrl or Si-HuR for 24 hours or used untransfected (Ctrl). HuR KO were cells with HuR gene deletion by CRISPR/Cas9. HuR WT were cells transfected with control sgRNA. (B) Representative images of immunofluorescence staining of Clauind-1 (green) performed 24 hours after transfection. Cell nuclei were DAPI (blue) stained.

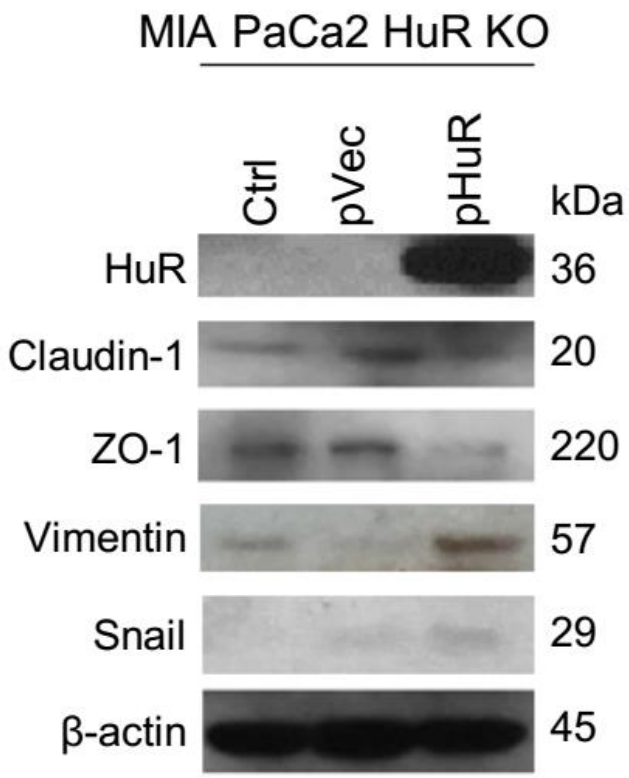

Figure 6.3. Re-expression of HuR inhibited expression of epithelial markers and promoted expression of mesenchymal markers in pancreatic cancer cells. Western blot of HuR and EMT markers using cell extracts of MIA PaCa-2 cells after transfection. β-actin was used as a loading control. Cells were transfected with either an empty vector (pVec) or pCDNA3.1-HuR (pHuR)for 48 hours.

6.1.2. Suppression of HuR inhibited pancreatic cancer cell migration and invasion *in vitro*

As EMT promotes cancer cells migration and invasion, we expected HuR knockdown in pancreatic cancer cells would inhibit migration and invasion. We performed wound healing assay and the Boyden Chamber invasion assay to evaluate the migration and invasion abilities of PANC-1 and MIA PaCa2 cells following HuR knockdown. In the wound healing assay, migration in both PANC-1 and MIA PaCa2 cells was significantly inhibited following si-HuR transfection (**Fig. 6.4.**). Consistently, HuR KO MIA PaCa-2 cells also had decreased ability to migrate (**Fig. 6.4.**).

Migration and invasion were further assessed by using either matrigel uncoated (for migration) or coated (for invasion) boyden chambers. Data show that siRNA-mediated inhibition of HuR (si-HuR) significantly inhibited migration of MIA PaCa2 cells, however, the invasion ability was not impaired. The transient nature of si-RNA mediated HuR knockdown may contribute to this result. In PANC-1 cells, si-HuR transfection was strong enough to inhibit both migration and invasion. HuR gene deletion in MIA PaCa2 cells significantly inhibited both migration and invasion compared with wild-type cells (**Fig 6.5.**). MIA PaCa2 HuR KO cells barely migrated at 48 hours and 60 hours, compared with both MIA PaCa2 WT cells and MIA PaCa2 si-HuR cells.

Because HuR also regulates cell proliferation, there is a possibility that the inhibition in migration/invasion detected here was due to inhibition in proliferation. To address this question, we examined the proliferation of si-HuR and HuR KO cells. Si-HuR MIA PaCa-2 cells had the same growth rate as the si-Ctrl cells and untreated cells (Ctrl) up to 72 hours (**Fig 6.6. A**), suggesting the inhibition in migration/invasion was independent of cell proliferation. There was a ~40% growth inhibition at 60 hours with HuR KO MIA PaCa-2 cells compared to wild type cells (**Fig 6.6. B**), and could contribute to the inhibition of gap-closing detected in the HuR KO

cells. Considering HuR KO cells were permanently and completely deleted with HuR, while si-HuR was temporary and not a 100% inhibition, it is likely that inhibition of HuR may first influence EMT and migration/invasion in the tested cells, and when the depletion of HuR is more severe, growth/proliferation were affected.

Considering that HuR re-expression in MIA PaCa2 HuR KO cells enhanced the expression of EMT markers, we examined migration and invasion in these cells. Data demonstrated that the restoration of HuR in MIA PaCa2 HuR KO cells significantly enhanced migration in wound healing assay compared with HuR KO cells (**Fig 6.7.**).

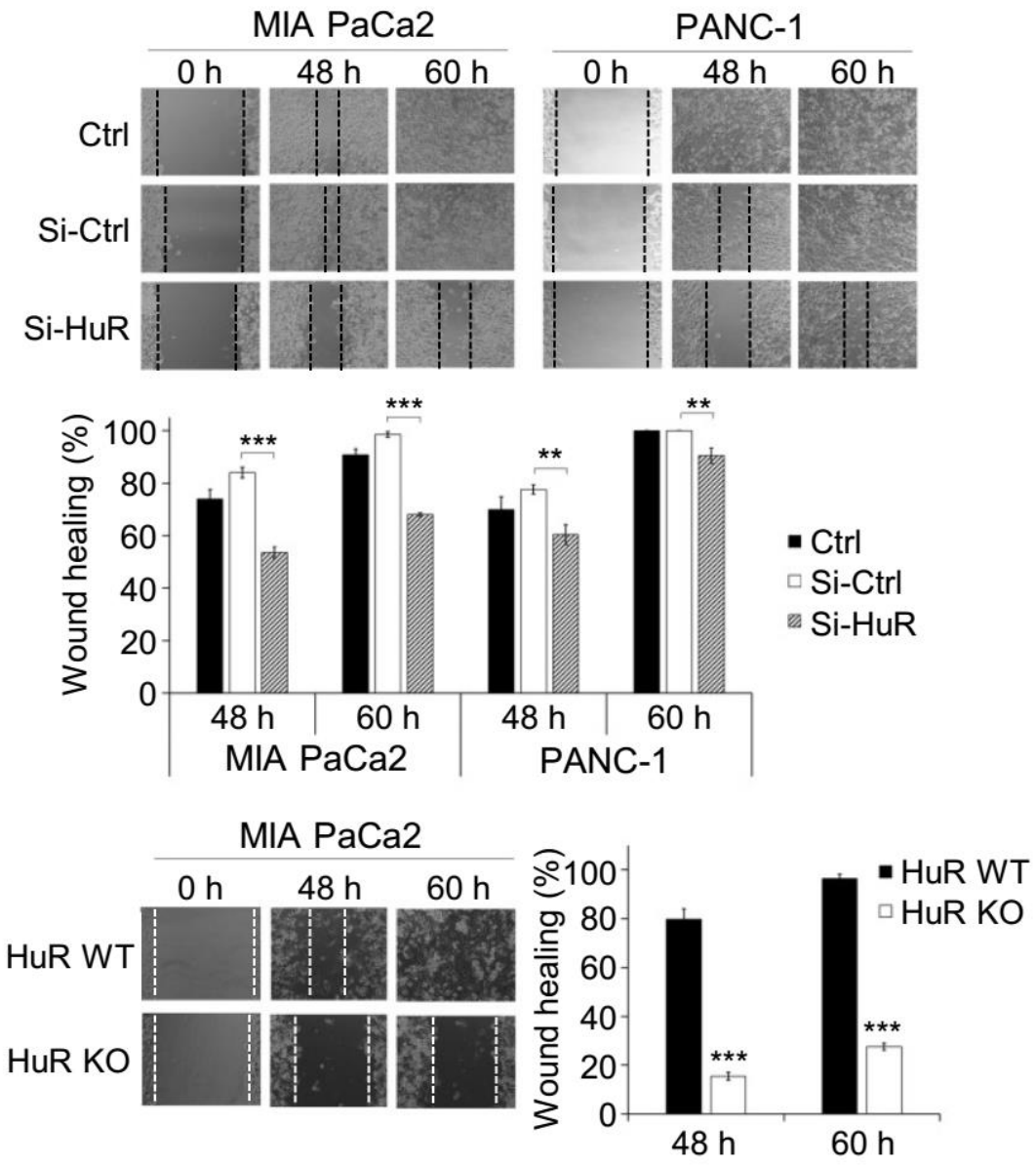

Figure 6.4. Suppression of HuR inhibited pancreatic cancer cell migration in wound healing assay. PANC-1 and MIA PaCa2 cells were transfected with either Si-Ctrl or Si-HuR for 24 hours, and then plated into 24-well plates to form confluent monolayer. Scratch was made on confluent monolayer cells with a 10µl pipette tip (0 hours). Cell migration was measured after 48 hours and 60 hours. Bar graph shows what percentage was covered by the cells. Bar graphs represent Mean ± SEM of ⩾ 3 repeats. **p < 0.01; ***p < 0.001 by one-way ANOVA-Tukey's test.

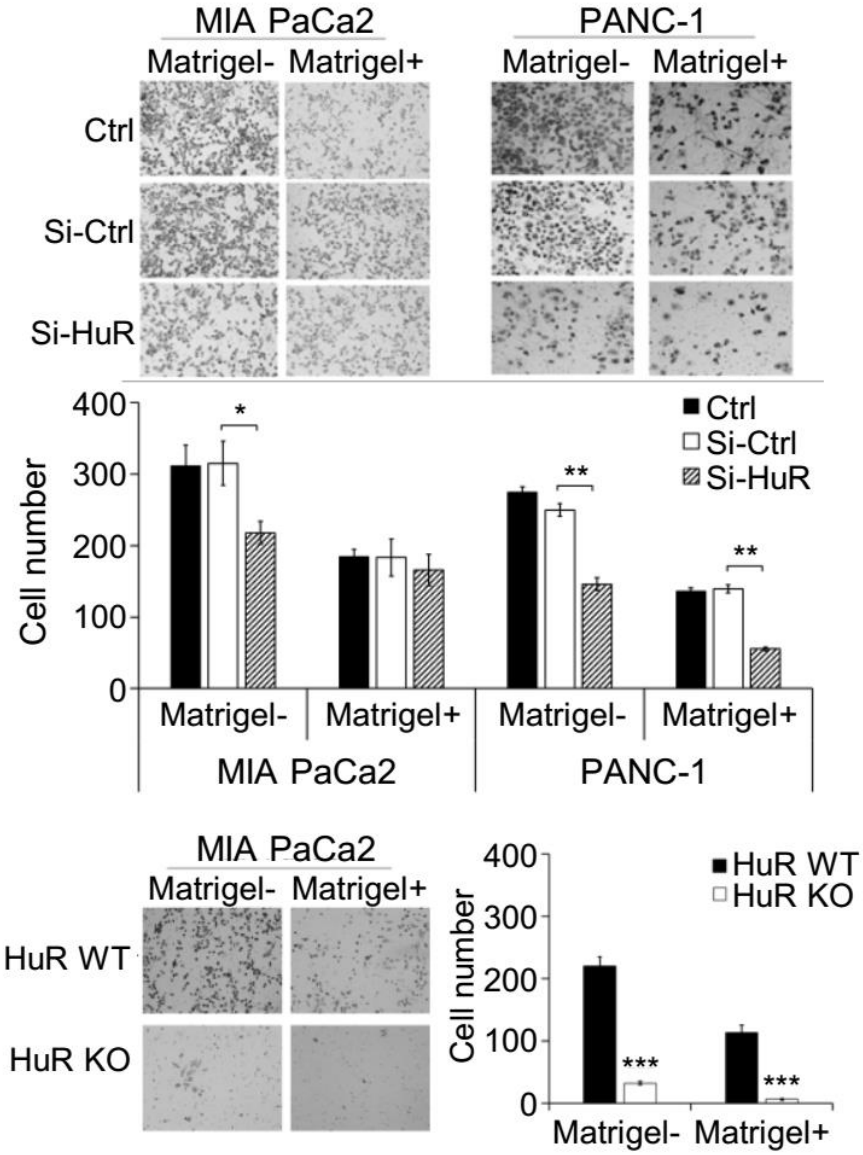

Figure 6.5. Suppression of HuR inhibited pancreatic cancer cell migration and invasion in boyden chamber invasion assay. PANC-1 and MIA PaCa2 cells were transfected with either Si-Ctrl or Si-HuR for 24 hours, and then plated into the boyden chambers. Cell migration (matrigel-) and invasion (matrigel+) were detected at 24 hours for PANC-1 cells and 48 hours for MIA PaCa-2 cells. Bar graphs show the Mean ± SEM of migrated/invaded cells per field of > 3 fields per experiment for 3 experiments. *$p < 0.05$; **$p < 0.01$; ***$p < 0.001$ by one-way ANOVA-Tukey's test.

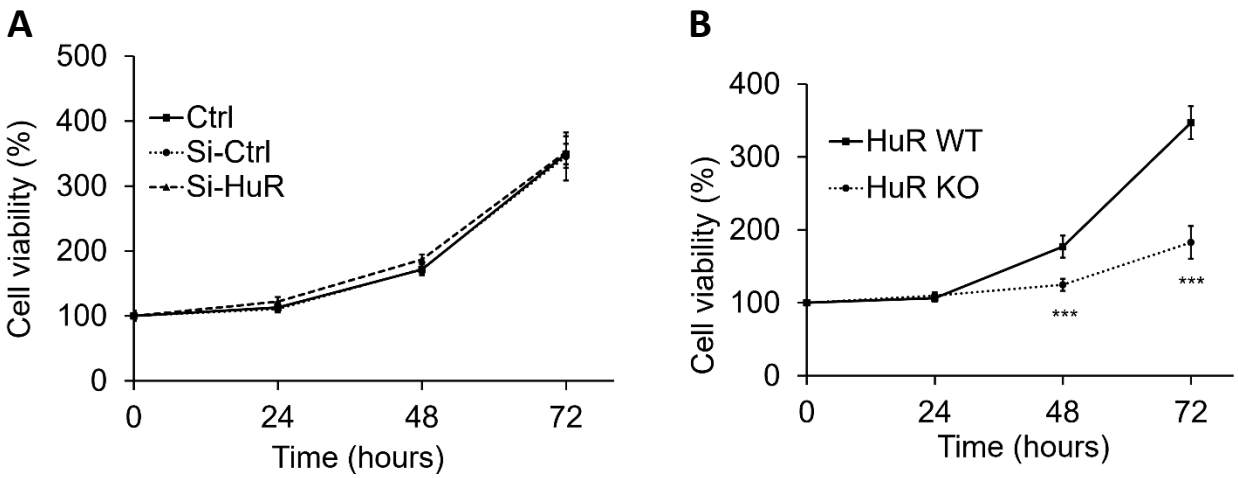

Figure 6.6. Growth curves of MIA PaCa-2 cells with HuR knockdown or deletion. (A) Si-HuR, cells transfected with si-RNA targeting HuR mRNA; Si-Ctrl, cells transfected with scramble si-RNA; Ctrl, cells not transfected. (B) HuR KO, cells deleted of HuR gene by CRISPR/Cas9 procedure; HuR WT, cells transfected with control sgRNA. All cells were plated in 96-well plates at the density of 3,000 cell/ well. Cell viabilities were detected by MTT assay at 0, 24, 48, and 72 hours. Data represents Mean ± SD of 4 experiments each done in 8 repeats. ***, $p<0.001$ with Student's t-test.

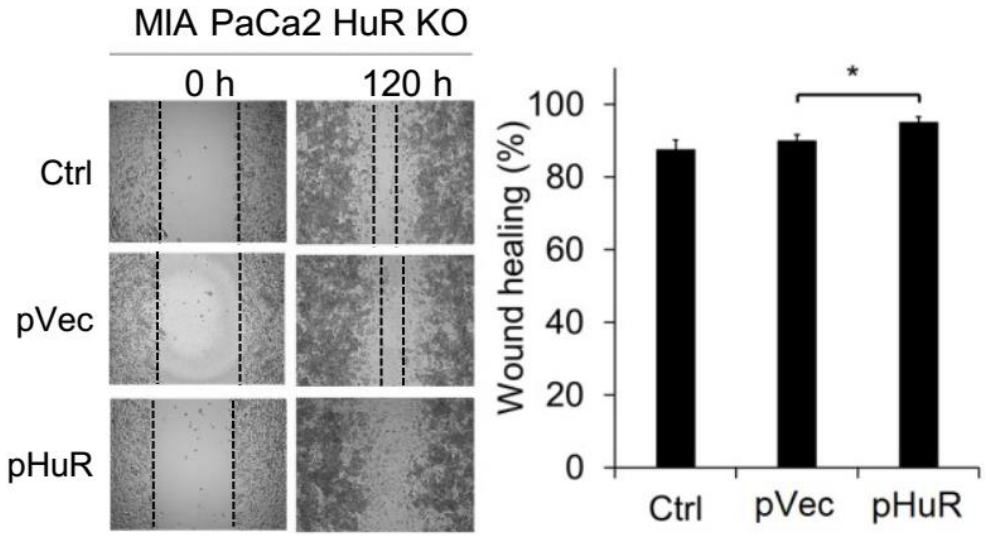

Figure 6.7. Re-expression of HuR in MIA PaCa2 HuR KO cells enhanced cell migration in wound healing assay. MIA PaCa2 HuR KO cells were transfected with either pVec or pHuR for 48 hours, and then plated into 24 well plates to form confluent monolayer. Scratch was made on confluent monolayer cells with a 10µl pipette tip (0 hour). Cell migration was measured after 120 hours. Bar graph shows what percentage was covered by the cells. Bar graphs represent Mean ± SEM of ⩾ 3 repeats. *, $p<0.05$ by one-way ANOVA-Tukey's test.

6.1.3. Suppression of HuR inhibited pancreatic CSCs *in vitro* and *in vivo*

As EMT is associated with the presence of CSCs, we examined the pancreatic CSCs first using tumor sphere formation assay. In both PANC-1 and MIA PaCa2 cells, the number and the size of tumor spheres were significantly decreased with si-RNA mediated HuR inhibition, indicating the inhibition of CSC population. HuR KO MIA PaCa2 cells had decreased number of spheres but the sizes of the spheres formed were not influenced (**Fig. 6.8.**).

As expected, the re-expression of HuR in MIA PaCa2 HuR KO cells increased the number of tumor spheres, with a moderate decrease in the size of tumor spheres formed (**Fig. 6.9.**). The increased number of tumor spheres indicated an increase in the number of CSCs. It is also possible that the loss of adhesion molecules in the tumor spheres contribute to the dissociation of tumor spheres, resulting in increased tumor sphere number.

As the CSC population is responsible for tumorigenicity *in vivo*, we compared the tumor formation rate of MIA PaCa2 HuR KO cells with that of the CRISPR/Cas9-control cells (HuR WT cells) in nude mice. HuR WT cells yielded 100% (16/16) tumor formation in 8 days after subcutaneous inoculation of 2×10^6 cells (day 8). Inoculation of the same number of HuR KO cells resulted in tumor formation rate of 25% (4/16) at day 8, which increased only to a final tumor formation rate of 37.5% (6/16) at day 21 **(Fig. 6.10. A)**. These data indicate that tumorigenicity of MIA PaCa2 cells was impaired with HuR gene deletion. We performed immunohistochemical staining to confirm the expression of HuR in MIA PaCa2 HuR WT tumors and MIA PaCa2 HuR KO tumors. As expected, HuR was not expressed in the HuR KO tumor cells **(Fig. 6.10. A)**. The tumor growth was also inhibited by HuR gene deletion. The HuR KO tumors grew significantly slower than the HuR WT tumors **(Fig. 6.10. B).**

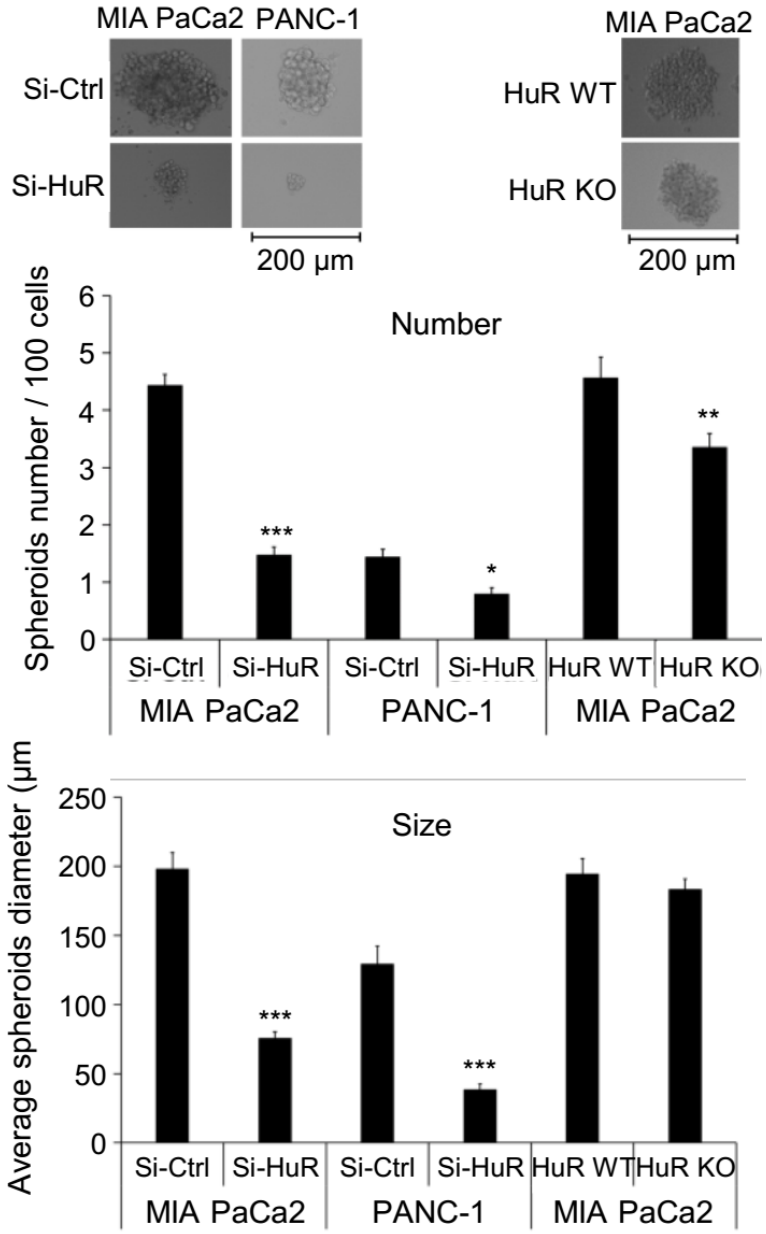

Figure 6.8. Suppression of HuR inhibited pancreatic CSCs in tumor sphere formation assay. PANC-1 and MIA PaCa2 cells were transfected with either Si-Ctrl or Si-HuR for 24 hours, and then seeded into the ultra-low attachment 96-well plates. The number and size of tumor spheres were measured at 14 days. Bar graphs show Mean ± SEM of 36 repeats. *$p < 0.05$; **$p < 0.01$; ***$p < 0.001$ by Student's t-test.

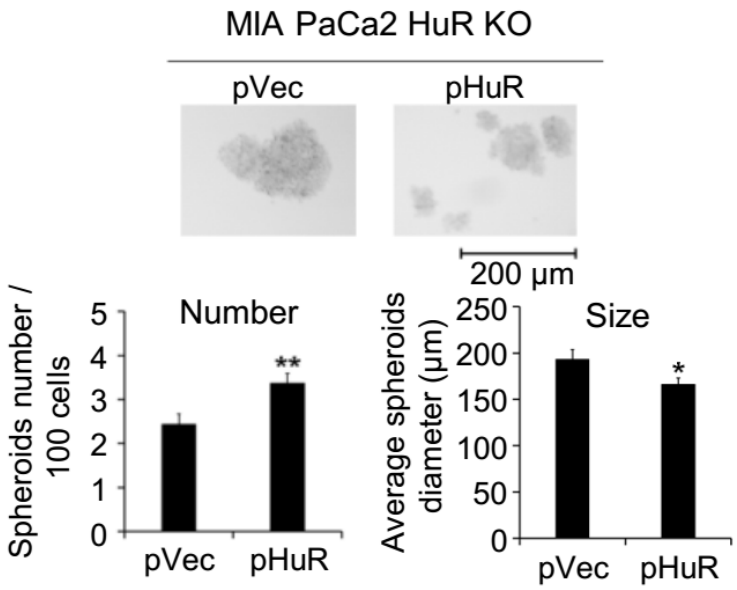

Figure 6.9. Re-expression of HuR promoted pancreatic CSCs in tumor sphere formation assay. PANC-1 and MIA PaCa2 cells were transfected with either Si-Ctrl or Si-HuR for 24 hours, and then seeded into the ultra-low attachment 96-well plates. The number and size of tumor spheres were measured at 14 days. Bar graphs show Mean ± SEM of 36 repeats. *p < 0.05; **p < 0.01 by Student's t-test.

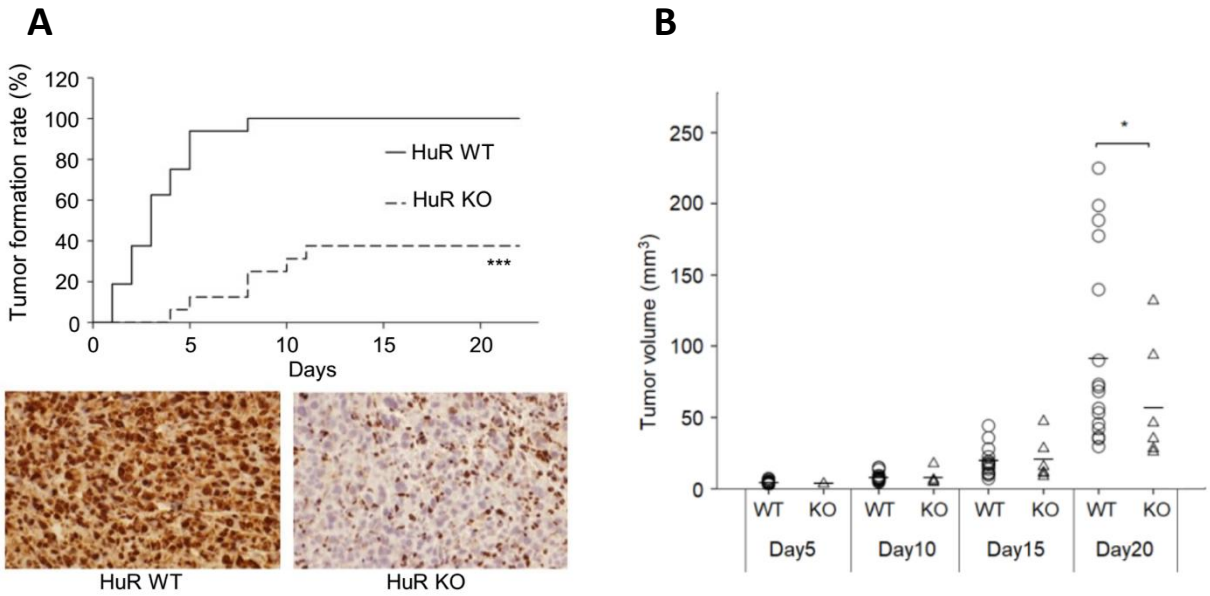

Figure 6.10. Suppression of HuR inhibited pancreatic cancer tumor formation and growth *in vivo*. (A) MIA PaCa-2 HuR WT cells and HuR KO cells were subcutaneously inoculated at the rate of $2x10^6$ cells per injection into the flank of nude mice (n=16 per group). ***p < 0.001 by Log-rank test. Immunohistochemistry staining was performed on paraffin embedded slides of collected tumors for HuR expression examination. (B) Tumor volume was measure with caliper. Each circle or triangle represents a tumor. The short bars show the mean tumor volume of each group. *p < 0.05 by Mann-Whitney U test.

6.1.4. HuR promoted EMT in pancreatic cancer by enhancing Snail

HuR typically regulates its target mRNAs by direct binding to the AU-rich elements (AREs) located in the 3'UTR of the target mRNAs, and thus protects the target mRNAs from degradation, resulting in increased expression.

We examined whether HuR bound to the mRNAs of important regulators of EMT and CSCs, using RNP-IP assay. Immunoprecipitation was performed in MIA PaCa2 total cell lysate with either anti-HuR antibody or IgG. The total RNA was extracted from the pull-down products, and then examined by RT-qPCR. mRNAs of a panel of EMT/CSC regulators showed strong association with HuR protein, including Snail, Slug, ZEB1, and β-catenin, as well as the mRNAs of the known HuR targets Msi1 and HuR (**Fig. 6.11. A**). The binding of HuR with these mRNAs were specific, since the expression of these mRNAs was hardly detected by a 40 cycle RT-qPCR amplification in the IgG pull-down products. As a comparison, MIA PaCa2 HuR KO cells were also used in the RNP-IP assay. As expected, due to the lack of HuR protein in the HuR KO cells, all these mRNAs were only detected at a background level in the pull-down products (**Fig. 6.11. A**). These data indicated that HuR bound to the mRNAs of a panel of EMT/CSC regulators in a cell-free system. Whether the binding of HuR to these putative target mRNAs is functionally important need to be further studied.

We hypothesized that the binding of HuR to these putative target mRNAs could protect these mRNAs from degradation. Both HuR WT and HuR KO MIA PaCa2 cells were treated with actinomycin D to block transcription, and then the stability of these mRNAs was detected in a 4-hour duration. We observed significantly enhanced degradation of Snail mRNA in HuR KO cells (**Fig. 6.11. B**). However, the stabilities of Slug, ZEB1, and β-catenin mRNAs were not altered with HuR KO (**Fig. 6.12. A**), despite the fact that they were bound to HuR in the cell-free

system. Consistently, the protein level of Snail was decreased with HuR knockdown (**Fig. 6.2.**), whereas the protein levels of Slug, Zeb1 and β-catenin were minimally influenced (**Fig. 6.12. B**). As Snail is a primary EMT-TF, the data illustrated that HuR regulated EMT progression by direct binding to Snail mRNA.

The direct interaction of HuR with the 3'UTR of Snail mRNA was then examined with a luciferase reporter assay. The full length 3'UTR and two truncated Snail mRNA 3'UTRs (ΔAREs, and AREs) were each constructed into the pmirGLO vector, which contains a firefly luciferase gene under the PGK promoter (**Fig. 6.13. A**). The sequence of ΔAREs did not contain the AREs, whereas the sequence of AREs contained a major cluster of the AREs in the 3'UTR of Snail mRNA. MIA PaCa2 HuR KO cells were then co-transfected with pHuR or pVec, and the pmirGLO plasmid containing each of the constructed 3'UTRs of Snail mRNA. Our data clearly show that HuR over-expression enhances the luminescence signal only with the presence of the AREs in the 3'UTR of Snail mRNA (Full length construct and AREs construct). When the AREs in the 3'UTR of Snail mRNA were absent (ΔAREs), the luminescence signal did not change with HuR over-expression (**Fig. 6.13. B**).

To further determine the functional importance of Snail in the HuR regulated EMT and migration, we over-expressed Snail in HuR KO MIA PaCa2 cells. The migration ability of the cells was then examined. Data showed that the restoration of Snail significantly increased migration of the HuR KO MIA PaCa2 cells (**Fig. 6.14.**).

Taken together, data here demonstrated that HuR directly bound to the AREs in the 3'UTR of Snail mRNA, and thus stabilized Snail mRNA from degradation, resulting in EMT progression and increased cell migration/invasion in pancreatic cancer cells.

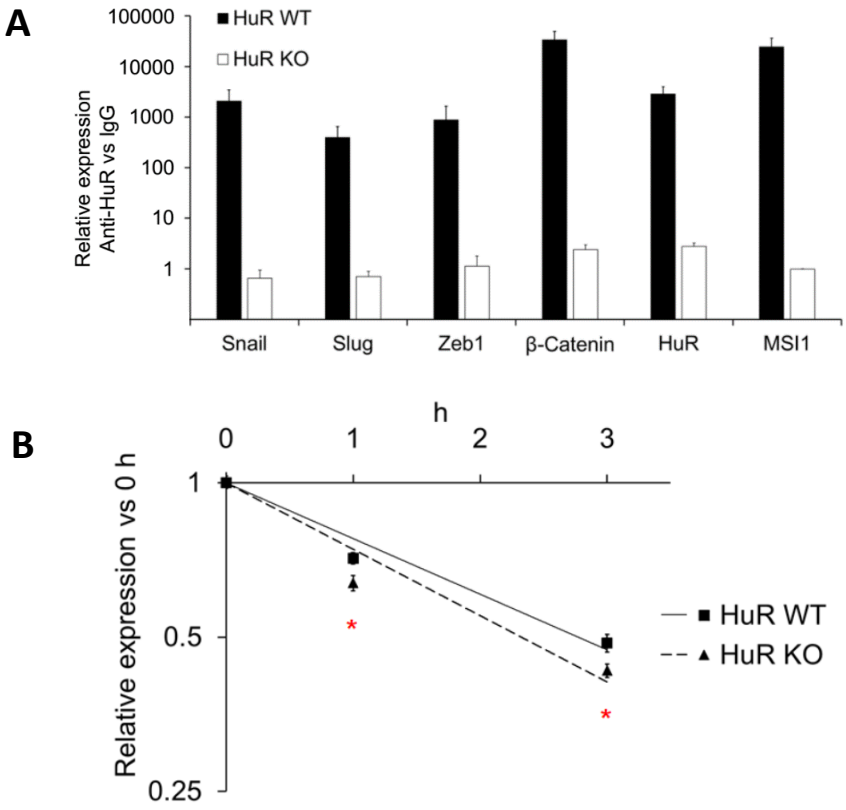

Figure 6.11. HuR bound to the mRNAs of EMT regulators. (A) RNP-IP detection of HuR binding mRNAs of EMT-related genes. Data for each individual mRNA was normalized to the IgG pull-down product of that mRNA. Bar graphs show Mean ± SEM of 9 repeats. (B) Stability of Snail mRNA in MIA PaCa-2 HuR WT and HuR KO cells. Transcription was blocked by actinomycin D (5 μg/ml) treatment 30 minutes before the first sample was collected (0 hours). Data shows Mean ± SEM of 9 repeats. *$p < 0.05$ by Student's t-test.

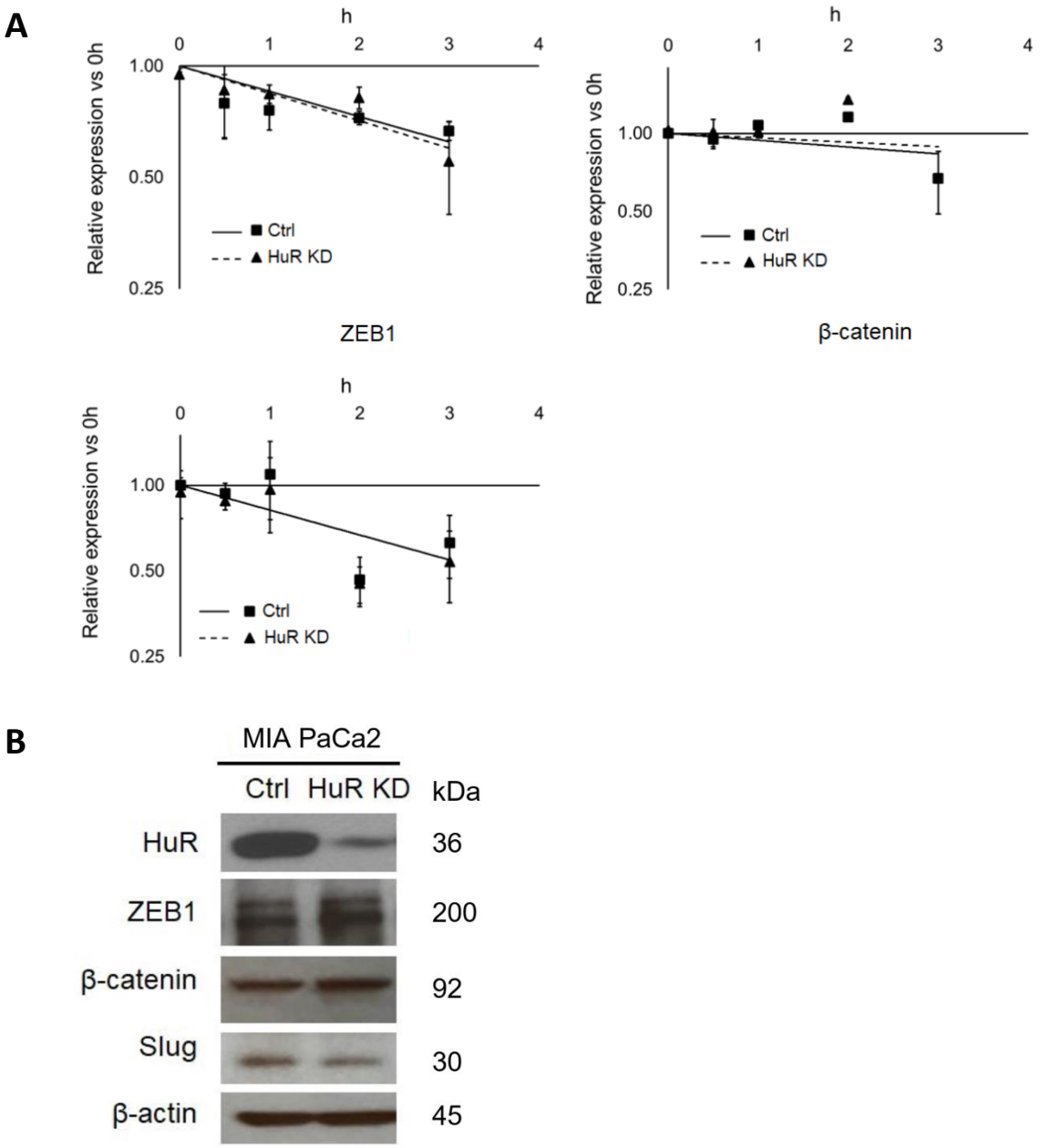

Figure 6.12. HuR suppression did not influence the mRNA stabilities and protein levels of ZEB1, β-catenin and Slug. (A) mRNA stability was detected by RT-qPCR. MIA PaCa2 cells were transfected with either Si-Ctrl (Ctrl) or Si-HuR (HuR KD) for 24 hours. Transcription was then blocked by actinomycin D (5 μg/ml) treatment 4 hours before the first sample was collected (0 h). (B) Protein levels were detected by western blot. β-actin was a loading control.

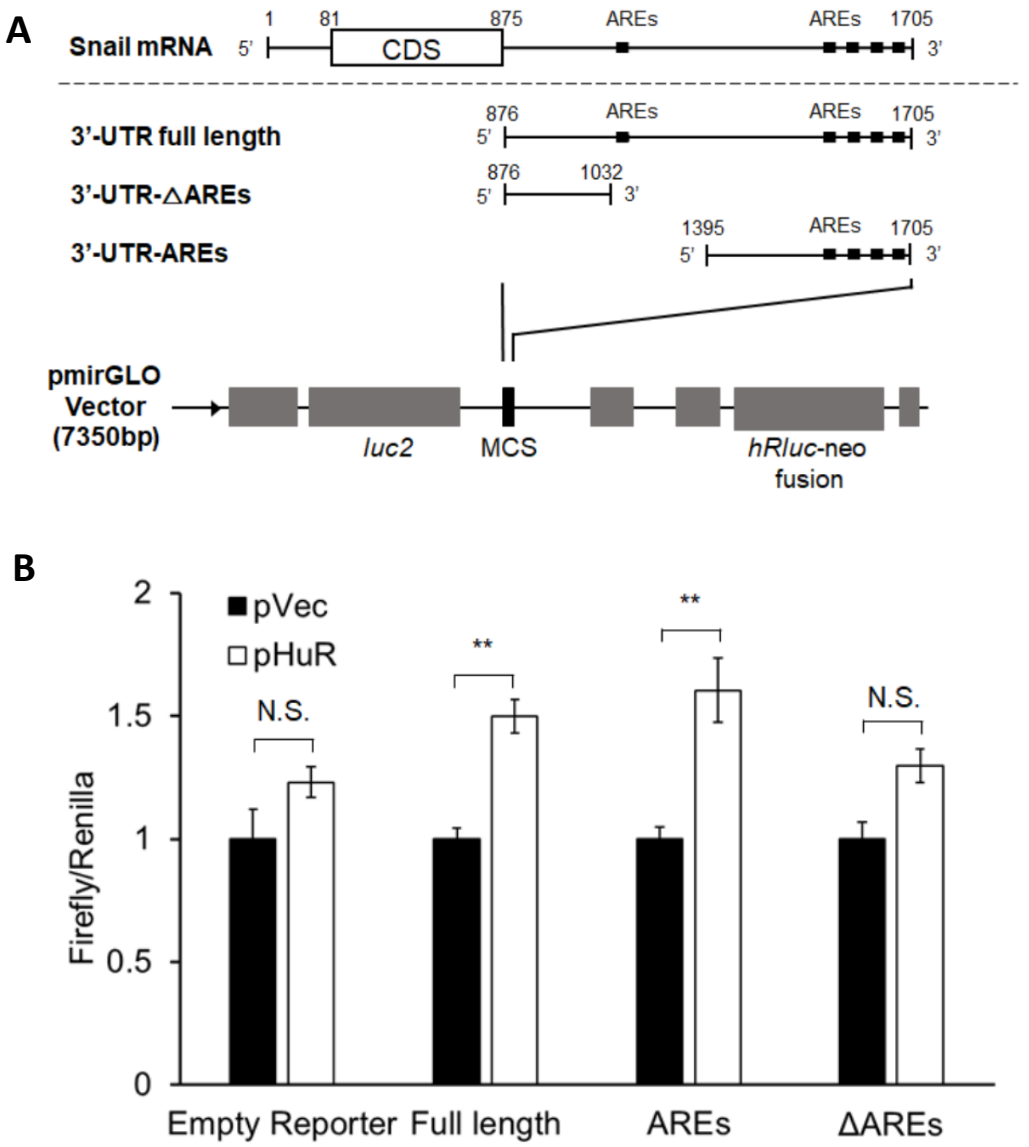

Figure 6.13. HuR direct bound to AREs in the 3'UTR of Snail mRNA. (A) Schematic diagram showing the constructions of dual-luciferase reporter (pmirGLO) with the full length and two truncations of the 3'UTR of Snail mRNA. (B) Dual-luciferase reporter assay. MIA PaCa-2 HuR KO cells were co-transfected with pHuR or pVec, and pmirGLO plasmid containing each of the constructed 3'UTRs of Snail mRNA (either the full length, AREs or ΔAREs, or empty reporter). **p < 0.01 by one-way ANOVA-Tukey's test.

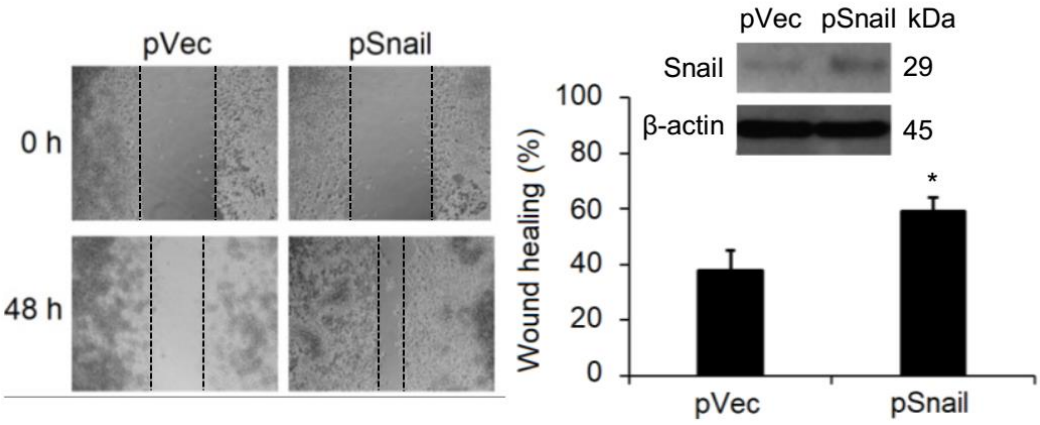

Figure 6.14. Re-expression of Snail in MIA PaCa2 HuR KO cells promoted cell migration in wound healing assay. Cells were transfected with empty vector (pVec) or pCDNA3.1-Snail plasmid (pSnail) for 48 hours. The level of Snail was examined by western-blot, using β-catenin as a loading control. Cells were then plated into 24-well plates to form confluent monolayer. Scratch was made on confluent monolayer cells with a 10µl pipette tip (0 hour). Cell migration was measured after 48 hours. Bar graph shows what percentage was covered by cells. Bar graphs represent Mean ± SEM of $\geqslant$ 3 repeats. *$p < 0.05$ by Student's t-test.

6.2. Discussion

In pancreatic cancer, higher HuR level is associated with higher tumor T stage in patients [374]. HuR is unlikely to be a tumor initiator in pancreas by itself, but rather facilitates tumor development [428]. Pancreas specific transgenic HuR mouse did not form spontaneous tumor, instead, the elevated intra-pancreas HuR level promoted a pancreatitis-like inflammatory microenvironment that could facilitate tumor development [428]. Specific silencing or knockout of HuR inhibited pancreatic cancer cell proliferation, migration, invasion, and disabled *in vivo* xenograft formation [429]. We hypothesized that HuR plays an important role in regulating pancreatic cancer cell EMT and stemness, and this regulation underlines the aggressiveness of the tumor in terms of invasion, metastasis, drug resistance and new tumor generation. Data here reveal that HuR enhances pancreatic cancer cell EMT, mainly by stabilizing Snail mRNAs and enhancing its protein expression. This enhancement in EMT promotes pancreatic cancer cell migration and invasion. The enhancement of EMT process by HuR also has implications in pancreatic CSC formation and maintenance. Inhibition of HuR dampened the ability of pancreatic cancer cell to migrate and invade, and inhibited tumor initiation in mice. These data add to our knowledge of the role that HuR is playing in tumor metastasis and cancer stem cells, which was not well understood before.

HuR is more and more recognized as a responder in the cells to various stresses and is involved in many physiological and pathological processes. Apparently, its function and the downstream genes regulated are different in different tissues and under different conditions. For example, under hypoxia HuR enhances VEGF and HIF-1α expression [430], whereas under oxidative stress HuR enhances expression of cyclins and sirtuins [431]. HuR is also shown to causally linked to the onset of inflammation in kidney disease [432], and contributes to liver fibrosis

[433], as well as many other pathological processes related to inflammation. In adipose tissue HuR protects against diet-induced obesity and insulin resistance [430]. The oncologic microenvironment and the cancer cell itself might provide a “stress” condition that upregulates and activates HuR, with mechanisms not yet understood. Data here show that HuR was differentially expressed in cancerous and normal pancreatic cells and mouse tissues, consistent with clinical reports of the association between HuR levels and pancreatic cancer. The results here showed that in pancreatic cancer cells, HuR bound to a panel of mRNAs of regulator genes in the process of cancer cell EMT, but apparently the binding did not influence protein expressions of all the bound mRNAs. Here, only Snail mRNA was stabilized and protein expression increased. The mechanism of this selectivity remains to be understood. Another unexplored area in this study is the potential interaction and crosstalk between the tumor microenvironment and HuR expression and function in the cancer cells and in the surrounding cells such as pancreatic stellate cells, immune cells, and fibroblasts.

In this study, we mainly focused on the relationship of HuR with pancreatic cancer EMT and CSCs. As a post-transcriptional regulator with a wide spectrum of downstream targets, it is undeniable that HuR may also regulates other biological events in pancreatic cancer, such as cancer cell proliferation, angiogenesis, and inflammation. Indeed, our data show that MIA PaCa2 HuR KO cells have an increased doubling time compared to the MIA PaCa2 HuR WT cells. The tumor growth of MIA PaCa2 HuR KO cells was also impaired *in vivo*, compared to the MIA PaCa2 HuR WT cells. It is possible that the inhibition of cell migration and invasion we detected in MIA PaCa2 HuR KO cells could be a combination of cell proliferation inhibition and migration/invasion inhibition. Interestingly, there was no difference between the doubling time of MIA PaCa2 si-Ctrl cells and MIA PaCa2 si-HuR cells, or PANC-1 si-Ctrl cells and PANC-1

si-HuR cells. Given that si-HuR is only a partial and transient suppression of HuR compared with gene deletion, and si-HuR in both MIA PaCa2 and PANC-1 cells inhibited migration and invasion, it is likely that HuR has more significant effects on cell migration/invasion than proliferation in the tested cells. Taken together, our studies illustrated that the inhibition of HuR in pancreatic cancer cells primarily inhibited the migration and invasion.

In summary, studies included in this chapter show that the suppression of HuR inhibited pancreatic cancer cell EMT and consequently inhibited migration, invasion, and CSCs through inhibition of the EMT-TF Snail. HuR directly binds to the AREs in the 3'UTR of Snail mRNA, resulting in the stabilization of Snail mRNA, increased level of Snail, and progression of EMT. Suppression of HuR enhances Snail mRNA degradation and Snail protein downregulation.

Chapter 7. A Novel HuR Inhibitor, KH-3, Inhibits Pancreatic Cancer EMT, Metastasis and CSCs *In Vitro* and *In Vivo*

In chapter 6, we demonstrated that the knockdown of HuR inhibited pancreatic cancer EMT, migration, invasion, and CSCs. Given that HuR has different levels in cancer cells versus normal cells, and given its function in tumor progression, targeting HuR has the potential to inhibit tumor growth, metastasis, and avoid drug resistance and tumor recurrence. Therefore, HuR is an attractive target for the development of novel drugs for pancreatic cancer management.

Efforts in developing small molecule inhibitors of HuR have not been successful so far. Especially, there is a lack of small molecules that directly interrupt HuR-mRNA binding. In this chapter, we identified a novel HuR inhibitor that directly binds to HuR and interrupts HuR-mRNA binding. We investigated its effects on pancreatic cancer progression, metastasis, and tumorigenesis *in vitro* and *in vivo*.

7.1. Results

7.1.1. Screening for inhibitors of pancreatic cancer EMT

In an effort to discover new inhibitors for pancreatic cancer EMT, Dr. Liang Xu's group at the University of Kansas developed a high throughput screening (HTS) assay to identify HuR inhibitors. A screening of about 6000 compounds, including 28 structural derivatives to the HDAC inhibitors SAHA and MS-275, found that compound KH-3 (**Fig. 7.1. A**) was one of the top hits. KH-3 is a structural derivative to SAHA and MS-275. Our study found that KH-3 reduced the viability of pancreatic cancer cell lines PANC-1 and BxPc-3 more potently than its parent compounds SAHA and MS-275 (**Fig. 7.1. B, C**). KH-3 had IC_{50} values of 21 μM for PANC-1 and 6.25 μM for BxPC-3 cells, while SAHA had IC_{50} values of >40 μM for PANC-1 and 16 μM for BxPC-3. MS-275 had IC_{50} values of >40 μM for PANC-1 and > 50 μM for BxPC-3 (**Fig. 7.1. D**). Neither KH-3 nor the parent compounds significantly affected the viability

of the normal pancreatic ductal epithelial cells hTERT-HPNE even at a concentration of 40 µM (**Fig. 7.1. D**).

We then examined the HDAC inhibition activity of KH-3 using SAHA and MS-275 as positive controls. As expected, both SAHA and MS-275 showed potent HDAC inhibition activity by increasing the acetylation of all four histones (H2A, H2B, H3, and H4). Surprisingly, KH-3 hardly showed any HDAC inhibiting activities, as it minimally increased the acetylation of the histones (H3 and H4) as compared to the control (**Fig. 7.2.**). The data indicate that KH-3 is not an HDAC inhibitor. Considering that KH-3 had the lowest IC_{50} values for pancreatic cancer cell proliferation, it should have other mechanism(s) of action than HDAC inhibition.

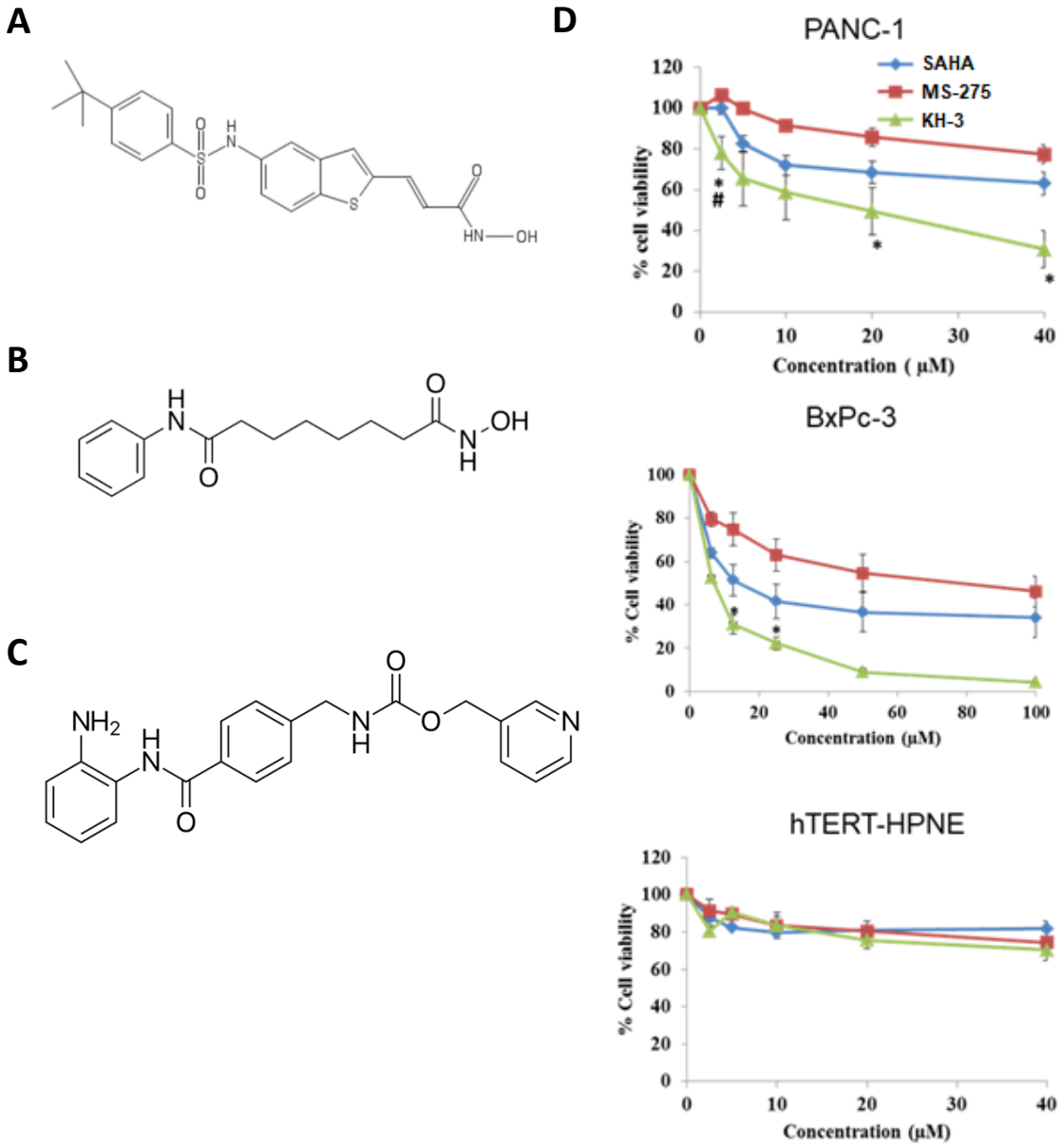

Figure 7.1. KH-3 reduced the cell viability of pancreatic cancer cell lines with limited effect on normal pancreatic ductal cells. (A) Structure of compound KH-3. (B) Structure of HDAC inhibitor SAHA. (C) Structure of HDAC inhibitor MS-275. (D) PANC-1, BxPc-3 and hTERT-HPNE cells were treated with increasing concentrations of either SAHA, MS-275 or KH-3. Cell viability was then measured by MTT assay after 48 hours for PANC-1 and hTERT-HPNE cells, and after 24 hours for BxPc-3 cells. *$p < 0.05$ versus MS-275; #$p < 0.05$ versus SAHA by Student's t-test.

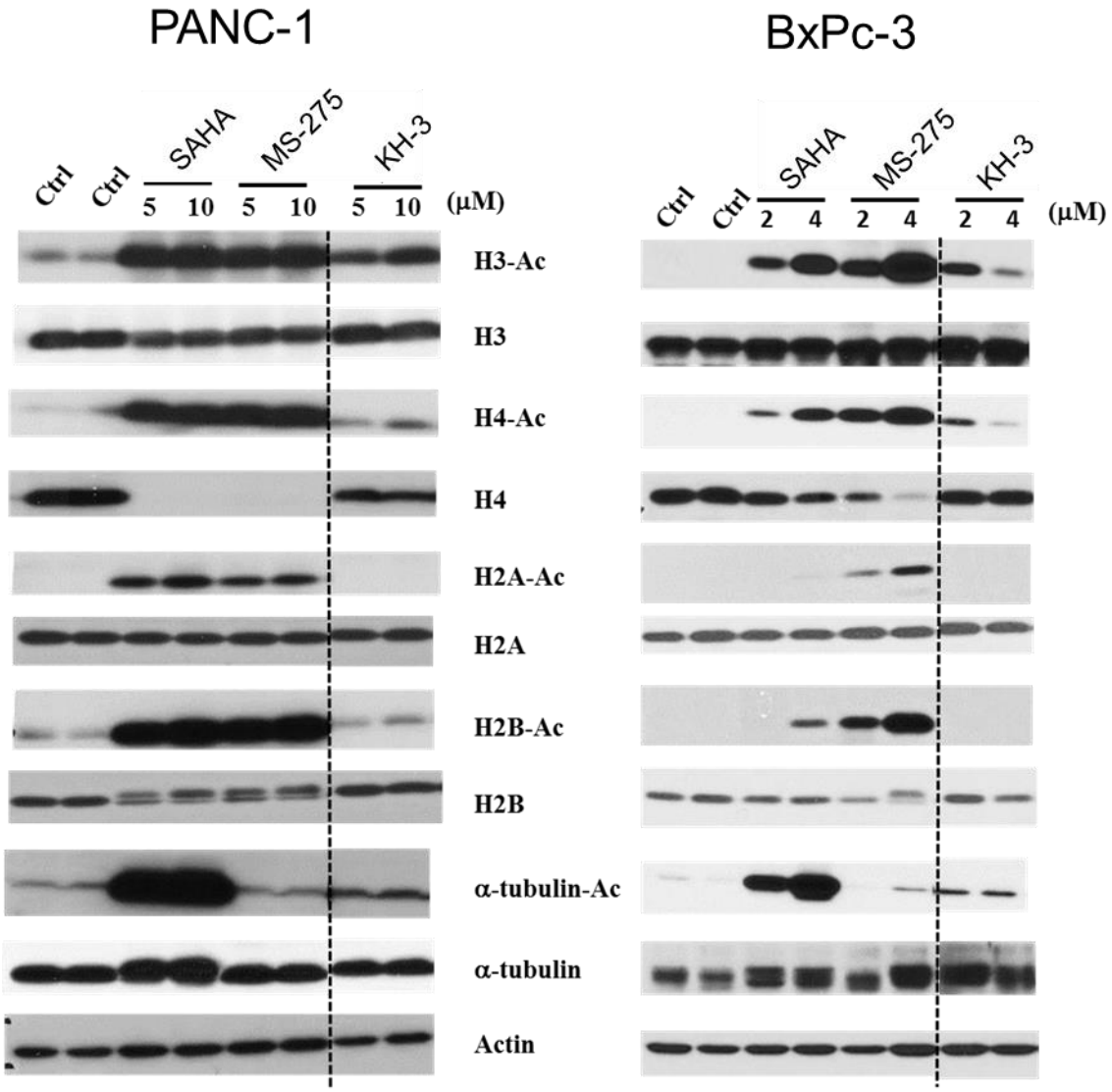

Figure 7.2. KH-3 lost HDAC inhibitory activity compared with parent compound SAHA and HDAC inhibitor MS-275. PANC-1 and BxPc-3 cells were treated with SAHA, MS-275, KH-3 or vehicle control (DMSO) for 24 hours. Acetylation of histones and α-tubulin was detected by western blot. Actin was used as a loading control.

7.1.2. A novel HuR inhibitor KH-3 disrupted HuR-mRNA interaction and inhibited pancreatic cancer cell viability depending on endogenous HuR level.

As KH-3 was identified as one of the top hits in the screening assay for HuR inhibitors, it is reasonable to examine the HuR binding infinity of KH-3. Direct binding of KH-3 with HuR was then examined by Surface Plasmon Resonance (SPR), a label-free technique to measure biomolecular interactions in real-time. The RNA recognition motifs (RRM1/2) of the human recombinant HuR protein were immobilized on the surface of the sensor chip. The data show that KH-3 bound to RRM1/2, resulting in an increase in the refractive index which change the measured resonance angle. The increase in resonance (RU) corresponded to the KH-3 concentration (**Fig. 7.3. A**). Through its binding, KH-3 disrupted HuR interaction with its known target mRNA, the Msi1 mRNA, with Ki values in nM range, as shown in the Fluorescence Polarization Assay (FPA) using the full-length HuR protein (**Fig. 7.3. B**), and in an Amplified Luminescent Proximity Homogeneous Assay (Alpha assay) using the RNA binding motifs RRM1/2 (**Fig. 7.3. C**). KH-1, which is a negative hit in the screening assay for HuR inhibitors, was used as a negative control. KH-1 did not disrupte HuR interactions with its known target mRNA, the Msi1 mRNA.

Endogenous HuR levels in PANC-1, MIA PaCa2, BxPc-3 and hTERT-HPNE Cells were quantified by western blot. The resulting expression levels correlated negatively with the IC_{50} values of KH-3 for the respective cell lines **(Fig 7.4.)**. MIA PaCa2 cells had the highest HuR protein abundance among the four tested cell lines and were the most sensitive to HuR treatment (IC_{50} = 5 µM). PANC-1 cells had the lowest HuR expression level and were the most resistant among the three cell lines (IC_{50} = 25 µM). BxPC-3 cells had an intermediate HuR expression level and the IC_{50} of KH-3 was in the middle (10 µM). The human pancreatic ductal

epithelial cell line, hTERT-HPEN, had the lowest abundance of HuR protein compared with the cancer cells, and the IC_{50} was the highest (IC_{50} >> 40 μM). The correlation between IC_{50} values and endogenous HuR level was tested by Pearson correlation coefficient method and a correlation coefficient value of -0.71 was found, indicating a strong inverse correlation. This inverse correlation of HuR expression levels and sensitivity to KH-3 treatment in the four tested cell lines suggested that KH-3 exerts its anti-pancreatic cancer activity through HuR (**Fig. 7.4.**)

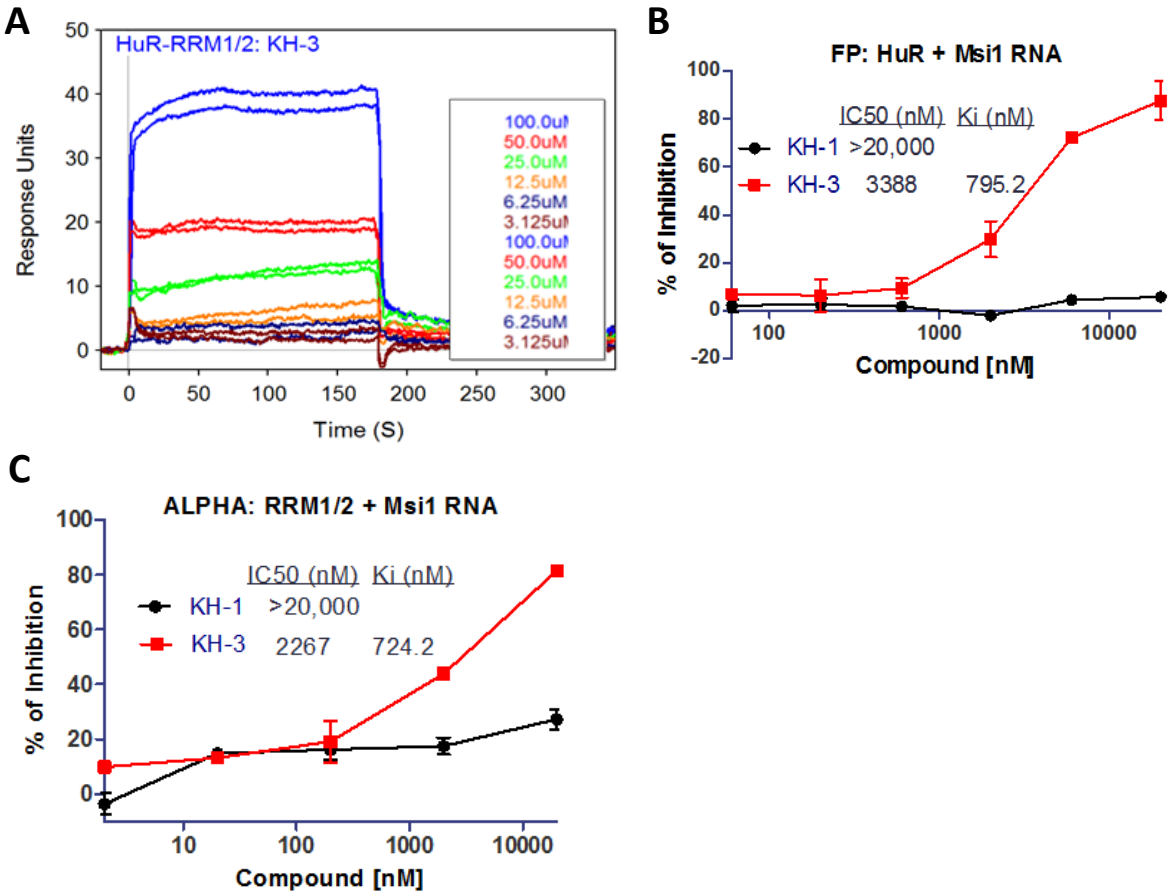

Figure 7.3. KH-3 was identified as an HuR inhibitor that directly binds to HuR and can disrupt HuR-mRNA interactions. (A) Surface plasmon resonance (SPR) assay showing direct binding of KH-3 to immobilized HuR-RRM1/2. (B) Fluorescence polarization (FP) assay showing interruption of KH-3 to the binding of MSI1 mRNA with HuR protein. A synthetic HDAC inhbitor KH-1 was used as negative control. Twenty-five nM full-length human HuR and 2 nM FITC-labeled 16-nt MSI1 RNA sequence was used. (C) Amplified Luminescent Proximity Homogeneous Assay (Alpha assay) showing KH-3 inhibited the binding of *MSI1* mRNA to HuR-RRM1/2. 100 nM His-tagged HuR RRM1/2 fragment and 25 nM biotinylated 16-nt *MSI1* mRNA sequence were used. KH-1 did not inhibit the binding of *MSI1* mRNA to HuR-RRM1/2. Labeled scramble 16-nt RNA was used as control. Ki values were calculated based on the Kd and the dose-response curves.

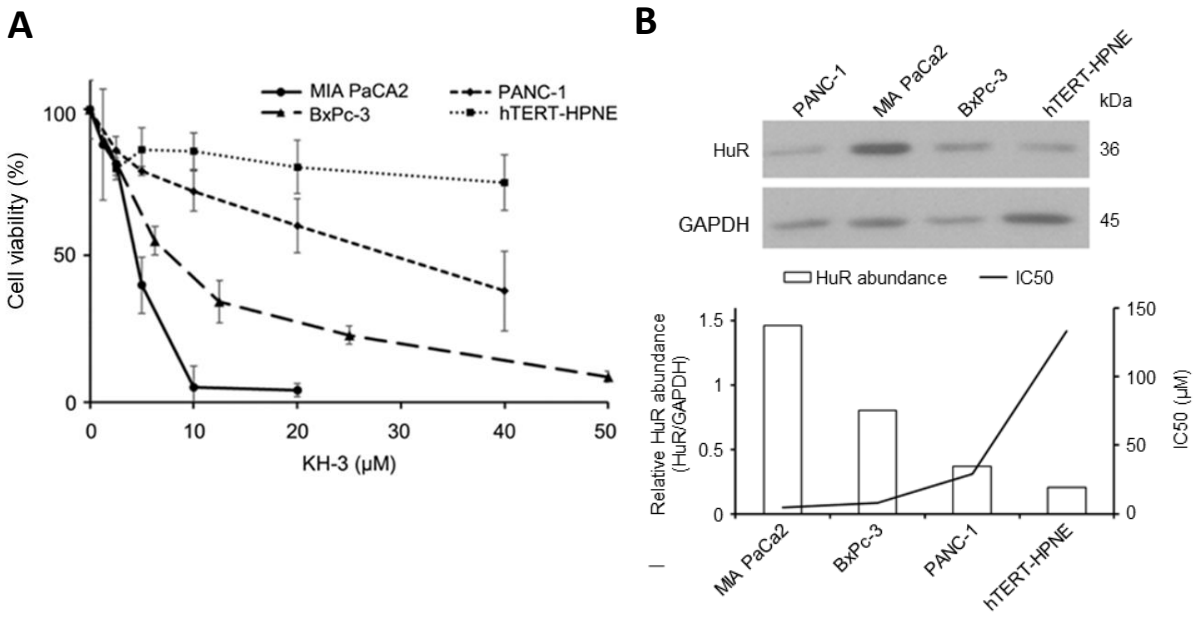

Figure 7.4. HuR protein amount negatively correlates with cell viability of different pancreatic cancer lines in the presence of KH-3. (A) PANC-1, MIA PaCa2, BxPc-3, and hTERT-HPNE cells were treated with increasing concentrations of KH-3. Cell viability was then measured by MTT assay after 48 hours. (B) Upper: Western blot showing endogenous HuR levels of the tested cell lines. Lower: Correlation of HuR levels and sensitivity of cells to KH-3 treatment. Bars show relative band density of HuR normalized to GAPDH, and the line shows IC_{50} values of KH-3.

7.1.3. KH-3 inhibited pancreatic cancer EMT, migration, invasion, and CSCs *in vitro* by inhibiting HuR functions

In chapter 6, we have demonstrated that the inhibition of HuR by either si-HuR or CRISPR/Cas9 based HuR gene deletion led to the inhibition of pancreatic cancer EMT, migration, invasion, and CSCs. As an HuR inhibitor, KH-3 was expected to mimic the effects of HuR downregulation on pancreatic cancer EMT, migration, invasion, and CSCs.

In order to investigate the effect of KH-3 on pancreatic cancer, the levels of EMT signature proteins were first examined by western blot. KH-3 treatment in both MIA PaCa2 and PANC-1 cells decreased Vimentin and Snail, two mesenchymal markers, and increased the epithelial marker Claudin-1 (**Fig. 7.5.**), mimicking HuR knockdown as shown in chapter 6 (**Fig. 6.2.**). The level of HuR was not changed with KH-3 treatment (**Fig. 7.5**), indicating that KH-3 exerted its function through interrupting HuR-mRNA binding rather than altering HuR expression.

A wound healing assay was then used to examine how cell migration was affected by KH-3 treatment. In both MIA PaCa2 and PANC-1 cells, KH-3 significantly inhibited cell migration in a dose dependent manner (**Fig. 7.6., 7.7.**). Knockdown of HuR by si-RNA and gene deletion by CRISPR/Cas were then used to examine the target specificity of KH-3. Consistent with data in Chapter 6 (**Fig. 6.4.**), in both MIA PaCa2 and PANC-1 cells, si-HuR reduced migration compared with the control treatment (**Fig. 7.6.**), and MIA PaCa2 HuR KO cells had dramatically inhibited cell migration (**Fig. 7.7.**). KH-3 did not show an additional effect on the cell migration in cells where HuR expression was suppressed (both si-HuR cells and HuR KO cells), indicating a loss-of-target effect for KH-3 (**Fig. 7.6., 7.7.**).

We then re-expressed HuR in HuR KO MIA PaCa2 cells by transfecting the cells with an HuR-expression plasmid (pHuR). After restoring HuR expression, KH-3 partially inhibited cell

migration (**Fig. 7.8.**). These data demonstrate that KH-3 induced inhibition of migration is dependent on HuR.

Cell invasion was further examined by the Boyden Chamber assay. KH-3 significantly inhibited both migration and invasion of MIA PaCa2 cells (**Fig. 7.9.**).

In addition, tumor sphere formation was also inhibited by KH-3 treatment. In PANC-1 cells, 10 μM of KH-3 eliminated the tumor spheres, while 4 μM of KH-3 had a similar effect in MIA PaCa2 cells. Also, in BxPC-3 cells, 8 μM of KH-3 significantly inhibited both the number and the size of tumor spheres (**Fig. 7.10.**).

Taken together, as an HuR inhibitor, KH-3 successfully mimicked the effects of HuR knockdown and inhibited pancreatic cancer cell EMT, migration, invasion, and CSCs. The inhibitory effects of KH-3 on pancreatic cancer was HuR dependent.

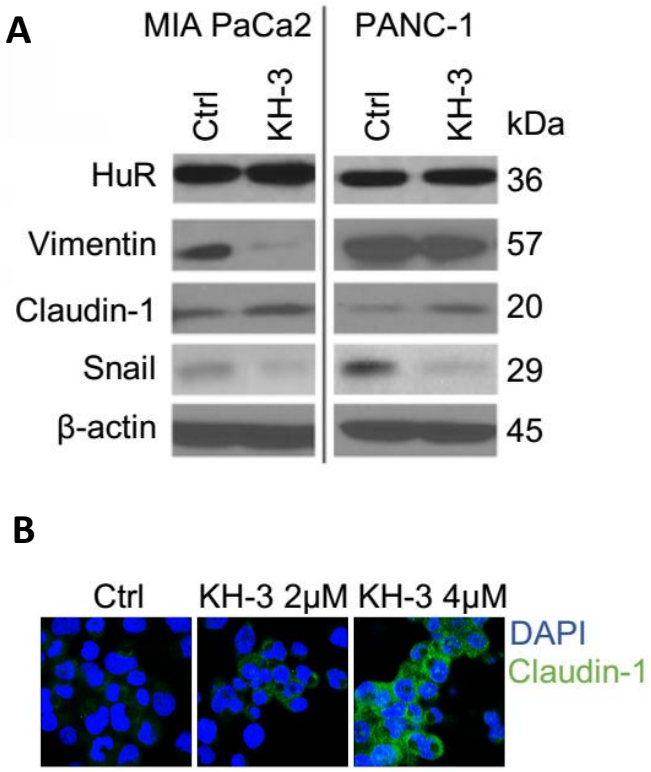

Figure 7.5. KH-3 inhibited expression of mesenchymal and promoted expression of epithelial markers in pancreatic cancer cells. (A) Western blots of MIA PaCa-2 and PANC-1 cells showing expression of HuR and EMT markers. β-actin was a loading control. MIA PaCa-2 cells were treated with 2 μM and PANC-1 cells with 5 μM KH-3 for 24 hours, based on their IC_{50} values. (B) Immunofluorescence staining for Claudin-1 in MIA PaCa-2 cells. Cells were treated with 2 μM and 4 μM KH-3 for 24 hours, and nuclei were DAPI stained.

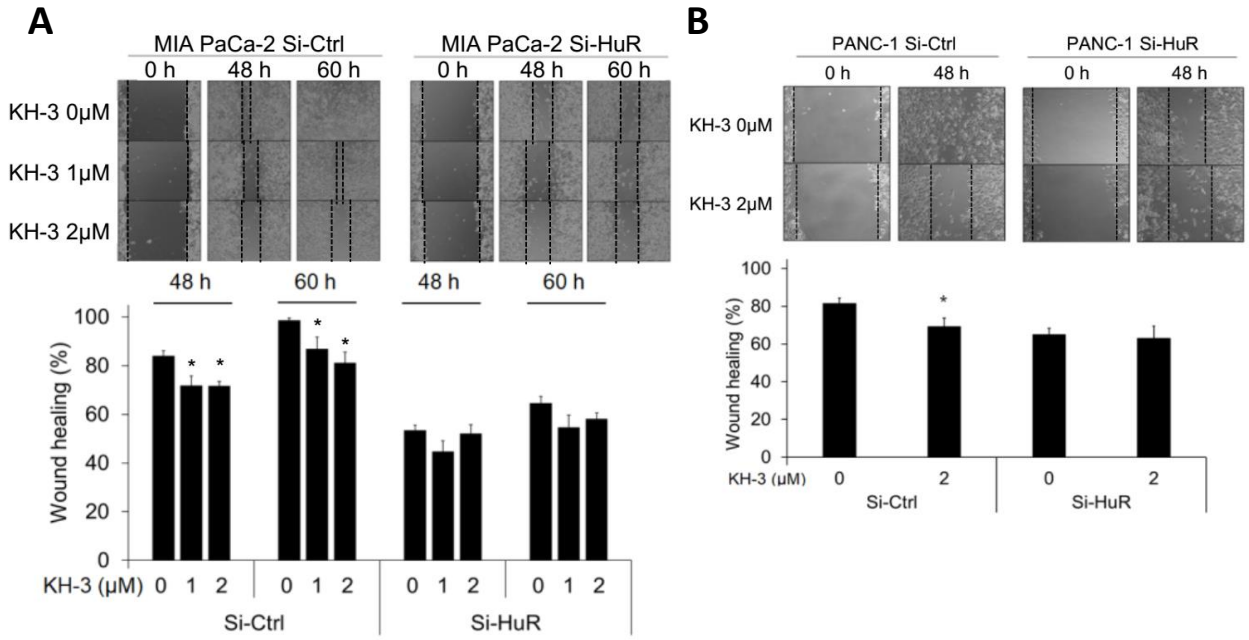

Figure 7.6. KH-3 inhibition of cell migration in MIA PaCa2 and PaCa2 cells was lost upon si-HuR treatment. MIA PaCa2 (A) and PANC-1 (B) cells were transfected with either si-Ctrl or si-HuR for 24 hours, and then plated into 24-well plates to form confluent monolayer. Scratches were made on confluent monolayers with a 10μL pipette tip (0 hours). MIA PaCa2 cells were then exposed to 1 μM and 2μM KH-3. PANC-1 cells were exposed to 2 μM KH-3. Cell migration was measured at 48 hours and 60 hours. Bar graph shows what percentage was covered by cells after 48 or 60 hours. The results represent mean ± SEM of ⩾ 3 repeats. *$p < 0.05$ by one-way ANOVA-Tukey's test (A) or Student's t-test (B) as compared to control.

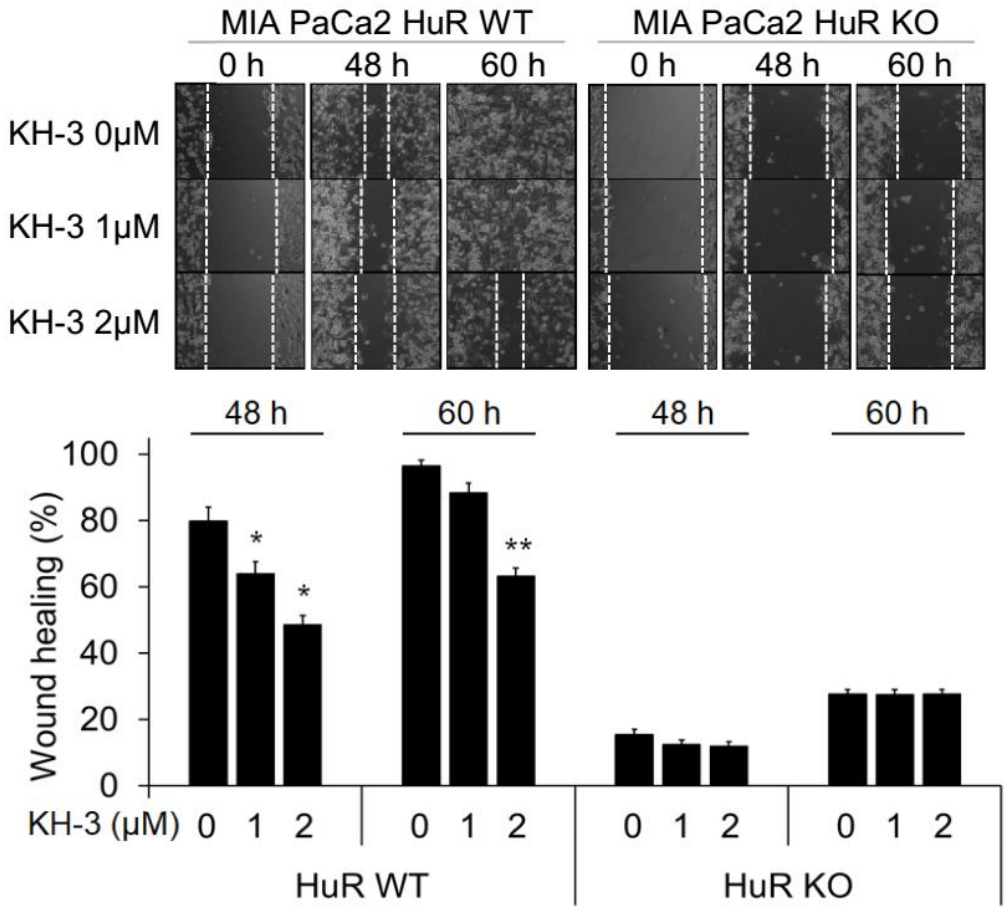

Figure 7.7. KH-3 inhibition of cell migration in MIA PaCa2 cells was lost after HuR knockout. The HuR gene was deleted in MIA PaCa2 cells by CRISPR/Cas9. Cells were plated into 24-well plates to form confluent monolayer. A scratch was made on confluent monolayer cells with a 10μL pipette tip (0 hour). Cells were then exposed to1 μM and 2μM KH-3 and cell migration was measured after 48 and 60 hours. Bar graph shows the percentage covered by cells. Bar graphs represent mean ± SEM of ⩾ 3 repeats. *$p < 0.05$; **$p < 0.01$ by one-way ANOVA-Tukey's test as compared to control.

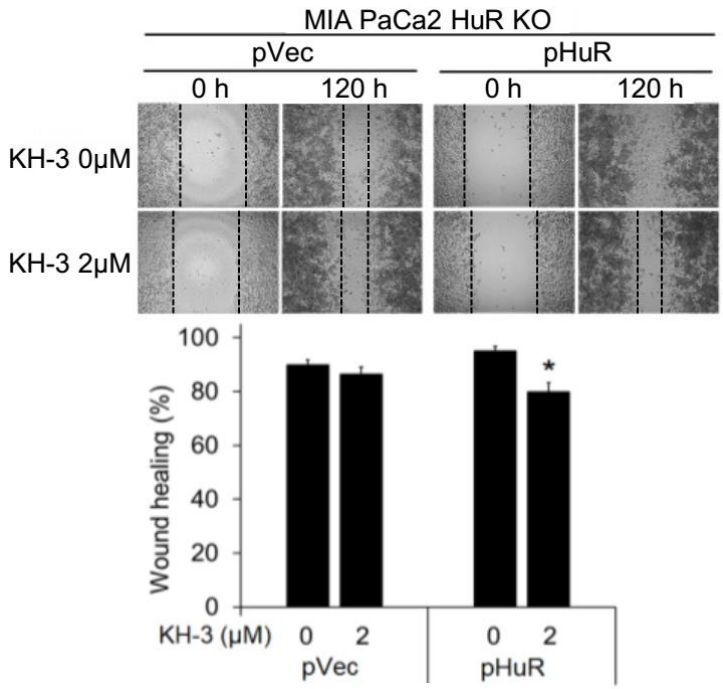

Figure 7.8. HuR re-expression in MIA PaCa2 HuR KO cells partially rescued the effect of KH-3. MIA PaCa2 HuR KO cells were generated by CRISPR/Cas9. Cells were then transfected with empty vector (pVec) or pcDNA3.1-HuR (pHuR) for 48 hours and then plated into 24-well plates to form confluent monolayers. A scratch was made on confluent monolayers with a 10μL pipette tip (0 hour). Some cells were then exposed to 2μM KH-3. Cell migration was measured after 120 hours. Bar graph shows the percentage covered by cells. Bar graphs represent mean ± SEM of ⩾ 3 repeats. *$p < 0.05$ by Student's t-test as compared to control.

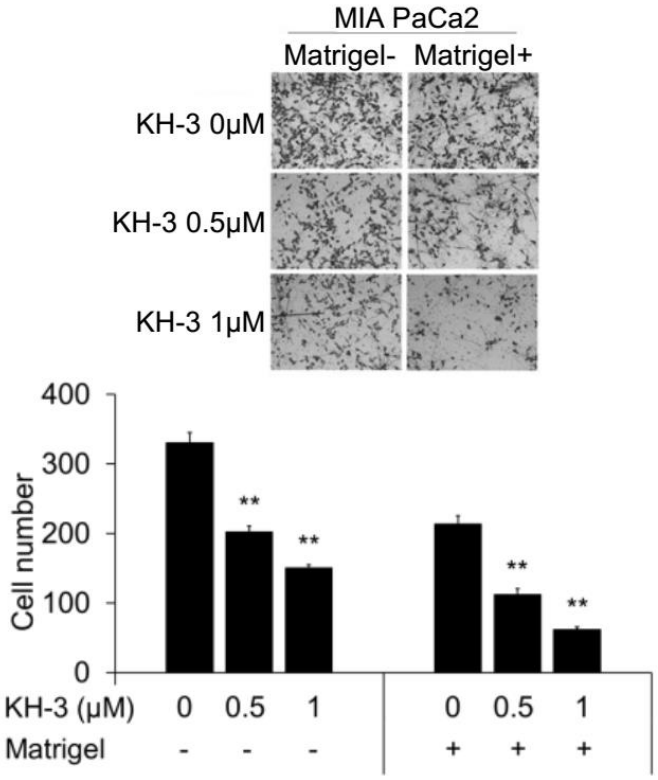

Figure 7.9. KH-3 inhibited the migration and invasion of MIA PaCa2 cells in the Boyden Chamber assay. MIA PaCa2 cells were plated into the Boyden Chamber in the presence of either 0, 0.5 or 1 μM KH-3. Cell migration (Matrigel-) and invasion (Matrigel+) were determined after 48 hours. Bar graphs show the mean ± SEM of migrated/invaded cells per field. Each treatment was triplicated. *$p < 0.05$; **$p < 0.01$ by one-way ANOVA-Tukey's test as compared to control.

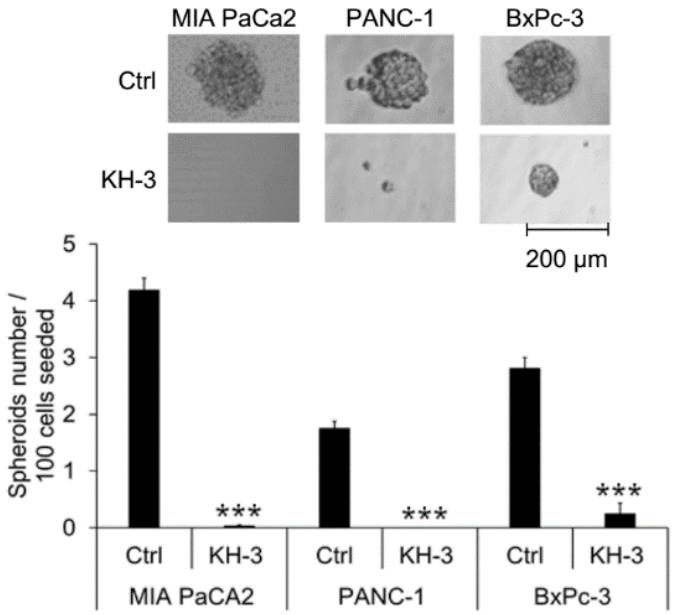

Figure 7.10. KH-3 inhibited pancreatic cancer tumor sphere formation. Cells were seeded at 100 cells/well in ultra-low attachment 96-well plates. MIA PaCa-2 cells were treated with 4 µM of KH-3, PANC-1 cells with 10 µM, and BxPC-3 cells 8 µM. Spheres were imaged and counted 14 days post seeding. Bar graphs show mean ± SEM of 36 repeats. ***$p < 0.001$ by one-way ANOVA-Tukey's test as compared to control.

7.1.4. KH-3 decreased Snail mRNA stability and protein expression.

Data in chapter 6 demonstrate that HuR bound to the mRNAs of a panel of EMT regulators (**Fig. 6.10., 6.11., 6.12.**). Here we examine the effects of KH-3 on the binding of HuR to its targets. We expected that upon KH-3 treatment, HuR target mRNAs would be less likely to co-precipitate with HuR. In order to prevent the re-binding of HuR with target mRNAs in a cell-free immunoprecipitation procedure, KH-3 was supplied in cell lysate buffer at the concentration of 2 μM. MIA PaCa2 cells were treated with 2 μM of KH-3 for 24 hours and total cell lysate was used for the pulldown assay. KH-3 significantly decreased the amounts of mRNAs of Snail, Slug, ZEB1, β-catenin, HuR and Msi1 in the pulled-down products (**Fig. 7.11. A**), consistent with but slightly less efficient than the HuR KO (**Fig. 6.10.**). Similar to HuR KO, KH-3 treatment (2 μM) enhanced Snail mRNA degradation (**Fig. 7.11. B**) and decreased the protein level of Snail (**Fig. 7.5.**).

As we identified Snail as a direct target of HuR in EMT regulations (**Fig. 6.12., 6.13.**), the effect of KH-3 on the binding of HuR with Snail mRNA was examined with the luciferase reporter assay. When pHuR and pmirGLO were co-transfected with the full-length Snail 3'UTR construct, or with AREs, KH-3 treatment reduced the luminescence signal (**Fig. 7.12.**), clearly demonstrating the disruption of the interaction of HuR with the 3'UTR of Snail mRNA. In the absence of HuR binding elements (ΔAREs), KH-3 had no effect on the luminescence signal (**Fig 7.12.**).

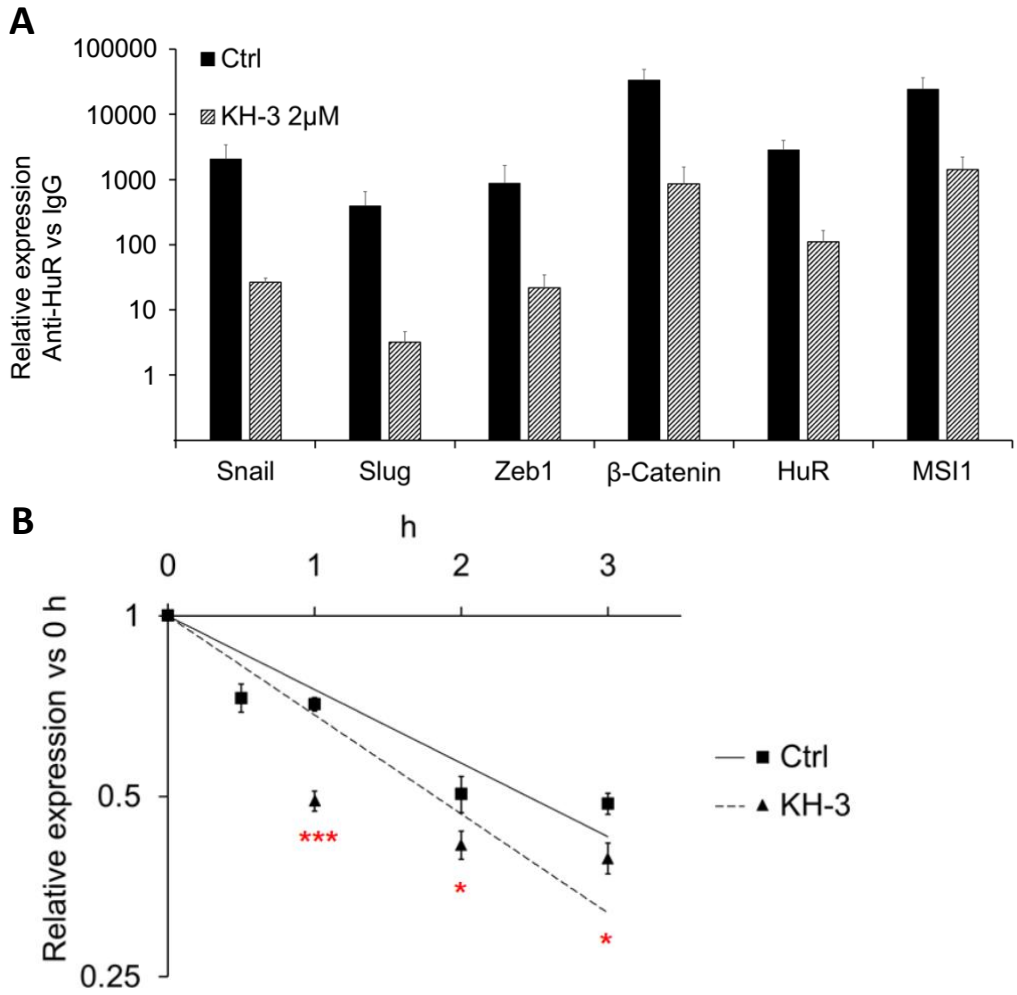

Figure 7.11. KH-3 disrupted the binding of HuR with the mRNAs of EMT regulators and impaired the stability of Snail mRNA. (A) RNP-IP assay. MIA PaCA-2 cells were treated with 2 μM of KH-3 for 24 hours. KH-3 was supplied in lysate buffer at the concentration of 2 μM. Total RNA from pull-down products of whole cell lysate were subjected to RT-qPCR detection. Data for each individual mRNA was normalized to the IgG pull-down product of that mRNA. Bar graphs show mean ± SEM of 9 repeats. (B) Stability of Snail mRNA in MIA PaCa-2 cells treated with KH-3. Transcription was blocked by actinomycin D (5 μg/ml) treatment 30 minutes before the cells were exposed to KH-3 (2 μM) (0 h). Data represent mean ± SEM of 9 repeats. *$p < 0.05$; ***$p < 0.001$ by Student's t-test as compared to control.

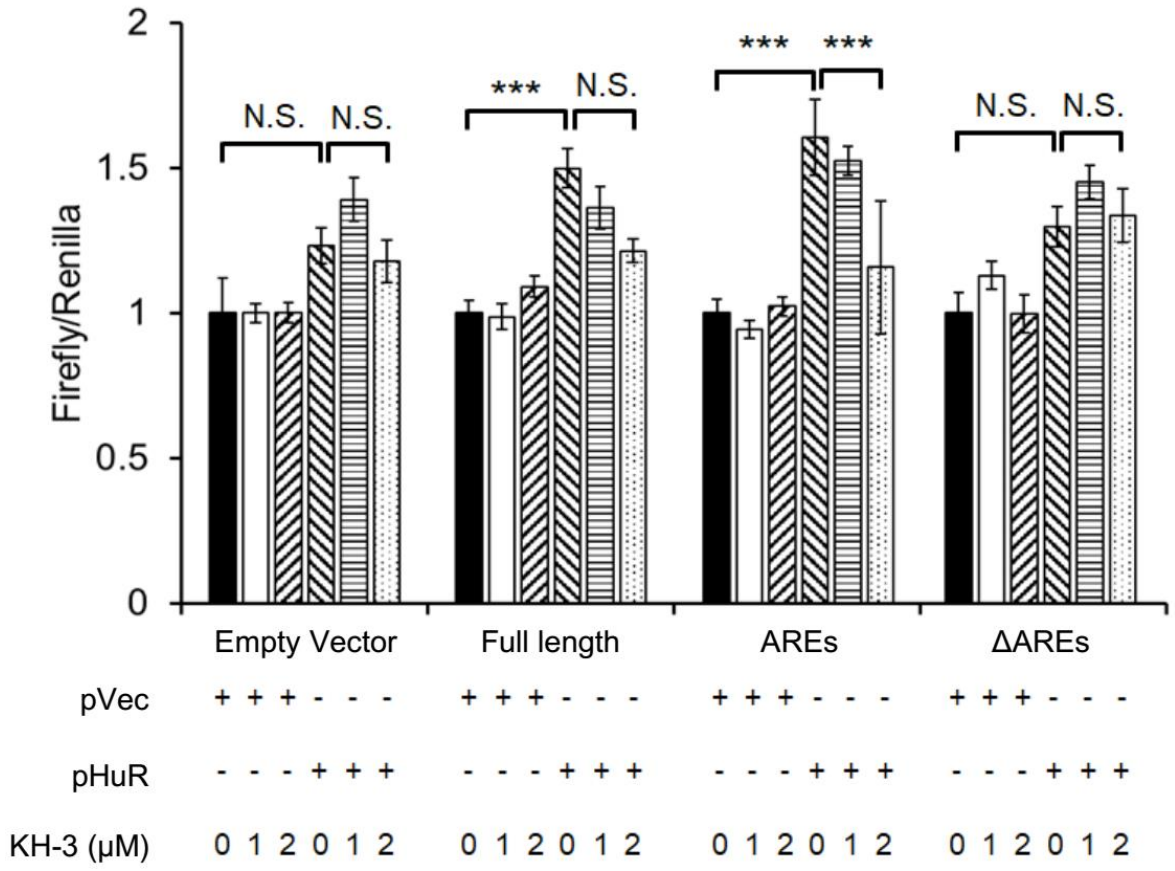

Figure 7.12. KH-3 disrupted the binding of HuR with the AREs in the 3'UTR of Snail mRNA in a dual-luciferase reporter assay. MIA PaCa-2 HuR KO cells were co-transfected with pHuR (or pVec) and the dual-luciferase reporter with Snail 3'UTR constructs (either the full length, AREs or ΔAREs, or empty vector). After 24 hours, cells were treated with KH-3 at indicated concentrations for an additional 24 hours. Data represent mean ± SEM of 9 repeats. ***$p < 0.001$ by one-way ANOVA-Tukey's as compared to control.

7.1.5. KH-3 inhibited HuR positive pancreatic cancer progression and metastasis *in vivo*.

The *in vivo* tumor inhibitory effect of KH-3 was then tested in a highly metastatic orthotopic xenograft model of pancreatic cancer outlined in **Figure 7.13 A**. Briefly, 2×10^5 PANC-1 cells were implanted into the pancreatic parenchyma of nude mice. This resulted in a 90% tumor formation rate in the pancreas, with ~ 60% of mice having metastasis in the liver and in the peritoneal cavity within 5 weeks, based on our previous experiences. For imaging purposes, PANC-1 cells were transfected with luciferase. Tumor progression was monitored by weekly imaging using an In Vivo Imaging System (IVIS). To avoid peritoneal metastatic lesions resulting from leak of injection, 5 mice (donor mice) were injected with the luciferase expressing PANC-1 cells (PANC-1-Luc2) and tumors were allowed to form for 4 weeks. Tumors in the pancreas of these donor mice were harvested and cut into ~1 mm^3 pieces and implanted into the pancreatic parenchyma of recipient mice. After 2 weeks, tumor development in the pancreas of the recipient mice was detected by imaging. Mice were then grouped, and treatment commenced (n = 9 for control group, n = 10 for each of KH-3 group and a positive control group of 5-FU treatment).

A pilot MTD (maximum tolerant dose) experiment was carried out to determine dose regimen to be used in treatment. Mice (n=3) were started at 50 mg/kg body weight of KH-3 daily, intraperitoneal injection (IP) for 3 consecutive days. No clinical signs of toxicities were observed. Dose was then escalated to 75 mg/kg for 3 days and when no signs of toxicities were observed, dose was increased to 100 mg/kg for 5 days. On day 5 of 100 mg/kg, reduction in activities were observed in mice. Dose was reduced to 3x weekly at 100 mg/kg, by IP injection. No clinical signs of toxicities were observed. The 100 mg/kg 3x weekly IP injection was

determined as the treatment dose. All treatment concerning KH-3 used this dose regimen. The dose regimen for 5-FU was 50 mg/kg based on literature reports [434, 435].

The treatment continued for 5 weeks when the control tumor bearing mice has poor body conditions. All mice were euthanized, and gross necropsy was performed. The data showed that KH-3 treatment significantly inhibited tumor growth and reduced tumor burden compared with the vehicle treated group (Control) (**Fig. 7.13. B, C**), while 5-FU did not show significant anti-tumor effects during the treatment. The final tumor weight in KH-3 treated mice was also significantly reduced compared with vehicle treated mice (**Fig. 7.13. D**). It is notable that 8 out of 10 mice in 5-FU group had tumors, whereas 10 out of 10 mice in KH-3 group and 9 out of 9 mice in control group had tumors. There are several possibilities to explain why these two mice in 5-FU group did not have tumor. It is possible that these two mice had better response to 5-FU from the beginning of treatment. However, because the other 8 mice in the groups apparently did not respond to 5-FU treatment and the final average tumor weight in 5-FU group was not reduced compared to untreated controls, it is not likely these 2 mice alone would have such a dramatic tumor regression. Another obvious possibility is that the tumor formation is heterogenic in individual mice. Our grouping was based on IVIS imaging results, which had a significant variation between individual mouse (the total flux ranging from 2.23×10^6 p/s to 1.09×10^9 p/s). As a comparison, the negative control mouse, which does not bear tumors, had a total flux of 6.19×10^5 p/s as the baseline. In addition, the two mice in 5-FU group without tumors had a significant lower readout in IVIS imaging during the treatment. Therefore, it is more likely that these two mice did not bear tumor and the imaging had false positive results when grouping.

No clinical signs of toxicity were observed in KH-3 treated mice and 5-FU treated mice during the treatment. There is a difference in body weight between control and KH-3 group after 21

days of treatment. However, because of tumor growth, it is yet difficult to attribute the changes in body weight to toxicity. Histological examination of the livers found no changes in the KH-3 group (**Fig. 7.14.**).

In order to precisely detect whether there were metastatic lesions in the liver, we used a bioluminescent assay by soaking the liver tissues in solutions of luciferin (10 mg/ml). A liver metastatic lesion gave positive bioluminescent signals which were detected by the IVIS system, while soaking the same tissues in PBS gave no signals (**Fig. 7.15. A**). All mouse livers were then collected and soaked in 10 mg/ml of luciferin and bioluminescence was examined. In the vehicle treated group (Ctrl), 5 out of 9 mice developed metastatic lesions in the liver (56%). In the 5-FU treated group, 4 out of 10 mice had liver metastatic lesions (40%), whereas in the KH-3 treated group, only 1 out of 10 mice developed liver metastasis (10%) (**Fig. 7.15. B, C**).

At the end of the *in vivo* study, tumor tissues were examined for EMT alterations by western blots. Consistent with *in vitro* data and the expected EMT inhibition, the epithelial markers Claudin-1 and ZO-1 were upregulated in the KH-3 treated mice, and Snail was downregulated (**Fig. 7.16. A**). The upregulated expression of Claudin-1 was further confirmed by immunofluorescence staining (**Fig. 7.16. B**). Immunohistochemistry confirmed the high expression level of HuR in the tumor tissues compared with the adjacent normal pancreatic tissues. KH-3 treatment did not change the expression level of HuR in the tumor tissues (**Fig. 7.16. C**).

To examine whether the inhibitory effects of KH-3 were dependent on HuR, an *in vivo* treatment was performed using MIA PaCa2 HuR KO tumors. MIA PaCa2 HuR KO cells were inoculated into both flanks of nude mice (n=16 in each group). Tumor formation and growth were closely

monitored with caliper measurement. The treatment started on the same day the cells were inoculated, with either KH-3 (100 mg/kg, IP, three times per week) or vehicle. Data demonstrated that KH-3 treatment did not affect either formation **(Fig. 7.17. A)** or growth **(Fig. 7.17. B)** of these HuR KO tumors. These data, together with the data in the orthotopic pancreatic cancer mouse model, strongly indicate that the KH-3 effects were dependent on the presence of HuR in the tumor.

A **Pancreatic tumor orthotopic xenograft mouse model *in vivo***

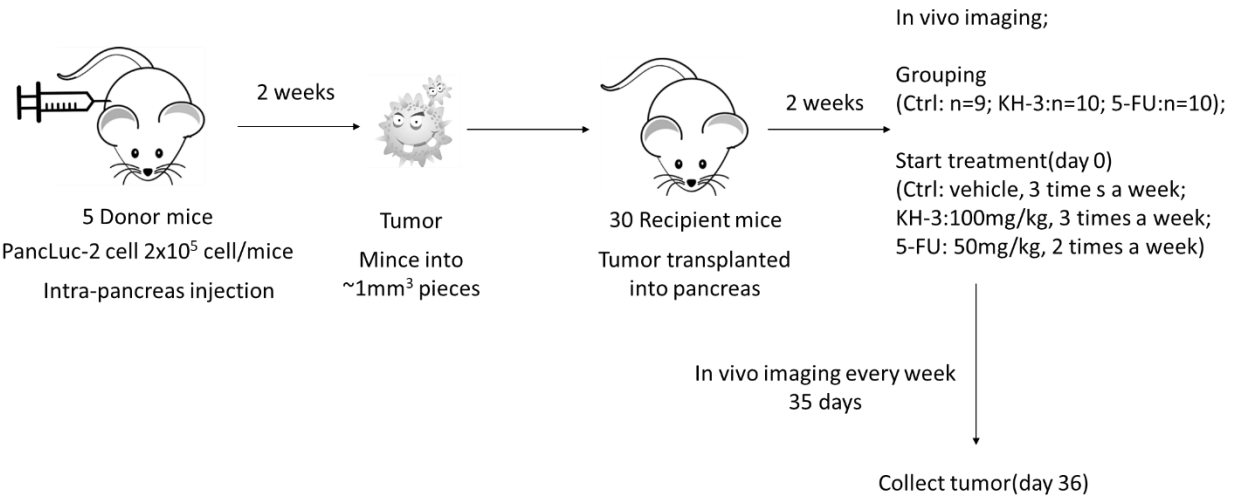

B

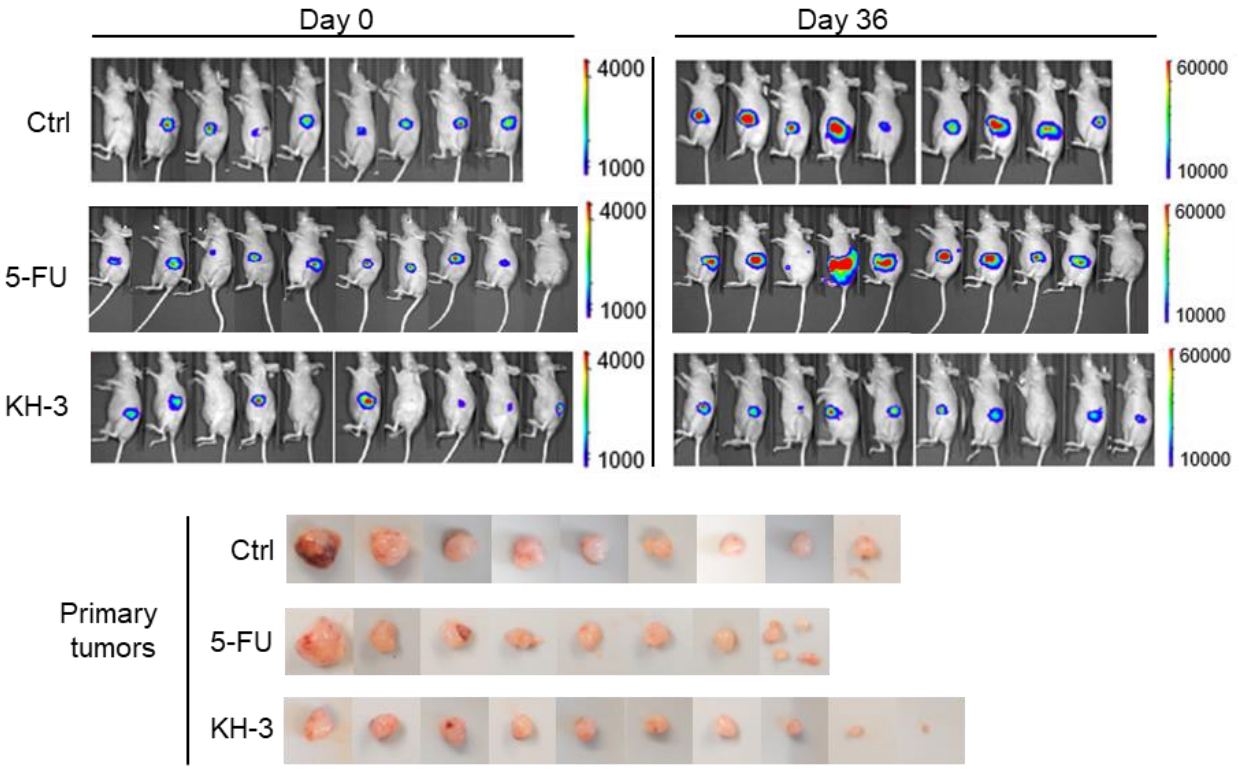

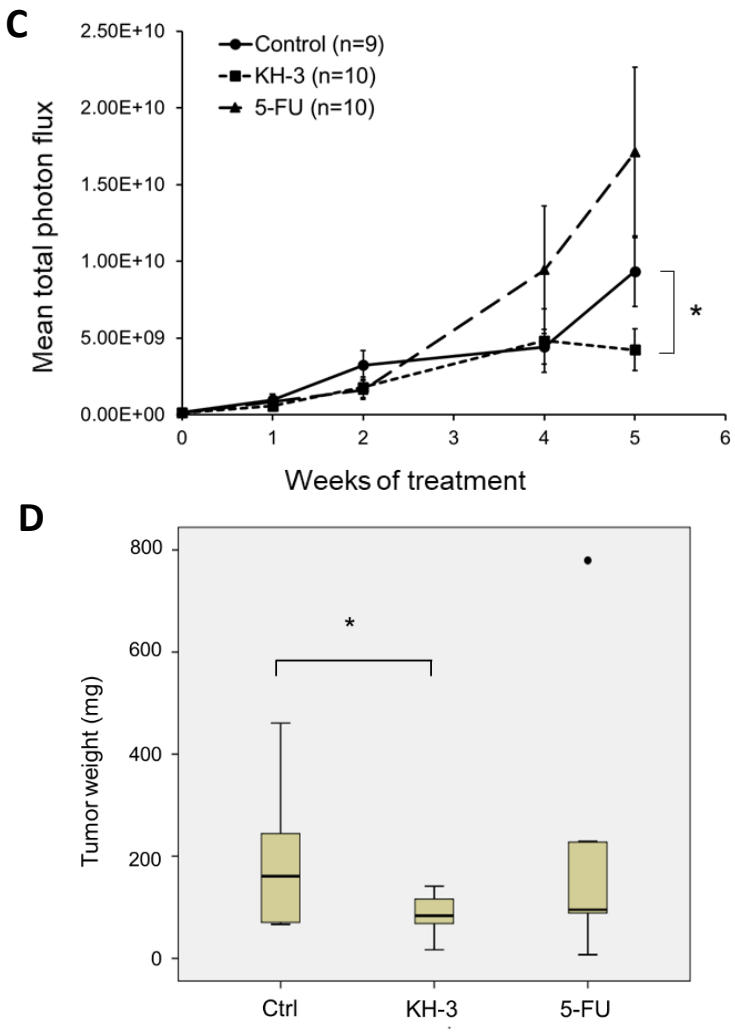

Figure 7.13. KH-3 inhibited growth of a HuR positive pancreatic cancer in an orthotopic xenograft mouse model. (A) Schematic diagram shows the workflow of the *in vivo* assay. (B) Upper: bioluminescence images of mice bearing PANC-1-Luc2 tumors treated with KH-3 (100mg/kg, 3 x weekly, n=10), or vehicle (Ctrl, n=9), or 5-FU (50 mg/kg, 2x weekly). Lower: Tumor in mouse pancreas at the end of treatment (Day 36). (C) Average tumor burden measured by using an IVIS, quantified as photons/sec/cm^2 (mean ± SEM). *$p < 0.05$ by one-way ANOVA-Tukey's test. (D) Average tumor weight at the end of the treatment. *$p < 0.05$ by one-way ANOVA-Tukey's test. The round dot in 5-FU group represents a statistical outlier tumor sample.

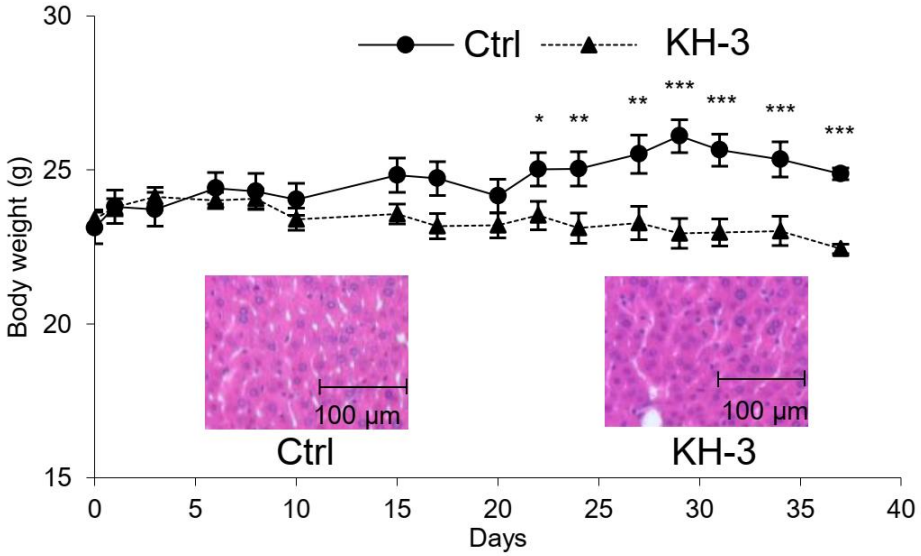

Figure 7.14. Body weight and liver histology of mice bearing PANC-1 tumors. KH-3, 100 mg/kg 3x weekly IP. Ctrl, vehicle control. Average body weight measured by digital scale (mean ± SEM). *p < 0.05; **p < 0.01; ***p < 0.001 by Student's t-test.

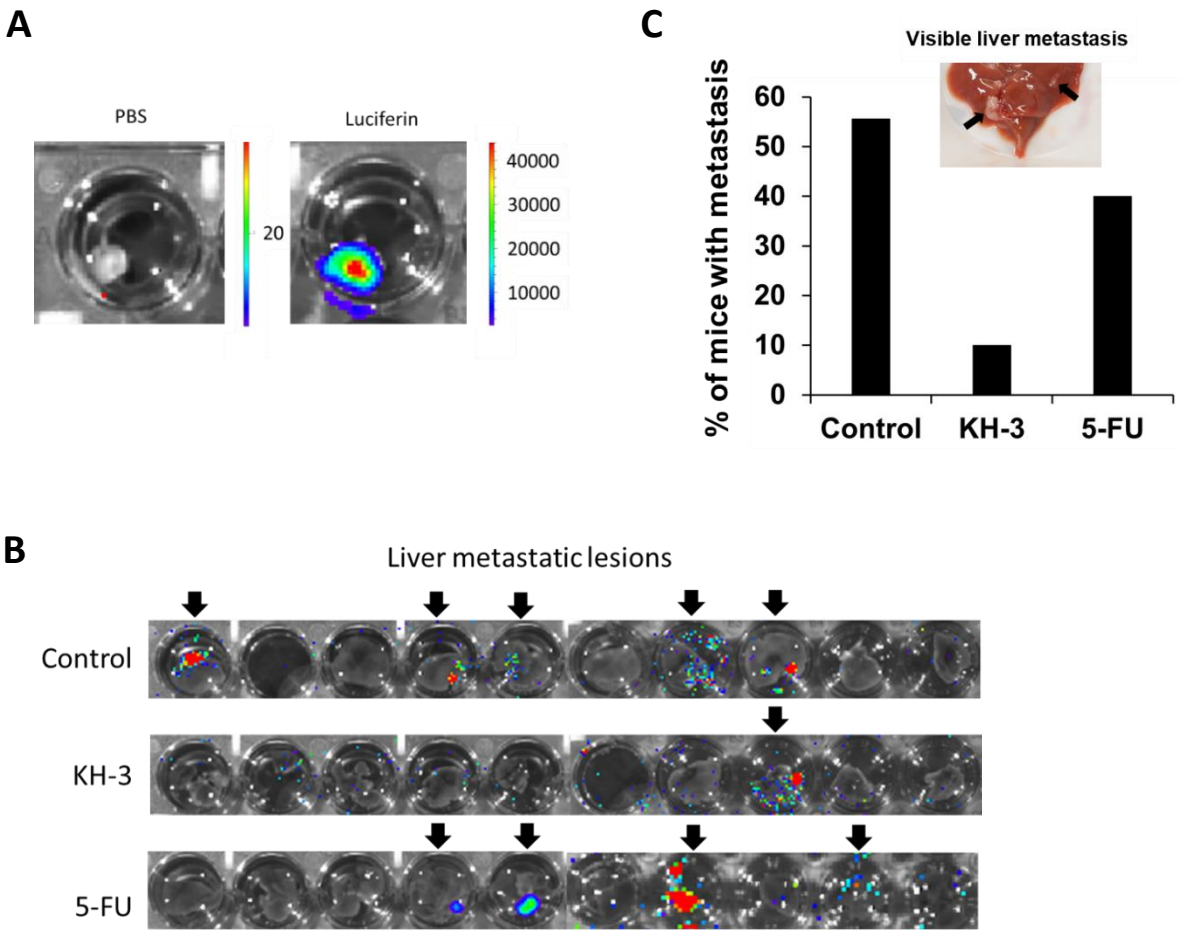

Figure 7.15. KH-3 inhibited metastasis of an HuR positive pancreatic cancer *in vivo*. (A) A visible liver metastatic lesion was soaked in PBS or D-luciferin for 5 minutes and then imaged with IVIS spectrum imaging system. (B) Mouse livers were collected and incubated with D-luciferin for 5 minutes before being imaged with an IVIS. Black arrows indicated positive bioluminescence in the liver which was considered as liver metastatic lesions. (C) Bar graph showed liver metastasis rate in control mice, KH-3 treated mice, and 5-FU treated mice. Images showed visible metastatic lesions.

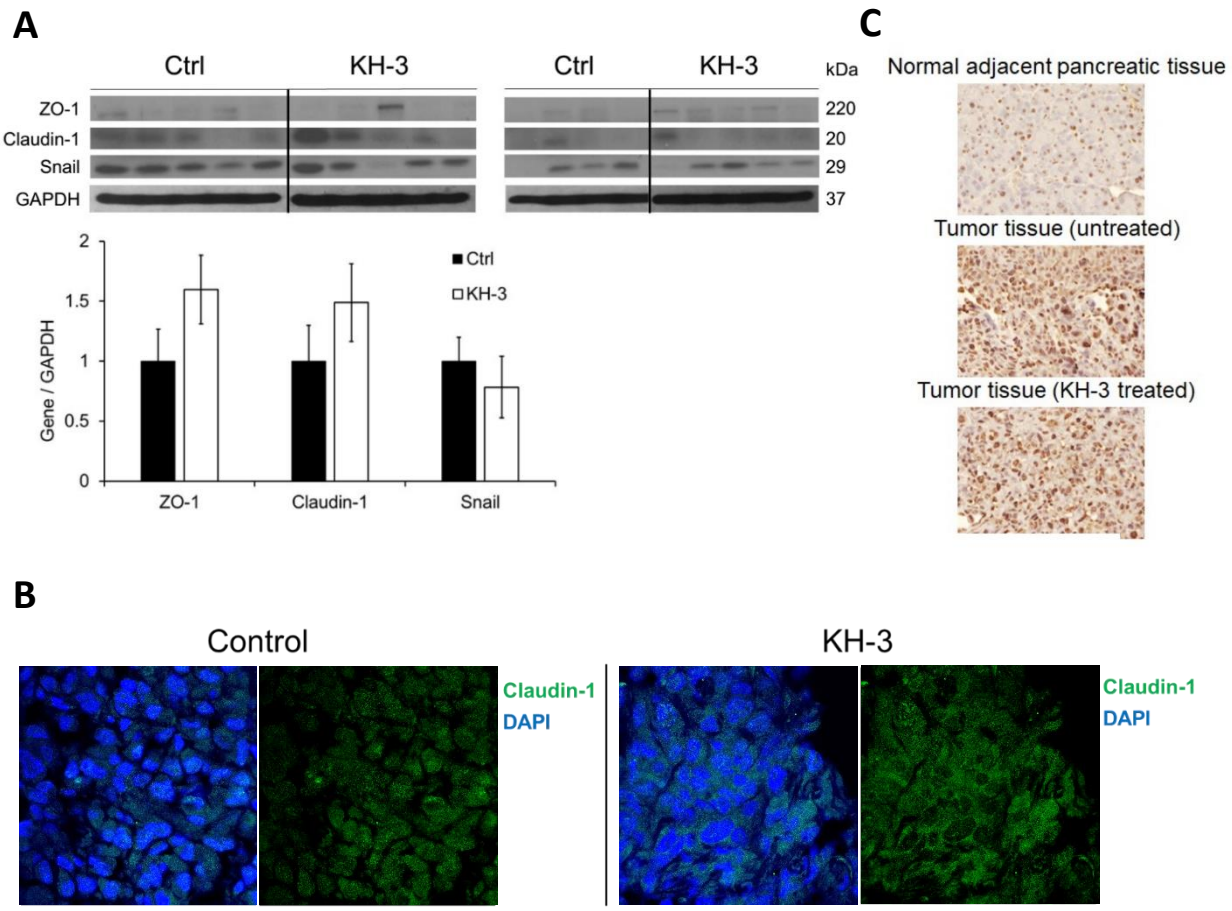

Figure 7.16. KH-3 inhibited the expression of EMT makers in pancreatic tumor tissues. (A) Western blot of mouse tumor tissues showing EMT markers. Bar graphs show average band intensity of each protein normalized to GAPDH. (B) Immunofluorescence staining showing increased Claudin-1 expression in KH-3 treated tumor, compare with vehicle treated tumor. (C) Immunohistochemistry showing HuR expression in tumor tissues and adjacent normal pancreatic tissues.

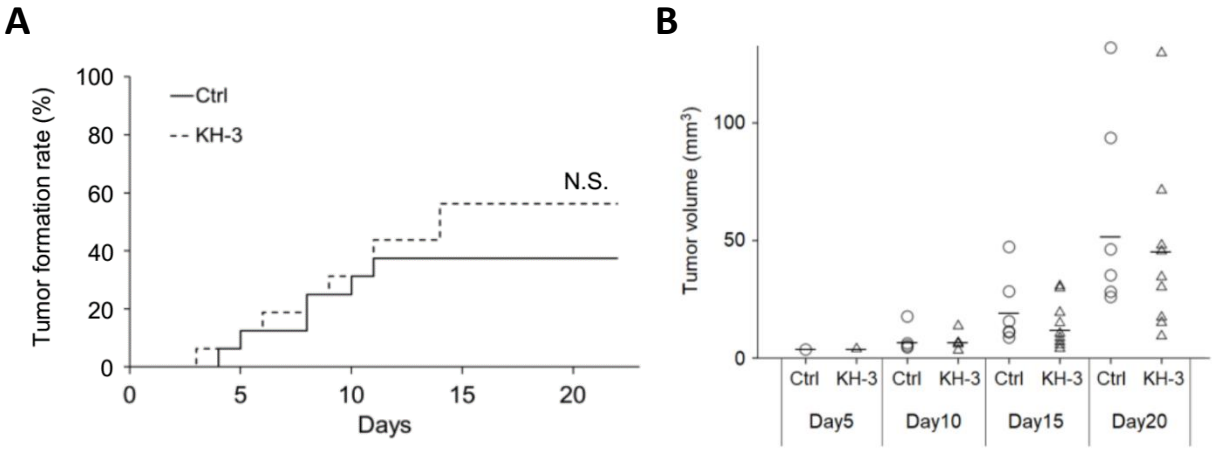

Figure 7.17. KH-3 did not influence the formation and growth of an HuR negative pancreatic tumor. (A) Subcutaneous tumor formation of MIA PaCa-2 HuR KO cells with and without KH-3 treatment (n=16 for each group). Log Rank test resulted in no significant difference. (B) Volume of the subcutaneous tumors formed in (A). Each circle or triangle represents a tumor. The short lines represent average tumor volume of each group. Mann–Whitney U tests on each day demonstrated no significant differences between treatment and control.

7.2. Discussion

Given the importance of HuR in EMT and CSC, along with its roles in other signaling pathways involved in cancer progression, it is intriguing to develop pharmacological inhibitors of HuR for the treatment of cancer. However, there has been little success with small molecules that inhibit HuR functions, partially due to the unclear structure of the RNA interacting pocket in the HuR protein [387]. The only small molecule advanced to early phase clinical trial is MS-444, a myosin light chain kinase inhibitor, which was found to interfere with nuclear-to-cytoplasmic translocation of HuR. However, there are multiple issues regarding specificity and toxicities [387]. Our data show that a novel compound, KH-3, works in a different way than MS-444. KH-3 binds to the RNA recognition motifs (RRM1/2) of the HuR protein and disrupts the HuR-mRNA interaction. Consequently, KH-3 inhibits pancreatic cancer cell EMT, migration, invasion, and CSCs, mimicking the effects of HuR knockdown.

It is a reasonable concern that KH-3 has residual HDAC inhibitory activity, due to the structure similarity to its parent compound, the HDAC inhibitor SAHA. However, our data show that KH-3 had only minimal HDAC inhibitory activity on the acetylation of histones H3 and H4, and even lost HDAC inhibitory activity on histones H2A and H2B. Our study demonstrated that KH-3 had target specificity to HuR within the effective dose range *in vitro* and *in vivo*. Data showed that when HuR was knocked down or deleted in MIA PaCa2 cells, KH-3 lost its inhibitory activity against cell migration at concentrations of 1 μM and 2 μM. *In vivo,* KH-3 (100 mg/kg, 3x week) inhibited the growth and metastasis of a HuR positive tumor but did not inhibit the formation and growth of tumors deficient of HuR at the same dose. Thus, the anti-tumor activities of KH-3 were unlikely due to the HDAC inhibition. Overall, in this dissertation, KH-3 demonstrated a good target specificity for HuR inhibition in pancreatic cancer cells. Structure-

activity relationship analysis could be further utilized to screen for KH-3 analogs with improved anti-tumor activities and other drug-like chemical and physical properties.

Currently, combination chemotherapy is widely used in cancer management and has shown favorable effects on a variety of tumors, compared with mono-chemotherapy. The major benefits of combination regimens are the synergistic effects of the drugs in targeting heterogenetic tumors and drug resistances by inhibiting different signaling pathways in tumor progression and metastasis. Here we demonstrated that KH-3 inhibited pancreatic cancer EMT and CSCs. The inhibition of EMT and CSCs could potentially increase effects of other anti-cancer drugs, because both EMT and CSCs are associated with drug resistance and tumor heterogeneity. Thus, investigating combination regimens of KH-3 and conventional chemotherapeutic agents for pancreatic cancer, such as gemcitabine, paclitaxel, 5-FU, and other drugs, could provide valuable information to conquer drug resistance and result in better efficacy.

Overall, being the first of its class, KH-3 showed the promise of using target-specific small molecules to inhibit HuR function by direct disruption of HuR-mRNA binding. Pharmacological inhibition of HuR holds the promise to comprehensively inhibit pancreatic cancer progress, metastasis, drug resistance, and tumor recurrence.

.

Chapter 8. Summary and Future Directions

Pancreatic cancer is expected to be the second-leading cause of cancer-related death by 2030, with 88,000 newly diagnosed patients and 63,000 death in the US [1]. Currently, there are only limited options in pancreatic cancer management: surgical removal as a curative method is only available to a small population of early stage pancreatic cancer patient; radiation therapy only has modest effect in both adjuvant and neoadjuvant settings; conventional chemotherapy has an overall low response rate in patients and usually comes along with multiple toxicities. Developing novel and effective anti-pancreatic cancer agents is essential. Considering that pancreatic cancer is highly metastatic, CSC-enriched, and chemo-resistant, pharmacological agents targeting metastasis related molecules and pathways, such as EMT-TFs and CSC-related proteins, have the promise to improve pancreatic cancer management. Clinical trials on various EMT-TF inhibitors and CSC-related protein/pathway inhibitors are ongoing. This dissertation describes efforts in investigating several novel approaches to inhibit pancreatic cancer progression and metastasis. Each has its own merits, shortcomings, and mechanisms need to be addressed in future development.

Chapter 4 and 5 demonstrated that two medical plant extracts, Pao and Rau, similarly inhibited pancreatic CSCs *in vitro* and *in vivo*. Pao and Rau are used as health supplements by the American public, and have been shown to have inhibitory effects on cell proliferation and apoptosis in ovarian, prostate, and pancreatic cancers [393, 397-399]. Our previous studies also showed that Pao and Rau induced apoptosis in pancreatic cancer cells and sensitized pancreatic cancer cells to gemcitabine treatment [398, 424]. In this dissertation, we discovered that Pao and Rau preferentially inhibited pancreatic CSCs than the general cancer cell population. Pao and Rau had a lower IC_{50} on a CSC enriched side population, and higher IC_{50}s on the non-stem-like population and the whole cancer cell population. Pao and Rau decreased the proportions of

$CD24^+CD44^+EpCAM^+$ pancreatic CSC population *in vitro*. In a subcutaneous xenograft mouse model, Pao and Rau significantly inhibited the tumor formation and growth, without obvious toxicity. Pao and Rau inhibited the expression of CSC-related protein, Nanog and β-catenin. The expression of CSC-related genes, such as *DPPA4*, *ESRRB*, *SOX2*, *TCL1*, and β -catenin downstream target genes, such as *BCL2L2*, *COX2* and *MYC*, were also suppressed with Pao and Rau treatment. Overall, our findings demonstrated that Pao and Rau hold the promise to inhibit pancreatic CSCs with limited toxicities.

Both Pao and Rau are complex mixtures of natural compounds. Applying natural compounds mixtures to cancer treatment have advantages and disadvantages. Medicinal plants have been proven to be good sources of anti-tumor compounds for clinical usage. Naturally Occurring Plant-based Anti-cancer Compound-Activity-Target Database (NPACT, http://crdd.osdd.net/raghava/npact/) has recorded approximately 1980 experimentally validated plant-derived natural anti-cancer compounds with their compound-target interactions [436, 437]. One of the advantages of plant-derived anti-tumor compounds is that they are generally more tolerated and non-toxic to normal human cells. Clinically, plant-derived chemotherapeutic drugs, such as paclitaxel, docetaxel and vincristine, have been approved by FDA for used in various types of cancer. In addition, Pao and Rau are also used as dietary supplements, indicating low toxicity. Thus, Pao and Rau are worth future investigation to contribute to clinical cancer management.

There are also some disadvantages using natural extract mixtures such as Pao and Rau in cancer treatment. First, the drug target(s) and mechanism(s) are hard to define, as the components could each have their own target(s) and/or mechanism(s), and the signaling pathways could crosstalk. The impurity can induce non-specificity in mechanism, which may result in increased off-target

side-effects. Second, the components in the extract may have different biological activities, which may influence the potency of the active intergradient in the mixture. Therefore, it is ideal to understand how each ingredient in the mixtures affects cancer cells, as well as oncogenes, tumor suppressor genes, and tumor-related regulatory pathways.

A reasonable next step is to identify the active ingredients in Pao and Rau which possess the anti-tumor activities, for future drug development. Recent studies have shown that Pao is enriched with β-carboline alkaloid and Rau contains 2,6-dimethoxybenzoquinone [438-440]. Both β-carboline alkaloid and 2,6-dimethoxybenzoquinone have been shown to possess the anti-tumor activities. Column chromatography can be used to make fragments of Pao and Rau, and anti-cancer activities can be tracked using cell viability assays. Once the active fragments are isolated, UPLC-MS-based methods can be applied to separate and identify pure compounds from Pao and Rau, and each of the compounds can be evaluated for their anti-tumor activities. Based on the isolated compounds, structure–activity relationship (SAR) analysis could also be deployed to develop potent analogs. The identification of active ingredients from Pao and Rau will provide potential prototype anti-tumor agents for drug discovery.

Paradoxically, it is possible that a pure active compound cannot be identified from these mixtures. Because in a medicinal plant extract, it is not rare that several ingredients work synergistically to exhibit the antitumor activities, and fragmentation will cause decrease or even loss of activities. Moreover, some ingredients may work on enhancing pharmacokinetic and pharmacodynamic features of the active ingredients, and separation of them could influence the absorption, distribution, metabolism and excretion of the active compounds and thus dampen the efficacy *in vivo*. Also, some ingredients may work on reducing side-effects of the active compounds, and separation would cause an increase in toxicity. If these scenarios happen, then it

is not beneficial to purify Pao and Rau to provide single active compound. Rather, a "fingerprint" chromatograph or spectrum could be obtained to mark the chemical characteristics of the signature components of Pao and Rau. This fingerprint can be used for quality control, and identification of Pao and Rau as therapeutic agents.

There is also a technical limitation in the studies of Pao and Rau presented in Chapter 4 and 5. CSC isolation procedure in this dissertation was not a "clean" method. We used a membrane permeable dye, DCV, to separate a side population. This method is efficient to obtain a subpopulation enriched with CSCs, but it is not a specific method to isolate CSCs. A more specific method is to use immunofluorescent staining of multiple cell surface markers and coupled flow cytometry isolation, such as isolation of $CD24^{+/}CD44^{+/}EpCAM^{+}$ cells as pancreatic CSCs. However, Pao and Rau have strong and broad-spectrum auto-fluorescence that interfered with the conjugated fluorophores of commonly available antibodies, therefore this method was not successful in our efforts. Several other cell surface markers could be used as CSC markers to isolated pancreatic CSCs, including CD133, CXCR4 and OCT4 [223].

EMT markers were not investigated in the metastasis inhibition induced by Pao and Rau due to limit of time. We have found that nuclear β-catenin and several downstream targets were decreased by Pao and Rau, as well as multiple CSC-related genes. However, EMT-related molecules have not been illustrated. Because EMT and CSCs are highly linked, and both contribute to pancreatic cancer metastasis, it is worthwhile to examine EMT markers and EMT-TFs with Pao and Rau treatment.

The mechanism(s) by which Pao and Rau induced CSC inhibition needs to be further investigated. Our study showed that Pao and Rau reduced both Nanog and nuclear β-catenin

levels, which are essential regulators in stem cell initiation and maintenance. Whether and how Pao and Rau interacted with Nanog and β-catenin signaling and/or other CSC-related genes remain unknown. Moreover, as mentioned above, this plant preparation contained a complex mixture of natural compounds. It is possible that Pao and Rau impacted other molecular targets and pathways that led to CSC inhibition. The direct targets involved in Pao and Rau induced pancreatic cancer inhibition are also worth investigation. Proteomic and bioinformatic methods could be employed for target identification.

In chapter 6, we illustrated the role of an RNA binding protein HuR in pancreatic cancer EMT and CSCs. By using si-HuR transfected cells and CRISPR/Cas9 HuR KO cells, we demonstrated that the knockdown of HuR repressed pancreatic cancer cell EMT, migration, and invasion. Restoration of HuR in HuR KO cells promoted EMT and migration. The stemness features, including tumor sphere formation ability and tumorigenicity in mice were also inhibited with HuR knockdown. RNP-IP identified a panel of EMT-TFs that directly bound to HuR. HuR directly bound to the AREs in the 3'UTR of *SNAI1* mRNA, leading to the stabilization of *SNAI1* mRNA and increased level of Snail. Taken together, data show that HuR served as an EMT promoting factor in pancreatic cancer by directly binding to and stabilizing *SNAI1* mRNA. Our data provide new insight into the function of HuR in pancreatic cancer metastasis.

As an AU-rich element binding protein (AUBP), HuR has a broad spectrum of target genes that are involved in multiple pathological events. The diverse functions of HuR in cancer development and progression include regulating tumor growth, tumorigenesis, angiogenesis, tumor inflammation, treatment response, and tumor microenvironment. In this dissertation, we mainly focused on the role of HuR in pancreatic cancer EMT, invasion, metastasis, and tumorigenicity. Other functions of HuR in pancreatic cancer are also worth studying. For

example, recently studies demonstrated that the overexpression of HuR in colon cancer cells promote the level of tumor-derived exosomes containing HuR as cargo [441]. The exosomal HuR may have functions to regulate nearby and even remote cells, and it also has the potential to serve as a serum-based cancer biomarker [441]. Whether these is exosomal HuR in pancreatic cancer is of interest. More comprehensive studies of the functions of HuR in pancreatic cancer will facilitate full understanding of the therapeutic and prognostic role of HuR in cancer management.

Some pancreatic cancer cells, e.g. MIA PaCa2 cells, lack E-cadherin expression. In our studies, Claudin-1, instead of E-cadherin, was found upregulated when HuR was knocked down. Studies in colorectal cancer found HuR directly binds to Claudin-1 mRNA and enhanced its expression, thus the inhibition of HuR inhibited Claudin-1 expression. This contradiction with our data can have at least two explanations. First, the knockdown of HuR destabilizes both *SNAI1* mRNA and *CLDN1* mRNA. Snail suppresses the expression of *CLDN1*. The reduction of Snail released the repression on Claudin-1 expression, and this overweight the inhibitory effects of HuR knockdown on Claudin-1 expression. Second, HuR could function as a translational repressor upon binding to *CLDN1* mRNA at the 5'UTR instead of 3'UTR, and therefore knockdown of HuR would upregulate the level of Claudin-1. By using a computational analysis, we identified putative IRESs in the 5'UTR of *CLDN1* mRNA, which is important to maintain the level of Claudin-1 via cap-independent translation. HuR could bind to the IRESs in the 5'UTR of *CLDN1* mRNA and suppress Claudin-1 expression. As a future continuation of the study, bicistronic luciferase reporter assay and other methods can be utilized to verify the presence of IRESs in the 5'UTR of *CLDN1* mRNA, and the binding of HuR.

Our lab recently developed a 3D invasion model to evaluate pancreatic cancer invasion *in vitro*, and it can be utilized to the study of HuR in migration and invasion in the future. In this model, pancreatic cancer cells are cultured as tumor spheres in type I collagen. The solidified collagen maintains the pancreatic tumor sphere in a 3D culture condition, and the metastatic cells grow in a radiant pattern from the tumor sphere. The 3D culture model provides better data in prediction of drug resistance and tumor metastasis because it better represents tumor microenvironments than the monolayer culture [442].

In chapter 7, a novel HuR inhibitor, KH-3, was tested for its HuR inhibition and anti-pancreatic cancer activities. KH-3 was identified as an HuR/mRNA disruptor by directly binding to the RNA-recognition motifs (RRMs) of HuR. Consistently, KH-3 treatment of pancreatic cancer cell lines successfully mimicked the HuR knockdown effects, resulting in the inhibition of pancreatic cancer cell migration, invasion, and sphere formation. KH-3 inhibited tumor progression and metastasis in an orthotopic pancreatic cancer xenograft mouse model. Importantly, the loss of function analysis demonstrated that KH-3 exerted its anti-pancreatic activity in an HuR dependent way *in vitro* and *in vivo.* Overall, our data showed that KH-3 as a first-of-its-class HuR inhibitor, was a potent inhibitor on pancreatic cancer progression and metastasis. Based on the central regulatory role of HuR in many oncogenic pathways, the clinical association of HuR overexpression with tumor stages, and the differential expression of HuR between normal and cancer cells, inhibiting HuR could comprehensively inhibit tumor growth, metastasis, and recurrence.

We demonstrated that KH-3 had a good target specificity on HuR inhibition within the effective dose range *in vitro* (~2 μM in MIA PaCa2 cells and ~10 μM in PANC-1 cells) and *in vivo* (~100mg/kg). A minimal to undetectable HDAC inhibitory activity of KH-3 was found *in vitro*,

because of the partial structure similarity to its parent compound SAHA. The loss of target analysis found that the anti-tumor activity of KH-3 was unlikely due to the HDAC inhibition. **A logical next step** is to perform structure-activity relationship analysis to screen KH-3 analogs with improved anti-tumor activities and other drug-like chemical and physical properties.

Based on our current finding, KH-3 is a highly hydrophobic molecule with limited water solubility. It is unknown yet how KH-3 is taken up by the cells. It is possible cell membrane transporters contributed to the effects of KH-3. Several bioinformatic and *in vitro* assays could be used to identify the cell membrane transporters of KH-3. For example, KH-3 may share the same transporters with structure similar compounds, such as HDAC inhibitors SAHA and MS-275. Furthermore, by using the chemical structure database, the compounds with similar structure to KH-3 and known transporters may be found. In addition, KH-3 combined with various transporter blockers could be applied to *in vitro* assays to identify the transporter of KH-3. The identification of transporters involved in KH-3 uptake can provide critical information in pharmacokinetic and pharmacodynamic feature of KH-3, which is important before KH-3 can advance to clinical studies.

Although we demonstrated that KH-3 inhibited pancreatic cancer progression and metastasis with an orthotopic pancreatic cancer mouse model, it is still worthwhile to test the efficacy and efficient of KH-3 on pancreatic cancer with patient derived xenografts (PDX) mouse models and *LSL-Kras*$^{G12D/+}$; *LSL-Trp53*$^{R172H/+}$; *Pdx-1-Cre* (KPC) genetically engineered mouse models (GEMM). The advantages of PDX models are that the tumor maintain histologic and genetic features of the original patients and have high clinical relevance and predictive value. KPC mice are immunocompetent and are a useful model to study tumor progression with intact immune

system. In addition, KPC mice provide spontaneously initiated tumors that mimic human disease with better clinically relevance.

Combination chemotherapy is widely used in pancreatic cancer patients to achieve a favorable outcome. Because Pao, Rau and KH-3 all inhibited pancreatic cancer EMT and CSC, and EMT and CSC are related to drug resistance, it is putative that Pao, Rau and KH-3 have great values to be used in combination with conventional chemotherapeutic agents. Pao and Rau sensitized pancreatic cancer cells to gemcitabine treatment [398, 424]. We have preliminary data in PANC-1 cells demonstrating a synergistic effect of the KH-3/5-FU combination. However, our preliminary *in vitro* data showed an antagonistic effect of KH-3/gemcitabine and KH-3/paclitaxel combinations (data not shown). Considering that gemcitabine and nab-paclitaxel are widely used first-line anti-pancreatic cancer agents, the possible antagonism of KH-3 with gemcitabine/paclitaxel may be a concern for its potential clinical development. However, these *in vitro* results have not been confirmed *in vivo*. Preliminary studies from our collaborators on KH-3 demonstrated a synergistic effect of KH-3 with docetaxel, an analog of paclitaxel, on breast cancer. As chemo-resistance is one of the major challenges in cancer management, it is worthwhile to explore combinations of Pao, Rau, or KH-3 with a wide variety of chemotherapeutic agents that are in preclinical and clinical studies to further understand its possible synergy and limitations. In addition, tumor recurrence is another major challenge in cancer management. Current studies suggested that the existence of CSCs is responsible for the tumor recurrence. The effects of Pao, Rau, and KH-3 on cancer recurrence is also worth studied in preclinical and clinical studies in the future.

Taken together, results of this dissertation provided basis for the development of novel EMT and CSC inhibitors, including Pao, Rau, and KH-3. They effectively inhibited pancreatic cancer cell migration, invasion, stemness features, which are major challenges in cancer management. We hope this work set a basis for future works to develop these and other novel EMT and CSC inhibitors for improvement of pancreatic cancer management.

References

1. Rahib, L., et al., *Projecting cancer incidence and deaths to 2030: the unexpected burden of thyroid, liver, and pancreas cancers in the United States.* Cancer Res, 2014. **74**(11): p. 2913-21.
2. Siegel, R.L., K.D. Miller, and A. Jemal, *Cancer statistics, 2019.* CA Cancer J Clin, 2019. **69**(1): p. 7-34.
3. Adamska, A., A. Domenichini, and M. Falasca, *Pancreatic Ductal Adenocarcinoma: Current and Evolving Therapies.* Int J Mol Sci, 2017. **18**(7).
4. Ryan, D.P., T.S. Hong, and N. Bardeesy, *Pancreatic adenocarcinoma.* N Engl J Med, 2014. **371**(11): p. 1039-49.
5. Hruban, R.H., et al., *Precursors to pancreatic cancer.* Gastroenterol Clin North Am, 2007. **36**(4): p. 831-49, vi.
6. Hruban, R.H., A. Maitra, and M. Goggins, *Update on pancreatic intraepithelial neoplasia.* Int J Clin Exp Pathol, 2008. **1**(4): p. 306-16.
7. Distler, M., et al., *Precursor lesions for sporadic pancreatic cancer: PanIN, IPMN, and MCN.* Biomed Res Int, 2014. **2014**: p. 474905.
8. Iacobuzio-Donahue, C.A., *Genetic evolution of pancreatic cancer: lessons learnt from the pancreatic cancer genome sequencing project.* Gut, 2012. **61**(7): p. 1085-94.
9. Castellano-Megías, V.M., et al., *Pathological features and diagnosis of intraductal papillary mucinous neoplasm of the pancreas.* World J Gastrointest Oncol, 2014. **6**(9): p. 311-24.
10. Yonezawa, S., et al., *Precursor lesions of pancreatic cancer.* Gut Liver, 2008. **2**(3): p. 137-54.
11. Crippa, S., et al., *Mucinous cystic neoplasm of the pancreas is not an aggressive entity: lessons from 163 resected patients.* Ann Surg, 2008. **247**(4): p. 571-9.
12. Zamboni, G., et al., *Mucinous cystic tumors of the pancreas: clinicopathological features, prognosis, and relationship to other mucinous cystic tumors.* Am J Surg Pathol, 1999. **23**(4): p. 410-22.
13. Jang, K.T., et al., *Clinicopathologic characteristics of 29 invasive carcinomas arising in 178 pancreatic mucinous cystic neoplasms with ovarian-type stroma: implications for management and prognosis.* Am J Surg Pathol, 2015. **39**(2): p. 179-87.
14. Nagtegaal, I.D., et al., *The 2019 WHO classification of tumours of the digestive system.* Histopathology, 2019.
15. Crippa, S., et al., *Quality of life in pancreatic cancer: analysis by stage and treatment.* J Gastrointest Surg, 2008. **12**(5): p. 783-93; discussion 793-4.
16. Waters, A.M. and C.J. Der, *KRAS: The Critical Driver and Therapeutic Target for Pancreatic Cancer.* Cold Spring Harb Perspect Med, 2018. **8**(9).
17. Der, C.J., T.G. Krontiris, and G.M. Cooper, *Transforming genes of human bladder and lung carcinoma cell lines are homologous to the ras genes of Harvey and Kirsten sarcoma viruses.* Proc Natl Acad Sci U S A, 1982. **79**(11): p. 3637-40.
18. Hobbs, G.A., C.J. Der, and K.L. Rossman, *RAS isoforms and mutations in cancer at a glance.* J Cell Sci, 2016. **129**(7): p. 1287-92.
19. Wennerberg, K., K.L. Rossman, and C.J. Der, *The Ras superfamily at a glance.* J Cell Sci, 2005. **118**(Pt 5): p. 843-6.
20. Scheffzek, K. and M.R. Ahmadian, *GTPase activating proteins: structural and functional insights 18 years after discovery.* Cell Mol Life Sci, 2005. **62**(24): p. 3014-38.

21. Vigil, D., et al., *Ras superfamily GEFs and GAPs: validated and tractable targets for cancer therapy?* Nat Rev Cancer, 2010. **10**(12): p. 842-57.
22. Zinsky, R., et al., *Analysis of KRAS Mutations of Exon 2 Codons 12 and 13 by SNaPshot Analysis in Comparison to Common DNA Sequencing.* Gastroenterol Res Pract, 2010. **2010**: p. 789363.
23. Stolze, B., et al., *Comparative analysis of KRAS codon 12, 13, 18, 61, and 117 mutations using human MCF10A isogenic cell lines.* Sci Rep, 2015. **5**: p. 8535.
24. Jones, S., et al., *Core signaling pathways in human pancreatic cancers revealed by global genomic analyses.* Science, 2008. **321**(5897): p. 1801-6.
25. Biankin, A.V., et al., *Pancreatic cancer genomes reveal aberrations in axon guidance pathway genes.* Nature, 2012. **491**(7424): p. 399-405.
26. Sausen, M., et al., *Clinical implications of genomic alterations in the tumour and circulation of pancreatic cancer patients.* Nat Commun, 2015. **6**: p. 7686.
27. Waddell, N., et al., *Whole genomes redefine the mutational landscape of pancreatic cancer.* Nature, 2015. **518**(7540): p. 495-501.
28. Witkiewicz, A.K., et al., *Whole-exome sequencing of pancreatic cancer defines genetic diversity and therapeutic targets.* Nat Commun, 2015. **6**: p. 6744.
29. Kanda, M., et al., *Presence of somatic mutations in most early-stage pancreatic intraepithelial neoplasia.* Gastroenterology, 2012. **142**(4): p. 730-733.e9.
30. McKay, M.M. and D.K. Morrison, *Integrating signals from RTKs to ERK/MAPK.* Oncogene, 2007. **26**(22): p. 3113-21.
31. Shaul, Y.D. and R. Seger, *The MEK/ERK cascade: from signaling specificity to diverse functions.* Biochim Biophys Acta, 2007. **1773**(8): p. 1213-26.
32. Soucek, L., et al., *Modelling Myc inhibition as a cancer therapy.* Nature, 2008. **455**(7213): p. 679-83.
33. Blasco, R.B., et al., *c-Raf, but not B-Raf, is essential for development of K-Ras oncogene-driven non-small cell lung carcinoma.* Cancer Cell, 2011. **19**(5): p. 652-63.
34. Hayes, T.K., et al., *Long-Term ERK Inhibition in KRAS-Mutant Pancreatic Cancer Is Associated with MYC Degradation and Senescence-like Growth Suppression.* Cancer Cell, 2016. **29**(1): p. 75-89.
35. Castellano, E. and J. Downward, *RAS Interaction with PI3K: More Than Just Another Effector Pathway.* Genes Cancer, 2011. **2**(3): p. 261-74.
36. Hemmings, B.A. and D.F. Restuccia, *PI3K-PKB/Akt pathway.* Cold Spring Harb Perspect Biol, 2012. **4**(9): p. a011189.
37. Wu, C.Y., et al., *PI3K regulation of RAC1 is required for KRAS-induced pancreatic tumorigenesis in mice.* Gastroenterology, 2014. **147**(6): p. 1405-16.e7.
38. Aguirre, A.J., et al., *Activated Kras and Ink4a/Arf deficiency cooperate to produce metastatic pancreatic ductal adenocarcinoma.* Genes Dev, 2003. **17**(24): p. 3112-26.
39. Cerilli, L.A., et al., *Analysis of chromosome 9p21 deletion and p16 gene mutation in salivary gland carcinomas.* Hum Pathol, 1999. **30**(10): p. 1242-6.
40. Caldas, C., et al., *Frequent somatic mutations and homozygous deletions of the p16 (MTS1) gene in pancreatic adenocarcinoma.* Nat Genet, 1994. **8**(1): p. 27-32.
41. Qiu, W., et al., *Disruption of p16 and activation of Kras in pancreas increase ductal adenocarcinoma formation and metastasis in vivo.* Oncotarget, 2011. **2**(11): p. 862-73.

42. Schulz, P., et al., *Inducible re-expression of p16 in an orthotopic mouse model of pancreatic cancer inhibits lymphangiogenesis and lymphatic metastasis.* Br J Cancer, 2008. **99**(1): p. 110-7.
43. Jeong, J., et al., *Clinical significance of p16 protein expression loss and aberrant p53 protein expression in pancreatic cancer.* Yonsei Med J, 2005. **46**(4): p. 519-25.
44. Morton, J.P., et al., *Mutant p53 drives metastasis and overcomes growth arrest/senescence in pancreatic cancer.* Proc Natl Acad Sci U S A, 2010. **107**(1): p. 246-51.
45. Dai, J.L., et al., *Dpc4 transcriptional activation and dysfunction in cancer cells.* Cancer Res, 1998. **58**(20): p. 4592-7.
46. Cao, D., et al., *Differential expression of multiple genes in association with MADH4/DPC4/SMAD4 inactivation in pancreatic cancer.* Int J Clin Exp Pathol, 2008. **1**(6): p. 510-7.
47. Blackford, A., et al., *SMAD4 gene mutations are associated with poor prognosis in pancreatic cancer.* Clin Cancer Res, 2009. **15**(14): p. 4674-9.
48. Kojima, K., et al., *Inactivation of Smad4 accelerates Kras(G12D)-mediated pancreatic neoplasia.* Cancer Res, 2007. **67**(17): p. 8121-30.
49. Izeradjene, K., et al., *Kras(G12D) and Smad4/Dpc4 haploinsufficiency cooperate to induce mucinous cystic neoplasms and invasive adenocarcinoma of the pancreas.* Cancer Cell, 2007. **11**(3): p. 229-43.
50. Ijichi, H., et al., *Aggressive pancreatic ductal adenocarcinoma in mice caused by pancreas-specific blockade of transforming growth factor-beta signaling in cooperation with active Kras expression.* Genes Dev, 2006. **20**(22): p. 3147-60.
51. Leung, L., et al., *Loss of canonical Smad4 signaling promotes KRAS driven malignant transformation of human pancreatic duct epithelial cells and metastasis.* PLoS One, 2013. **8**(12): p. e84366.
52. Ballehaninna, U.K. and R.S. Chamberlain, *The clinical utility of serum CA 19-9 in the diagnosis, prognosis and management of pancreatic adenocarcinoma: An evidence based appraisal.* J Gastrointest Oncol, 2012. **3**(2): p. 105-19.
53. McGuigan, A., et al., *Pancreatic cancer: A review of clinical diagnosis, epidemiology, treatment and outcomes.* World J Gastroenterol, 2018. **24**(43): p. 4846-4861.
54. Strasberg, S.M., J.A. Drebin, and N.J. Soper, *Evolution and current status of the Whipple procedure: an update for gastroenterologists.* Gastroenterology, 1997. **113**(3): p. 983-94.
55. Barbier, L., et al., *Impact of total pancreatectomy: short- and long-term assessment.* HPB (Oxford), 2013. **15**(11): p. 882-92.
56. Kleeff, J., et al., *Distal pancreatectomy: risk factors for surgical failure in 302 consecutive cases.* Ann Surg, 2007. **245**(4): p. 573-82.
57. Zakaria, H.M., et al., *Total pancreatectomy: Short- and long-term outcomes at a high-volume pancreas center.* World J Gastrointest Surg, 2016. **8**(9): p. 634-642.
58. Kalser, M.H. and S.S. Ellenberg, *Pancreatic cancer. Adjuvant combined radiation and chemotherapy following curative resection.* Arch Surg, 1985. **120**(8): p. 899-903.
59. Klinkenbijl, J.H., et al., *Adjuvant radiotherapy and 5-fluorouracil after curative resection of cancer of the pancreas and periampullary region: phase III trial of the EORTC gastrointestinal tract cancer cooperative group.* Ann Surg, 1999. **230**(6): p. 776-82; discussion 782-4.

60. Smeenk, H.G., et al., *Long-term survival and metastatic pattern of pancreatic and periampullary cancer after adjuvant chemoradiation or observation: long-term results of EORTC trial 40891.* Ann Surg, 2007. **246**(5): p. 734-40.
61. Neoptolemos, J.P., et al., *A randomized trial of chemoradiotherapy and chemotherapy after resection of pancreatic cancer.* N Engl J Med, 2004. **350**(12): p. 1200-10.
62. Versteijne, E., et al., *Preoperative radiochemotherapy versus immediate surgery for resectable and borderline resectable pancreatic cancer (PREOPANC trial): study protocol for a multicentre randomized controlled trial.* Trials, 2016. **17**(1): p. 127.
63. Tienhoven, G.V., et al., *Preoperative chemoradiotherapy versus immediate surgery for resectable and borderline resectable pancreatic cancer (PREOPANC-1): A randomized, controlled, multicenter phase III trial.* 2018. **36**(18_suppl): p. LBA4002-LBA4002.
64. Rivas-Aravena, A., et al., *The Elav-like protein HuR exerts translational control of viral internal ribosome entry sites.* Virology, 2009. **392**(2): p. 178-185.
65. Manegold, C., *Gemcitabine (Gemzar) in non-small cell lung cancer.* Expert Rev Anticancer Ther, 2004. **4**(3): p. 345-60.
66. Seidman, A.D., *Gemcitabine as single-agent therapy in the management of advanced breast cancer.* Oncology (Williston Park), 2001. **15**(2 Suppl 3): p. 11-4.
67. Hansen, S.W., *Gemcitabine in the treatment of ovarian cancer.* Int J Gynecol Cancer, 2001. **11 Suppl 1**: p. 39-41.
68. Alvarellos, M.L., et al., *PharmGKB summary: gemcitabine pathway.* Pharmacogenet Genomics, 2014. **24**(11): p. 564-74.
69. Plunkett, W., et al., *Gemcitabine: metabolism, mechanisms of action, and self-potentiation.* Semin Oncol, 1995. **22**(4 Suppl 11): p. 3-10.
70. Huang, P., et al., *Action of 2',2'-difluorodeoxycytidine on DNA synthesis.* Cancer Res, 1991. **51**(22): p. 6110-7.
71. Casper, E.S., et al., *Phase II trial of gemcitabine (2,2'-difluorodeoxycytidine) in patients with adenocarcinoma of the pancreas.* Invest New Drugs, 1994. **12**(1): p. 29-34.
72. Burris, H.A., 3rd, et al., *Improvements in survival and clinical benefit with gemcitabine as first-line therapy for patients with advanced pancreas cancer: a randomized trial.* J Clin Oncol, 1997. **15**(6): p. 2403-13.
73. Earl, H.M., et al., *Effects of the addition of gemcitabine, and paclitaxel-first sequencing, in neoadjuvant sequential epirubicin, cyclophosphamide, and paclitaxel for women with high-risk early breast cancer (Neo-tAnGo): an open-label, 2x2 factorial randomised phase 3 trial.* Lancet Oncol, 2014. **15**(2): p. 201-12.
74. Iyer, G., et al., *Multicenter Prospective Phase II Trial of Neoadjuvant Dose-Dense Gemcitabine Plus Cisplatin in Patients With Muscle-Invasive Bladder Cancer.* 2018. **36**(19): p. 1949-1956.
75. Unno, M., et al., *Randomized phase II/III trial of neoadjuvant chemotherapy with gemcitabine and S-1 versus upfront surgery for resectable pancreatic cancer (Prep-02/JSAP-05).* 2019. **37**(4_suppl): p. 189-189.
76. Neuhaus, P., et al., *CONKO-001: Final results of the randomized, prospective, multicenter phase III trial of adjuvant chemotherapy with gemcitabine versus observation in patients with resected pancreatic cancer (PC).* 2008. **26**(15_suppl): p. LBA4504-LBA4504.
77. Horwitz, S.B., *Taxol (paclitaxel): mechanisms of action.* Ann Oncol, 1994. **5 Suppl 6**: p. S3-6.

78. Whitehead, R.P., et al., *Phase II trial of paclitaxel and granulocyte colony-stimulating factor in patients with pancreatic carcinoma: a Southwest Oncology Group study.* J Clin Oncol, 1997. **15**(6): p. 2414-9.
79. Sharma, U.S., S.V. Balasubramanian, and R.M. Straubinger, *Pharmaceutical and physical properties of paclitaxel (Taxol) complexes with cyclodextrins.* J Pharm Sci, 1995. **84**(10): p. 1223-30.
80. Gelderblom, H., et al., *Cremophor EL: the drawbacks and advantages of vehicle selection for drug formulation.* Eur J Cancer, 2001. **37**(13): p. 1590-8.
81. Gebbia, N. and V. Gebbia, *Single agent paclitaxel in the treatment of unresectable and/or metastatic pancreatic adenocarcinoma.* Eur J Cancer, 1996. **32a**(10): p. 1822-3.
82. Oettle, H., et al., *Paclitaxel as weekly second-line therapy in patients with advanced pancreatic carcinoma.* Anticancer Drugs, 2000. **11**(8): p. 635-8.
83. Maeda, S., et al., *Paclitaxel as second-line chemotherapy in patients with gemcitabine-refractory pancreatic cancer: a retrospective study.* Int J Clin Oncol, 2011. **16**(5): p. 539-45.
84. Shukuya, T., et al., *Weekly Paclitaxel after failure of gemcitabine in pancreatic cancer patients with malignant ascites: a retrospective study.* Jpn J Clin Oncol, 2010. **40**(12): p. 1135-8.
85. Lam, A.P., et al., *Phase II study of paclitaxel plus the protein kinase C inhibitor bryostatin-1 in advanced pancreatic carcinoma.* Am J Clin Oncol, 2010. **33**(2): p. 121-4.
86. Kim, Y.J., et al., *Phase II study of 5-fluorouracil and paclitaxel in patients with gemcitabine-refractory pancreatic cancer.* Cancer Chemother Pharmacol, 2009. **63**(3): p. 529-33.
87. Gradishar, W.J., *Taxanes for the treatment of metastatic breast cancer.* Breast Cancer (Auckl), 2012. **6**: p. 159-71.
88. Hosein, P.J., et al., *A phase II trial of nab-Paclitaxel as second-line therapy in patients with advanced pancreatic cancer.* Am J Clin Oncol, 2013. **36**(2): p. 151-6.
89. Von Hoff, D.D., et al., *Gemcitabine plus nab-paclitaxel is an active regimen in patients with advanced pancreatic cancer: a phase I/II trial.* J Clin Oncol, 2011. **29**(34): p. 4548-54.
90. Von Hoff, D.D., et al., *Increased survival in pancreatic cancer with nab-paclitaxel plus gemcitabine.* N Engl J Med, 2013. **369**(18): p. 1691-703.
91. Jordan, V.C., *A Retrospective: On Clinical Studies with 5-Fluorouracil.* Cancer Res, 2016. **76**(4): p. 767-8.
92. Malet-Martino, M. and R. Martino, *Clinical studies of three oral prodrugs of 5-fluorouracil (capecitabine, UFT, S-1): a review.* Oncologist, 2002. **7**(4): p. 288-323.
93. Colucci, G., et al., *Randomized phase III trial of gemcitabine plus cisplatin compared with single-agent gemcitabine as first-line treatment of patients with advanced pancreatic cancer: the GIP-1 study.* J Clin Oncol, 2010. **28**(10): p. 1645-51.
94. Berlin, J.D., et al., *Phase III study of gemcitabine in combination with fluorouracil versus gemcitabine alone in patients with advanced pancreatic carcinoma: Eastern Cooperative Oncology Group Trial E2297.* J Clin Oncol, 2002. **20**(15): p. 3270-5.
95. Louvet, C., et al., *Gemcitabine in combination with oxaliplatin compared with gemcitabine alone in locally advanced or metastatic pancreatic cancer: results of a GERCOR and GISCAD phase III trial.* J Clin Oncol, 2005. **23**(15): p. 3509-16.

96. Herrmann, R., et al., *Gemcitabine plus capecitabine compared with gemcitabine alone in advanced pancreatic cancer: a randomized, multicenter, phase III trial of the Swiss Group for Clinical Cancer Research and the Central European Cooperative Oncology Group.* J Clin Oncol, 2007. **25**(16): p. 2212-7.
97. Poplin, E., et al., *Phase III, randomized study of gemcitabine and oxaliplatin versus gemcitabine (fixed-dose rate infusion) compared with gemcitabine (30-minute infusion) in patients with pancreatic carcinoma E6201: a trial of the Eastern Cooperative Oncology Group.* J Clin Oncol, 2009. **27**(23): p. 3778-85.
98. Kulke, M.H., et al., *Randomized phase II study of gemcitabine administered at a fixed dose rate or in combination with cisplatin, docetaxel, or irinotecan in patients with metastatic pancreatic cancer: CALGB 89904.* J Clin Oncol, 2009. **27**(33): p. 5506-12.
99. Heinemann, V., et al., *Randomized phase III trial of gemcitabine plus cisplatin compared with gemcitabine alone in advanced pancreatic cancer.* J Clin Oncol, 2006. **24**(24): p. 3946-52.
100. Neoptolemos, J.P., et al., *Comparison of adjuvant gemcitabine and capecitabine with gemcitabine monotherapy in patients with resected pancreatic cancer (ESPAC-4): a multicentre, open-label, randomised, phase 3 trial.* Lancet, 2017. **389**(10073): p. 1011-1024.
101. Conroy, T., et al., *FOLFIRINOX versus gemcitabine for metastatic pancreatic cancer.* N Engl J Med, 2011. **364**(19): p. 1817-25.
102. Kalluri, R. and R.A. Weinberg, *The basics of epithelial-mesenchymal transition.* J Clin Invest, 2009. **119**(6): p. 1420-8.
103. Dongre, A. and R.A. Weinberg, *New insights into the mechanisms of epithelial-mesenchymal transition and implications for cancer.* Nat Rev Mol Cell Biol, 2019. **20**(2): p. 69-84.
104. Lamouille, S., J. Xu, and R. Derynck, *Molecular mechanisms of epithelial-mesenchymal transition.* Nat Rev Mol Cell Biol, 2014. **15**(3): p. 178-96.
105. Shapiro, L., et al., *Structural basis of cell-cell adhesion by cadherins.* Nature, 1995. **374**(6520): p. 327-37.
106. Blaschuk, O.W., et al., *Identification of a cadherin cell adhesion recognition sequence.* Dev Biol, 1990. **139**(1): p. 227-9.
107. Hong, S.M., et al., *Loss of E-cadherin expression and outcome among patients with resectable pancreatic adenocarcinomas.* Mod Pathol, 2011. **24**(9): p. 1237-47.
108. von Burstin, J., et al., *E-cadherin regulates metastasis of pancreatic cancer in vivo and is suppressed by a SNAIL/HDAC1/HDAC2 repressor complex.* Gastroenterology, 2009. **137**(1): p. 361-71, 371.e1-5.
109. Pignatelli, M., et al., *Loss of membranous E-cadherin expression in pancreatic cancer: correlation with lymph node metastasis, high grade, and advanced stage.* J Pathol, 1994. **174**(4): p. 243-8.
110. Anderson, J.M. and C.M. Van Itallie, *Physiology and function of the tight junction.* Cold Spring Harb Perspect Biol, 2009. **1**(2): p. a002584.
111. Tang, V.W. and D.A. Goodenough, *Paracellular ion channel at the tight junction.* Biophys J, 2003. **84**(3): p. 1660-73.
112. Poliak, S., et al., *Distinct claudins and associated PDZ proteins form different autotypic tight junctions in myelinating Schwann cells.* J Cell Biol, 2002. **159**(2): p. 361-72.

113. Hamazaki, Y., et al., *Multi-PDZ domain protein 1 (MUPP1) is concentrated at tight junctions through its possible interaction with claudin-1 and junctional adhesion molecule.* J Biol Chem, 2002. **277**(1): p. 455-61.
114. Tokes, A.M., et al., *Claudin-1, -3 and -4 proteins and mRNA expression in benign and malignant breast lesions: a research study.* Breast Cancer Res, 2005. **7**(2): p. R296-305.
115. Shibutani, M., et al., *Low expression of claudin-1 and presence of poorly-differentiated tumor clusters correlate with poor prognosis in colorectal cancer.* Anticancer Res, 2013. **33**(8): p. 3301-6.
116. Nakagawa, S., et al., *Expression of CLDN1 in colorectal cancer: a novel marker for prognosis.* Int J Oncol, 2011. **39**(4): p. 791-6.
117. Sheehan, G.M., et al., *Loss of claudins-1 and -7 and expression of claudins-3 and -4 correlate with prognostic variables in prostatic adenocarcinomas.* Hum Pathol, 2007. **38**(4): p. 564-9.
118. Kominsky, S.L., et al., *Loss of the tight junction protein claudin-7 correlates with histological grade in both ductal carcinoma in situ and invasive ductal carcinoma of the breast.* Oncogene, 2003. **22**(13): p. 2021-33.
119. Usami, Y., et al., *Reduced expression of claudin-7 correlates with invasion and metastasis in squamous cell carcinoma of the esophagus.* Hum Pathol, 2006. **37**(5): p. 569-77.
120. Blanchard, A.A., et al., *Claudins 1, 3, and 4 protein expression in ER negative breast cancer correlates with markers of the basal phenotype.* Virchows Arch, 2009. **454**(6): p. 647-56.
121. Lu, S., et al., *Claudin expression in high-grade invasive ductal carcinoma of the breast: correlation with the molecular subtype.* Mod Pathol, 2013. **26**(4): p. 485-95.
122. Kinugasa, T., et al., *Selective up-regulation of claudin-1 and claudin-2 in colorectal cancer.* Anticancer Res, 2007. **27**(6a): p. 3729-34.
123. Dhawan, P., et al., *Claudin-1 regulates cellular transformation and metastatic behavior in colon cancer.* J Clin Invest, 2005. **115**(7): p. 1765-76.
124. Resnick, M.B., et al., *Claudin expression in gastric adenocarcinomas: a tissue microarray study with prognostic correlation.* Hum Pathol, 2005. **36**(8): p. 886-92.
125. Johnson, A.H., et al., *Expression of tight-junction protein claudin-7 is an early event in gastric tumorigenesis.* Am J Pathol, 2005. **167**(2): p. 577-84.
126. Tassi, R.A., et al., *Claudin-7 expression in human epithelial ovarian cancer.* Int J Gynecol Cancer, 2008. **18**(6): p. 1262-71.
127. Suh, Y., et al., *Claudin-1 induces epithelial-mesenchymal transition through activation of the c-Abl-ERK signaling pathway in human liver cells.* Oncogene, 2013. **32**(41): p. 4873-82.
128. Chao, Y.C., et al., *Claudin-1 is a metastasis suppressor and correlates with clinical outcome in lung adenocarcinoma.* Am J Respir Crit Care Med, 2009. **179**(2): p. 123-33.
129. Chang, T.L., et al., *Claudin-1 has tumor suppressive activity and is a direct target of RUNX3 in gastric epithelial cells.* Gastroenterology, 2010. **138**(1): p. 255-65.e1-3.
130. Kondo, J., et al., *Claudin-1 expression is induced by tumor necrosis factor-alpha in human pancreatic cancer cells.* Int J Mol Med, 2008. **22**(5): p. 645-9.
131. Liu, M., et al., *ZIP4 Promotes Pancreatic Cancer Progression by Repressing ZO-1 and Claudin-1 through a ZEB1-Dependent Transcriptional Mechanism.* Clin Cancer Res, 2018. **24**(13): p. 3186-3196.

132. Fletcher, D.A. and R.D. Mullins, *Cell mechanics and the cytoskeleton.* Nature, 2010. **463**(7280): p. 485-92.
133. Mendez, M.G., S. Kojima, and R.D. Goldman, *Vimentin induces changes in cell shape, motility, and adhesion during the epithelial to mesenchymal transition.* Faseb j, 2010. **24**(6): p. 1838-51.
134. Gilles, C., et al., *Transactivation of vimentin by beta-catenin in human breast cancer cells.* Cancer Res, 2003. **63**(10): p. 2658-64.
135. Lang, S.H., et al., *Enhanced expression of vimentin in motile prostate cell lines and in poorly differentiated and metastatic prostate carcinoma.* Prostate, 2002. **52**(4): p. 253-63.
136. Al-Saad, S., et al., *The prognostic impact of NF-kappaB p105, vimentin, E-cadherin and Par6 expression in epithelial and stromal compartment in non-small-cell lung cancer.* Br J Cancer, 2008. **99**(9): p. 1476-83.
137. Walsh, N., et al., *Identification of pancreatic cancer invasion-related proteins by proteomic analysis.* Proteome Sci, 2009. **7**: p. 3.
138. Liu, C.Y., et al., *Vimentin contributes to epithelial-mesenchymal transition cancer cell mechanics by mediating cytoskeletal organization and focal adhesion maturation.* Oncotarget, 2015. **6**(18): p. 15966-83.
139. Toiyama, Y., et al., *Increased expression of Slug and Vimentin as novel predictive biomarkers for lymph node metastasis and poor prognosis in colorectal cancer.* Carcinogenesis, 2013. **34**(11): p. 2548-57.
140. Liu, T., et al., *Dysregulated expression of Slug, vimentin, and E-cadherin correlates with poor clinical outcome in patients with basal-like breast cancer.* J Surg Oncol, 2013. **107**(2): p. 188-94.
141. Wu, Y. and B.P. Zhou, *Snail: More than EMT.* Cell Adh Migr, 2010. **4**(2): p. 199-203.
142. Peinado, H., D. Olmeda, and A. Cano, *Snail, Zeb and bHLH factors in tumour progression: an alliance against the epithelial phenotype?* Nat Rev Cancer, 2007. **7**(6): p. 415-28.
143. Zhou, B.P., et al., *Dual regulation of Snail by GSK-3beta-mediated phosphorylation in control of epithelial-mesenchymal transition.* Nat Cell Biol, 2004. **6**(10): p. 931-40.
144. Vinas-Castells, R., et al., *The hypoxia-controlled FBXL14 ubiquitin ligase targets SNAIL1 for proteasome degradation.* J Biol Chem, 2010. **285**(6): p. 3794-805.
145. Domínguez, D., et al., *Phosphorylation regulates the subcellular location and activity of the snail transcriptional repressor.* Mol Cell Biol, 2003. **23**(14): p. 5078-89.
146. Peinado, H., et al., *Snail mediates E-cadherin repression by the recruitment of the Sin3A/histone deacetylase 1 (HDAC1)/HDAC2 complex.* Mol Cell Biol, 2004. **24**(1): p. 306-19.
147. Medici, D., E.D. Hay, and B.R. Olsen, *Snail and Slug promote epithelial-mesenchymal transition through beta-catenin-T-cell factor-4-dependent expression of transforming growth factor-beta3.* Mol Biol Cell, 2008. **19**(11): p. 4875-87.
148. Stemmer, V., et al., *Snail promotes Wnt target gene expression and interacts with beta-catenin.* Oncogene, 2008. **27**(37): p. 5075-80.
149. Cano, A., et al., *The transcription factor snail controls epithelial-mesenchymal transitions by repressing E-cadherin expression.* Nat Cell Biol, 2000. **2**(2): p. 76-83.
150. Hojo, N., et al., *Snail knockdown reverses stemness and inhibits tumour growth in ovarian cancer.* Sci Rep, 2018. **8**(1): p. 8704.

151. Hotz, B., et al., *Epithelial to mesenchymal transition: expression of the regulators snail, slug, and twist in pancreatic cancer.* Clin Cancer Res, 2007. **13**(16): p. 4769-76.
152. Yin, T., et al., *Expression of snail in pancreatic cancer promotes metastasis and chemoresistance.* J Surg Res, 2007. **141**(2): p. 196-203.
153. Nishioka, R., et al., *SNAIL induces epithelial-to-mesenchymal transition in a human pancreatic cancer cell line (BxPC3) and promotes distant metastasis and invasiveness in vivo.* Exp Mol Pathol, 2010. **89**(2): p. 149-57.
154. Yang, X., et al., *Silencing Snail suppresses tumor cell proliferation and invasion by reversing epithelial-to-mesenchymal transition and arresting G2/M phase in non-small cell lung cancer.* Int J Oncol, 2017. **50**(4): p. 1251-1260.
155. Zhang, A., et al., *Reduced expression of Snail decreases breast cancer cell motility by downregulating the expression and inhibiting the activity of RhoA GTPase.* Oncol Lett, 2013. **6**(2): p. 339-346.
156. Azmi, A.S., et al., *Systems analysis reveals a transcriptional reversal of the mesenchymal phenotype induced by SNAIL-inhibitor GN-25.* BMC Syst Biol, 2013. **7**: p. 85.
157. Vandewalle, C., F. Van Roy, and G. Berx, *The role of the ZEB family of transcription factors in development and disease.* Cell Mol Life Sci, 2009. **66**(5): p. 773-87.
158. Sanchez-Tillo, E., et al., *ZEB1 represses E-cadherin and induces an EMT by recruiting the SWI/SNF chromatin-remodeling protein BRG1.* Oncogene, 2010. **29**(24): p. 3490-500.
159. Zhang, J., et al., *Involvement of ZEB1 and E-cadherin in the invasion of lung squamous cell carcinoma.* Mol Biol Rep, 2013. **40**(2): p. 949-56.
160. Zhou, Y.M., et al., *Clinicopathological significance of ZEB1 protein in patients with hepatocellular carcinoma.* Ann Surg Oncol, 2012. **19**(5): p. 1700-6.
161. Zhang, G.J., et al., *High expression of ZEB1 correlates with liver metastasis and poor prognosis in colorectal cancer.* Oncol Lett, 2013. **5**(2): p. 564-568.
162. Bronsert, P., et al., *Prognostic significance of Zinc finger E-box binding homeobox 1 (ZEB1) expression in cancer cells and cancer-associated fibroblasts in pancreatic head cancer.* Surgery, 2014. **156**(1): p. 97-108.
163. Rhodes, L.V., et al., *Dual regulation by microRNA-200b-3p and microRNA-200b-5p in the inhibition of epithelial-to-mesenchymal transition in triple-negative breast cancer.* Oncotarget, 2015. **6**(18): p. 16638-52.
164. Yang, Y., et al., *ZEB1 sensitizes lung adenocarcinoma to metastasis suppression by PI3K antagonism.* J Clin Invest, 2014. **124**(6): p. 2696-708.
165. Shen, A., et al., *Pien Tze Huang inhibits metastasis of human colorectal carcinoma cells via modulation of TGF-beta1/ZEB/miR-200 signaling network.* Int J Oncol, 2015. **46**(2): p. 685-90.
166. Kurahara, H., et al., *Epithelial-mesenchymal transition and mesenchymal-epithelial transition via regulation of ZEB-1 and ZEB-2 expression in pancreatic cancer.* J Surg Oncol, 2012. **105**(7): p. 655-61.
167. Sakata, J., et al., *Inhibition of ZEB1 leads to inversion of metastatic characteristics and restoration of paclitaxel sensitivity of chronic chemoresistant ovarian carcinoma cells.* Oncotarget, 2017. **8**(59): p. 99482-99494.
168. Ren, J., et al., *Inhibition of ZEB1 reverses EMT and chemoresistance in docetaxel-resistant human lung adenocarcinoma cell line.* J Cell Biochem, 2013. **114**(6): p. 1395-403.

169. Wellner, U., T. Brabletz, and T. Keck, *ZEB1 in Pancreatic Cancer.* Cancers (Basel), 2010. **2**(3): p. 1617-28.
170. Jones, S., *An overview of the basic helix-loop-helix proteins.* Genome Biol, 2004. **5**(6): p. 226.
171. Hamamori, Y., et al., *Regulation of histone acetyltransferases p300 and PCAF by the bHLH protein twist and adenoviral oncoprotein E1A.* Cell, 1999. **96**(3): p. 405-13.
172. Barnes, R.M. and A.B. Firulli, *A twist of insight - the role of Twist-family bHLH factors in development.* Int J Dev Biol, 2009. **53**(7): p. 909-24.
173. Yang, F., et al., *SET8 promotes epithelial-mesenchymal transition and confers TWIST dual transcriptional activities.* Embo j, 2012. **31**(1): p. 110-23.
174. Ohuchida, K., et al., *Twist, a novel oncogene, is upregulated in pancreatic cancer: clinical implication of Twist expression in pancreatic juice.* Int J Cancer, 2007. **120**(8): p. 1634-40.
175. Yang, M.H. and K.J. Wu, *TWIST activation by hypoxia inducible factor-1 (HIF-1): implications in metastasis and development.* Cell Cycle, 2008. **7**(14): p. 2090-6.
176. Pai, H.C., et al., *Moscatilin inhibits migration and metastasis of human breast cancer MDA-MB-231 cells through inhibition of Akt and Twist signaling pathway.* J Mol Med (Berl), 2013. **91**(3): p. 347-56.
177. Na, Y.R., et al., *Bone morphogenetic protein 7 induces mesenchymal-to-epithelial transition in melanoma cells, leading to inhibition of metastasis.* Cancer Sci, 2009. **100**(11): p. 2218-25.
178. Satoh, K., et al., *Up-regulation of MSX2 enhances the malignant phenotype and is associated with twist 1 expression in human pancreatic cancer cells.* Am J Pathol, 2008. **172**(4): p. 926-39.
179. Srivastava, R.K., et al., *Sulforaphane synergizes with quercetin to inhibit self-renewal capacity of pancreatic cancer stem cells.* Front Biosci (Elite Ed), 2011. **3**: p. 515-28.
180. Komiya, Y. and R. Habas, *Wnt signal transduction pathways.* Organogenesis, 2008. **4**(2): p. 68-75.
181. MacDonald, B.T., K. Tamai, and X. He, *Wnt/β-catenin signaling: components, mechanisms, and diseases.* Dev Cell, 2009. **17**(1): p. 9-26.
182. Yook, J.I., et al., *Wnt-dependent regulation of the E-cadherin repressor snail.* J Biol Chem, 2005. **280**(12): p. 11740-8.
183. Arensman, M.D., et al., *The CREB-binding protein inhibitor ICG-001 suppresses pancreatic cancer growth.* Mol Cancer Ther, 2014. **13**(10): p. 2303-14.
184. Manegold, P., et al., *Differentiation Therapy Targeting the β-Catenin/CBP Interaction in Pancreatic Cancer.* Cancers (Basel), 2018. **10**(4).
185. Ko, A.H., et al., *Final results of a phase Ib dose-escalation study of PRI-724, a CBP/beta-catenin modulator, plus gemcitabine (GEM) in patients with advanced pancreatic adenocarcinoma (APC) as second-line therapy after FOLFIRINOX or FOLFOX.* 2016. **34**(15_suppl): p. e15721-e15721.
186. El-Khoueiry, A.B., et al., *A phase I first-in-human study of PRI-724 in patients (pts) with advanced solid tumors.* 2013. **31**(15_suppl): p. 2501-2501.
187. Xu, J., S. Lamouille, and R. Derynck, *TGF-beta-induced epithelial to mesenchymal transition.* Cell Res, 2009. **19**(2): p. 156-72.
188. Katsuno, Y., S. Lamouille, and R. Derynck, *TGF-beta signaling and epithelial-mesenchymal transition in cancer progression.* Curr Opin Oncol, 2013. **25**(1): p. 76-84.

189. Dhasarathy, A., et al., *The transcription factors Snail and Slug activate the transforming growth factor-beta signaling pathway in breast cancer.* PLoS One, 2011. **6**(10): p. e26514.
190. Gregory, P.A., et al., *An autocrine TGF-beta/ZEB/miR-200 signaling network regulates establishment and maintenance of epithelial-mesenchymal transition.* Mol Biol Cell, 2011. **22**(10): p. 1686-98.
191. Zhang, Y.E., *Non-Smad pathways in TGF-beta signaling.* Cell Res, 2009. **19**(1): p. 128-39.
192. Melisi, D., et al., *Galunisertib plus gemcitabine vs. gemcitabine for first-line treatment of patients with unresectable pancreatic cancer.* British Journal of Cancer, 2018. **119**(10): p. 1208-1214.
193. Kopan, R. and M.X. Ilagan, *The canonical Notch signaling pathway: unfolding the activation mechanism.* Cell, 2009. **137**(2): p. 216-33.
194. Wang, Z., et al., *The role of Notch signaling pathway in epithelial-mesenchymal transition (EMT) during development and tumor aggressiveness.* Curr Drug Targets, 2010. **11**(6): p. 745-51.
195. Li, Y., et al., *Regulation of EMT by Notch signaling pathway in tumor progression.* Curr Cancer Drug Targets, 2013. **13**(9): p. 957-62.
196. Mazur, P.K., et al., *Notch2 is required for progression of pancreatic intraepithelial neoplasia and development of pancreatic ductal adenocarcinoma.* Proc Natl Acad Sci U S A, 2010. **107**(30): p. 13438-43.
197. Abel, E.V., et al., *The Notch pathway is important in maintaining the cancer stem cell population in pancreatic cancer.* PLoS One, 2014. **9**(3): p. e91983.
198. Agrawal, N., et al., *Exome sequencing of head and neck squamous cell carcinoma reveals inactivating mutations in NOTCH1.* Science, 2011. **333**(6046): p. 1154-7.
199. Hanlon, L., et al., *Notch1 functions as a tumor suppressor in a model of K-ras-induced pancreatic ductal adenocarcinoma.* Cancer Res, 2010. **70**(11): p. 4280-6.
200. Du, Z., et al., *HepaCAM inhibits the malignant behavior of castration-resistant prostate cancer cells by downregulating Notch signaling and PF-3084014 (a gamma-secretase inhibitor) partly reverses the resistance of refractory prostate cancer to docetaxel and enzalutamide in vitro.* Int J Oncol, 2018. **53**(1): p. 99-112.
201. Wu, C.X., et al., *Notch Inhibitor PF-03084014 Inhibits Hepatocellular Carcinoma Growth and Metastasis via Suppression of Cancer Stemness due to Reduced Activation of Notch1-Stat3.* Mol Cancer Ther, 2017. **16**(8): p. 1531-1543.
202. Huber, M.A., et al., *NF-kappaB is essential for epithelial-mesenchymal transition and metastasis in a model of breast cancer progression.* J Clin Invest, 2004. **114**(4): p. 569-81.
203. O'Shea, J.J., et al., *The JAK-STAT Pathway: Impact on Human Disease and Therapeutic Intervention.* 2015. **66**(1): p. 311-328.
204. Fisher, R., L. Pusztai, and C. Swanton, *Cancer heterogeneity: implications for targeted therapeutics.* Br J Cancer, 2013. **108**(3): p. 479-85.
205. Nguyen, L.V., et al., *Cancer stem cells: an evolving concept.* Nat Rev Cancer, 2012. **12**(2): p. 133-43.
206. Makino, S., *Further evidence favoring the concept of the stem cell in ascites tumors of rats.* Ann N Y Acad Sci, 1956. **63**(5): p. 818-30.

207. Hamburger, A.W. and S.E. Salmon, *Primary bioassay of human tumor stem cells.* Science, 1977. **197**(4302): p. 461-3.
208. Sell, S., *On the stem cell origin of cancer.* Am J Pathol, 2010. **176**(6): p. 2584-494.
209. Fulawka, L., P. Donizy, and A. Halon, *Cancer stem cells--the current status of an old concept: literature review and clinical approaches.* Biol Res, 2014. **47**(1): p. 66.
210. Lapidot, T., et al., *A cell initiating human acute myeloid leukaemia after transplantation into SCID mice.* Nature, 1994. **367**(6464): p. 645-8.
211. Bonnet, D. and J.E. Dick, *Human acute myeloid leukemia is organized as a hierarchy that originates from a primitive hematopoietic cell.* Nat Med, 1997. **3**(7): p. 730-7.
212. Collins, A.T., et al., *Prospective identification of tumorigenic prostate cancer stem cells.* Cancer Res, 2005. **65**(23): p. 10946-51.
213. O'Brien, C.A., et al., *A human colon cancer cell capable of initiating tumour growth in immunodeficient mice.* Nature, 2007. **445**(7123): p. 106-10.
214. Eramo, A., et al., *Identification and expansion of the tumorigenic lung cancer stem cell population.* Cell Death Differ, 2008. **15**(3): p. 504-14.
215. Al-Hajj, M., et al., *Prospective identification of tumorigenic breast cancer cells.* Proc Natl Acad Sci U S A, 2003. **100**(7): p. 3983-8.
216. Yang, Z.F., et al., *Identification of local and circulating cancer stem cells in human liver cancer.* Hepatology, 2008. **47**(3): p. 919-28.
217. Li, C., et al., *Identification of pancreatic cancer stem cells.* Cancer Res, 2007. **67**(3): p. 1030-7.
218. Clarke, M.F., et al., *Cancer stem cells--perspectives on current status and future directions: AACR Workshop on cancer stem cells.* Cancer Res, 2006. **66**(19): p. 9339-44.
219. Shiozawa, Y., et al., *Cancer stem cells and their role in metastasis.* Pharmacol Ther, 2013. **138**(2): p. 285-93.
220. Vinogradov, S. and X. Wei, *Cancer stem cells and drug resistance: the potential of nanomedicine.* Nanomedicine (Lond), 2012. **7**(4): p. 597-615.
221. Yu, Y., G. Ramena, and R.C. Elble, *The role of cancer stem cells in relapse of solid tumors.* Front Biosci (Elite Ed), 2012. **4**: p. 1528-41.
222. Liu, H., et al., *Cancer stem cells from human breast tumors are involved in spontaneous metastases in orthotopic mouse models.* Proc Natl Acad Sci U S A, 2010. **107**(42): p. 18115-20.
223. Hermann, P.C., et al., *Distinct populations of cancer stem cells determine tumor growth and metastatic activity in human pancreatic cancer.* Cell Stem Cell, 2007. **1**(3): p. 313-23.
224. Cristofanilli, M., et al., *Circulating tumor cells, disease progression, and survival in metastatic breast cancer.* N Engl J Med, 2004. **351**(8): p. 781-91.
225. Cohen, S.J., et al., *Relationship of circulating tumor cells to tumor response, progression-free survival, and overall survival in patients with metastatic colorectal cancer.* J Clin Oncol, 2008. **26**(19): p. 3213-21.
226. Danila, D.C., et al., *Circulating tumor cell number and prognosis in progressive castration-resistant prostate cancer.* Clin Cancer Res, 2007. **13**(23): p. 7053-8.
227. Ma, J., et al., *Isolation of tumorigenic circulating melanoma cells.* Biochem Biophys Res Commun, 2010. **402**(4): p. 711-7.
228. Theodoropoulos, P.A., et al., *Circulating tumor cells with a putative stem cell phenotype in peripheral blood of patients with breast cancer.* Cancer Lett, 2010. **288**(1): p. 99-106.

229. An, Y. and W.M. Ongkeko, *ABCG2: the key to chemoresistance in cancer stem cells?* Expert Opin Drug Metab Toxicol, 2009. **5**(12): p. 1529-42.
230. Jiang, Y., et al., *Expressions of putative cancer stem cell markers ABCB1, ABCG2, and CD133 are correlated with the degree of differentiation of gastric cancer.* Gastric Cancer, 2012. **15**(4): p. 440-50.
231. Nakai, E., et al., *Enhanced MDR1 expression and chemoresistance of cancer stem cells derived from glioblastoma.* Cancer Invest, 2009. **27**(9): p. 901-8.
232. Li, L. and R. Bhatia, *Stem cell quiescence.* Clin Cancer Res, 2011. **17**(15): p. 4936-41.
233. Karnoub, A.E., et al., *Mesenchymal stem cells within tumour stroma promote breast cancer metastasis.* Nature, 2007. **449**(7162): p. 557-63.
234. Massard, C., E. Deutsch, and J.C. Soria, *Tumour stem cell-targeted treatment: elimination or differentiation.* Ann Oncol, 2006. **17**(11): p. 1620-4.
235. Amariglio, N., et al., *Donor-derived brain tumor following neural stem cell transplantation in an ataxia telangiectasia patient.* PLoS Med, 2009. **6**(2): p. e1000029.
236. Liu, C., et al., *Multiple tumor types may originate from bone marrow-derived cells.* Neoplasia, 2006. **8**(9): p. 716-24.
237. Kelly, P.N., et al., *Tumor growth need not be driven by rare cancer stem cells.* Science, 2007. **317**(5836): p. 337.
238. McCulloch, E.A. and J.E. Till, *Perspectives on the properties of stem cells.* Nat Med, 2005. **11**(10): p. 1026-8.
239. Passegue, E., et al., *Normal and leukemic hematopoiesis: are leukemias a stem cell disorder or a reacquisition of stem cell characteristics?* Proc Natl Acad Sci U S A, 2003. **100 Suppl 1**: p. 11842-9.
240. Plaks, V., N. Kong, and Z. Werb, *The cancer stem cell niche: how essential is the niche in regulating stemness of tumor cells?* Cell Stem Cell, 2015. **16**(3): p. 225-38.
241. Shibue, T. and R.A. Weinberg, *EMT, CSCs, and drug resistance: the mechanistic link and clinical implications.* Nat Rev Clin Oncol, 2017. **14**(10): p. 611-629.
242. Ailles, L.E. and I.L. Weissman, *Cancer stem cells in solid tumors.* Curr Opin Biotechnol, 2007. **18**(5): p. 460-6.
243. Gopalan, V., F. Islam, and A.K. Lam, *Surface Markers for the Identification of Cancer Stem Cells.* Methods Mol Biol, 2018. **1692**: p. 17-29.
244. Reid, P.A., et al., *Current understanding of cancer stem cells: Review of their radiobiology and role in head and neck cancers.* Head Neck, 2017. **39**(9): p. 1920-1932.
245. Kuşoğlu, A. and Ç. Biray Avcı, *Cancer stem cells: A brief review of the current status.* Gene, 2019. **681**: p. 80-85.
246. Liu, X., et al., *Yamanaka factors critically regulate the developmental signaling network in mouse embryonic stem cells.* Cell Res, 2008. **18**(12): p. 1177-89.
247. Takahashi, K. and S. Yamanaka, *Induction of pluripotent stem cells from mouse embryonic and adult fibroblast cultures by defined factors.* Cell, 2006. **126**(4): p. 663-76.
248. Müller, M., et al., *The role of pluripotency factors to drive stemness in gastrointestinal cancer.* Stem Cell Research, 2016. **16**(2): p. 349-357.
249. Storms, R.W., et al., *Isolation of primitive human hematopoietic progenitors on the basis of aldehyde dehydrogenase activity.* Proc Natl Acad Sci U S A, 1999. **96**(16): p. 9118-23.
250. Yu, C., et al., *ALDH activity indicates increased tumorigenic cells, but not cancer stem cells, in prostate cancer cell lines.* In Vivo, 2011. **25**(1): p. 69-76.

251. Telford, W.G., et al., *Side population analysis using a violet-excited cell-permeable DNA binding dye.* Stem Cells, 2007. **25**(4): p. 1029-36.
252. Nomura, A., et al., *CD133 initiates tumors, induces epithelial-mesenchymal transition and increases metastasis in pancreatic cancer.* Oncotarget, 2015. **6**(10): p. 8313-22.
253. Glumac, P.M. and A.M. LeBeau, *The role of CD133 in cancer: a concise review.* Clin Transl Med, 2018. **7**(1): p. 18.
254. Skoda, J., et al., *Co-Expression of Cancer Stem Cell Markers Corresponds to a Pro-Tumorigenic Expression Profile in Pancreatic Adenocarcinoma.* PloS one, 2016. **11**(7): p. e0159255-e0159255.
255. Peng, Y., et al., *Angiogenin interacts with ribonuclease inhibitor regulating PI3K/AKT/mTOR signaling pathway in bladder cancer cells.* Cell Signal, 2014. **26**(12): p. 2782-92.
256. Hwang, W.L., et al., *SNAIL regulates interleukin-8 expression, stem cell-like activity, and tumorigenicity of human colorectal carcinoma cells.* Gastroenterology, 2011. **141**(1): p. 279-91, 291.e1-5.
257. Chen, Y.C., et al., *Aldehyde dehydrogenase 1 is a putative marker for cancer stem cells in head and neck squamous cancer.* Biochem Biophys Res Commun, 2009. **385**(3): p. 307-13.
258. Leung, E.L., et al., *Non-small cell lung cancer cells expressing CD44 are enriched for stem cell-like properties.* PLoS One, 2010. **5**(11): p. e14062.
259. Ding, Q., et al., *CD133 facilitates epithelial-mesenchymal transition through interaction with the ERK pathway in pancreatic cancer metastasis.* Mol Cancer, 2014. **13**: p. 15.
260. Wei, Z.R., et al., *Low tristetraprolin expression promotes cell proliferation and predicts poor patients outcome in pancreatic cancer.* Oncotarget, 2016. **7**(14): p. 17737-50.
261. Mani, S.A., et al., *The epithelial-mesenchymal transition generates cells with properties of stem cells.* Cell, 2008. **133**(4): p. 704-15.
262. Morel, A.P., et al., *Generation of breast cancer stem cells through epithelial-mesenchymal transition.* PLoS One, 2008. **3**(8): p. e2888.
263. Hennessy, B.T., et al., *Characterization of a naturally occurring breast cancer subset enriched in epithelial-to-mesenchymal transition and stem cell characteristics.* Cancer Res, 2009. **69**(10): p. 4116-24.
264. Zhou, W., et al., *Snail contributes to the maintenance of stem cell-like phenotype cells in human pancreatic cancer.* PLoS One, 2014. **9**(1): p. e87409.
265. Wellner, U., et al., *The EMT-activator ZEB1 promotes tumorigenicity by repressing stemness-inhibiting microRNAs.* Nat Cell Biol, 2009. **11**(12): p. 1487-95.
266. Kong, D., et al., *Cancer Stem Cells and Epithelial-to-Mesenchymal Transition (EMT)-Phenotypic Cells: Are They Cousins or Twins?* Cancers (Basel), 2011. **3**(1): p. 716-29.
267. Mladinich, M., D. Ruan, and C.H. Chan, *Tackling Cancer Stem Cells via Inhibition of EMT Transcription Factors.* Stem Cells Int, 2016. **2016**: p. 5285892.
268. Mao, J., et al., *Roles of Wnt/beta-catenin signaling in the gastric cancer stem cells proliferation and salinomycin treatment.* Cell Death Dis, 2014. **5**: p. e1039.
269. Hoffmeyer, K., et al., *Wnt/beta-catenin signaling regulates telomerase in stem cells and cancer cells.* Science, 2012. **336**(6088): p. 1549-54.
270. Wang, J., B.A. Sullenger, and J.N. Rich, *Notch signaling in cancer stem cells.* Adv Exp Med Biol, 2012. **727**: p. 174-85.

271. Ye, J., et al., *Higher notch expression implies poor survival in pancreatic ductal adenocarcinoma: A systematic review and meta-analysis.* Pancreatology, 2018. **18**(8): p. 954-961.
272. Zhang, S., et al., *Notch signaling via regulation of RB and p-AKT but not PIK3CG contributes to MIA PaCa-2 cell growth and migration to affect pancreatic carcinogenesis.* Oncol Lett, 2018. **15**(2): p. 2105-2110.
273. Aaronson, D.S. and C.M. Horvath, *A road map for those who don't know JAK-STAT.* Science, 2002. **296**(5573): p. 1653-5.
274. Jatiani, S.S., et al., *Jak/STAT pathways in cytokine signaling and myeloproliferative disorders: approaches for targeted therapies.* Genes Cancer, 2010. **1**(10): p. 979-93.
275. Schindler, C., D.E. Levy, and T. Decker, *JAK-STAT signaling: from interferons to cytokines.* J Biol Chem, 2007. **282**(28): p. 20059-63.
276. Hernandez-Vargas, H., et al., *Methylome analysis reveals Jak-STAT pathway deregulation in putative breast cancer stem cells.* Epigenetics, 2011. **6**(4): p. 428-39.
277. Duzagac, F., et al., *JAK/STAT pathway interacts with intercellular cell adhesion molecule (ICAM) and vascular cell adhesion molecule (VCAM) while prostate cancer stem cells form tumor spheroids.* J buon, 2015. **20**(5): p. 1250-7.
278. Lin, L., et al., *STAT3 signaling pathway is necessary for cell survival and tumorsphere forming capacity in ALDH(+)/CD133(+) stem cell-like human colon cancer cells.* Biochem Biophys Res Commun, 2011. **416**(3-4): p. 246-51.
279. Lin, L., et al., *STAT3 is necessary for proliferation and survival in colon cancer-initiating cells.* Cancer Res, 2011. **71**(23): p. 7226-37.
280. Han, Z., et al., *Inhibition of STAT3 signaling targets both tumor-initiating and differentiated cell populations in prostate cancer.* Oncotarget, 2014. **5**(18): p. 8416-28.
281. Macha, M.A., et al., *Guggulsterone decreases proliferation and metastatic behavior of pancreatic cancer cells by modulating JAK/STAT and Src/FAK signaling.* Cancer Lett, 2013. **341**(2): p. 166-77.
282. Ren, X., et al., *Identification of Niclosamide as a New Small-Molecule Inhibitor of the STAT3 Signaling Pathway.* ACS Med Chem Lett, 2010. **1**(9): p. 454-9.
283. Wang, C., et al., *Niclosamide Inhibits Cell Growth and Enhances Drug Sensitivity of Hepatocellular Carcinoma Cells via STAT3 Signaling Pathway.* J Cancer, 2018. **9**(22): p. 4150-4155.
284. Arend, R.C., et al., *Niclosamide and its analogs are potent inhibitors of Wnt/beta-catenin, mTOR and STAT3 signaling in ovarian cancer.* Oncotarget, 2016. **7**(52): p. 86803-86815.
285. Gyamfi, J., et al., *Niclosamide reverses adipocyte induced epithelial-mesenchymal transition in breast cancer cells via suppression of the interleukin-6/STAT3 signalling axis.* Sci Rep, 2019. **9**(1): p. 11336.
286. Li, R., et al., *Niclosamide overcomes acquired resistance to erlotinib through suppression of STAT3 in non-small cell lung cancer.* Mol Cancer Ther, 2013. **12**(10): p. 2200-12.
287. Lu, L., et al., *Activation of STAT3 and Bcl-2 and reduction of reactive oxygen species (ROS) promote radioresistance in breast cancer and overcome of radioresistance with niclosamide.* Oncogene, 2018. **37**(39): p. 5292-5304.
288. You, S., et al., *Disruption of STAT3 by niclosamide reverses radioresistance of human lung cancer.* Mol Cancer Ther, 2014. **13**(3): p. 606-16.

289. Varjosalo, M. and J. Taipale, *Hedgehog: functions and mechanisms.* Genes Dev, 2008. **22**(18): p. 2454-72.
290. Choudhry, Z., et al., *Sonic hedgehog signalling pathway: a complex network.* Ann Neurosci, 2014. **21**(1): p. 28-31.
291. Po, A., et al., *Hedgehog controls neural stem cells through p53-independent regulation of Nanog.* Embo j, 2010. **29**(15): p. 2646-58.
292. Clement, V., et al., *HEDGEHOG-GLI1 signaling regulates human glioma growth, cancer stem cell self-renewal, and tumorigenicity.* Curr Biol, 2007. **17**(2): p. 165-72.
293. Lee, C.J., J. Dosch, and D.M. Simeone, *Pancreatic cancer stem cells.* J Clin Oncol, 2008. **26**(17): p. 2806-12.
294. Ulasov, I.V., et al., *Inhibition of Sonic hedgehog and Notch pathways enhances sensitivity of CD133(+) glioma stem cells to temozolomide therapy.* Mol Med, 2011. **17**(1-2): p. 103-12.
295. Heiden, K.B., et al., *The sonic hedgehog signaling pathway maintains the cancer stem cell self-renewal of anaplastic thyroid cancer by inducing snail expression.* J Clin Endocrinol Metab, 2014. **99**(11): p. E2178-87.
296. Batsaikhan, B.E., et al., *Cyclopamine decreased the expression of Sonic Hedgehog and its downstream genes in colon cancer stem cells.* Anticancer Res, 2014. **34**(11): p. 6339-44.
297. Huang, F.T., et al., *Inhibition of hedgehog signaling depresses self-renewal of pancreatic cancer stem cells and reverses chemoresistance.* Int J Oncol, 2012. **41**(5): p. 1707-14.
298. Schaefke, B., et al., *The evolution of posttranscriptional regulation.* Wiley Interdiscip Rev RNA, 2018: p. e1485.
299. Friedman, R.C., et al., *Most mammalian mRNAs are conserved targets of microRNAs.* Genome Res, 2009. **19**(1): p. 92-105.
300. Bartel, D.P., *MicroRNAs: target recognition and regulatory functions.* Cell, 2009. **136**(2): p. 215-33.
301. Rhoades, M.W., et al., *Prediction of plant microRNA targets.* Cell, 2002. **110**(4): p. 513-20.
302. Schwarz, D.S., et al., *Evidence that siRNAs function as guides, not primers, in the Drosophila and human RNAi pathways.* Mol Cell, 2002. **10**(3): p. 537-48.
303. Lim, L.P., et al., *Microarray analysis shows that some microRNAs downregulate large numbers of target mRNAs.* Nature, 2005. **433**(7027): p. 769-73.
304. Liu, J., et al., *MicroRNA-dependent localization of targeted mRNAs to mammalian P-bodies.* Nat Cell Biol, 2005. **7**(7): p. 719-23.
305. Zhang, J. and L. Ma, *MicroRNA control of epithelial-mesenchymal transition and metastasis.* Cancer Metastasis Rev, 2012. **31**(3-4): p. 653-62.
306. Park, S.M., et al., *The miR-200 family determines the epithelial phenotype of cancer cells by targeting the E-cadherin repressors ZEB1 and ZEB2.* Genes Dev, 2008. **22**(7): p. 894-907.
307. Li, Y., et al., *Up-regulation of miR-200 and let-7 by natural agents leads to the reversal of epithelial-to-mesenchymal transition in gemcitabine-resistant pancreatic cancer cells.* Cancer Res, 2009. **69**(16): p. 6704-12.
308. Dykxhoorn, D.M., et al., *miR-200 enhances mouse breast cancer cell colonization to form distant metastases.* PLoS One, 2009. **4**(9): p. e7181.

309. Le, M.T., et al., *miR-200-containing extracellular vesicles promote breast cancer cell metastasis.* J Clin Invest, 2014. **124**(12): p. 5109-28.
310. Aslakson, C.J. and F.R. Miller, *Selective events in the metastatic process defined by analysis of the sequential dissemination of subpopulations of a mouse mammary tumor.* Cancer Res, 1992. **52**(6): p. 1399-405.
311. Yamakuchi, M., M. Ferlito, and C.J. Lowenstein, *miR-34a repression of SIRT1 regulates apoptosis.* Proc Natl Acad Sci U S A, 2008. **105**(36): p. 13421-6.
312. Chen, Y. and G. Varani, *Protein families and RNA recognition.* Febs j, 2005. **272**(9): p. 2088-97.
313. Lunde, B.M., C. Moore, and G. Varani, *RNA-binding proteins: modular design for efficient function.* Nat Rev Mol Cell Biol, 2007. **8**(6): p. 479-90.
314. Hentze, M.W., et al., *A brave new world of RNA-binding proteins.* Nat Rev Mol Cell Biol, 2018. **19**(5): p. 327-341.
315. Shaw, G. and R. Kamen, *A conserved AU sequence from the 3' untranslated region of GM-CSF mRNA mediates selective mRNA degradation.* Cell, 1986. **46**(5): p. 659-67.
316. Chen, C.Y. and A.B. Shyu, *AU-rich elements: characterization and importance in mRNA degradation.* Trends Biochem Sci, 1995. **20**(11): p. 465-70.
317. Bakheet, T., B.R. Williams, and K.S. Khabar, *ARED 3.0: the large and diverse AU-rich transcriptome.* Nucleic Acids Res, 2006. **34**(Database issue): p. D111-4.
318. Benjamin, D. and C. Moroni, *mRNA stability and cancer: an emerging link?* Expert Opin Biol Ther, 2007. **7**(10): p. 1515-29.
319. Nagai, K., et al., *Crystal structure of the RNA-binding domain of the U1 small nuclear ribonucleoprotein A.* Nature, 1990. **348**(6301): p. 515-20.
320. Liker, E., et al., *The structure of the mRNA export factor TAP reveals a cis arrangement of a non-canonical RNP domain and an LRR domain.* Embo j, 2000. **19**(21): p. 5587-98.
321. Oubridge, C., et al., *Crystal structure at 1.92 A resolution of the RNA-binding domain of the U1A spliceosomal protein complexed with an RNA hairpin.* Nature, 1994. **372**(6505): p. 432-8.
322. Varani, L., et al., *The NMR structure of the 38 kDa U1A protein - PIE RNA complex reveals the basis of cooperativity in regulation of polyadenylation by human U1A protein.* Nat Struct Biol, 2000. **7**(4): p. 329-35.
323. Fan, X.C. and J.A. Steitz, *HNS, a nuclear-cytoplasmic shuttling sequence in HuR.* Proc Natl Acad Sci U S A, 1998. **95**(26): p. 15293-8.
324. Brennan, C.M. and J.A. Steitz, *HuR and mRNA stability.* Cell Mol Life Sci, 2001. **58**(2): p. 266-77.
325. Ma, W.J., et al., *Cloning and characterization of HuR, a ubiquitously expressed Elav-like protein.* J Biol Chem, 1996. **271**(14): p. 8144-51.
326. Scheiba, R.M., et al., *The C-terminal RNA binding motif of HuR is a multi-functional domain leading to HuR oligomerization and binding to U-rich RNA targets.* RNA Biol, 2014. **11**(10): p. 1250-61.
327. Rebane, A., A. Aab, and J.A. Steitz, *Transportins 1 and 2 are redundant nuclear import factors for hnRNP A1 and HuR.* Rna, 2004. **10**(4): p. 590-9.
328. Wang, J., et al., *Multiple functions of the RNA-binding protein HuR in cancer progression, treatment responses and prognosis.* Int J Mol Sci, 2013. **14**(5): p. 10015-41.
329. Kakuguchi, W., et al., *HuR knockdown changes the oncogenic potential of oral cancer cells.* Mol Cancer Res, 2010. **8**(4): p. 520-8.

330. Giles, K.M., et al., *The 3'-untranslated region of p21WAF1 mRNA is a composite cis-acting sequence bound by RNA-binding proteins from breast cancer cells, including HuR and poly(C)-binding protein.* J Biol Chem, 2003. **278**(5): p. 2937-46.
331. Nabors, L.B., et al., *HuR, a RNA stability factor, is expressed in malignant brain tumors and binds to adenine- and uridine-rich elements within the 3' untranslated regions of cytokine and angiogenic factor mRNAs.* Cancer Res, 2001. **61**(5): p. 2154-61.
332. Young, L.E., et al., *The mRNA binding proteins HuR and tristetraprolin regulate cyclooxygenase 2 expression during colon carcinogenesis.* Gastroenterology, 2009. **136**(5): p. 1669-79.
333. Annabi, B., et al., *Inhibition of MMP-9 secretion by the anti-metastatic PSP94-derived peptide PCK3145 requires cell surface laminin receptor signaling.* Anticancer Drugs, 2006. **17**(4): p. 429-38.
334. Yi, J., et al., *Reduced nuclear export of HuR mRNA by HuR is linked to the loss of HuR in replicative senescence.* Nucleic Acids Res, 2010. **38**(5): p. 1547-58.
335. Al-Ahmadi, W., et al., *Alternative polyadenylation variants of the RNA binding protein, HuR: abundance, role of AU-rich elements and auto-Regulation.* Nucleic Acids Res, 2009. **37**(11): p. 3612-24.
336. Carballo, E., W.S. Lai, and P.J. Blackshear, *Evidence that tristetraprolin is a physiological regulator of granulocyte-macrophage colony-stimulating factor messenger RNA deadenylation and stability.* Blood, 2000. **95**(6): p. 1891-9.
337. Sawaoka, H., et al., *Tristetraprolin binds to the 3'-untranslated region of cyclooxygenase-2 mRNA. A polyadenylation variant in a cancer cell line lacks the binding site.* J Biol Chem, 2003. **278**(16): p. 13928-35.
338. Garneau, N.L., J. Wilusz, and C.J. Wilusz, *The highways and byways of mRNA decay.* Nat Rev Mol Cell Biol, 2007. **8**(2): p. 113-26.
339. Cougot, N., S. Babajko, and B. Seraphin, *Cytoplasmic foci are sites of mRNA decay in human cells.* J Cell Biol, 2004. **165**(1): p. 31-40.
340. Valencia-Sanchez, M.A., et al., *Control of translation and mRNA degradation by miRNAs and siRNAs.* Genes Dev, 2006. **20**(5): p. 515-24.
341. Galban, S., et al., *RNA-binding proteins HuR and PTB promote the translation of hypoxia-inducible factor 1alpha.* Mol Cell Biol, 2008. **28**(1): p. 93-107.
342. Durie, D., et al., *RNA-binding protein HuR mediates cytoprotection through stimulation of XIAP translation.* Oncogene, 2011. **30**(12): p. 1460-9.
343. Ishimaru, D., et al., *Regulation of Bcl-2 expression by HuR in HL60 leukemia cells and A431 carcinoma cells.* Mol Cancer Res, 2009. **7**(8): p. 1354-66.
344. Bhattacharyya, S.N., et al., *Relief of microRNA-mediated translational repression in human cells subjected to stress.* Cell, 2006. **125**(6): p. 1111-24.
345. Kawai, T., et al., *Translational control of cytochrome c by RNA-binding proteins TIA-1 and HuR.* Mol Cell Biol, 2006. **26**(8): p. 3295-307.
346. Lopez de Silanes, I., et al., *Identification of a target RNA motif for RNA-binding protein HuR.* Proc Natl Acad Sci U S A, 2004. **101**(9): p. 2987-92.
347. Kullmann, M., et al., *ELAV/Hu proteins inhibit p27 translation via an IRES element in the p27 5'UTR.* Genes Dev, 2002. **16**(23): p. 3087-99.
348. Meng, Z., et al., *Alterations in RNA-binding activities of IRES-regulatory proteins as a mechanism for physiological variability and pathological dysregulation of IGF-IR*

translational control in human breast tumor cells. J Cell Physiol, 2008. **217**(1): p. 172-83.
349. Yeh, C.H., et al., *RNA-binding protein HuR interacts with thrombomodulin 5'untranslated region and represses internal ribosome entry site-mediated translation under IL-1 beta treatment.* Mol Biol Cell, 2008. **19**(9): p. 3812-22.
350. Kim, H.H., et al., *HuR recruits let-7/RISC to repress c-Myc expression.* Genes Dev, 2009. **23**(15): p. 1743-8.
351. Kang, M.J., et al., *NF-kappaB activates transcription of the RNA-binding factor HuR, via PI3K-AKT signaling, to promote gastric tumorigenesis.* Gastroenterology, 2008. **135**(6): p. 2030-42, 2042.e1-3.
352. Jeyaraj, S.C., et al., *Transcriptional control of human antigen R by bone morphogenetic protein.* J Biol Chem, 2010. **285**(7): p. 4432-40.
353. Abdelmohsen, K., et al., *miR-519 reduces cell proliferation by lowering RNA-binding protein HuR levels.* Proc Natl Acad Sci U S A, 2008. **105**(51): p. 20297-302.
354. Guo, X., Y. Wu, and R.S. Hartley, *MicroRNA-125a represses cell growth by targeting HuR in breast cancer.* RNA Biol, 2009. **6**(5): p. 575-83.
355. Roff, A.N., et al., *MicroRNA-570-3p regulates HuR and cytokine expression in airway epithelial cells.* Am J Clin Exp Immunol, 2014. **3**(2): p. 68-83.
356. Abdelmohsen, K., et al., *Ubiquitin-mediated proteolysis of HuR by heat shock.* Embo j, 2009. **28**(9): p. 1271-82.
357. Izquierdo, J.M., *Hu antigen R (HuR) functions as an alternative pre-mRNA splicing regulator of Fas apoptosis-promoting receptor on exon definition.* J Biol Chem, 2008. **283**(27): p. 19077-84.
358. Wang, H., et al., *Promotion of exon 6 inclusion in HuD pre-mRNA by Hu protein family members.* Nucleic Acids Res, 2010. **38**(11): p. 3760-70.
359. Keene, J.D., *Why is Hu where? Shuttling of early-response-gene messenger RNA subsets.* Proc Natl Acad Sci U S A, 1999. **96**(1): p. 5-7.
360. Doller, A., et al., *Protein kinase C alpha-dependent phosphorylation of the mRNA-stabilizing factor HuR: implications for posttranscriptional regulation of cyclooxygenase-2.* Mol Biol Cell, 2007. **18**(6): p. 2137-48.
361. Kim, H.H., et al., *Nuclear HuR accumulation through phosphorylation by Cdk1.* Genes Dev, 2008. **22**(13): p. 1804-15.
362. Abdelmohsen, K., et al., *Phosphorylation of HuR by Chk2 regulates SIRT1 expression.* Mol Cell, 2007. **25**(4): p. 543-57.
363. Costantino, C.L., et al., *The role of HuR in gemcitabine efficacy in pancreatic cancer: HuR Up-regulates the expression of the gemcitabine metabolizing enzyme deoxycytidine kinase.* Cancer Res, 2009. **69**(11): p. 4567-72.
364. Burkhart, R.A., et al., *HuR is a post-transcriptional regulator of core metabolic enzymes in pancreatic cancer.* RNA Biol, 2013. **10**(8): p. 1312-23.
365. Lal, S., et al., *HuR posttranscriptionally regulates WEE1: implications for the DNA damage response in pancreatic cancer cells.* Cancer Res, 2014. **74**(4): p. 1128-40.
366. Blanco, F.F., et al., *The mRNA-binding protein HuR promotes hypoxia-induced chemoresistance through posttranscriptional regulation of the proto-oncogene PIM1 in pancreatic cancer cells.* Oncogene, 2016. **35**(19): p. 2529-41.

367. Zarei, M., et al., *Posttranscriptional Upregulation of IDH1 by HuR Establishes a Powerful Survival Phenotype in Pancreatic Cancer Cells.* Cancer Res, 2017. **77**(16): p. 4460-4471.
368. Li, Y., et al., *Involvement of post-transcriptional regulation of FOXO1 by HuR in 5-FU-induced apoptosis in breast cancer cells.* Oncol Lett, 2013. **6**(1): p. 156-160.
369. McAllister, F., et al., *dCK expression correlates with 5-fluorouracil efficacy and HuR cytoplasmic expression in pancreatic cancer: a dual-institutional follow-up with the RTOG 9704 trial.* Cancer Biol Ther, 2014. **15**(6): p. 688-98.
370. Tatarian, T., et al., *Cytoplasmic HuR Status Predicts Disease-free Survival in Resected Pancreatic Cancer: A Post-hoc Analysis From the International Phase III ESPAC-3 Clinical Trial.* Ann Surg, 2018. **267**(2): p. 364-369.
371. Heinonen, M., et al., *Cytoplasmic HuR expression is a prognostic factor in invasive ductal breast carcinoma.* Cancer Res, 2005. **65**(6): p. 2157-61.
372. Wang, J., et al., *Predictive and prognostic significance of cytoplasmic expression of ELAV-like protein HuR in invasive breast cancer treated with neoadjuvant chemotherapy.* Breast Cancer Res Treat, 2013. **141**(2): p. 213-24.
373. Giaginis, C., et al., *Elevated Hu-Antigen Receptor (HuR) Expression is Associated with Tumor Aggressiveness and Poor Prognosis but not with COX-2 Expression in Invasive Breast Carcinoma Patients.* Pathol Oncol Res, 2018. **24**(3): p. 631-640.
374. Richards, N.G., et al., *HuR status is a powerful marker for prognosis and response to gemcitabine-based chemotherapy for resected pancreatic ductal adenocarcinoma patients.* Ann Surg, 2010. **252**(3): p. 499-505; discussion 505-6.
375. Heinonen, M., et al., *Prognostic role of HuR in hereditary breast cancer.* Clin Cancer Res, 2007. **13**(23): p. 6959-63.
376. Lim, S.J., et al., *Cytoplasmic expression of HuR is related to cyclooxygenase-2 expression in colon cancer.* Cancer Res Treat, 2009. **41**(2): p. 87-92.
377. Miyata, Y., et al., *High expression of HuR in cytoplasm, but not nuclei, is associated with malignant aggressiveness and prognosis in bladder cancer.* PLoS One, 2013. **8**(3): p. e59095.
378. Xu, W., et al., *Knockdown of HuR represses osteosarcoma cells migration, invasion and stemness through inhibition of YAP activation and increases susceptibility to chemotherapeutic agents.* Biomed Pharmacother, 2018. **102**: p. 587-593.
379. D'Uva, G., et al., *Beta-catenin/HuR post-transcriptional machinery governs cancer stem cell features in response to hypoxia.* PLoS One, 2013. **8**(11): p. e80742.
380. Jimbo, M., et al., *Targeting the mRNA-binding protein HuR impairs malignant characteristics of pancreatic ductal adenocarcinoma cells.* Oncotarget, 2015. **6**(29): p. 27312-31.
381. Nakanishi, S., et al., *MS-444, a new inhibitor of myosin light chain kinase from Micromonospora sp. KY7123.* J Antibiot (Tokyo), 1995. **48**(9): p. 948-51.
382. Blanco, F.F., et al., *Impact of HuR inhibition by the small molecule MS-444 on colorectal cancer cell tumorigenesis.* Oncotarget, 2016. **7**(45): p. 74043-74058.
383. Wang, J., et al., *Anti-cancer effects of the HuR inhibitor, MS-444, in malignant glioma cells.* Cancer Biol Ther, 2019. **20**(7): p. 979-988.
384. D'Agostino, V.G., et al., *Dihydrotanshinone-I interferes with the RNA-binding activity of HuR affecting its post-transcriptional function.* Sci Rep, 2015. **5**: p. 16478.

385. Lal, P., et al., *Regulation of HuR structure and function by dihydrotanshinone-I.* Nucleic Acids Res, 2017. **45**(16): p. 9514-9527.
386. Guo, J., et al., *Inhibiting cytoplasmic accumulation of HuR synergizes genotoxic agents in urothelial carcinoma of the bladder.* Oncotarget, 2016. **7**(29): p. 45249-45262.
387. Meisner, N.C., et al., *Identification and mechanistic characterization of low-molecular-weight inhibitors for HuR.* Nat Chem Biol, 2007. **3**(8): p. 508-15.
388. Wu, X., et al., *Identification and validation of novel small molecule disruptors of HuR-mRNA interaction.* ACS Chem Biol, 2015. **10**(6): p. 1476-84.
389. Manzoni, L., et al., *Interfering with HuR-RNA Interaction: Design, Synthesis and Biological Characterization of Tanshinone Mimics as Novel, Effective HuR Inhibitors.* J Med Chem, 2018. **61**(4): p. 1483-1498.
390. Chae, M.J., et al., *Chemical inhibitors destabilize HuR binding to the AU-rich element of TNF-alpha mRNA.* Exp Mol Med, 2009. **41**(11): p. 824-31.
391. Sanjana, N.E., O. Shalem, and F. Zhang, *Improved vectors and genome-wide libraries for CRISPR screening.* Nat Methods, 2014. **11**(8): p. 783-784.
392. Shalem, O., et al., *Genome-scale CRISPR-Cas9 knockout screening in human cells.* Science, 2014. **343**(6166): p. 84-87.
393. Bemis, D.L., et al., *beta-carboline alkaloid-enriched extract from the amazonian rain forest tree pao pereira suppresses prostate cancer cells.* J Soc Integr Oncol, 2009. **7**(2): p. 59-65.
394. Steele, J.C., et al., *Indole and beta-carboline alkaloids from Geissospermum sericeum.* J Nat Prod, 2002. **65**(1): p. 85-8.
395. Mbeunkui, F., et al., *In vitro antiplasmodial activity of indole alkaloids from the stem bark of Geissospermum vellosii.* J Ethnopharmacol, 2012. **139**(2): p. 471-7.
396. Reina, M., et al., *Indole alkaloids from Geissospermum reticulatum.* J Nat Prod, 2012. **75**(5): p. 928-34.
397. Yu, J. and Q. Chen, *The plant extract of Pao pereira potentiates carboplatin effects against ovarian cancer.* Pharm Biol, 2014. **52**(1): p. 36-43.
398. Yu, J., J. Drisko, and Q. Chen, *Inhibition of pancreatic cancer and potentiation of gemcitabine effects by the extract of Pao Pereira.* Oncol Rep, 2013. **30**(1): p. 149-56.
399. Chang, C., et al., *Pao Pereira Extract Suppresses Castration-Resistant Prostate Cancer Cell Growth, Survival, and Invasion Through Inhibition of NFkappaB Signaling.* Integr Cancer Ther, 2014. **13**(3): p. 249-58.
400. Vermeulen, L., et al., *Single-cell cloning of colon cancer stem cells reveals a multi-lineage differentiation capacity.* Proc Natl Acad Sci U S A, 2008. **105**(36): p. 13427-32.
401. Kim, S.Y., et al., *Cancer Stem Cells Protect Non-Stem Cells From Anoikis: Bystander Effects.* J Cell Biochem, 2016. **117**(10): p. 2289-301.
402. Goodell, M.A., S. McKinney-Freeman, and F.D. Camargo, *Isolation and characterization of side population cells.* Methods Mol Biol, 2005. **290**: p. 343-52.
403. Richard, V., et al., *Side Population Cells as Prototype of Chemoresistant, Tumor-Initiating Cells.* BioMed Research International, 2013. **2013**: p. 517237.
404. Li, C., C.J. Lee, and D.M. Simeone, *Identification of human pancreatic cancer stem cells.* Methods Mol Biol, 2009. **568**: p. 161-73.
405. Ajani, J.A., et al., *Cancer stem cells: the promise and the potential.* Semin Oncol, 2015. **42 Suppl 1**: p. S3-17.

406. Takebe, N., et al., *Targeting cancer stem cells by inhibiting Wnt, Notch, and Hedgehog pathways.* Nat Rev Clin Oncol, 2011. **8**(2): p. 97-106.
407. Cheng, P., et al., *Nanog down-regulates the Wnt signaling pathway via β-catenin phosphorylation during epidermal stem cell proliferation and differentiation.* Cell Biosci, 2015. **5**.
408. Yong, X., et al., *Helicobacter pylori upregulates Nanog and Oct4 via Wnt/beta-catenin signaling pathway to promote cancer stem cell-like properties in human gastric cancer.* Cancer Lett, 2016. **374**(2): p. 292-303.
409. Takao, Y., T. Yokota, and H. Koide, *Beta-catenin up-regulates Nanog expression through interaction with Oct-3/4 in embryonic stem cells.* Biochem Biophys Res Commun, 2007. **353**(3): p. 699-705.
410. Amini, S., et al., *The expressions of stem cell markers: Oct4, Nanog, Sox2, nucleostemin, Bmi, Zfx, Tcl1, Tbx3, Dppa4, and Esrrb in bladder, colon, and prostate cancer, and certain cancer cell lines.* Anat Cell Biol, 2014. **47**(1): p. 1-11.
411. Salmaggi, A., et al., *Glioblastoma-derived tumorospheres identify a population of tumor stem-like cells with angiogenic potential and enhanced multidrug resistance phenotype.* Glia, 2006. **54**(8): p. 850-60.
412. Nagare, R.P., et al., *Cancer Stem Cells - Are Surface Markers Alone Sufficient?* Curr Stem Cell Res Ther, 2017. **12**(1): p. 37-44.
413. Reya, T., et al., *Stem cells, cancer, and cancer stem cells.* Nature, 2001. **414**(6859): p. 105-11.
414. La Barre, J., *Hypotensive effects of the completely dereserpinised extract of Rauwolfia vomitoria.* Arzneimittelforschung, 1973. **23**(4): p. 600-5.
415. Gbolade, A., *Ethnobotanical study of plants used in treating hypertension in Edo State of Nigeria.* J Ethnopharmacol, 2012. **144**(1): p. 1-10.
416. Pesewu, G.A., R.R. Cutler, and D.P. Humber, *Antibacterial activity of plants used in traditional medicines of Ghana with particular reference to MRSA.* J Ethnopharmacol, 2008. **116**(1): p. 102-11.
417. Kweifio-Okai, G., *Antiinflammatory activity of a Ghanaian antiarthritic herbal preparation: I.* J Ethnopharmacol, 1991. **33**(3): p. 263-7.
418. La Barre, J. and J. Castiau, *[Effect of reserpine-free Rauwolfia vomitoria extract on gastric motility in dogs].* C R Seances Soc Biol Fil, 1957. **151**(12): p. 2222-4.
419. Isaiah, A.M., et al., *Vitamin e supplementation with rauwolfia vomitoria root bark extract improves hematological indices.* N Am J Med Sci, 2012. **4**(2): p. 86-9.
420. Bemis, D.L., et al., *Anti-prostate cancer activity of a beta-carboline alkaloid enriched extract from Rauwolfia vomitoria.* Int J Oncol, 2006. **29**(5): p. 1065-73.
421. Iwu, M.M. and W.E. Court, *Root alkaloids of Rauwolfia vomitoria afz.* Planta Med, 1977. **32**(1): p. 88-99.
422. Beljanski, M. and M.S. Beljanski, *Three alkaloids as selective destroyers of cancer cells in mice. Synergy with classic anticancer drugs.* Oncology, 1986. **43**(3): p. 198-203.
423. Chen, Q., et al., *Antitumor and neurotoxic effects of novel harmine derivatives and structure-activity relationship analysis.* Int J Cancer, 2005. **114**(5): p. 675-82.
424. Yu, J. and Q. Chen, *Antitumor Activities of Rauwolfia vomitoria Extract and Potentiation of Gemcitabine Effects Against Pancreatic Cancer.* Integr Cancer Ther, 2014. **13**(3): p. 217-25.

425. Oettle, H. and P. Neuhaus, *Adjuvant therapy in pancreatic cancer: a critical appraisal.* Drugs, 2007. **67**(16): p. 2293-310.
426. Renouf, D. and M. Moore, *Evolution of systemic therapy for advanced pancreatic cancer.* Expert Rev Anticancer Ther, 2010. **10**(4): p. 529-40.
427. Yu, J., et al., *Antitumor Activities of Rauwolfia vomitoria Extract and Potentiation of Carboplatin Effects Against Ovarian Cancer.* Curr Ther Res Clin Exp, 2013. **75**: p. 8-14.
428. Peng, W., et al., *Elevated HuR in Pancreas Promotes a Pancreatitis-Like Inflammatory Microenvironment That Facilitates Tumor Development.* Mol Cell Biol, 2018. **38**(3).
429. Lal, S., et al., *CRISPR Knockout of the HuR Gene Causes a Xenograft Lethal Phenotype.* Mol Cancer Res, 2017. **15**(6): p. 696-707.
430. Hung, K.F., et al., *Human antigen R protein modulates vascular endothelial growth factor expression in human corneal epithelial cells under hypoxia.* J Formos Med Assoc, 2019.
431. Abdelmohsen, K., et al., *Posttranscriptional gene regulation by RNA-binding proteins during oxidative stress: implications for cellular senescence.* Biol Chem, 2008. **389**(3): p. 243-55.
432. Shang, J. and Z. Zhao, *Emerging role of HuR in inflammatory response in kidney diseases.* Acta Biochim Biophys Sin (Shanghai), 2017. **49**(9): p. 753-763.
433. Woodhoo, A., et al., *Human antigen R contributes to hepatic stellate cell activation and liver fibrosis.* Hepatology, 2012. **56**(5): p. 1870-82.
434. Bruckner, H.W., et al., *Leucovorin and 5-fluorouracil as a treatment for disseminated cancer of the pancreas and unknown primary tumors.* Cancer Res, 1988. **48**(19): p. 5570-2.
435. Rick, F.G., et al., *Combination of gastrin-releasing peptide antagonist with cytotoxic agents produces synergistic inhibition of growth of human experimental colon cancers.* Cell Cycle, 2012. **11**(13): p. 2518-25.
436. Aung, T.N., et al., *Understanding the Effectiveness of Natural Compound Mixtures in Cancer through Their Molecular Mode of Action.* International journal of molecular sciences, 2017. **18**(3): p. 656.
437. Mangal, M., et al., *NPACT: Naturally Occurring Plant-based Anti-cancer Compound-Activity-Target database.* Nucleic Acids Res, 2013. **41**(Database issue): p. D1124-9.
438. Bemis, D.L., et al., *beta-carboline alkaloid-enriched extract from the amazonian rain forest tree pao pereira suppresses prostate cancer cells.* Journal of the Society for Integrative Oncology, 2009. **7**(2): p. 59-65.
439. Morris Kupchan, S. and M.E. Obasi, *A Note on the Occurrence of 2,6-Dimethoxybenzoquinone in Rauwolfia vomitoria**Received December 11, 1959, from the Department of Pharmaceutical Chemistry. University of Wisconsin, Madison.* Journal of the American Pharmaceutical Association (Scientific ed.), 1960. **49**(4): p. 257-258.
440. Rizzello, C.G., et al., *Synthesis of 2-methoxy benzoquinone and 2,6-dimethoxybenzoquinone by selected lactic acid bacteria during sourdough fermentation of wheat germ.* Microbial cell factories, 2013. **12**: p. 105-105.
441. Preet, R., et al., *105 The RNA Binding Protein HuR Enhances Exosome Secretion in Colorectal Cancer.* Gastroenterology, 2016. **150**(4): p. S27.
442. Li, C.L., et al., *Survival advantages of multicellular spheroids vs. monolayers of HepG2 cells in vitro.* Oncol Rep, 2008. **20**(6): p. 1465-71.